



---

# **Universidad de Valladolid**

Facultad de Ciencias

Departamento de Química Física y  
Química Inorgánica

TESIS DOCTORAL:

## **Biomolecules and interstellar molecules: structure, interactions and spectroscopic characterization**

Presentada por Elena Rita Alonso Alonso  
para optar al grado de  
Doctor por la Universidad de Valladolid

Dirigida por:

Prof. Jose Luis Alonso Hernández



Esta investigación ha sido financiada por:

**Ministerio de Ciencia e Innovación**

Plan Nacional I+D+I

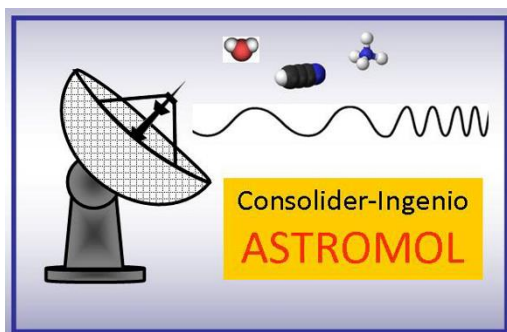
CTQ-2013-40717-P

CTQ-2016-76393-P

FPI Grant: CTQ-2014-067776



Consolider-Ingenio  
MINECO CSD2009-00038  
**(ASTROMOL)**



(FP/2007-2013)/ERC-  
SyG-2013 Grant  
Agreement n. 610256  
**NANOCOSMOS**

**nanocosmos**



European Research Council  
Established by the European Commission



JCyL-VA077U16  
**Junta de  
Castilla y León**





Dicen que ningún camino fácil te llevará a algo que merezca la pena, y es cierto, que no he escuchado a nadie decir que el camino que se recorre durante una tesis doctoral es un camino de rosas. Lo que si tengo claro es que no lo podría haber recorrido sola. A pesar de que bajo la autoría de esta Memoria sólo conste mi nombre, son muchas las personas que me han acompañado durante este arduo camino, y qué menos, que dedicarles unas pequeñas palabras, aunque sea la milésima parte de lo que en verdad se merecen.

Primero de todo agradecer al Prof. José Luis Alonso por haberme guiado durante todo este tiempo. Tengo claro que no podría haber elegido a nadie mejor para aprender todo sobre la espectroscopia molecular, pero no es lo único que me llevo. Tu incansable ejemplo de entusiasmo, constancia, honestidad y de “tirar para adelante” venga lo que venga no deja indiferente a nadie.

A todos los pasados y presentes miembros del GEM, especialmente a Iker, Lucie y Santi, por toda vuestra ayuda que ha contribuido enormemente a mi formación durante este periodo.

Al Prof. G.A. Blake y a su grupo en California Institute of Technology, por haberme acogido durante 4 meses dándome la oportunidad de participar y aprender de su investigación.

A mis padres, por todo su cariño y apoyo incondicional. No hay palabras para describir lo agradecida que os estoy por todo lo que habéis hecho por mí. No podría haber llegado hasta aquí sin vosotros. Gracias por quererme y enseñarme a querer incondicionalmente.

A mi familia y a la familia Alonso Galiana por estar a mi lado siempre.

A mis amigos, en especial a Sara A., Mery, Sara C., Pati, Kewei, Yaiza y Manu, por ser mi válvula de escape en innumerables ocasiones, por creer en mí cuando ni yo misma lo hago, por hacerme ver el vaso medio lleno, por enseñarme a comerme el mundo y no la cabeza, y sobre todo, por sacar lo mejor de mí.



# INDEX

---

ABSTRACT.....	page 1
INTRODUCCIÓN.....	page 11
1. Antecedentes.....	page 13
2. Moléculas y biomoléculas en fase gas.....	page 15
2.1. Efecto exo-anomérico.....	page 18
2.1. Edulcorantes artificiales.....	page 20
2.1. Ácidos fenólicos.....	page 23
2.1. Dipéptidos.....	page 25
3. Astrofísica molecular: moléculas del medio interestelar.....	page 28
3.1. Moléculas prebióticas.....	page 30
3.1.1. Ácido acrílico.....	page 33
3.1.2. Formato de vinilo.....	page 34
3.1.3. Metoxiamina.....	page 35
3.1.4. N-metil hidroxilamina.....	page 37
3.1.5. Cianuro de isopropilo.....	page 38
3.2. Precursores de aminoácidos..	page 39
3.2.1. Aminoacetonitrilo.....	page 40
3.2.2. Glicinamida.....	page 41
3.2.3. Hidantoina.....	page 43
4. Referencias.....	page 44
EXPERIMENTAL METHODOLOGY.....	page 49
CHAPTER I. A structural expression of exo-anomeric effect.....	page 65
CHAPTER II. The sweet structures of D-sorbitol.....	page 79
CHAPTER III. Saccharine.....	page 91

CHAPTER IV. The conformational map of phenolic acids.....	page 103
CHAPTER V. The role of amino acid side chains in stabilizing dipeptides: The laser ablation Fourier transform microwave spectrum of Ac-Val-NH <sub>2</sub> .....	page 115
CHAPTER VI. Waveguide CP-FTMW and millimeter wave spectra of s-cis and s-trans-acrylic acid.....	page 129
CHAPTER VII. Millimeter Wave Spectrum and Astronomical Search for Vinyl Formate.....	page 143
CHAPTER VIII. The rotational spectrum of methoxyamine up to 480 GHz: a laboratory study and astronomical search....	page 157
CHAPTER IX. Laboratory millimeter wave spectrum of N-methylhydroxylamine.....	page 175
CHAPTER X. A Comprehensive Rotational Study of Interstellar Iso-propyl Cyanide up to 480 GHz.....	page 191
CHAPTER XI. Rotational Spectra in 29 Vibrationally Excited States of Interstellar Aminoacetonitrile.....	page 211
CHAPTER XII. The glycine precursor glycinamide caught in the gas phase: A laser-ablation jet-cooled rotational study...	page 225
CHAPTER XIII. Laser ablated hydantoin: a high resolution rotational study.....	page 235
CONCLUSIONS AND FUTURE TRENDS.....	page 247
APPENDIX: Supplementary information.....	page 255





# ABSTRACT

---





Nowadays, structure-property relationships are at the heart of modern molecular approaches to biomolecular systems. Knowledge of the different geometries adopted by biomolecules is crucial to gain insight into their biological functions. The structures are the result of a subtle, yet complex, balance between a significant number of different interactions, both intrinsic and environmental. Gas phase studies thus become essential, to overcome the competition between intra- and intermolecular interactions into tuning the overall conformational behavior. Microwave spectroscopy, considered the most definitive gas phase structural probe, can distinguish between different conformational structures since they have different spectroscopic constants and give separate rotational spectra. However, it suffers a severe limitation: it has been limited to molecular specimens having an appreciable vapor pressure. In general, large molecules, those of biological importance, have low vapor pressures and tend to undergo thermal reactions and degradation upon heating, making them out of reach for structural studies in the gas phase. In the last decade, rotational studies of biomolecules have entered in a new stage with the combination of laser ablation LA techniques and narrowband MB-FTMW and broadband CP-FTMW Fourier transform microwave techniques in supersonic jets, developed in our laboratories over the last years, overcoming the problems of thermal decomposition associated with conventional heating methods.

Monosaccharides are the primary building blocks of many essential carbohydrate systems. They play a crucial role in many fundamental biochemical processes ranging from energy metabolism to recognition. Stereoelectronic hyperconjugation factors, like those associated with anomeric or gauche effects, as well as the cooperative OH...O chains extended along the entire molecule, are the main factors driving the conformational behavior. Structural signatures for **exo-anomeric effect** have been extracted from the archetypal methyl- $\beta$ -D-xyloside using broadband Fourier transform microwave spectroscopy combined with laser ablation. Spectrum analysis allows the determination of a set of rotational constants, which has been unequivocally attributed to conformer  $cc$ - $\beta$ - ${}^4C_1$   $g^-$ , corresponding to the global minimum of the potential energy surface, where the

aglycon residue (CH<sub>3</sub>) orientation contributes to the maximization of the exo-anomeric effect. Further analysis allowed the determination of the  $r_s$  structure, based on the detection of 11 isotopologues, derived from the presence of six <sup>13</sup>C and five <sup>18</sup>O atoms be observed in their natural abundances. The observed glycosidic C<sub>1</sub>–O<sub>1</sub> bond length decrease (1.38 Å) can be interpreted regarding the exo-anomeric effect. As such, the exo-anomeric effect presents itself as one of the leading driving forces controlling the shape of many biologically essential oligosaccharides.

Since early last century, abundant research has addressed the link between sweetness and the structure of sweeteners. None of these theories has been able to offer a unified explanation regarding the sweetness-structure relation until Shallenberger and Acree's proposal. They observed that the sweetness depends on the strength of two H-bonds by which the sweetener is bound to the sweet receptor. They established that one of the two electronegative atoms might act as a proton donor (AH) in the hydrogen bond interaction and the other as acceptor (B). These two groups form what is called the *glucophore*, which refers to the part of the sweetener that interacts with the sweet receptor. In the gas phase isolation conditions of a supersonic expansion, three different conformers have been revealed for the artificial sweetener **D-sorbitol**, investigated for the first time using a combination of chirped pulse Fourier transform microwave spectroscopy (CP-FTMW) coupled with laser ablation (LA) source. All conformers are over-stabilized by a network of five-cooperative intramolecular hydrogen bonds between vicinal hydroxyl groups in clockwise or counterclockwise arrangements. They all share a characteristic structural signature: the O<sub>1</sub>H...O<sub>2</sub> intramolecular hydrogen bond that fulfills the requirements of the glucophore proposed by Shallenberger's molecular theory of sweet taste. It is well known that the compounds that have sweet taste have different functionalities. **Saccharine**, as the vast of artificial sweeteners, has been discovered by an accidental event during organic synthesis. It is a broad commonly used artificial sweetener whose sodium salt is applied in several foods and in the production of several pharmaceuticals compounds whose structure consists in a benzoic sulfimide. The jet-cooled rotational spectrum of solid samples of

saccharine (m.p.= 228°C) has also been investigated in the isolation condition of a supersonic expansion. In saccharine, AH is the imino group and B a sulfoxide oxygen atom. Present results provide the first linkage between sweetness and structure in artificial sweeteners.

The benefits of vaporization by laser ablation and the high resolution and sensitivity attained by the LA-CP-FTMW have provided the first conformational map of the simplest phenolic acids of ***trans*-cinnamic** and ***p*-coumaric**. Two conformers of *trans*-cinnamic acid and four conformers of *trans*-*p*-coumaric acid have been characterized under the isolation conditions of a supersonic expansion. The spectroscopic constants derived from the analysis of the rotational spectra compared with those predicted theoretically provide an unmatched means to achieve an unambiguous identification of the observed species.

The first step towards fully understands protein folding requires detailed information on the intrinsic conformational preferences of small and peptide mimics. Dipeptide mimics (containing two peptide linkages, -CO-NH-) have received much attention because they represent the peptides smallest realistic and representative systems for designing local conformational effects in peptides and proteins. LA-MB-FTMW spectroscopy has studied the steric effects imposed by the isopropyl group of valine in the conformational stabilization of the capped dipeptide **N-acetyl-L-valinamide (Ac-Val-NH<sub>2</sub>)**. The rotational and quadrupole coupling constants of the two <sup>14</sup>N nuclei determined in this work show that this dipeptide exists as a mixture of C<sub>7</sub><sup>eq</sup> and C<sub>5</sub> conformers in the supersonic expansion. The conformers are stabilized by a C=O···H-N intramolecular hydrogen bond closing a seven- or a five-membered ring, respectively. The observation of both conformers is in good agreement with previous results on the related dipeptides containing different residues, confirming that the polarity/non-polarity of the side chains of the amino acid is responsible for the conformational locking/unlocking. The large isopropyl group is not able to prevent the less stable C<sub>5</sub> conformer from forming, but it destabilizes the C=O···H-N interaction.

Up to date, over 190 molecules have been unambiguously identified in the interstellar medium due to the ongoing astronomical observations complemented with elaborated laboratory studies. Many of these molecules are organic containing abundant interstellar elements H, C, N, and O and are found mainly in the hot cores, i.e., in the regions of prolific star formation with temperatures higher than 100 K through the interpretation of molecular line surveys at millimeter and submillimeter wavelengths. The identification of specific species requires direct comparison of the particular frequencies observed in interstellar space with spectroscopic measurements of known species in a laboratory experiment. The vast amount of data generated by the ALMA motivates laboratory spectroscopists to record and analyze rotational spectra of potential interstellar molecules and to fulfill the first requirement for unequivocal identification of new molecules in space, i.e., the availability of transition frequencies with high accuracy from microwave to sub-millimeter wave range. A general procedure has been introduced combining different time and frequency domain spectroscopic tools of different importance for providing the precise set of spectroscopic constants that could be used to search for this species in the ISM.

The millimeter wave spectrum of **acrylic acid** ( $\text{CH}_2=\text{CH}-\text{COOH}$ ), the simplest unsaturated carboxylic acid, was measured and analyzed from 130 to 360 GHz. Additional measurements from 18 to 26.5 GHz were also made using a waveguide CP-FTMW spectrometer. More than 4000 rotational lines were assigned to *s-cis*- and *s-trans*-acrylic acid in their ground vibrational states leading to the precise determination of rotational, quartic and first complete set of sextic centrifugal distortion constants. New laboratory data of acrylic acid were then used to search for its spectral features in Orion KL, Sgr B2, and W51 molecular clouds. An upper limit to the column density of acrylic acid in Orion KL is provided.

Previous detections of methyl and ethyl formate make other small substituted formates potential candidates for observation in the interstellar medium. Among them, **vinyl formate** is one of the most straightforward unsaturated carboxylic esters. This work aims to provide direct experimental frequencies of the ground vibrational state of vinyl formate in a broad

spectral range for astrophysical use. The room-temperature rotational spectrum of vinyl formate has been measured from 80 to 360 GHz and analyzed in terms of Watson's semirigid rotor Hamiltonian. More than 2.600 transitions were assigned, and a new set of spectroscopic constants was accurately determined. Spectral features of vinyl formate were then searched for in Orion KL, Sgr B2(N), B1-b, and TMC-1 molecular clouds. Upper limits to the column density of vinyl formate are provided.

**Methoxamine** is a potential interstellar amine that has been predicted by gas-grain chemical models for the formation of complex molecules. This work aims to provide direct experimental frequencies of its ground-vibrational state in the millimeter- and submillimeter-wave regions to achieve its detection in the interstellar medium. Methoxamine was chemically liberated from its hydrochloride salt, and its rotational spectrum was recorded at room temperature from 75 to 480 GHz. Many observed transitions revealed A–E splitting caused by the internal rotation of the methyl group, which had to be treated with specific internal rotation codes. Over 400 lines were assigned for the most stable conformer, and a precise set of derived spectroscopic constants was used to search for spectral features of methoxamine in the Orion KL, Sgr B2, B1-b, and TMC-1 molecular clouds. Upper limits to the column density of methoxamine were derived.

The pure rotational spectrum of **N-methyl hydroxylamine** ( $\text{CH}_3\text{NHOH}$ ), a potential candidate in the interstellar medium, has been studied in the millimeter-wave region up to 360 GHz. The molecule was liberated from its hydrochloride salt, and the ground and six lowest excited vibrational states of the most stable trans conformation, as well as the  $^{13}\text{C}$  isotopologue in natural abundance, have been measured and analyzed. From the measured ground state A–E splittings, a barrier hindering the methyl internal rotation  $V_3 = 1245.8$  (46)  $\text{cm}^{-1}$  has been derived. The sub-Doppler Lamb-dip technique has been employed to resolve the  $^{14}\text{N}$  hyperfine structure of intense transitions. The spectroscopic constants reported in the present study constitute a robust set of laboratory data to support future searches of N-methyl hydroxylamine in the interstellar medium.

A detailed analysis of the rotational spectra of the interstellar **iso-propyl cyanide** has been carried out up to 480 GHz using three different high-resolution spectroscopic techniques. Jet-cooled broadband chirped pulse Fourier transform microwave spectroscopy from 6 to 18 GHz allowed us to measure and analyze the ground-state rotational transitions of all singly substituted  $^{13}\text{C}$  and  $^{15}\text{N}$  isotopic species in their natural abundances. The monohydrate of isopropyl cyanide, in which the water molecule bounds through a stronger  $\text{O}-\text{H}\cdots\text{N}$  and weaker bifurcated  $(\text{C}-\text{H})_2\cdots\text{O}$  hydrogen bonds in a Cs configuration, has also been detected in the supersonic expansion. Stark-modulation spectroscopy in the microwave and millimeter wave range from 18 to 75 GHz allowed us to analyze the vibrational satellite pattern arising from pure rotational transitions in the low-lying vibrational excited states. Finally, assignments and measurements were extended through the millimeter and submillimeter wave region. The room temperature rotational spectra made possible the assignment and analysis of pure rotational transitions in 19 vibrationally excited states. Significant perturbations were found above 100 GHz in most of the observed excited states. Due to the complexity of the interactions and importance of this astrophysical region for future radio astronomic detection, both a graphical plot approach and a coupled fit have been used to assign and measure almost 10,000 new lines.

The number of unidentified lines in the millimeter and submillimeter wave surveys of the interstellar medium has overgrown. The significant contributions are due to rotational transitions in excited vibrational states of relatively few molecules that are called the “astrophysical weeds.” The assignments and analyses of rotational spectra in the low-lying vibrational states of not yet identified astrophysical species are needed to address this problem. The necessary data to deal with spectral lines from astrophysical weeds species can be obtained from detailed laboratory rotational measurements in the microwave and millimeter wave region. One of the interstellar molecules to be considered is **aminoacetonitrile**, which has received attention due to its implication in the chemical synthesis of the smallest amino acid, glycine. We report a detailed spectroscopic investigation of the interstellar aminoacetonitrile, a possible precursor molecule of glycine.

Using a combination of Stark and frequency-modulation microwave and millimeter wave spectroscopies, we observed and analyzed the room-temperature rotational spectra of 29 excited states with energies up to  $1000\text{ cm}^{-1}$ . We also observed the  $^{13}\text{C}$  isotopologues in the natural abundance. The extensive data set of more than 2000 new rotational transitions will support further identifications of amino acetonitrile in the interstellar medium.

The detection of glycine in the interstellar medium (ISM) is one of the most pursued targets for the researchers in the astrochemistry and astrophysics. The famous Strecker reaction which remains the most often proposed synthesis of glycine in the interstellar medium ISM, include the participation the precursors of aminoacetonitrile and glycinamide that also are candidates to be present in the ISM. Hence, in 2008, aminoacetonitrile was discovered in SgrB2 by the rotational spectroscopy data. Thus, if the hydrolysis of aminoacetonitrile occurs in the gas phase or the grains of the ISM, **glycinamide** should also be present in the interstellar medium. The microwave spectrum of glycinamide successfully liberated in the gas phase by laser ablation of its hydrochloride salt, is now first reported. The experimental constants are of significant importance for possible future identifications of glycinamide precursor in the ISM.

Laser ablation techniques coupled with broadband and narrowband Fourier transform microwave spectroscopies have allowed the high-resolution rotational study of solid **hydantoin**, an essential target in astrochemistry as a possible precursor of glycine. The complicated hyperfine structure arising from the presence of two  $^{14}\text{N}$  nuclei in non-equivalent positions has been resolved and interpreted regarding the nuclear quadrupole coupling interactions. The results reported in this work provide a solid base for the interstellar searches of hydantoin in the astrophysical surveys. The values of the nuclear quadrupole coupling constants have also been discussed in terms of the electronic environment around the respective nitrogen atom.





# INTRODUCCIÓN

---



## 1. ANTECEDENTES

---

La presente tesis doctoral se ha realizado en los Laboratorios de Espectroscopia y Bioespectroscopia del Grupo de Espectroscopia Molecular (GEM) de la Universidad de Valladolid, Unidad Asociada del CSIC, ubicados en el Edificio Quifima del Parque Científico y en el marco del proyecto del Plan Nacional **CTQ2013-40717-P: Biomoléculas y moléculas del medio interestelar: estructura, interacciones y caracterización espectroscópica**, del que soy becaria FPI. Éste tiene en la actualidad continuidad con el **CTQ2016-76393-P: Biomoléculas y moléculas del medio interestelar: Relaciones Estructura-Propiedad, Quiralidad y Caracterización Espectroscópica**, así como en el proyecto concedido por la Junta de Castilla y León (**VA077U16: Relación estructura-propiedad en edulcorantes**), en los que se viene igualmente desarrollado mi temática de investigación. Al amparo de estos proyectos, se ha desarrollado y construido en nuestros laboratorios una nueva instrumentación que combina la ablación láser, expansiones supersónicas y técnicas de microondas en el dominio del tiempo, conocidas por los acrónimos LA-MB-FTMW (Laser Ablation Molecular Beam Fourier Transform Microwave) y LA-CP-FTMW (Laser Ablation Chirped Pulse Fourier Transform Microwave) que están haciendo posible los primeros estudios estructurales de biomoléculas en condiciones de práctico aislamiento en fase gas. Con estas técnicas, se está superando el grave inconveniente de la vaporización de sólidos de biomoléculas, evitando los procedimientos clásicos de calentamiento que causan su descomposición. En el periodo de mi tesis, me he implicado en nuevos experimentos con estas técnicas de alta resolución pudiendo extraer de los espectros de rotación los parámetros espectroscópicos que conducen a revelar sus estructuras más estables así como a desvelar las interacciones intramoleculares que las estabilizan. En algunos casos ha sido posible establecer las relaciones existentes entre la estructura y ciertas propiedades relevantes como la del dulzor.

Igualmente, y en total sinergia con Grupo de Astrofísica Molecular del ICMM (CSIC, Madrid), se están abordado estudios espectroscópicos de posibles moléculas del medio

interestelar (ISM) en los que estoy participando. Nuestras medidas de laboratorio, resultantes de los estudios espectroscópicos en las regiones milimétrica y submilimétrica del espectro electromagnético, sobre posibles moléculas candidatas, son directamente comparadas con las emisiones captadas por los diferentes observatorios de ALMA (Atacama Large Millimeter Array, Chile) e IRAM (Granada) procedentes de diversas regiones del ISM (Sagitario y Orion principalmente). Ello hace posible la identificación inequívoca de una nueva especie química en el ISM. Estos resultados son de gran importancia en el modelado del universo y en las investigaciones sobre el origen de la vida. Con la participación de nuestra Unidad Asociada CSIC en el proyecto **Consolider-Ingenio MINECO CSD2009-00038 (ASTROMOL)** y en la actualidad en el proyecto europeo **(FP/2007-2013) / ERC-SyG-2013 Grant Agreement n. 610256 NANOCOSMOS**, se han construido en el GEM nuevas configuraciones instrumentales en estas regiones de altas frecuencias que han facilitado el descubrimiento de nuevas especies del ISM.

El contenido de la presente Memoria, desarrollado en el contexto de los proyectos aquí mencionados, debe entenderse en dos grandes vertientes. Una primera centrada en el estudio estructural de moléculas y biomoléculas, en el que abordan importantes aspectos de las relaciones estructura-propiedad y efecto *exo*-anómero, entre otros. Una segunda, dedicada al estudio de moléculas prebióticas y precursores de aminoácidos susceptibles de poder ser detectadas en el ISM. Un resumen de los resultados obtenidos se aborda en las siguientes secciones.

## 2. MOLECULAS Y BIOMOLECULAS EN FASE GAS.

---

Nuestra aproximación químico-física al estudio de sistemas biológicos es reduccionista; pasa por caracterizar el comportamiento de sus constituyentes más elementales denominados *building blocks* a escala molecular, con la intención de enlazar sus comportamientos y predecir el mismo a escala macroscópica, considerando al sistema como un todo. Esta aproximación es radicalmente opuesta a la que habitualmente se realiza en los campos de la Biología y Bioquímica que consideran a los sistemas como un todo, tratando de explicar la maquinaria de su funcionamiento a través de datos macroscópicos procedentes de metodologías clásicas. Esta aproximación conlleva un alto grado de especulación al carecer del necesario soporte experimental a nivel molecular.

El medio natural en el que se desenvuelven las biomoléculas son las fases condensadas, donde su comportamiento está condicionado, no sólo por sus interacciones intramoleculares siempre presentes, sino también por las interacciones intermoleculares con el medio. Así, los estudios espectroscópicos al uso (IR, Raman, NMR...etc) que se realizan en fases condensadas, no aportan datos sobre la molécula como ente aislado, y no dan información sobre las propiedades intrínsecas de estos sistemas. Simplemente decir que, para entender el comportamiento estructural y funcional en su medio natural, es obligado analizar y racionalizar su comportamiento estructural en ausencia de interacciones intermoleculares, es decir, en las condiciones de aislamiento que brinda la fase gas. Con esta información en fase gas, y con el estudio de los pertinentes complejos intermoleculares también en fase gas, podemos establecer un primer nexo con su posible comportamiento en los medios biológicos. Además, las diferentes estructuras tridimensionales obtenidas en condiciones de aislamiento en fase gas, ayudan a establecer con menor ambigüedad posibles relaciones estructura-propiedad.

Las condiciones que brinda una expansión supersónica<sup>1,2</sup> son las idóneas para llevar a cabo este tipo de estudios en fase gas, siendo el entorno experimental deseable en los

experimentos químico-físicos y espectroscópicos. El enfriamiento adiabático de moléculas en el jet supersónico aumenta, en general, la población de los niveles más bajos de energía incrementando la intensidad de las transiciones y simplificando los espectros, particularmente los de rotación. Así, la espectroscopia de microondas en el dominio del tiempo con transformada de Fourier acoplada a un jet supersónico y conocida con el acrónimo MB-FTMW<sup>3,4</sup> (Molecular-Beam Fourier Transform Microwave Spectroscopy) se ha confirmado como la técnica espectroscópica de mayor potencial en la investigación estructural en fase gas.

Conjuga las ventajas de la espectroscopia en el dominio del tiempo (elevada sensibilidad y resolución) con las propias de la expansión supersónica (entorno libre de colisiones e interacciones, enfriamiento ro-vibracional, etc.). Resulta idónea para la determinación de estructuras moleculares ya que su sensibilidad posibilita la caracterización de especies isotópicas en abundancia natural, así como la generación y caracterización en la expansión supersónica de especies inestables con interacciones intermoleculares de diferente naturaleza y entidad (complejos de van der Waals y con enlace de hidrógeno). Con la construcción del primer espectrómetro MB-FTMW<sup>5</sup> en España, el Grupo de Espectroscopia Molecular (GEM) de la Universidad de Valladolid inició su andadura con las primeras caracterizaciones de enlaces de hidrógeno axial y ecuatorial<sup>6,7,8,9,10</sup> y la generación y caracterización estructural de un gran número de complejos intermoleculares (ver por ejemplo).<sup>11,12,13,14,15</sup> El estudio de interacciones débiles con enlace de hidrógeno con el grupo dador es el C-H, responsables de las estructuras terciaria y cuaternaria de las proteínas, fue igualmente motivo de interesantes aportaciones (ver por ejemplo<sup>16,17,18,19</sup>).

Sin embargo, toda la potencialidad esta técnica no resulta aplicable a un gran número de sólidos orgánicos con elevados puntos de fusión y baja volatilidad, como son las biomoléculas. Su labilidad térmica hace inviable su vaporización con los métodos clásicos de calentamiento sin producir la descomposición térmica. Importantes *building blocks* como aminoácidos, bases nitrogenadas, péptidos, neurotransmisores y azúcares,

resultaban inaccesibles a estos estudios de alta resolución en fase gas. La aplicación de un pulso láser intenso y focalizado produce la vaporización instantánea de un sólido orgánico y constituye una alternativa a los métodos clásicos de calentamiento. La ablación láser introducida, entre otros, por el premio Nobel Smalley,<sup>20</sup> es habitual en técnicas como MALDI y espectrometría de masas.<sup>21,22</sup> Su implementación en la espectroscopia de rotación no resulta tan evidente. En este contexto, nuestro grupo de investigación ha venido investigando exitosamente durante más de una década dispositivos de ablación láser acoplados a la técnica MB-FTMW en expansiones supersónicas<sup>23</sup> dando lugar a una nueva técnica desarrollada en nuestro laboratorio denominada LA-MB-FTMW (Laser Ablation Molecular-Beam Fourier Transform Microwave Spectroscopy).<sup>24</sup> Más recientemente, nuevos dispositivos de ablación láser han sido acoplados a las nuevas técnicas de banda ancha CP-FTMW (Chirp Pulsed Fourier Transform Microwave)<sup>25</sup> que agilizan enormemente las labores de asignación e interpretación de los espectros.<sup>26</sup> El tandem de técnicas LA-MB-FTMW y LA-CP-FTMW, descritas en la Metodología Experimental (pág. 49), ha hecho posible el estudio a escala molecular de sistemas biológicos en condiciones de práctico aislamiento en fase gas, y a un nivel de detalle impensables hasta el presente. Simplemente mencionar los resultados obtenidos en estos últimos años en aminoácidos naturales (ej.: tirosina,<sup>27</sup> triptófano,<sup>28</sup> histidina<sup>29</sup>), dipéptidos naturales más simples (ej.: Ac-Pro-NH<sub>2</sub>,<sup>30</sup> Ac-Ser-NH<sub>2</sub>,<sup>31</sup> gly-gly<sup>32</sup>), aminoalcoholes (ej.: fenilglicinol<sup>33</sup>), nucleósidos (ej.: uridina<sup>34</sup>), carbohidratos (ej.:  $\alpha$  y  $\beta$ -D-glucosa,<sup>35</sup>  $\alpha$ -D-Galactosa,<sup>36</sup> desoxiribosa,<sup>37</sup> eritrosa,<sup>38</sup> xilosa,<sup>39</sup> D-glucosamina,<sup>40</sup> D-fructosa<sup>41</sup>), neurotransmisores (dopamina,<sup>42</sup> norefredina,<sup>43</sup> etc. ), fármacos (aspirina,<sup>44</sup> vitamina C<sup>45</sup>).

Los resultados y conclusiones obtenidos en estos últimos trabajos, han motivado nuevas problemáticas que se han abordado por primera vez en el desarrollo de mi tesis doctoctoral. Algunas de ellas abren nuevas líneas de investigación. En los siguientes apartados se hace un resumen de las mismas, junto con los resultados obtenidos más significativos

## 2.1. EFECTO *EXO-ANOMÉRICO*: Evidencias estructurales.

El efecto anomérico es un efecto estereoelectrónico que describe la tendencia que, en carbohidratos, se manifiesta por la tendencia que los tienen sustituyentes polares adyacentes al heteroátomo del anillo a la posición axial frente a la ecuatorial en principio más estable.<sup>46,47,48</sup> Este efecto se racionaliza habitualmente con la teoría de orbitales moleculares. La interacción hiperconjugativa  $n \rightarrow \sigma^*$  entre el par no enlazante ( $n$ ) de electrones en el orbital molecular del O<sub>5</sub> del anillo (ver Fig. 1) y un orbital molecular vacío anti-enlazante ( $\sigma^*$ ) del enlace C<sub>1</sub>-O<sub>1</sub> del centro anomérico del acetal axial está favorecida por la disposición antiperiplana. Esta preferencia por la posición axial se ha constatado en los estudios experimentales de la  $\alpha$ -D-glucosa,<sup>35</sup>  $\alpha$ -D-Galactosa<sup>36</sup> y D-xilosa<sup>39</sup> que adoptan, en todos los casos, una configuración del anillo <sup>4</sup>C<sub>1</sub> favorecida por el efecto *endo*-anomérico (anomérico).

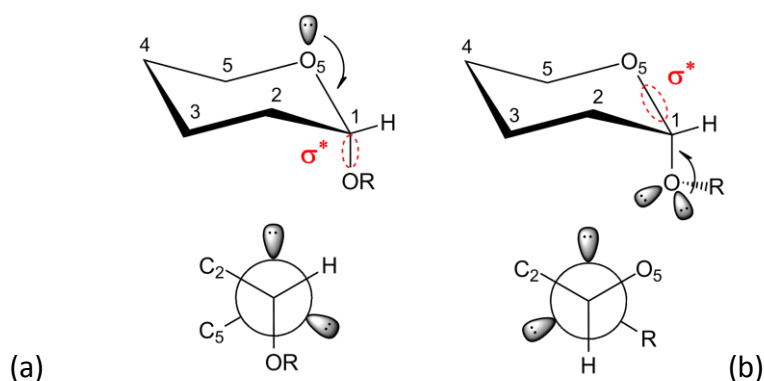


**Figura 1.** (a) Acetal axial mostrando el efecto *endo*-anomérico que estabiliza el anómero axial. (b) disposición antiperiplana del par no enlazante del grupo alcoxi *exo*-cíclico respecto al orbital  $\sigma^*$  del enlace C<sub>1</sub>-O<sub>5</sub> en el efecto *exo*-anomérico.

Como se muestra en la Fig. 1b, si el aglicón (grupo alcoxi -OR) adopta la orientación espacial adecuada, cabe también la interacción del par ( $n$ ) no enlazante del alcoxi con el orbital molecular desocupado  $\sigma^*$  del enlace C<sub>1</sub>-O<sub>5</sub> en una disposición igualmente antiperiplana. Aunque no hay diferencias conceptuales entre ambos, se reserva el término *exo*-anomérico para este último. El efecto *endo*-anomérico estabiliza la configuración axial



del sustituyente polar en el que a su vez tiene lugar el efecto *exo*-anomérico; sus efectos quedan enmascarados por los propios del *endo*-anomérico dominante. Mientras que son numerosas las pruebas y manifestaciones experimentales del efecto anomérico, son nulas las existentes para *exo*-anomérico a pesar de su papel relevante en las uniones o-glicosídicas.

La investigación iniciada sobre el efecto *exo*-anomérico ha considerado la molécula del metil  $\beta$ -D-xilopiranos (Fig.2) como arquetipo; la posición ecuatorial del aglicón únicamente posibilita el efecto *exo*-anomérico. Su sólido se vaporiza mediante ablación láser, las moléculas vaporizadas se siembran en gas Ne y se expanden adiabáticamente.

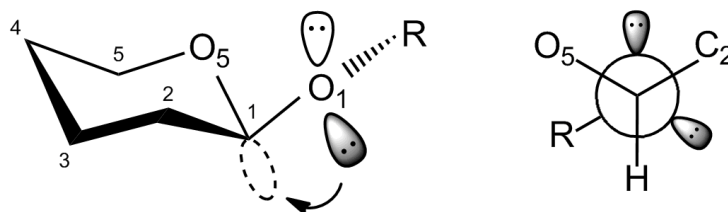


**Figura 2.** Acetal ecuatorial que muestra el efecto *exo*-anomérico por la configuración antiperiplana que estabiliza el anómero axial. Al lado se presenta la proyección de Newman a lo largo del enlace  $C_1-O_1$ .

Su espectro de rotación en el dominio del tiempo de banda ancha se obtiene mediante la técnica de CP-FTMW. El único rotámero detectado en la expansión corresponde al conformero  $cc\text{-}\beta\text{-}^4C_1$  g- con una orientación del aglicón que maximiza el efecto *exo*-anomérico.<sup>49</sup>

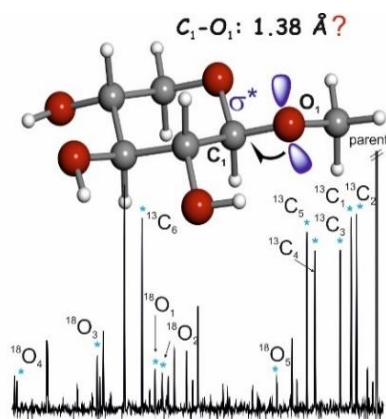


**Figure 3.** Fragmento de espectro donde se observa una transición parent y las correspondientes a los isotopólogos monosustituídos. Esquema de la molécula de la metilxilopiranos con la interacción entre orbitales debido al efecto *exo*-anomérico.

La gran sensibilidad lograda en el experimento ha hecho posible la caracterización de todas las especies isotópicas de  $^{13}\text{C}$  y  $^{18}\text{O}$  (ver Fig.3) en su abundancia natural (1% y 0,4% respectivamente) y determinar con gran precisión la estructura molecular (distancias y ángulos de enlace) con gran precisión. La distancia obtenida para el enlace glucosídico  $\text{C}_1\text{-O}_1$  de 1.38 Å es notablemente inferior a los valores típicos en el rango 1.42-1.44 Å.<sup>50,51</sup> Este acortamiento del enlace solo puede explicarse en base a los efectos hiperconjugativos derivados del efecto *exo*-anomérico. Estos resultados han abierto una nueva línea de investigación sobre la unión glucosídica en la que el efecto *exo*-anomérico juega un papel relevante.

## 2.2. EDULCORANTES ARTIFICIALES: Relaciones estructura-dulzor

El uso de los edulcorantes artificiales se extiende cada día más en nuestra cadena alimenticia debido, fundamentalmente, a su bajo aporte calórico. El dulzor es una propiedad que poseen compuestos con muy distinta funcionalidad. Desde inicios del pasado siglo, han sido numerosos los estudios encaminados a esclarecer la relación entre la propiedad del dulzor y la estructura de los compuestos dulces.<sup>52,53,54</sup> Ninguno de ellos condujo a una explicación unificada hasta que, en la década de los sesenta, Shallenberger y Acree<sup>55,56</sup> propusieron su teoría molecular del dulzor. Ésta atribuye el dulzor a la presencia de pares de grupos funcionales, uno actuando como dador de protones (AH) y el otro como aceptor (B), formando lo que se denomina glucóforo (ver Fig.4) que interacciona mediante enlaces de hidrógeno con dos grupos funcionales análogos de los receptores de nuestro paladar. Los átomos A y B del glucóforo son átomos electronegativos que, según Shallenberger deben estar separados entre 2.5 y 4 Å. Una tercera zona de interacción hidrófoba o de Van der Waals ( $\gamma$ -site), capaz en principio de realzar el dulzor, fue posteriormente propuesta por Iker formando lo que se conoce como triángulo del dulzor (A-H,B,  $\gamma$ ).<sup>57,58,59</sup> Nuevos modelos y teorías sobre el dulzor han sido más recientemente desarrolladas,<sup>60,61</sup> pero todas ellas confluyen en el rasgo estructural común del glucóforo.

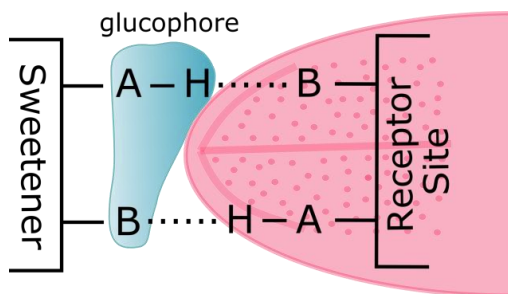


**Figura 4.** Esquema de la estructura del glucóforo y su interacción con el receptor.

Cuando estas teorías fueron formuladas, la información estructural sobre edulcorantes estaba restringida a fases condensadas. No se conocía la estructura tridimensional de los edulcorantes que posibilitara la identificación de rasgos estructurales relacionados con glucóforos. Así, muchos de los edulcorantes eran descubiertos accidentalmente.<sup>62</sup> Nuestras técnicas espectroscópicas de microondas hacen posible hoy día la identificación inequívoca de las estructuras más estables de los sólidos de edulcorantes, en las condiciones de aislamiento de la expansión supersónica. Un primer estudio de edulcorantes naturales de cetohexosas<sup>63,64</sup> ha evidenciado la repercusión de nuestras técnicas en esta importante temática.

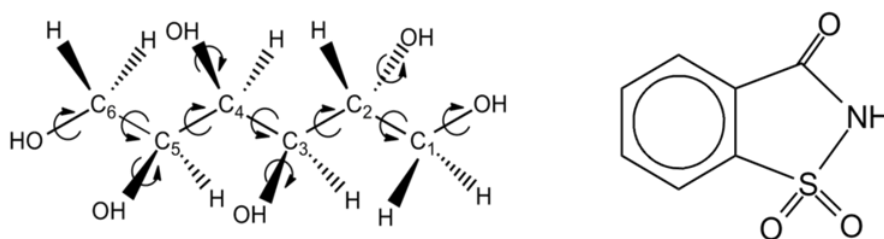


**Figura 5.** Esquemas de los edulcorantes del D-sorbitol (2S,3R,4R,5R)-hexane-1,2,3,4,5,6 hexol y sacarina (1,1-dioxo-1,2-benzothiazol-3-one) con funcionalidades muy distintas.

En esta investigación se ha abordado el estudio de los edulcorantes artificiales del sorbitol y sacarina (Fig.5), con funcionalidades tan distintas, que nos ayuden a racionalizar las posibles relaciones estructura-propiedad. El complejo entramado de enlaces de hidrógeno intramoleculares que se produce en la familia de polialcoholes ( $C_6H_{14}O_6$ ) a la que pertenece el sorbitol, manitol y dulcitol entre otros, está aún por esclarecer. Dentro del

elevado número de confórmeros que potencialmente pueden formarse en estas cadenas alicíclicas cabe esperar que, en algunos de ellos, existan rasgos estructurales comunes atribuibles a glucóforos pudiendo así justificarse el dulzor de estos compuestos. En el Capítulo II de esta Memoria se recoge el estudio del D-sorbitol, primer polyalcohol estudiado en fase gas, elegido como arquetipo del comportamiento de los denominados como “*sugar alcohols*”. Las tres estructuras detectadas<sup>65</sup> (ver Fig.6) se sobreestabilizan por un entramado de cinco enlaces de hidrógeno cooperativos. Todas ellas comparten la interacción  $O_1H \cdots O_2$  que cumple con los requisitos del glucóforo: el grupo  $O_1H$  actúa como donante de protón (AH) y el  $O_2$  como aceptor (B) de la propuesta de Shallenberger. Se han acometido igualmente los estudios del D-dulcitol y D-manitol y los primeros resultados apuntan a la existencia de “*sweet structures*” semejantes a las detectadas en el D-Sorbitol.

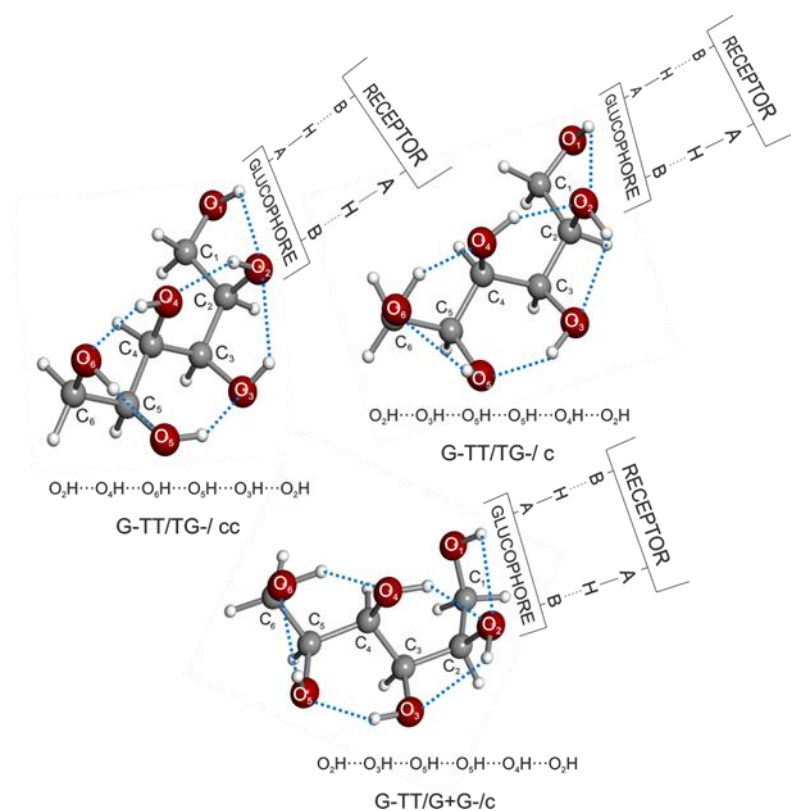


**Figura 6.** Los tres confórmeros detectados en el D-sorbitol en los que se significa el entramado de cinco enlaces de hidrógeno intramoleculares y la existencia del *glucophore* común en todos ellos.

Sobre el primer edulcorante descubierto en 1878, la sacarina, no existían estudios en fase gas. La presencia de un cromóforo favorece siempre la fotofragmentación limitando la eficacia de la vaporización láser.<sup>66</sup> El experimento ha resultado finalmente viable y el análisis del espectro de rotación ha permitido establecer la simetría  $C_s$  de la sacarina e identificar el glucóforo: NH (AH) grupo donante y O (B) de la sulfona como receptor (ver Fig.7). Todos los detalles del estudio de la Sacarina se recogen en el capítulo III.

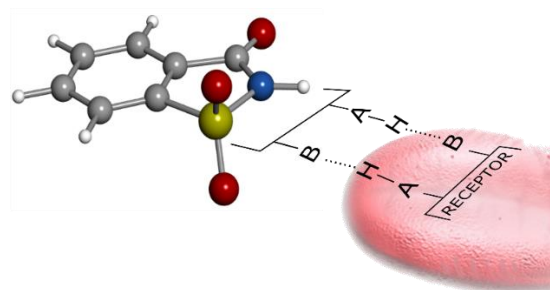


**Figura 7.** La sacarina su esquema de interacción glucóforo-receptor

### 2.3. ÁCIDOS FENÓLICOS: Panorama conformacional.

Los ácidos fenólicos son compuestos bioactivos<sup>67</sup> que se encuentran presentes en frutas, verduras, plantas medicinales y aromáticas entre otros, y además de tener un papel vital en la industria farmacéutica<sup>68,69</sup> poseen propiedades antioxidantes<sup>70</sup> y anticancerígenas,<sup>71,72</sup> entre otras.<sup>73,74,75,76,77</sup> Sin embargo, no existen datos estructurales de estos sistemas, importantes para desvelar sus mecanismos de actuación. Los ácidos trans-cinámico y p-cumárico son dos de los ácidos fenólicos más importantes y representativos de la familia de ácidos fenólicos. El ácido trans-cinámico (tCA) es el más simple. Tiene dos posibles configuraciones, s-cis y s-trans (fig.8) debido según la disposición del grupo carboxilo. El ácido trans-p-cumárico (tpCA) deriva del cinámico añadiendo un grupo OH en la posición para en el anillo fenólico. Así, cada configuración s-cis o s-trans del tCA origina dos configuraciones syn(s) o anti(a) dependiendo de la posición del grupo OH. Se trata de compuestos sólidos con puntos de fusión elevados (133°C y 213°C para el tCA y tpCA respectivamente) que ha imposibilitado hasta el presente su estudio en fase gas

(descomponen por calentamiento) por lo que su panorama conformacional no está constatado. Haciendo uso de nuestras técnicas de vaporización por ablación láser acopladas a técnicas de microondas con transformadas de Fourier, se ha logrado obtener por primera vez los espectros de rotación. Dado su elevado tamaño molecular, la experimentación se ha realizado en la región de baja frecuencia, entre 2 y 8 GHz, utilizándose una nueva configuración de nuestra instrumentación LA-CP-FTMW.

Los datos espectroscópicos obtenidos, son directamente comparables con aquellos predichos teóricamente, constituyendo una herramienta única para discriminación e identificación los conformeros en la expansión supersónica. Dos han sido los conformeros detectados para el tCA (s-cis y s-trans) y cuatro para el tpCA (s-cis-a, s-cis-s, s-trans-a, s-trans-s) estableciéndose su planariedad en todos los casos.<sup>78</sup> La investigación se detalla en el capítulo IV.

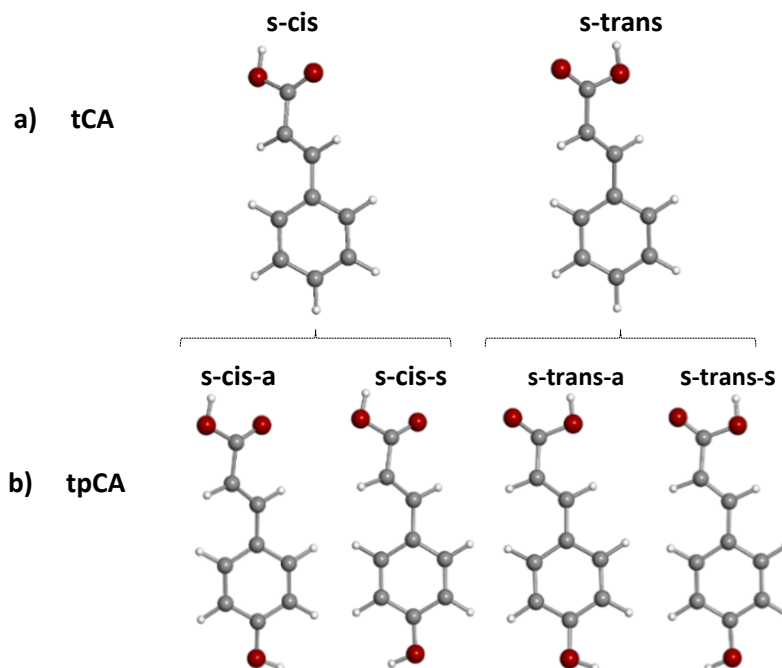


**Figura 8.** a) Configuraciones s-cis y s-trans del ácido trans-cinámico. b) Configuraciones del trans-p-cumárico generadas con disposiciones anti (a) o syn (s) del grupo hidroxilo.

## 2.4. DIPEPTIDOS: El papel de la cadena lateral.

Las proteínas son las moléculas más versátiles en los sistemas vivos que realizan funciones relevantes en los procesos biológicos, existiendo una relación directa entre su estructura y una determinada propiedad funcional.<sup>79,80,81</sup> Para entender la estructura de una proteína, es necesario conocer el comportamiento de sus eslabones que las constituyen, es decir, de los *building blocks* de aminoácidos y dipéptidos, desvelando las interacciones intramoleculares que estabilizan sus estructuras. Los experimentos en fase gas, en el seno de una expansión supersónica, resultan idóneos ya que se evitan todas las interacciones intermoleculares que inevitablemente ocurren en las fases condensadas.<sup>82,83</sup> Una de las temáticas importantes de nuestro grupo de investigación, ligada a nuestro estudio de aminoácidos,<sup>23</sup> es el estudio de dipéptidos como unidades elementales de las cadenas peptídicas. La gran labilidad de estos compuestos dificulta su vaporización y su estudio estructural en fase gas. Hasta 2017 no fue posible el estudio del dipéptido más simple de la Glicilglicina (Gly-Gly)<sup>84</sup> gracias a las últimas mejoras de nuestra instrumentación.

En principio, las terminaciones amino (*N-terminal*) y carboxílica (*C-terminal*) de los dipéptidos naturales pueden originar interacciones que no existen en las cadenas peptídicas. Si pretendemos mimetizar su comportamiento en las cadenas peptídicas se recurre a sustituir uno de los H del NH<sub>2</sub> por el grupo acetil Ac (CH<sub>3</sub>-C=O) y el grupo carboxílico por el grupo amida (CO-NH<sub>2</sub>) formando dipéptidos protegidos (*capped peptides*).<sup>68</sup> Nuestros primeros estudios en los prototipos de la Ac-Ala-NH<sub>2</sub><sup>85</sup> y N-acetilglicinamida (Ac-Gly-NH<sub>2</sub>)<sup>86</sup> desvelaron la existencia de las dos configuraciones C<sub>7</sub><sup>eq</sup> y C<sub>5</sub> de la Fig.9, estabilizadas por enlaces de hidrógeno O⋯H-N intramoleculares cerrando ciclos de siete y cinco miembros respectivamente. En el dipéptido de la prolina Ac-Pro-NH<sub>2</sub> la presencia del anillo restringe la flexibilidad de la cadena y únicamente la configuración C<sub>7</sub><sup>eq</sup> se observa experimentalmente.<sup>87</sup> El análisis de la estructura hiperfina de cuadrupolo nuclear de <sup>14</sup>N hizo posible una estimación de los ángulos de Ramachandran.<sup>88</sup>

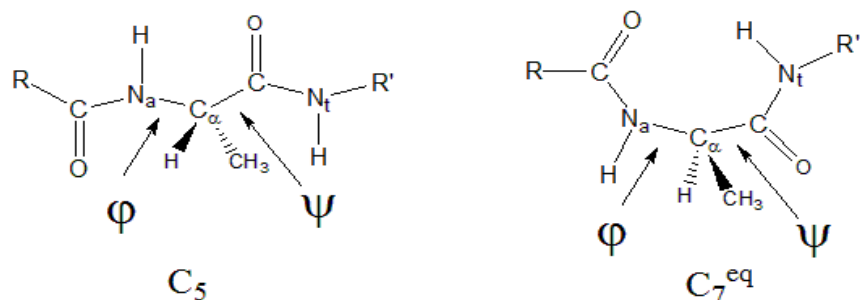


**Figure 9.** Esquemas de las configuraciones  $C_5$  y  $C_7^{eq}$  para los péptidos terminados de fórmula  $RCO-Ala-NHR'$  con  $R, R' = Me / H$ .  $\phi$   $[C(O)-N_a-C_\alpha-C(O)]$  y  $\psi$   $[N_a-C_\alpha-C(O)-N_t]$  son los ángulos de Ramachandran.

Partiendo de estas dos configuraciones arquetipo  $C_7^{eq}$  y  $C_5$  presentes en los dipéptidos más simples, el efecto que una cadena lateral polar ha sido recientemente analizado en el dipéptido *N*-acetyl-L-serinamide ( $Ac-Ser-NH_2$ ).<sup>89</sup> La configuración  $C_7^{eq}$  sobre estabilizada por dos nuevas interacciones intramoleculares  $NH\cdots OH$  y  $OH\cdots O=C$  (ver Fig. 10) que surgen de la presencia de la cadena lateral polar ( $-CH_2OH$ ) de la serina, ha resultado ser la dominante y única detectada en el jet supersónico. Las cadenas polares de los residuos de aminoácidos afectan al equilibrio  $C_7^{eq}/C_5$  de los dipéptidos.

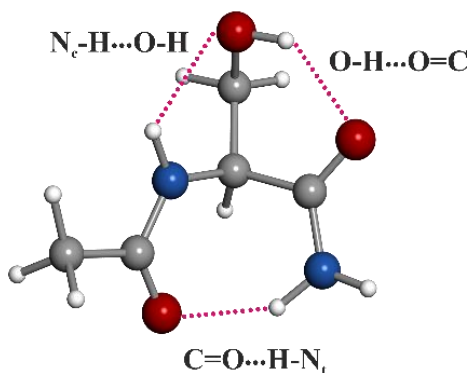


**Figura 10.** El conformero  $C_7^{eq}$  observado en el dipéptido  $Ac-Ser-NH_2$  en el que se significan, aparte de la interacción  $C=O\cdots HN$ , las interacciones extras  $NH\cdots OH$  y  $OH\cdots O=C$  originadas por la cadena polar de la serina.



Cabe ahora preguntarse, ¿cómo afectarán los efectos estéricos de una cadena lateral apolar voluminosa? Para responder a esta cuestión se ha realizado el estudio del dipéptido de la Ac-Val-NH<sub>2</sub><sup>90</sup> con la cadena lateral isopropilo (-CH(CH<sub>3</sub>)<sub>2</sub>), lo suficientemente voluminosa para poner en evidencia los efectos estéricos. Adelantar que los dos conforméres de la Fig. 11 correspondientes a las configuraciones C<sub>7</sub><sup>eq</sup> y C<sub>5</sub> han sido inequívocamente identificados en el estudio espectroscópico del capítulo V. Todo parece indicar, que los efectos estéricos no parecen afectar significativamente al equilibrio C<sub>7</sub><sup>eq</sup>/C<sub>5</sub> de los dipéptidos.

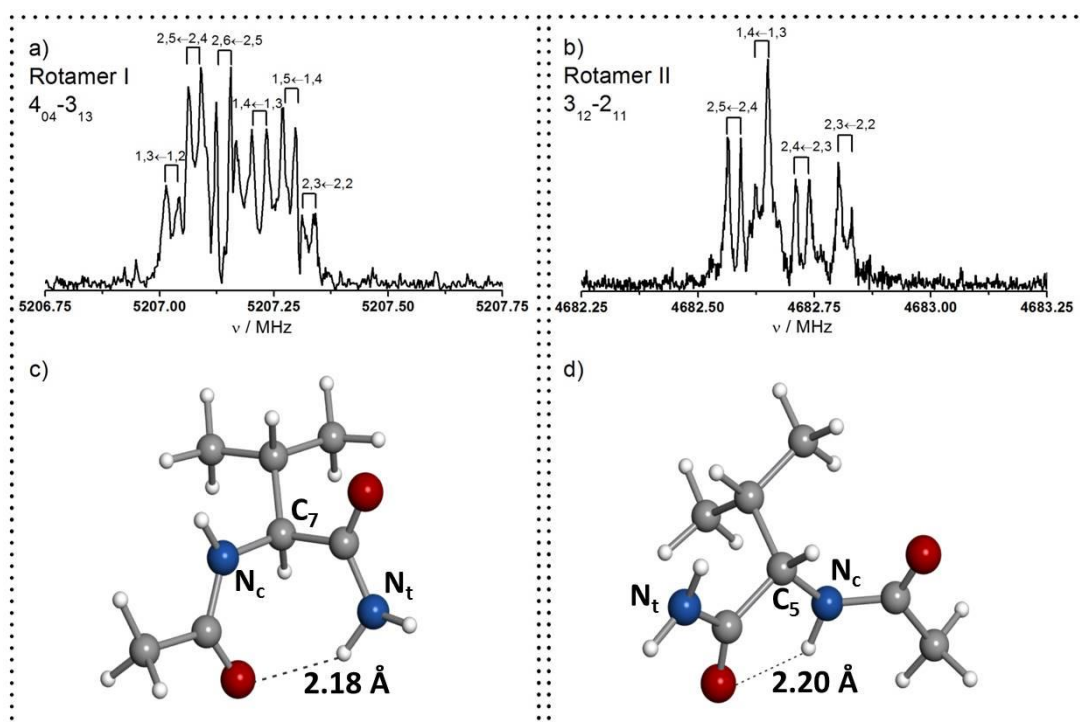


**Figura 3.** Los conforméres C<sub>7</sub><sup>eq</sup> y C<sub>5</sub> observados en el dipéptido de la Ac-Val-NH<sub>2</sub> mostrando la compleja estructura hiperfina de cuadrupolo nuclear de las transiciones.

Toda esta información, obtenida en los eslabones (dipéptidos), resulta de gran relevancia y pueden ponerse en su debido contexto con los datos recopilados por Mons et al.<sup>91</sup>

### 3. ASTROFISICA MOLECULAR: MOLÉCULAS DEL MEDIO INTERESTELAR (ISM).

---

El medio interestelar contiene materia que está concentrada en regiones frías conocidas como nubes interestelares. Estas nubes están compuestas de gas y pequeños granos de partículas, siendo la especie dominante el hidrógeno, ya sea en su forma atómica o molecular. La mayoría de esta materia ha sido eyectada por estrellas viejas o moribundas, y las nubes interestelares más densas normalmente se las asocia con la formación de nuevas estrellas<sup>92</sup> y, por tanto, en la formación de sistemas planetarios como el nuestro. Conocer las moléculas que están presentes en el medio interestelar nos ayuda a entender la formación y evolución de nuestro sistema planetario y, por ende, el origen de la vida.<sup>93,94,95</sup>

Hasta no hace muchos años, estaba extendida la idea de que las condiciones extremas del medio interestelar ISM eran del todo hostiles para la formación de especies orgánicas. Sin embargo, la detección de más de 190 moléculas identificadas en el medio interestelar (ISM) en las últimas décadas ha contribuido a desterrar definitivamente esa idea. Hasta el presente, en base a las observaciones de la radioastronomía en sinergia con los datos espectroscópicos obtenidos en los laboratorios. La identificación de una nueva especie en el ISM requiere una comparación directa de las frecuencias de emisión de los observatorios procedentes del ISM con las medidas espectroscópicas realizadas en laboratorio en las regiones milimétrica y submilimétrica<sup>96,97,98</sup> del espectro electromagnético sobre especies conocidas. La resolución sin precedentes de las nuevas observaciones de ALMA (Atacama Large Millimeter/submillimeter Array) combinada con datos espectroscópicos de laboratorio en alta resolución ofrece una oportunidad única para explorar la complejidad molecular del ISM. Todo ello supone un continuo reto a los experimentos de laboratorio para la generación de nuevos datos espectroscópicos tanto de moléculas estables ya conocidas como de nuevas especies inestables susceptibles de generarse en las condiciones del medio interestelar.<sup>99</sup>

En los últimos años, el GEM viene adaptando y desarrollando nueva instrumentación para la realización de experimentos en las regiones centimétrica, milimétrica y submilimétrica del espectro electromagnético.<sup>100,101,102,103</sup> En el marco de los proyectos Consolider y Nanocosmos se han realizado las primeras identificaciones del etil mercaptano  $\text{CH}_3\text{CH}_2\text{SH}$ <sup>104</sup> y  $\text{HMgNC}$ <sup>105</sup> en el ISM, a las que se han unido la más recientes del etil metil éter  $\text{CH}_3\text{CH}_2\text{OCH}_3$ <sup>106</sup> y metilisocianato  $\text{CH}_3\text{NCO}$ .<sup>107</sup> Esta última es de particular relevancia ya que es una de las moléculas más abundantes en el ISM, detectada recientemente en el cometa 67P/Churyumov-Gerasimenko<sup>108</sup> y en el experimento COSAC (Cometary Sampling and Composition) a bordo de la plataforma Rosetta. En todas estas identificaciones se han utilizado datos espectroscópicos de nuestro laboratorio. Igualmente se han analizado los espectros del fenol  $\text{C}_6\text{H}_5\text{OH}$ ,<sup>109</sup> acroleína  $\text{CH}_2\text{CHCHO}$ <sup>110</sup> y metil vinil éter  $\text{CH}_2\text{CH}_2\text{OCH}_3$ <sup>111</sup> sobre las que se han realizado identificaciones tentativas. La selección de las moléculas prebióticas susceptibles de estudio espectroscópico está siempre guiada por la similitud funcional con las ya identificadas, así como por los modelos cinéticos elaborados por los astrofísicos. En el diagrama de la Fig.12 aparecen los rangos cubiertos por la instrumentación disponible en el GEM junto a los correspondientes a los observatorios más importantes actualmente operativos.

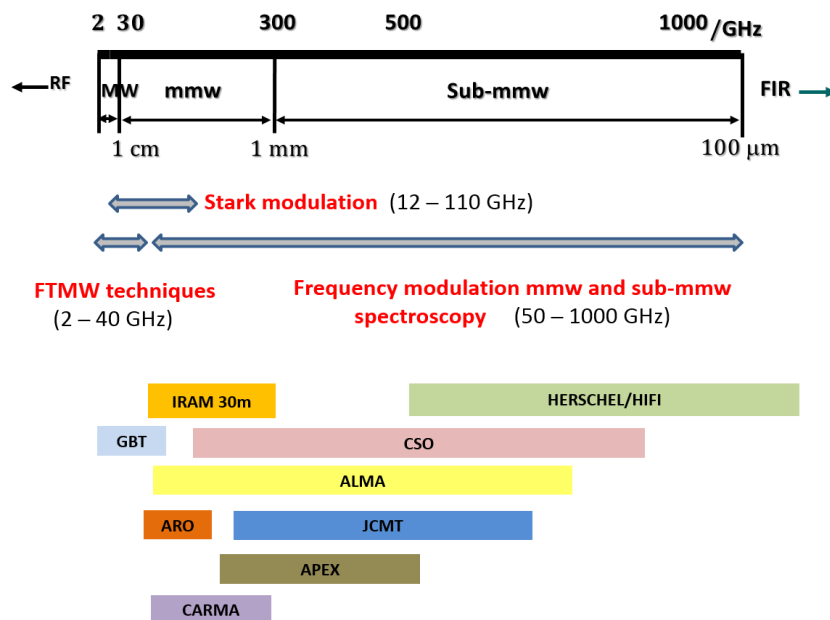


**Figura 4.** Rangos de frecuencia cubiertos en nuestros laboratorios junto a los diferentes rangos de los principales observatorios.

### 3.1. MOLÉCULAS PREBIÓTICAS

El término prebiótico fue utilizado por el bioquímico ruso Oparin y Haldane<sup>112,113</sup> para elaborar una hipótesis sobre el origen de la vida. Esta hipótesis afirma que la vida se generó de forma espontánea gracias a las particulares condiciones que hubo en las primeras etapas de la historia de la Tierra, hace más de 4.000 millones de años. Cuando se formó la Tierra la atmósfera primitiva constituida por metano, amoníaco, nitrógeno, vapor de agua, etc., era muy distinta a la actual. La mezcla de estos gases, expuesta a la radiación solar y a las descargas eléctricas de las constantes tormentas, originaría moléculas orgánicas llamadas prebióticas.<sup>114</sup> Estas moléculas, cada vez más complejas, dieron lugar a aminoácidos (elementos constituyentes de las proteínas) y ácidos nucleicos. Según Oparin, estas primeras moléculas quedaron atrapadas en las charcas de aguas poco profundas formadas en el litoral del océano primitivo donde continuaron evolucionando y diversificándose. Esta hipótesis fue posteriormente reforzada por el conocido experimento de Miller-Urey<sup>115</sup> que demostró que moléculas orgánicas complejas de aminoácidos y azúcares podían sintetizarse a partir de moléculas más simples de hidrógeno, metano, amoníaco y agua. Esta teoría endógena sobre el origen de la materia orgánica y de la vida es el que viene prevaleciendo en estas últimas décadas. Una parte importante de la investigación de la presente Memoria recoge estudios espectroscópicos de moléculas prebióticas que aportan nuevos y valiosos datos de laboratorio que pueden hacer posible la identificación de nuevas moléculas en el ISM. Con este fin, y para lograr la mayor sinergia posible, se ha puesto en marcha una estrategia en nuestros estudios de laboratorio para conectar con los registros “*survey*” obtenidos en diferentes regiones del ISM y analizados por el grupo de Astrofísica del CSIC. Las diferentes etapas en las que se ejecuta dicha estrategia están recogidas en el diagrama de bloques de la fig. 13.

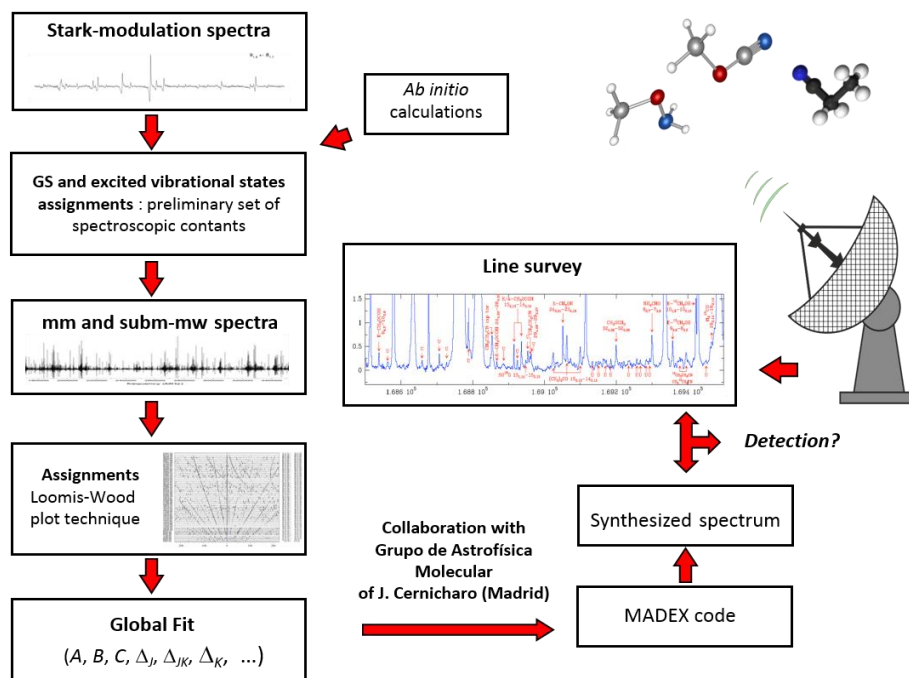


**Figura 5.** Diagrama de bloques de las etapas de la estrategia utilizada.

Todos los estudios de los espectros de rotación se inician en la región centimétrica de bajas frecuencias (entre 8 y 40 GHz) conocida como la región de microondas MW en la que se utiliza la modulación de Stark. Se trata de experimentos en el dominio de frecuencias y en condiciones de equilibrio termodinámico. Se procede en esta primera etapa a la asignación del espectro de rotación tanto en el estado fundamental de vibración como en los estados excitados de las vibraciones de baja frecuencia que están poblados a la temperatura ambiente de trabajo. En ocasiones, las espectroscopias con transformadas de Fourier en el dominio del tiempo acopladas a una expansión supersónica facilitan la identificación de especies isotópicas en su abundancia natural. Si se trata de sólidos orgánicos, como en el caso de precursores de amino ácidos, se hacen intervenir dispositivos de vaporización con ablación láser. Todas estas técnicas están descritas en la sección dedicada a la Metodología Experimental. En esta primera etapa, el análisis de los espectros conduce a la determinación de las constantes de rotación  $A$ ,  $B$ ,  $C$  y, en la mayoría de los casos, a una primera estimación de la contribución de la distorsión centrífuga, plasmada en una primera estimación de sus constantes.

En la siguiente etapa de la experimentación se procede al registro de los espectros de rotación en las regiones milimétrica y submilimétrica partiendo de 75GHz y alcanzando hasta los 480 GHz, regiones del espectro donde tienen lugar las observaciones de radioastronomía de los observatorios. Las técnicas utilizadas, descritas en La Metodología Experimental, están basadas en dispositivos de multiplicación de frecuencia de última generación. Las moléculas estudiadas son alicíclicas, muy flexibles (con modos normales de muy baja frecuencia) y fácilmente deformables por la distorsión centrífuga. Así, las predicciones de rotor rígido o semirígido realizadas con las constantes espectroscópicas de la etapa anterior no son lo suficientemente precisas para la asignación inequívoca de las transiciones en unos espectros con una alta densidad espectral y miles de señales en los registros. No sólo son los efectos de la distorsión centrífuga los que contribuyen a estas desviaciones, sino que las perturbaciones por resonancias de Fermi y acoplamientos de Coriolis dificultan enormemente la interpretación y asignación de los espectros. Todo ello obliga a nuevas estrategias en la asignación y análisis de los espectros. Los denominados Loomis-Wood Plot<sup>116</sup> resultan de gran utilidad en los análisis de las progresiones de transiciones, sobre todo en el análisis de los espectros de rotación en estados excitados de vibración. El modelado teórico *ab initio*, resulta igualmente de gran ayuda. El análisis de los espectros requiere del uso de Hamiltonianos de rotación que incorporan todas las correcciones antes mencionadas que supone el ajuste de un elevado número de parámetros espectroscópicos susceptibles de determinar con las transiciones medidas. Dada la gran complejidad del problema, algunos de estos parámetros adolecen de significación física, pero permiten la reproducción del espectro en amplias regiones de frecuencia, incluso en las que se carece de experimentación. Son finalmente estos parámetros espectroscópicos los que la astrofísica necesita para generar el espectro que denomina “sintetizado” que tiene en cuenta las condiciones del medio interestelar. Este es el que se finalmente se compara con los “*surveys*” disponibles procedentes de las observaciones en distintas regiones del ISM; el que hace finalmente posible identificación de la especie química estudiada en laboratorio.

Durante el periodo de mi tesis doctoral he realizado y participado en los estudios de moléculas prebióticas conteniendo los elementos más abundantes H, C, O, N presentes en el medio interestelar (ISM). En las secciones siguientes se realiza un breve esbozo sobre las mismas. La información detallada se recoge en los capítulos correspondientes.

### **3.1.1 Ácido acrílico: Espectro de milimétricas del s-cis y s-trans**

Las regiones de Orion KL y Sgr B2 poseen una rica actividad química y son siempre objetivo primordial de investigación para la astroquímica. Las nuevas observaciones de ALMA, con mayor sensibilidad y resolución angular que las provenientes de los radiotelescopios convencionales, exigen nuevos datos de laboratorio con el fin de crear un atlas de frecuencias e intensidades de moléculas potencialmente existentes en las regiones observadas. Una de ellas, el ácido acrílico (2-propenoico,  $\text{CH}_2=\text{CH}-\text{COOH}$ ), es el ácido carboxílico insaturado más simple. Comparte funcionalidad ( $-\text{COOH}$  y  $-\text{CH}=\text{CH}_2$ ) con otras moléculas como las del ácido fórmico, ácido acético, alcohol vinílico y propenal ya detectadas en el ISM por lo que resulta un candidato lógico. Su espectro de rotación ha sido medido y analizado en la región de milimétricas entre 130 y 360 GHz. Medidas adicionales en la región de microondas entre 18 y 26.5 GHz han sido igualmente incluidas dentro de un total de más de 4000 transiciones correspondientes a los dos isómeros s-cis y s-trans ácido acrílico de la Fig.14. La precisión de las constantes espectroscópicas obtenidas<sup>117</sup> ha posibilitado su búsqueda en las nubes moleculares de Orion KL, Sgr B2 y W51. Aunque la detección es aún tentativa, se ha podido establecer un límite superior de la columna de densidad en Orion KL. Los detalles de la investigación están recogidos en el capítulo VI de la Memoria.

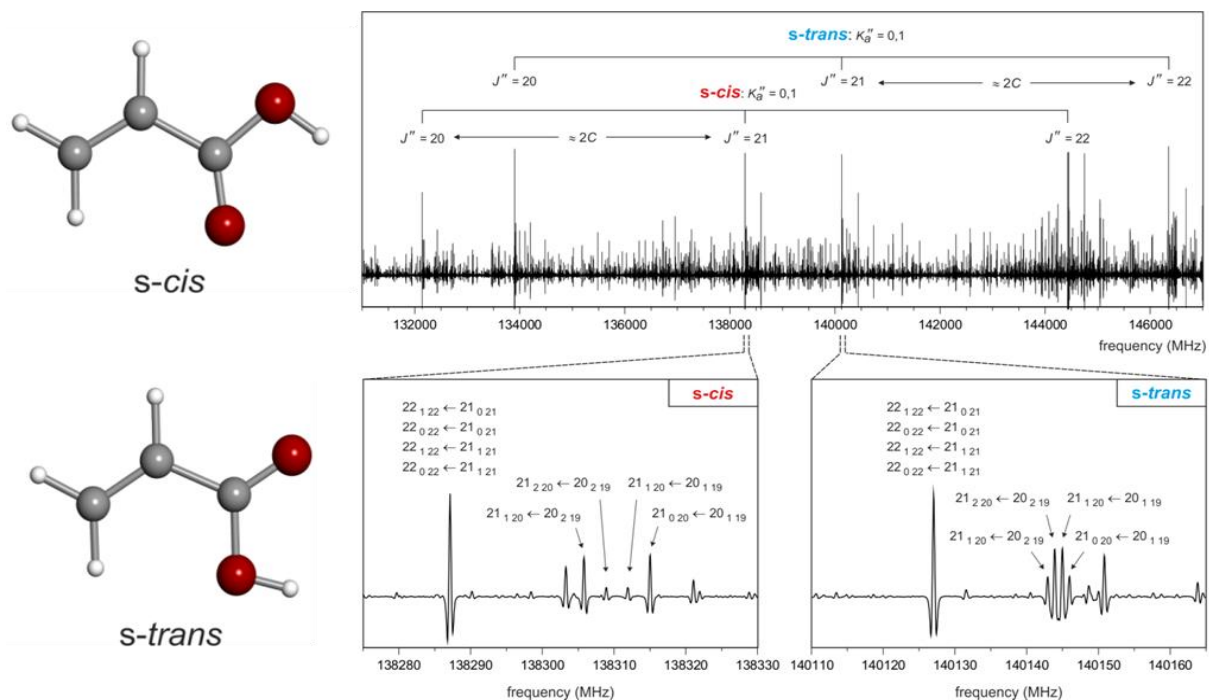


**Figura 6.** Isómeros s-cis y s-trans del ácido acrílico junto a una sección del espectro de milimétricas y pormenores del mismo detallando asignaciones.

### 3.1.2 Formato de Vinilo: Espectro de milimétricas y búsqueda en el ISM.

La elección de nuevos candidatos a identificar se justifica por las analogías funcionales con las moléculas ya identificadas y las posibles reacciones químicas que puedan tener lugar en la región observada. Así, los correspondientes al formato de etilo ( $\text{CH}_3\text{CH}_2\text{OCOH}$ ) ha sido recientemente identificado en Sgr B2(N)<sup>118</sup> y Orion KL<sup>119</sup>. El hecho de que otras moléculas con el grupo vinilo tales como cianuro de vinilo ( $\text{CH}_2=\text{CHCN}$ ),<sup>120</sup> alcohol vinílico ( $\text{CH}_2=\text{CHOH}$ )<sup>121</sup> y propileno ( $\text{CH}_2=\text{CHCH}_3$ )<sup>122</sup> entre otras, han sido igualmente identificadas en dichas regiones, hacen del formato de vinilo ( $\text{CH}_2=\text{CHOCHO}$ ) sea un serio candidato en el ISM. Su búsqueda no ha podido llevarse a cabo hasta el presente por la carencia de medidas de laboratorio lo suficientemente precisas en el rango de milimétricas. La investigación descrita en el capítulo VII, asigna y analiza más de 2600 transiciones del



formato de vinilo medidas en el rango de 80 a 360 GHz. La precisión de los parámetros espectroscópicos obtenidos con el análisis, han permitido una primera búsqueda en las regiones de Orion KL y Sgr B2. Aún no ha sido posible su detección, pero nuestros datos se siguen utilizando en investigaciones en otras regiones del ISM como las de formación de nuevas estrellas donde las concentraciones del formato de metilo se predicen más elevadas. En todo caso, los valores de las columnas de densidad obtenidas tanto en el estudio anterior del ácido acrílico<sup>117</sup> como en éste de este del formato de vinilo<sup>123</sup> parecen indicar que los mecanismos de producción de especies vinílicas en las regiones de Orion KL y Sgr B2 están preferentemente asociadas con grupos ciano (-CN).

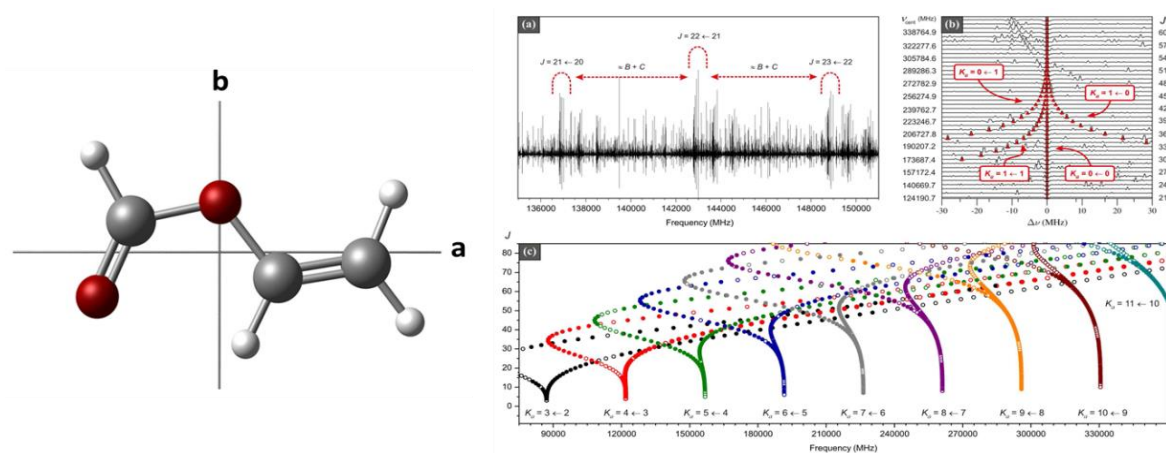


**Figura 15.** El isómero cis-trans más estable del formato de vinilo, un sector del espectro de milimétricas y los Loomis–Wood-type plot ilustrando la convergencia de ciertas progresiones de transiciones.

### 3.1.3. Metoxiamina: Su estudio espectroscópico entre 80 y 480 GHz.

Hasta el presente, muy pocas moléculas conteniendo el grupo  $\text{-NH}_2$  han sido identificadas en el ISM. La más significativa, la formamida ( $\text{NH}_2\text{CHO}$ ) detectada en 1971 por Rubin et al.<sup>124</sup> Con posterioridad la metil amina ( $\text{CH}_3\text{NH}_2$ )<sup>125</sup> cianamida ( $\text{NH}_2\text{CN}$ ),<sup>126</sup> acetamida ( $\text{CH}_3\text{CONH}_2$ )<sup>127</sup> y el aminoacetonitrilo ( $\text{NH}_2\text{CH}_2\text{CN}$ )<sup>128</sup> han sido también identificados. Por otra parte, Garrod et al.<sup>129</sup> predicen la formación de metoxiamina ( $\text{CH}_3\text{ONH}_2$ ) e hidroxilamina ( $\text{NH}_2\text{OH}$ ) con abundancias significativas. Mientras que esta

última ha sido buscada en diversas fuentes interestelares,<sup>130</sup> la metoxiamina no ha sido aún investigada dada su inestabilidad. En la investigación descrita en el capítulo VIII, la metoxiamina se ha liberado *in situ* partiendo de su sal de clorhidrato y su espectro de rotación y se ha analizado en el rango de 75 a 480GHz. Muchas de las transiciones observadas presentan desdoblamientos A, E debido a los efectos de la rotación interna del grupo metilo, que complica el análisis.

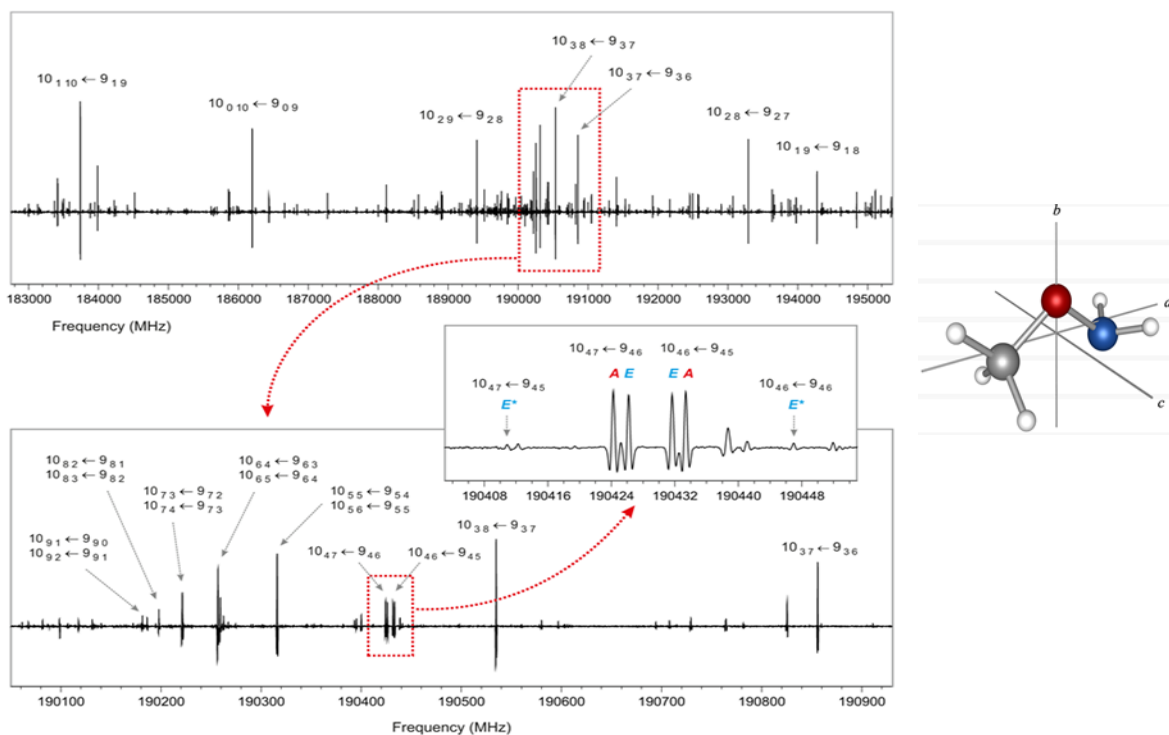


**Figura 16.** La metoxiamina y una porción de su espectro en el que se muestran los desdoblamientos A, E debidos a la rotación interna del grupo metilo.

Con los datos proporcionados en nuestro estudio, la metoxiamina aún no ha sido identificada<sup>131</sup> en las regiones de formación de estrellas en Orion KL y Sgr B2, aunque todo hace pensar que, con las abundancias predichas con los modelos químicos y las recientes observaciones de los observatorios con mayor sensibilidad y resolución, será posible pronto su detección.

### 3.1.4. N-metilhidroxilamina: Su espectro de rotación hasta 360GHz

La N-metil hidroxilamina ( $\text{CH}_3\text{NHOH}$ ) es un derivado de la metil amina en la que un hidrógeno del grupo amino ha sido sustituido por un hidroxilo. Está predicha su existencia con cierta abundancia en nubes moleculares calientes (hot cores)<sup>129</sup> caracterizadas por su alta densidad y elevadas temperaturas. Su espectro puro de rotación ha sido estudiado en la región de milimétricas hasta 360GHz.<sup>132</sup> Más de 2000 transiciones han sido medidas para el estado fundamental y seis estados excitados de vibración correspondientes a los modos normales de baja frecuencia mostrados en la fig.17. Igualmente, los isotopólogos de  $^{13}\text{C}$  en su abundancia natural han sido medidos y analizados. Las constantes espectroscópicas obtenidas en este estudio constituyen un conjunto de datos de laboratorio muy precisos para afrontar la búsqueda de la N-metilhidroxilamina en el ISM.

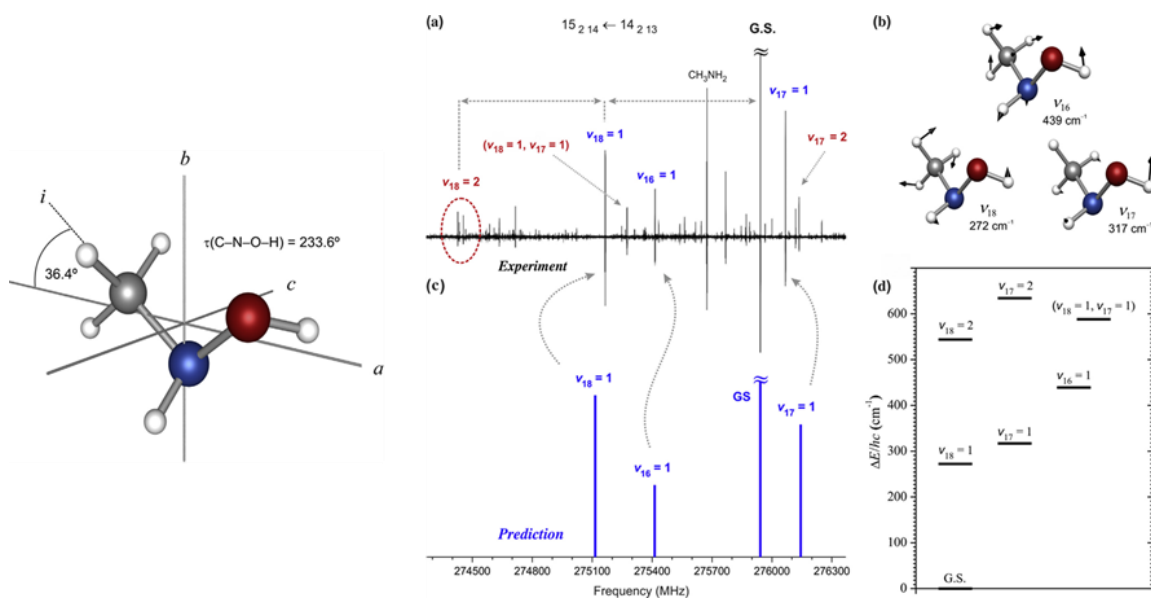


**Figura 17.** La N-metil hidroxilamina y una porción de su espectro en el que se muestran las transiciones satélites correspondientes a los espectros de rotación en los estados excitados de las vibraciones de baja frecuencia.

### 3.1.4. Cianuro de isopropilo: Un análisis exhaustivo de su espectro de rotación.

La reciente detección del cianuro de isopropilo en el ISM<sup>133</sup> ha resultado ser de gran relevancia al tratarse de la primera molécula con cadena ramificada detectada en el espacio. Esta detección ha permitido establecer una primera conexión entre la química interestelar y la composición de los meteoritos en los que los aminoácidos ramificados son dominantes.<sup>134</sup> Dada su importancia, se ha realizado en nuestros laboratorios un estudio exhaustivo de su espectro de rotación, desde 6 a 480 GHz, utilizando tres técnicas de alta resolución distintas. CP-FT-MW (chirped pulse Fourier transform microwave spectroscopy) entre 6 y 18 GHz con la que se han identificado las especies isotópicas <sup>13</sup>C y <sup>15</sup>N en su abundancia natural así como el monohidrato generado en la expansión supersónica del experimento (ver Fig.18). El espectro de microondas con modulación de Stark en el rango de 18 a 75 GHz ha permitido en análisis de los espectros de rotación en 19 estados de vibración, asignación extendida al rango de milimétricas y submilimétricas en las que se han observado perturbaciones muy significativas entre estados excitados. Toda la información que se aporta en nuestra investigación,<sup>135</sup> consistente en el análisis de más de 10.000 transiciones, hará posible la identificación de nuevas señales del cianuro de isopropilo en las diferentes regiones del ISM que actualmente se realizan por los diferentes observatorios. El estudio del cianuro de isopropilo se recoge en el capítulo X.

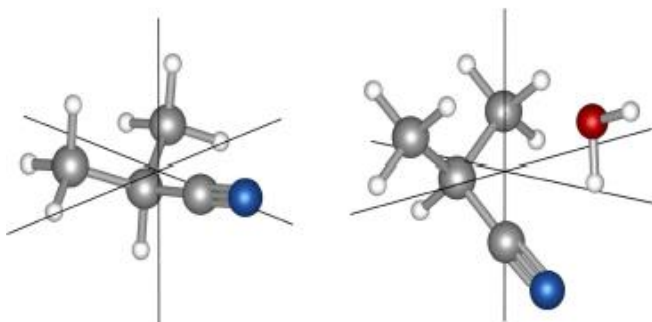


**Figura 18.** El cianuro de isopropilo y su monohidrato.

### 3.2. PRECURSORES DE AMINOÁCIDOS.

La detección de la glicina, el aminoácido más elemental, en el ISM es uno de los grandes objetivos de los investigadores en el campo de la astroquímica y astrofísica. Su presencia constataría la existencia de una química compleja en dicho medio que haría posible la síntesis de los denominados “ladrillos de la vida” (*building blocks*).<sup>136</sup> Han sido varios los intentos de identificación publicados<sup>137,138</sup> pero pronto negados con contundencia.<sup>139</sup> Aunque el descubrimiento de la glicina aún no ha sido posible, son numerosos los estudios teóricos sobre los posibles mecanismos de su formación.<sup>140,141,142,143,144,145</sup> Algunos incluyen la participación de otras moléculas, precursores de la glicina, que son igualmente candidatas a detectarse en el ISM.<sup>146</sup> Así, la famosa reacción de Strecker,<sup>147</sup> una mezcla de amoníaco, cianuro de hidrógeno, aldehído y agua reaccionan para dar aminoacetonitrilo ( $\text{H}_2\text{N}-\text{CH}_2-\text{CN}$ ). Éste, tanto en laboratorio como en condiciones del medio interestelar, se transforma en glicina por hidrólisis.<sup>148,149</sup> Esta reacción sigue siendo la más aceptada en la síntesis de la glicina.<sup>150,151</sup> Por otra parte, la hidrólisis del aminoacetonitrilo ocurre a través del intermediato de la glicinamida ( $\text{H}_2\text{N}-\text{CH}_2-\text{CONH}_2$ )<sup>152</sup> que, finalmente, se hidroliza para dar glicina y amoníaco.

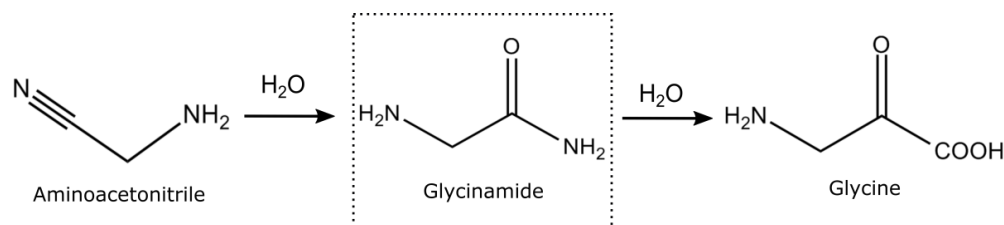


**Figura 19.** Esquema de la reacción de Strecker

De todo lo anterior se deduce que, el estudio espectroscópico de precursores y su detección en el ISM están importante como la de los propios *building blocks*, con el fin de llegar a entender los procesos químicos que llevan a su formación. Aunque en diferentes contextos, tres han sido los precursores de la glicina cuyos estudios se han abordado

durante la realización de mi tesis doctoral: aminoacetonitrilo, glicinamida e hidantoina, cuyos resultados se esbozan en los siguientes apartados.

### **3.2.1. Amino acetonitrilo: Espectros de rotación en 29 estados excitados de vibración.**

El número de líneas no identificadas en el medio interestelar se incrementa de forma inexorablemente a medida que se incrementa la sensibilidad y resolución de las observaciones de radioastronomía. La contribución más importante procede de transiciones de rotación en estados excitados de vibración de un reducido número de moléculas que, por su abundancia en el medio interestelar o por su flexibilidad, poseen estados excitados de vibración lo suficientemente poblados para generar espectros de rotación que contaminan los registros y dificultan la identificación de nuevas especies. Este problema, conocido en la literatura como *astrophysical weeds*<sup>153</sup> se aborda primero en los laboratorios mediante un análisis exhaustivo de los espectros de rotación en los estados excitados de las vibraciones de baja frecuencia. El aminoacetonitrilo ( $\text{H}_2\text{NCH}_2\text{CN}$ ), precursor de la glicina fue detectado en SgrB2 en 2008.<sup>154</sup> Esta región se caracteriza por la elevada temperatura del gas, lo cual sugiere que muchas de las líneas observadas pertenezcan a estados excitados de vibración.<sup>155</sup> Mediante la combinación de nuestras técnicas de la región de centimétricas hasta submilimétricas, se ha analizado el espectro de rotación de hasta 29 estados excitados de vibración<sup>156</sup> (ver Fig.20 con energías de hasta  $1000\text{ cm}^{-1}$  respecto al estado fundamental de vibración).

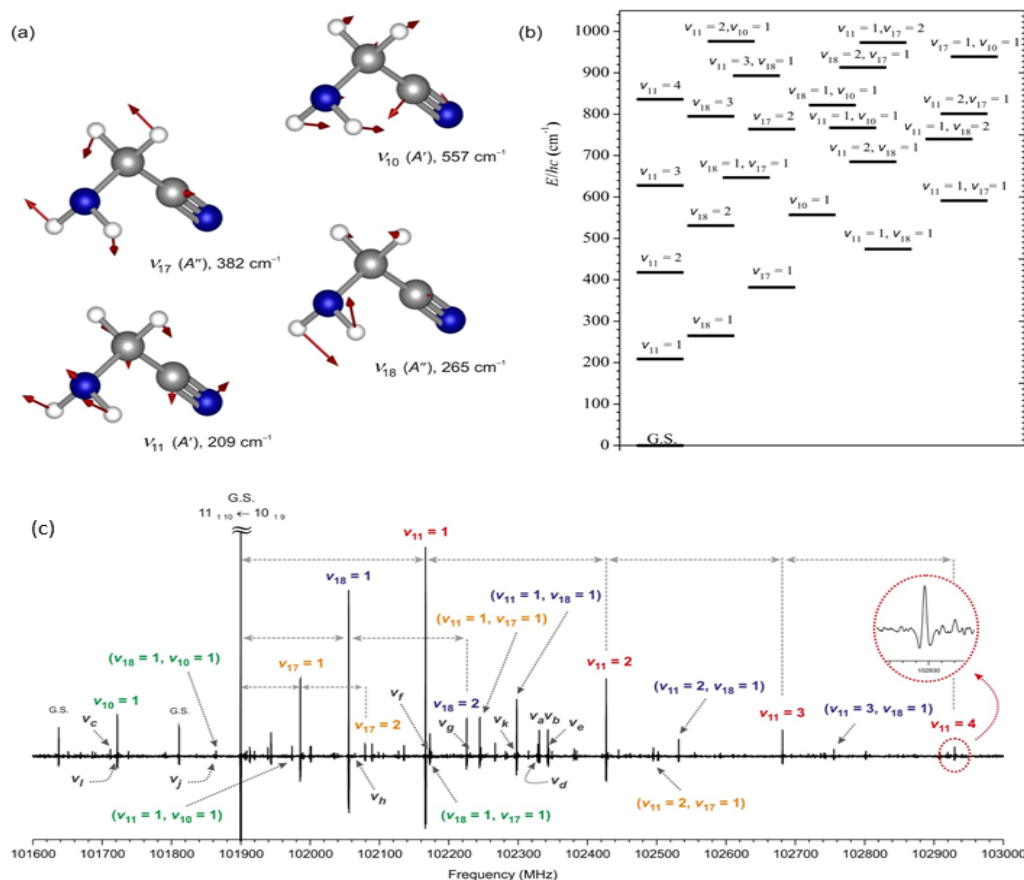


**Figure 20.** (a) Visualización esquemática de los 4 modos de vibración más bajos del aminoacetonitrilo  $\nu_{11}$ ,  $\nu_{18}$ ,  $\nu_{17}$  y  $\nu_{10}$ . (b) Diagrama de los niveles de energía vibracionales predichos por debajo de  $1000\text{cm}^{-1}$  resultado de los 4 modos de vibración más bajos. (c) Sección de 1.5 GHz del espectro del aminoacetonitrilo en la región de milimétrica donde se muestran los estados excitados asignados alrededor del ground state.

El extenso conjunto de datos recogidos en el cap. XI, con más de 2000 nuevas transiciones, permitirá la identificación de nuevas transiciones del aminoacetonitrilo en el medio interestelar que ayuden a aliviar el problema de minimizar el problema.

### 1.3.1.2. Glicinamida: Estudio de microondas mediante ablación láser.

A diferencia del aminoacetonitrilo ( $\text{H}_2\text{N}-\text{CH}_2-\text{CN}$ ), la glicinamida ( $\text{H}_2\text{N}-\text{CH}_2-\text{CONH}_2$ ) no ha sido aún detectada en el ISM debido a la carencia de datos de su espectro de rotación. Se trata de un sólido muy inestable que se dispensa comercialmente en forma de clorhidrato de glicinamida (m.p.  $86\text{ }^\circ\text{C}$ ). La glicinamida es un intermediato en la formación de la glicina

por lo que es un candidato a estar presente en el medio interestelar: los datos espectroscópicos de laboratorio son imprescindibles para su identificación. En la investigación llevada a cabo en nuestros laboratorios se ha utilizado la ablación láser para liberar la forma neutra de la glicinamida a partir del clorhidrato. El espectro de microondas ha sido por primera vez caracterizado con nuestra técnica de LA-CP-FTMW entre 6 y 12 GHz (Fig. 21a). Todas las transiciones de rotación aparecen con una compleja estructura hiperfina (Fig.21b) con un elevado número de componentes que no pueden resolverse adecuadamente en el espectro de banda ancha. Ello es debido al acoplamiento de cuadrupolo nuclear de los dos núcleos  $^{14}\text{N}$  que posee la glicinamida y que complica en gran medida el análisis del espectro. Para ello, ha sido fundamental la gran resolución de nuestra técnica de cavidad LA-MB-FTMW que resuelve definitivamente el espectro (ver Fig. 21c) haciendo posible su análisis. Esta primera caracterización de la glicinamida en la región centimétrica es el primer paso para una posible identificación en el ISM. El estudio de la glicinamida se recoge en el capítulo XII.

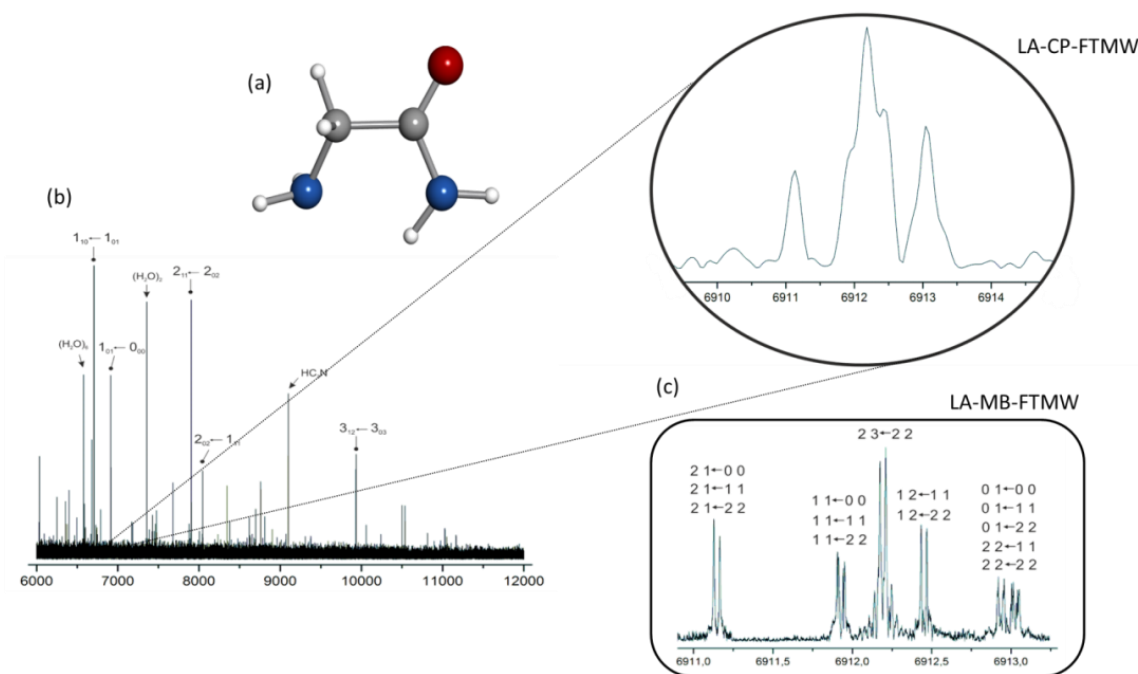


**Figura 21.** (a) Estructura de la glicinamida. (b) Espectro de rotación de banda ancha entre 6 y 12 GHz con zoom a la transición  $1_{01} \leftarrow 0_{00}$ . (c) Espectro de MB-FTMW de la transición  $1_{01} \leftarrow 0_{00}$  con la estructura hiperfina resuelta.



### 3.1.2. La ablación del sólido de la Hidantoina: Estudio de su espectro de rotación.

La hidantoina ( $C_3H_4O_2N_2$ ) es considerada como uno de los precursores de la glicina en el medio interestelar<sup>157,158</sup> y su origen extraterrestre está probada por su presencia en los meteoritos (condritas).<sup>159</sup> Al tratarse de una molécula heterocíclica conteniendo nitrógeno, se presume que participa en la formación de oligopéptidos y polipéptidos<sup>160</sup> así como de ser un intermediato del  $HCN_6$  molécula crucial en el origen de la vida.<sup>161</sup>

La hidantoina, es un sólido con alto punto de fusión (m.p. 220 °C) y térmicamente lábil por lo que no puede transferirse fácilmente a fase gas por calentamiento sin sufrir una grave descomposición térmica. En 2017 Ozeki et al. han logrado una primera caracterización de su espectro en la región de milimétricas mediante calentamiento a 150 °C.<sup>162</sup> Sin embargo, la compleja estructura de cuadrupolo nuclear debida a la presencia de dos núcleos de  $^{14}N$  en posiciones no equivalentes del anillo no pudo ser resuelta dada la pobre resolución del experimento. En nuestro estudio de alta resolución en la región de centimétricas<sup>163</sup> se han utilizado nuestros dispositivos de ablación láser acoplados a las técnicas de microondas con transformadas de Fourier (ver capítulo metodología experimental) para resolver y analizar la estructura de cuadrupolo nuclear y completar así todos los parámetros espectroscópicos que puedan hacer posible la identificación de este importante precursor en el medio interestelar. Los valores de las constantes de acoplamiento de cuadrupolo obtenidos para los núcleos  $N_3$  y  $N_5$  han sido discutidos en el contexto de su entorno electrónico en la molécula. Todos los detalles del estudio figuran en el capítulo XIII de la Memoria.

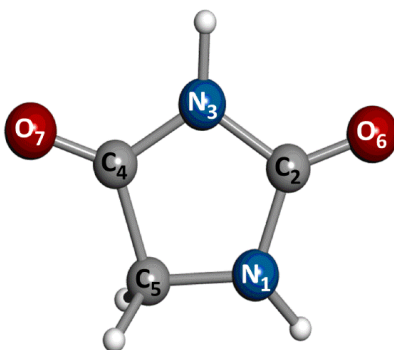


**Figure 22.** La forma bicetona de la hidantoina observada.

## 4. REFERENCIAS

---

- <sup>1</sup> Levy DH, Laser spectroscopy of cold gas-phase molecules. *Annu Rev Phys Chem.*, 1980, 31:197,
- <sup>2</sup> Scoles G, Atomic and molecular beam methods, vol 1. Oxford University Press, New York/Oxford, ed.1988
- <sup>3</sup> T. J. Balle, W. H. Flygare, *Rev. Sci. Instrum.*, 1981, 52, 33.
- <sup>4</sup> U. Andresen, H. Dreizler, J.-U. Grabow, W. Stahl, *Rev. Sci. Instrum.*, 1990, 61, 3694.
- <sup>5</sup> J. L. Alonso, F. J. Lorenzo, J. C. López, A. Lesarri, S. Mata, H. Dreizler, *Chem. Phys.*, 1997, 218, 267.
- <sup>6</sup> S. Antolínez, J. C. López, J. L. Alonso, *Angew. Chem. Int. Ed.*, 1999, 38, 1772.(VIP)
- <sup>7</sup> M. E. Sanz, J. C. López, J. L. Alonso, *Chem. Eur. J.*, 1999, 5, 3293.
- <sup>8</sup> M. E. Sanz, J. C. López, J. L. Alonso, *Chem. Eur. J.*, 2002, 8, 4265.
- <sup>9</sup> M. E. Sanz, A. Lesarri, J.C. Lopez, J. L. Alonso, *Angew. Chem. Int. Ed.*, 2001, 40, 935.
- <sup>10</sup> S. Blanco, A. Lesarri, J. C. López, J. L. Alonso, *Chem. Eur. J.*, 2002, 8, 1603.
- <sup>11</sup> S. Antolinez, A. Lesarri, J. C. López, J. L. Alonso, *Chem. Eur. J.*, 2000, 6, 3345.
- <sup>12</sup> S. Antolinez, J. C. López, J. L. Alonso, *Chem. Phys. Lett.*, 2000, 323, 130.
- <sup>13</sup> J. L. Alonso, J. C. López, S. Blanco, A. Lesarri, F.J. Lorenzo, *J. Chem. Phys.*, 2000, 113, 2760.
- <sup>14</sup> J. C. López, S. Blanco, A. Lesarri, M. E. Sanz, F. J. Lorenzo, J. L. Alonso, *J. Chem. Phys.*, 2001, 114, 9421
- <sup>15</sup> M. E. Sanz, V. M. Sanz, J. C. López, J. L. Alonso, *Chem. Phys. Lett.*, 2001, 342, 31
- <sup>16</sup> Y. Tatamitani, L. Bingxin, J. Shimada, T. Ogata, P. Ottaviani, A. Maris, W. Caminati, J. L. Alonso., *J. Am. Chem. Soc.*, 2002, 124, 2739.
- <sup>17</sup> J. L. Alonso, S. Antolínez, S. Blanco, A. Lesarri, J. C. López, W. Caminati. *J. Am. Chem. Soc.*, 2004, 126, 3244.
- <sup>18</sup> W. Caminati, J. C. López, J. L. Alonso, J.-U. Grabow, *Angew. Chem. Int. Ed.*, 2005, 44, 2.(VIP)
- <sup>19</sup> J. C. López, W. Caminati, J. L. Alonso, *Angew. Chem. Int. Ed.*, 2006, 118, 296.
- <sup>20</sup> T. G. Dietz, M. A. Duncan, D. E. Powers, R. E. Smalley, *J. Chem. Phys.*, 1981, 74, 6511.
- <sup>21</sup> K. Tanaka, H. Waki, Y. Ido, S. Akita, Y. Yoshida, T. Yoshida, "Protein and Polymer Analyses up to m/z 100 000 by Laser Ionization. Time-of flight Mass Spectrometry", *Rapid Commun. Mass Spectrom.* 1988, 2, 151
- <sup>22</sup> R. J. Levis, *Annu. Rev. Phys. Chem.*, 1994, 45, 483
- <sup>23</sup> "Microwave Spectroscopy of Biomolecular Building Blocks": J.L. Alonso, J.C.López, *Topics in Current Chemistry*, Vol. 364 Springer, Heidelberg, 2015, pp.335–402.
- <sup>24</sup> J. L. Alonso, C. Pérez, M. E. Sanz, J. C. López, S. Blanco, *Phys. Chem. Chem. Phys.*, 2009, 11, 617-627
- <sup>25</sup> G. G. Brown, B. C. Dian, K. O. Douglass, S. M. Geyer, S. T. Shipman and B. H. Pate, *Rev. Sci. Instrum.*, 2008, 79
- <sup>26</sup> S. Mata, I. Peña, C. Cabezas, J. C. López and J. L. Alonso *J. Mol. Spectrosc.*, 2012, 280, 91-96
- <sup>27</sup> C. Pérez, S. Mata, C. Cabezas, J. C. López, J. L. Alonso, *J. Phys. Chem. A*, 2015, 119 (16), 3731–3735
- <sup>28</sup> M. E. Sanz, C. Cabezas, S. Mata, J. L. Alonso, *J. Chem. Phys.*, 2014, 140, 204308
- <sup>29</sup> C. Bermúdez, S. Mata, C. Cabezas, J. L. Alonso, *Angew. Chem. Int. Ed.*, 2014, 53, 11015,
- <sup>30</sup> C. Cabezas, M. Varela, J. L. Alonso, *ChemPhysChem.*, 2013, 14, 2539-2543.
- <sup>31</sup> C. Cabezas, R. Martinus, R. Anouk, I. Peña, J. L. Alonso, *Phys.Chem.Chem.Phys.*, 2015, 17, 20274-20280,
- <sup>32</sup> C. Cabezas, M. Varela, J.L. Alonso *Angew. Chem. Int. Ed.* 2017, 56, 6420 –6425,
- <sup>33</sup> A. Simão, I. Peña, C. Cabezas, J. L. Alonso, *Chemical Physics Letters*, 2014, 616–617 184-188,
- <sup>34</sup> I. Peña, C. Cabezas, J. L. Alonso, *Angew. Chem. Int. Ed.*,(2015, 54, 2991-2994
- <sup>35</sup> J. L. Alonso, M. A. Lozoya, I. Peña, J. C. López, C. Cabezas, S. Mata, S. Blanco, *Chem. Sci.*, 2014, 5, 515-522
- <sup>36</sup> I. Peña, C. Cabezas, J. L. Alonso, *Chem. Commun.*, 2015, 51, 10115
- <sup>37</sup> I. Peña, E. J. Cocinero, C. Cabezas, A. Lesarri, S. Mata, P. Écija, A. M. Daly, A. Cimas, C. Bermúdez, F. J. Basterretxea, S. Blanco, J. A. Fernández, J. C. López, F. Castaño, J. L. Alonso, *Angew. Chem. Int. Ed.*, 2013 52, 11840-11845.; E. J. Cocinero, A. Lesarri, P. Écija, F. J. Basterretxea, Jens-Uwe Grabow, J. A. Fernández, F. Castaño, *Angew. Chem. Int. Ed.*, 2012, 51, 3119 –3124.
- <sup>38</sup> C. Cabezas, I. Peña, A. M. Daly, J. L. Alonso, *ChemCommun.*, 2013, 49, 10826-10828
- <sup>39</sup> I. Peña, S. Mata, A. Martín, C. Cabezas, A. M. Daly, J. L. Alonso, *Phys. Chem. Chem. Phys.*, 2013, 15, 18243-18248
- <sup>40</sup> I. Peña, L. Kolesniková, C. Cabezas, C. Bermúdez, M. Berdakin, A. Simão, J. L. Alonso, *Phys. Chem. Chem. Phys.*, 2014, 16, 23244-23250

- <sup>41</sup> C. Bermúdez, I. Peña, C. Cabezas, A. M. Daly, J. L. Alonso, *ChemPhysChem*, 2013, 14(5), 893-895; E.J.Cocinero, Davis, F. J. Basterretxea, J. A. Fernández, F. Castaño, *J. Am. Chem. Soc.*, 2013, 135 (7), 2845–2852
- <sup>42</sup> C.Cabezas, I.Peña, J.C.López, J.L.Alonso. *J Phys Chem Lett.*, 2013, 4(3), 486-490,
- <sup>43</sup> J.L. Alonso, M.E. Sanz, J.C. López, V. Cortijo; *J. Am. Chem. Soc.*, 2009, 131 (12), 4320-4326
- <sup>44</sup> C. Cabezas, J. L. Alonso, J. C. López and S. Mata, *Angew. Chem. Int. Ed.*, 2012, 51: 1375–1378.
- <sup>45</sup> I. Peña, A. M. Daly, C. Cabezas, S. Mata, C. Bermúdez, A. Niño, J.C. López, J-U. Grabow, and J. L. Alonso *J. Phys. Chem. Lett.*, 2013, 4(1), pp 65–69
- <sup>46</sup> J.T. Edward. Stability of Glycosides to Acid Hydrolysis. *Chem. Ind. (Lond.)*, 1955, 36, 1102-1104.
- <sup>47</sup> R. U. Lemieux.; P. Chü, in 133rd National Meeting of the American Chemical Society 31N, 1958, American Chemical Society.
- <sup>48</sup> R.U. Lemieux. *Molecular Rearrangements*. John Wiley and Sons, New York, 1964, p.709.
- <sup>49</sup> E. R. Alonso, I. Peña, C. Cabezas, and José L. Alonso, *J. Phys. Chem. Lett.* 2016, 7, 845–850.
- <sup>50</sup> Kuchitsu, K., "Structure of Free Poliatomic Molecules", Springer-Verlag Berlin Heidelberg New York, 1998.
- <sup>51</sup> Anslyn, E.V.; Dougherty, D. A. "Modern Physical Organic Chemistry" University Science Book, Sausalito, 2006.
- <sup>52</sup> G. Cohn, *Die organischen Geschmacksstoffe*, F. Siemenroth, 1914.
- <sup>53</sup> E. Oertly and R. G. Myers, *J. Am. Chem. Soc.*, 1919, 41, 855-867.
- <sup>54</sup> T. Kaneko, *J. Chem. Soc. (Japan)*, 1938, 29, 433-439
- <sup>55</sup> R. S. Shallenberger and T. E. Acree, *Nature*, 1967, 216, 480-482.
- <sup>56</sup> R. S. Shallenberger, T.E. Acree and C. Y. Lee, *Nature*, 1969, 221, 555-556.
- <sup>57</sup> L. B. Kier, *J. Pharm. Sci.*, 1972, 61, 1394-1397.
- <sup>58</sup> A. van der Heijden, L. B. P. Brussel and H. G. Peer, *Food Chem.*, 1978, 3, 207-211.
- <sup>59</sup> T.Yamazaki, E. Benedetti, D. Kent and M. Goodman, *Angew.Chem. Int. Ed.*, 1994, 33, 1437-1451.
- <sup>60</sup> (a) C. Nofre and J.M. Tinti, *Food Chemistry*, 1996, 56, 263-274. (b) R. S. Shallenberger, *Food Chemistry*, 1996, 56,209-214
- <sup>61</sup> R.S.Shallenberger, "*Taste Chemistry*". Springer-Verlag New York, 2012
- <sup>62</sup> R.H.Goldsmith, *J.Chem. Educ.*, 1987, 64, 954-955.
- <sup>63</sup> C.Bermúdez, I.Peña, C.Cabezas, A.M.Daly, J.L. Alonso *ChemPhysChem*. 2013, 14, 893 – 895
- <sup>64</sup> C. Bermúdez, I. Peña, S. Mata, J.L. Alonso, *Chemistry*. 2016, 22(47):16829-16837.
- <sup>65</sup> E.R. Alonso, L. Kolesniková and José L. Alonso, *Angew. Chem.* 2018, submitted.
- <sup>66</sup> M. E. Sanz, C. Cabezas, S. Mata, and J. L. Alonso, *J. Chem. Phys.* ,2014, 140, 204308
- <sup>67</sup> Vogt, T. Phenylpropanoid Biosynthesis. *Mol. Plant* 2010, 3, 2–20.
- <sup>68</sup> Dixon, R. A. *Nature* 2001, 411, 843–847.
- <sup>69</sup> Sharma, P. *J.Chem. Pharm. Res.*, 2011, 3, 403–423.
- <sup>70</sup> Shang, Y.-J.; Liu, B.-Y.; Zhao, M.-M. *Czech J. Food Sci.* 2015, 33.
- <sup>71</sup> De, P.; Baltas, M.; Bedos-Belval, F. *Curr. Med. Chem.* 2011, 18, 1672–1703.
- <sup>72</sup> Liu, L.; Hudgins, W. R.; Shack, S.; Yin, M. Q.; Samid, D. *Int. J. Cancer* 1995, 62, 345–350.
- <sup>73</sup> Guzman, J. D. *Molecules* 2014, 19, 19292–19349.
- <sup>74</sup> Jitareanu, A.; Tataringa, G.; Zbancioc, A. M.; Tuchilus, C.; Stanescu, U. *Rev. Med. Chir. Soc. Med. Nat. Iasi*. 2011, 115, 965–971.
- <sup>75</sup> Korose, B.; Sova, M.; Turk, S.; Krasevec, N.; Novak, M.; Lah, L.; Stojan, J.; Podobnik, B.; Berne, S.; Zupanec, N. *J. Appl. Microbiol.* 2014, 116, 955–966S
- <sup>76</sup> Pragasam, S. J.; Venkatesan, V.; Rasool, M. *Inflammation* 2013, 36, 169–176.
- <sup>77</sup> Guven, M.; Aras, A. B.; Akman, T.; Sen, H. M.; Ozkan, A.; Salis, O.; Sehitoglu, I.; Kalkan, Y.; Silan, C.; Deniz, M. *Iran J. Basic Med. Sci.* 2015, 18, 356–363.
- <sup>78</sup> V.Cortijo, E.R.Alonso, S.Mata and J.L.Alonso, *J.Phys.Chem.A*, 2018 DOI: 10.1021/acs.jpca.7b08882
- <sup>79</sup> H. A. Lehninger, D. Nelson and M. Cox, *Lehninger Principles of Biochemistry*, W. H. Freeman, 2008.
- <sup>80</sup> Y. Park and V. Helms, *Bioinformatics*, 2007, 23, 701–708.
- <sup>81</sup> Schermann J.P, *Spectroscopy and Modelling of Biomolecular Building Blocks* , Elsevier Amsterdam 2008
- <sup>82</sup> E. G. Robertson and J. P. Simons, *Phys. Chem. Chem. Phys.*, 2001, 3, 1–18.
- <sup>83</sup> M. S. De Vries and P. Hobza, *Annu. Rev. Phys. Chem.*, 2007, 58, 585–612.
- <sup>84</sup> C.Cabezas, M. Varela, J.L. Alonso; *Angew. Chem. Int. Ed.* 2017, 56, 6420 –6425
- <sup>85</sup> C. Cabezas, M. Varela, V. Cortijo, A. I. Jimenez, I. Peña, A.M. Daly, J. C. Lopez, C. Cativiela and J. L. Alonso, *Phys.Chem. Chem. Phys.*, 2013, 15, 2580.

- 
- <sup>86</sup> C. Puzzarini, M. Biczysko, V. Barone, L. Largo, I. Pena, C.Cabezas and J. L. Alonso, *J. Phys. Chem. Lett.*, 2014, 5, 534–540.
- <sup>87</sup> C. Cabezas, M. Varela and J. L. Alonso, *ChemPhysChem*, 2013, 14, 2539–2543.
- <sup>88</sup> G. N. Ramachandran C. Ramakrishnan V. Sasisekharan, *J. Mol. Biol.*, 1963, 7, 95–99
- <sup>89</sup> C. Cabezas, M. A. T. Robben, A. M. Rijs, I. Pena and J. L. Alonso, *Phys. Chem. Chem. Phys.*, 2015, 17, 20274–20280.
- <sup>90</sup> I. León, E. R. Alonso, S. Mata, C. Cabezas, M. A. Rodríguez, J.-U. Grabowb and J. L. Alonso, *Phys. Chem. Chem. Phys.*, 2017, 19, 24985.
- <sup>91</sup> M.P. Gaigeot and M. Mons, *Topics in Current Chemistry*, Springer, Heidelberg, 2015, 364, pp.225–271.
- <sup>92</sup> J. Demaison, K. Sarka, E.A. Cohen. *Spectroscopy from Space*. NATO science series. Kluwer Academic Publishers, 2000.
- <sup>93</sup> S. Kwok. *Organic Matter in the Universe*. Wiley, 2012.
- <sup>94</sup> A.G.G.M. Tielens. *The Physics and Chemistry of the Interstellar Medium*. Cambridge University Press, 2005.
- <sup>95</sup> A.M. Shaw, *Astrochemistry*, Wiley, 2006.
- <sup>96</sup> D.E. Woon, 2017. <<http://www.astrochymist.org/>>
- <sup>97</sup> J.E. Beckman and J.P. Phillips. *Submillimetre wave astronomy*. Cambridge University Press. 1982
- <sup>98</sup> S. Schlemmer, H. Mutschke, T. Giesen, C. Jäger, *Laboratory Astrochemistry : From Molecules through Nanoparticles to Grains*. Ed Wiley-VCH, 2014. DOI: 10.1002/9783527653133
- <sup>99</sup> J. Cernicharo, R. Bachiller. *The Molecular Universe*. Proceedings of the 280<sup>th</sup> Symposium of the International Astronomical Union. Cambridge University Press, 2011.
- <sup>100</sup> A. M. Daly, C. Bermúdez, A. Lopez, B. Tercero, J.C. Pearson, N. Marcelino, J.L. Alonso, *J. Cernicharo ApJ*, 2013, 768:81
- <sup>101</sup> L. Kolesníková, E. R. Alonso, S. Mata, and J. L. Alonso, *ApJ Supp.Series* 2017, 229:26 (8pp)
- <sup>102</sup> C. Cabezas, S. Mata, A.M. Daly, A. Martín, J.L. Alonso, J. Cernicharo, *J.Mol.Spectros.*, 2012, 278,31–34
- <sup>103</sup> C. Cabezas, C. Barrientos, A. Largo, J.C. Guillemin and J.L. Alonso, *Phys.Chem.Chem.Phys.* 2016,18, 28538.
- <sup>104</sup> L. Kolesníková, B.Tercero, J.Cernicharo, J.L.Alonso, A.M.Daly, B.P. Gordon and S.T.Shipman *ApJ*, 2014, 784, L7.
- <sup>105</sup> C. Cabezas, J. Cernicharo, J.L. Alonso, M. Agúndez, S. Mata, M. Guelin, I. Peña, *ApJ*, 2013, 775:133.
- <sup>106</sup> B.Tercero, J.Cernicharo, A.López, N.Brouillet, L.Kolesníková, R.A.Motiyenko, L.Margulès, J.L. Alonso, J.C.Guillemin, *A&A*, 2015, 582, L1
- <sup>107</sup> J. Cernicharo, Z. Kisiel, B. Tercero, L. Kolesníková, I. R. Medvedev, A. López, S. Fortman, M. Winnewisser, F. C.deLucia, J.L.Alonso, J.-C.Guillemin, *A&A*, 2016, 587, L4.
- <sup>108</sup> F. Goesman, H. Rosenbauer et al., *Science*, 2015, 6247, 349.
- <sup>109</sup> L. Kolesníková, A.M. Daly, J.L. Alonso, B. Tercero, J.Cernicharo, *J. Mol. Spectrosc.*, 2013, 289, 13–20.
- <sup>110</sup> A.M. Daly, C. Bermúdez, L. Kolesníková, J.L. Alonso. *ApJS* 2015, 218:30 (7pp)
- <sup>111</sup> A.M. Daly, L. Kolesníková, S. Mata, J.L. Alonso *J. Mol. Spectrosc.*, 2014, 306, 11–18.
- <sup>112</sup> A.I. Oparin , *The origin of the life*, McMillan The origin of the life. 1938
- <sup>113</sup> J.B.S. Haldane, *Rationalist Annual*, 1929,148,3–10
- <sup>114</sup> P. Thaddeus, *Phil. Trans.R.Soc.B*, 2006, 1681–87
- <sup>115</sup> S.L. Miller and H.C. Urey *Science*, 1959, 130, 245–251.
- <sup>116</sup> Z. Kisiel, L. Pszczółkowski, I.R. Medvedev, et al. *J.Mol.Spectros.* 2005,233,231
- <sup>117</sup> E.R. Alonso, L. Kolesníková, I. Peña, S.T. Shipman, B. Tercero, J. Cernicharo and J.L. Alonso. *J.Mol. Spectros.* 2015, 316, 84–89
- <sup>118</sup> A. Belloche, , H. S. P Müller, K. M., P. Schilke and C. Comito, *A&A*, 2013, 559, A47
- <sup>119</sup> B. Tercero, I. Kleiner, J. Cernicharo, et al., *ApJL*, 2013, 770, L13
- <sup>120</sup> A. López, B. Tercero, Z. Kisiel, A. M. Daly, C. Bermúdez, H. Calcutt, N. Marcelino, S. Viti, B. J. Drouin, I. R. Medvedev, C. F. Neese, L. Pszczółkowski, J. L. Alonso, and J. Cernicharo, *A&A*, 2014, 572, A44 and references therein.
- <sup>121</sup> B.E. Turner and A. J. Apponi, *ApJL*, 2001, 561, L207
- <sup>122</sup> N. Marcelino, J. Cernicharo, M. Agúndez, et al., *ApJL*, 2007, 665, L127
- <sup>123</sup> E. R. Alonso, L. Kolesníková, B. Tercero, C. Cabezas, J. L. Alonso, J. Cernicharo, and J.-C. Guillemin *ApJ*, 2016, 832:42 (5pp)
- <sup>124</sup> Rubin, R., G.W. Swenson, J., Benson, R., Tigelaar, H., & Flygare, W., *ApJ*, 1971, 169, L39
- <sup>125</sup> Kaifu, N., Morimoto, M., Nagane, K., et al. 1974, *ApJ*, 191, L135

- <sup>126</sup> Turner, B., Liszt, H., Kaifu, N., & Kisliakov, A. 1975, *ApJ*, 201, L149
- <sup>127</sup> Hollis, J. M., Lovas, F. J., Remijan, A. J., et al. 2006, *ApJ*, 643, L25
- <sup>128</sup> Belloche, A., Menten, K. M., Comito, C., et al. 2008, *A&A*, 482, 179
- <sup>129</sup> Garrod, R. T., Weaver, S. L. W., & Herbst, E. 2008, *ApJ*, 682, 283
- <sup>130</sup> McGuire, B. A., Carroll, P. B., Dollhopf, N. M., et al. 2015, *ApJ*, 812, 76
- <sup>131</sup> L. Kolesníková, B. Tercero, E. R. Alonso, J.-C. Guillemin, J. Cernicharo, and J. L. Alonso *A&A*, 2018, 609, A24
- <sup>132</sup> L. Kolesníková, E.R. Alonso, S. Mata, J.L. Alonso. *J.Mol.Spectros.*, 2017. 335, 54–60
- <sup>133</sup> A. Belloche, R. T. Garrod, H. S. P. Müller, & K. M. Menten, 2014, *Sci*, 345, 1584
- <sup>134</sup> J. Cronin, S. Pizzarello, 1983, *AdSpR*, 3, 5
- <sup>135</sup> L. Kolesníková, E. R. Alonso, S. Mata, J. Cernicharo, and J. L. Alonso, *ApJ Supp.Series*, 2017, 233:24
- <sup>136</sup> S. Kwok in “Organic Matter in the Universe”, Wiley-VCH, 2012.
- <sup>137</sup> R. D. Brown, P. D. Godfrey, J. W. V. Storey, M.-P. Bassez, B. J. Robinson, R. A. Batchelor, M. G. McCulloch, O. E. H. Rydbeck, A. G. Hjalmarson, *MNRAS*, 1979, 186, 5P-8P.
- <sup>138</sup> Y.J. Kuan, S. B. Charnley, H.-C. Huang, W.-L. Tseng, and Z. Kisiel, *ApJ*, 2003, 593:848–867,
- <sup>139</sup> A Rigorous Attempt to Verify Interstellar Glycine L. E. Snyder, F. J. Lovas, J. M. Hollis, D. N. Friedel, P. R. Jewell, A. Remijan, V. V. Ilyushin, E. A. Alekseev, S. F. Dyubko, *ApJ*, 2005, 619:914–919.
- <sup>140</sup> L. Largo, C. Barrientos, V. M. Rayón, A. Largo, P. Redondo *Int. J. Mass Spectr.*, 2010, 295 21–25.
- <sup>141</sup> P. Redondo, A. Largo, and C. Barrientos *A&A*, 2015, 579, A125
- <sup>142</sup> A. Largo, P. Redondo, C. Barrientos, *Int. J. Quantum Chem*, 2004, 98, 355–360
- <sup>143</sup> V. A. Basiuk, K. Kobayashi, *Viva Origino*, 2002, 30 54 – 62
- <sup>144</sup> V. A. Basiuk *J. Phys. Chem. A* 2001, 105, 4252-4258
- <sup>145</sup> J.-B. Bossa, F. Duvernay, P. Theulé, F. Borget, L. d’Hendecourt, and T. Chiavassa, *A&A*, 2009, 506, 601–608.
- <sup>146</sup> A. Rimola, M. Sodupe and P. Ugliengo *Phys. Chem. Chem. Phys.*, 2010, 12, 5285–5294.
- <sup>147</sup> (a) A. Strecker, *Ann.Chem.Pharm.*, 1850, 75,27-45; (b) A. Strecker, *Ann.Chem.Pharm.*, 1854, 91, 349-351.
- <sup>148</sup> W. K. Anslow, H. King. *Org. Synth.* 1925, 4, 31 DOI: 10.15227/orgsyn.004.0031.
- <sup>149</sup> M. Wyzlic and A. H. Soloway *Tetrahedron Lett.* 1992, Vol. 33, No. 49, 7489-7490.
- <sup>150</sup> J. C. Aponte, J. E. Elsila, D. P. Glavin, S. N. Milam, S. B. Charnley, J. P. Dworkin *ACS Earth Space Chem.* 2017, 1, 3–13
- <sup>151</sup> H.-S. Zhu and J.-J. Ho *J. Phys. Chem. A* 2004, 108, 3798-3805.
- <sup>152</sup> Rimola, A., Sodupe, M., & Ugliengo, P. *Computational Study of Interstellar Glycine Formation Occurring at Radical Surfaces of Water-ice Dust Particles* 2012, *ApJ*, 754, 24
- <sup>153</sup> Fortman, S. M., Medvedev, I. R., Neese, C. F., & De Lucia, F. C., *ApJ*, 2010,725,1682
- <sup>154</sup> A. Belloche, K. M. Menten, C. Comito, H. S. P. Müller, P. Schilke, J. Ott, S. Thorwirth and C. Hieret, *A&A*, 2008, 482, 179-196.
- <sup>155</sup> Belloche, A., Müller, H. S. P., Menten, K. M., Schilke, P., & Comito, C. 2013, *A&A*, 559, A47
- <sup>156</sup> L. Kolesníková, E. R. Alonso, S. Mata, and J. L. Alonso, *ApJ Supp. Series* 2017,229:26(8pp)
- <sup>157</sup> Y. Kebukawa, Q. H. S. Chan, S. Tachibana, K. Kobayashi, and M. E Zolensky, 2017, *Sci. Adv.* 3(3), e1602093.
- <sup>158</sup> P. de Marcellus, M. Bertrand, M. Nuevo, F. Westall and L. Le Sergeant d’Hendecourt, *Astrobiology*, 2011, 11 (9), 847-854.
- <sup>159</sup> A. Shimoyama and R. Ogasawara, *Origins of life and evolution of the biosphere*, 2002, 32 (2), 165-179
- <sup>160</sup> C. Huber, W. Eisenreich, S. Hecht and G. Wächtershäuser, *Science*, 2003, 301 (5635), 938-940.
- <sup>161</sup> J. D. Sutherland, *Angew. Chem. Int. Ed.*, 2016, 55 (1), 104-121.
- <sup>162</sup> H. Ozeki, R. Miyahara, H. Ihara, S. Todaka, K. Kobayashi and M. Ohishi, *A&A*, 2017, 600, A44.
- <sup>163</sup> E. R. Alonso, L. Kolesníková and J. L. Alonso, *J.Chem.Phys.* 2017, 147, 124312.



# EXPERIMENTAL METHODOLOGY

---

*This chapter describes all the experimental techniques used in the investigation based on high-resolution rotational spectroscopy techniques in the microwave, millimeter and submillimeter wave ranges. This chapter dedicates two main sections to the laser ablation time domain microwave spectroscopy and frequency domain spectroscopy.*





## 1. LASER ABLATION TIME DOMAIN FOURIER TRANSFORM MICROWAVE SPECTROSCOPY

---

Microwave spectroscopy has long been considered to be a robust method for precise determination of structures of any gaseous molecular system of moderate size, being able to distinguish between different conformational structures of a molecule, and considered the source of the majority of gas-phase structural data known nowadays.<sup>1,2</sup> The only requirement is that the molecule has a nonzero electric dipole moment.<sup>3</sup> The research done can be classified in two different targets: the study of molecules and biomolecules, with the aim of unveiling their structure and their possible relationship structure-property, and the study of molecules candidates to be present in the interstellar medium (ISM), to enable their identification. Microwave spectroscopy in combination with supersonic jets have led to the development of two different families of techniques: those using a narrow band molecular beam (MB-FTMW)<sup>4,5,6</sup> and more recently developed, the wideband chirped pulse FTMW spectroscopy (CP-FTMW<sup>7</sup> and IMPACT FTMW<sup>8</sup>). What distinguishes the FTMW techniques is the possibility of analyzing all the populated species present in the jet separately, be they tautomers, conformers, or isotopomers, due to its extremely high resolution (sub-Doppler) and sensitivity. Also, small hyperfine effects arising from electric or magnetic interactions, such as nuclear electric quadrupole coupling, can be fully resolved, providing insight into the molecule electronic properties. Finally, the observation of tunneling doublings in the case of large amplitude motions, such as those arising from internal rotation or inversion, can give information on the intramolecular dynamics associated with these motions. These techniques have been widely used in the study of gaseous or easily vaporized compounds, weakly bounded complexes,<sup>9,10,11</sup> and even short-lived species generated in situ by electric discharges.<sup>12,13,14,15,16</sup> In our laboratory, it has been used to study axial/equatorial equilibria<sup>17,18,19,20</sup> in hydrogen-bonded complexes and weak C-H...O bonds,<sup>21,22,23,24</sup> and has been combined with electric discharges to generate and characterize new unstable compounds.<sup>25,26,27,28</sup>

The only inconvenient of working in gas-phase is the need of vaporizing the solid compounds. Some molecules, and specifically biomolecules, have extremely low vapor pressures at room temperatures, and a lot of them tend to decompose by the standard heating methods, already implemented in several laboratories.<sup>29,30,31</sup> For that reason, complete series of molecules of biological interest, such as building blocks, have escaped microwave spectroscopy studies. The pioneering works of Brown<sup>32</sup> or Suenram<sup>33</sup> and co-workers on molecular building blocks were carried out using such heating methods but, in many cases, thermal instability constituted a critical drawback. To overcome this trouble, a laser ablation system, which has been proved to be an efficient method for vaporizing solid samples,<sup>34</sup> has been developed in our laboratory in the past years coupled with microwave spectroscopic techniques, which allows vaporizing the sample using a Nd-YAG picosecond laser without perturbing or decomposing the compound. Laser-based vaporization techniques coupled with spectroscopic techniques<sup>35,36,37,38</sup> have been used for gas-phase studies. However, until recently, there have been few attempts to incorporate laser ablation into MB-FTMW spectrometers.<sup>39,40,41,42,43,44</sup> Suenram et al.<sup>39</sup> and Walker and Gerry<sup>40</sup> independently developed two laser ablation devices in combination with molecular-beam Fourier transform microwave spectroscopy (LA-MB-FTMW) to investigate the rotational spectra of metal oxides and halides. These devices failed when applied to organic solids.<sup>43,44</sup> Over the last few years, several MB-FTMW spectrometers which implement laser ablation sources to vaporize molecules in the throat of the nozzle have been configured in our laboratories. This approach, laser-ablation molecular-beam Fourier transform microwave (LA-MB-FTMW) spectroscopy,<sup>45</sup> was initially tested with several organic solids.<sup>46,47</sup> With the initial design<sup>48</sup> and progressive improvements,<sup>49,50</sup>(and references therein) relevant biomolecules have been studied to identify and characterize their most stable conformations in the gas phase. This approach has been followed in other laboratories.<sup>51</sup> More recently, laser ablation sources have been incorporated into broadband CP-FTMW spectrometers,<sup>52,53</sup> extending the application of this method to a large number of thermally fragile systems with high melting points. All the techniques

mentioned above use time-domain measurements of the emission radiation of the molecules.

A supersonic free jet produces cold, isolated, gas phase molecules, providing the suitable conditions to carry out our experiments. It is established under adiabatic conditions when high-pressure gas is expanded into a high vacuum ( $10^{-5}$ - $10^{-6}$ mbar) through a small orifice of a nozzle.<sup>54,55,56</sup> The molecules of the compound under study are seeded, after being laser ablated, in a carrier gas that usually is Neon and rarely Argon, at high pressure (1-20bar). If the pressure in the reservoir is high enough and the nozzle orifice is still much larger than the mean free path of the gas, many collisions take place in the high-density region near the orifice. These collisions induce the acceleration of the molecules in the proximity of the nozzle at the same time that increase the directionality of the flow. All this results in a jet of directed molecules with a narrow distribution of velocity and also kinetically cold, which means that only the lower energy levels of the rotational species present in the supersonic jet are populated.

In the following sections, the FTMW spectrometers used to carry out the experiments in this thesis are presented, the narrow band molecular beam coupled with laser ablation (LA-MB-FTMW)<sup>49,50</sup> (and references therein) and the broad-band Chirped pulse spectrometer coupled with laser ablation (LA-CP-FTMW).<sup>52,53</sup>

### **1.1. Narrowband Laser Ablation Molecular Beam Fourier Transform Microwave (LA-MB-FTMW) spectrometers.**

A complete description of the experimental setup of the LA-MB-FTMW spectrometers developed in this laboratory has been given elsewhere.<sup>45,50</sup> The instrument has three main blocks: a laser ablation system, an evacuated Fabry–Pérot cavity, and an FTMW spectrometer (see Fig 1.). To couple the ablation system for efficiently vaporizing the solid sample, the backside of one of the mirrors of the Fabry–Pérot resonator is modified so that it can hold a pulsed-jet nozzle especially designed. The samples are prepared as solid rods,

explained in next section. The solid sample rod is then placed vertically in the laser ablation nozzle where a focused laser beam impinges the sample laterally and produces its vaporization. The fourth (266 nm) or third (355 nm) harmonic from a picosecond (ca. 200 ps, 25 mJ/ pulse) Q-switched Nd:YAG laser has been used in the experiments reported in this thesis. Reproducibility of the ablation process is improved by a continuous translation and rotation of the sample rod, exposing new sample surface to each laser pulse.

Time-domain spectroscopy needs a source of excitation to be able to capture the emission of the molecules under study. In Fourier transform microwave spectroscopy a microwave source is used to excite the molecules, then the free induction decay FID as a consequence of the return of the population to the lower energy level is captured in the time domain, for later, using the Fourier transform, transform it to the frequency domain.

A typical experimental cycle<sup>50</sup> (see Fig. 1) starts with a pulse of carrier gas (stagnation pressures 2–8 bar of Ne, gas pulse typically 0.5 ms). After an adequate delay, a short laser pulse hits the sample rod producing, the vaporization of the solid. The ablated molecules are then seeded in the carrier gas, which expands supersonically between the two mirrors of the Fabry–Pérot resonator (see Fig 1a). In the supersonic expansion, the seeded molecules suffer a substantial cooling of the rotational and vibrational degrees of freedom, and individual conformers froze into the ground vibrational state of the corresponding potential energy well. Thus, the conformer distribution before the expansion may be preserved if the interconversion barriers between conformers are high enough. Molecular collisions gradually disappear as the expansion proceeds, in such a way that the different species can be probed in a virtually isolated environment by Fourier transform microwave (FTMW) spectroscopy. A short microwave pulse (typically 0.3  $\mu$ s) is subsequently applied, which produces a macroscopic polarization of the species in the jet (see Fig. 1b). Once the excitation pulse ceases, the molecular emission signal (FID, free induction decay) is captured in the time domain (see Fig 1c). Its Fourier transformation to the frequency domain yields the molecular rotational transitions which appear as Doppler doublets because the supersonic jet travels parallel to the resonator axis. The frequencies are calculated as the arithmetic mean of the Doppler doublets with an accuracy better than 3

kHz. A new experimental cycle can start once the vacuum cavity has been evacuated, and a repetition rate of 2 Hz is usually employed. For weak signals, hundreds of cycles must be added coherently. To probe the jet at different microwave frequencies or conduct a frequency scan, the Fabry–Pérot resonator is tuned mechanically under computer control. The timing of the whole experiment, in particular, the delay of the laser concerning the molecular pulse, is crucial for an optimum signal. Laser pulse energy is also critical.

Two different instruments that cover a different range of frequencies are present in our laboratory and used in this Ph.D. The oldest one covers from 6-18GHz,<sup>50a</sup> for standard size molecules. For large molecular systems, another instrument has been recently built which covers the range from 2 to 8GHz.<sup>50b</sup> Both have the same experimental procedure explained before and represented in fig. 1.

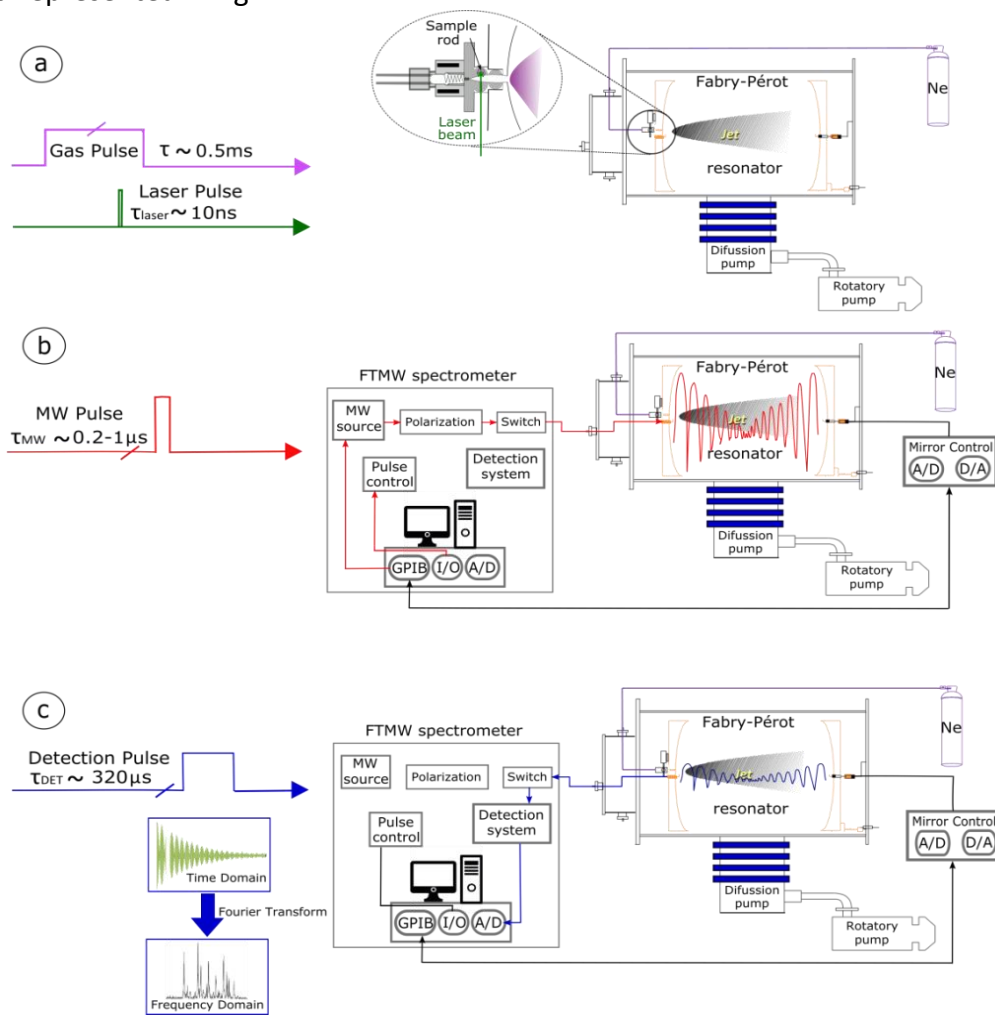


**Figure 1.** Pulse sequence for a single experimental LA-MB-FTMW cycle<sup>50</sup>

## **1.2 Broadband Laser Ablation Chirp Pulsed Fourier Transform (LA-CP-FTMW) spectrometers.**

The most recent instrument incorporated into the field of high-resolution microwave spectroscopy is a spectrometer that although follows the same principles as the MB-FTMW, in this case, the microwave polarization pulse consists on a fast linear sweep, called chirp, which contains the full range of frequencies being explored. This spectrometer, called Chirp Pulse Fourier Transform (CP-FTMW), has been developed at the University of Virginia in the group of Prof. Pate.<sup>7</sup> The most outstanding advantage of this new spectrometer is that the time of acquisition of the spectra is significantly reduced, which makes the search of the different coexisting species in the jet much more efficient. A pair of CP-FTMW spectrometers, operating in different frequency ranges, have been built in our laboratory. The first one covers from 6-18 GHz and the recently built from 2-8 GHz. In the 6-18GHz configuration, we can operate with horns (6-18GHz), situated in a perpendicular arrangement to the supersonic jet, or parabolic set (2-32GHz), situated in a coaxially to the supersonic jet (see fig 3a and 3c). The 2-8GHz instrument only operates with a set of horns, also in a perpendicular position to the supersonic jet, with an analog configuration as the 6-18GHz instrument illustrated in fig 3. As it has been implemented in the MB-FTMW spectrometer, for vaporizing solid samples it has been installed in both spectrometers a laser ablation system. It consists in both cases in a Nd:YAG picosecond laser. It operates in the fourth (266 nm) or third (355 nm) harmonic (ca. 200 ps, 25 mJ / pulse). A motor controller allows a DC motor to rotate and translate the rod up and down along the injection system to achieve the maximum exploitation of the sample.

The experiment cycle for the CP-FTMW spectrometer is as follows (fig. 3b): The experiment is triggered with a molecular pulse of 1,000  $\mu$ s duration which drives the carrier gas flow through the pulsed valve source. The laser pulse hits the solid and vaporizes the sample after an adequate delay ( $\sim$ 850  $\mu$ s). Four individual broadband-chirped excitation pulses, of 4  $\mu$ s width, are spaced by 18  $\mu$ s. Each one gives a broadband rotational spectrum, with a total of four for each injection cycle. Then, 2  $\mu$ s after each excitation pulse ceases,

the rotational free induction decay is acquired for 10  $\mu\text{s}$ . The internal pulse generator of the valve driver is used to create the digital pulses involved in the laser generation. Since the sample injection is perpendicular to the microwave field, the transit time of the polarized molecular jet is quite short and linewidths of about 100 kHz full-width-half-maximum (FWHM) are achieved.

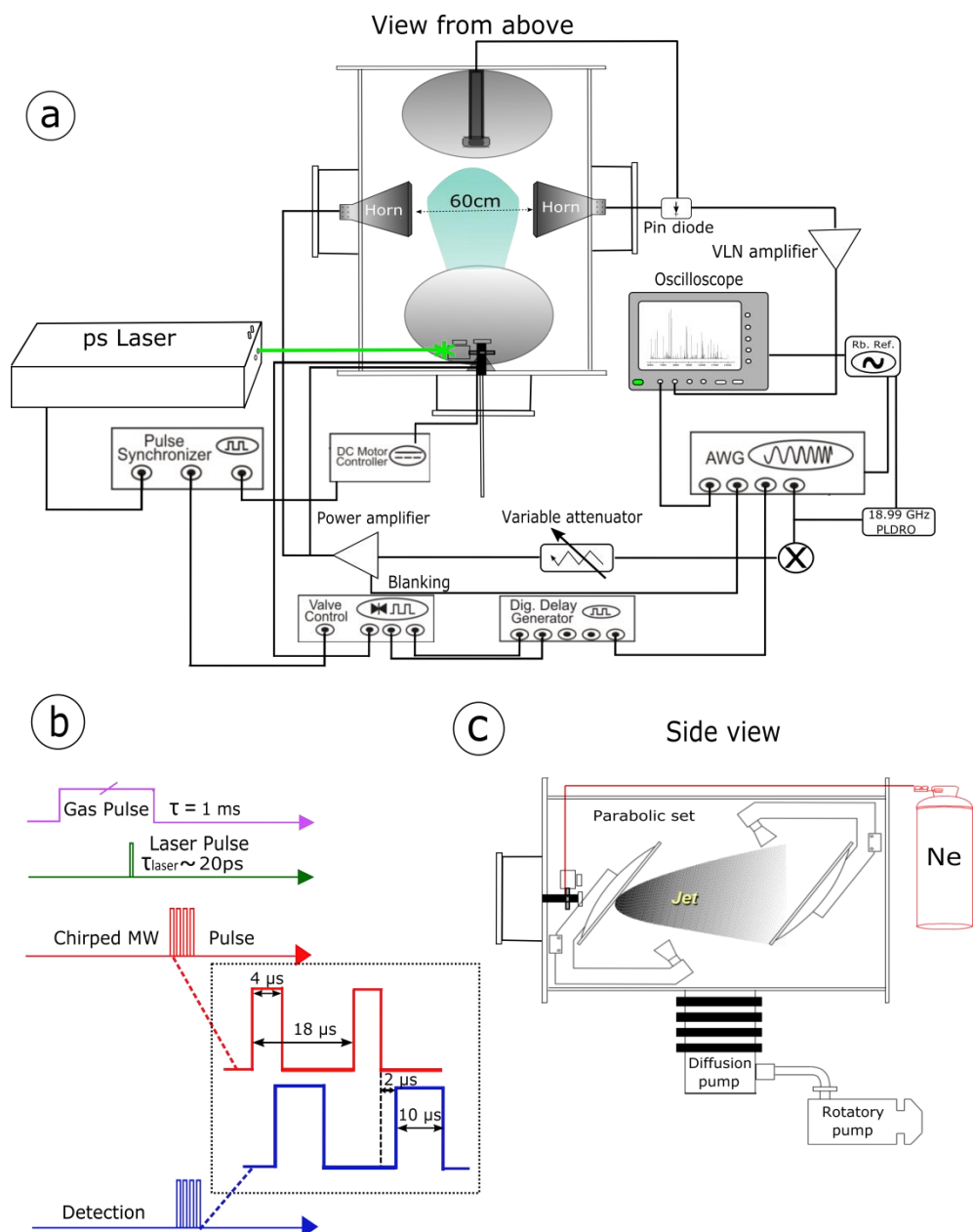


**Figure 2.** (a) Schematic of the CP-FTMW spectrometer operating in the 6-18GHz bandwidth. (b) Experiment cycle for LA-MB-FTMW spectrometer. (c) Side view of the LA-CP-FTMW spectrometer where the parabolic set is appreciated.

## 2. FREQUENCY DOMAIN SPECTROSCOPY

---

Another topic of the investigation is the study of molecules which are potential candidates to be present in the ISM. The purpose of this topic is to measure the rotational spectra of these molecules in the same range in which molecules emit radiation from ISM, and it is captured by radio telescopes, to be able to identify the molecule. The laboratory data is a necessary tool to carry out this task. However, the observations of the ISM are at high frequencies, so the spectrometers employed need to cover high frequencies ranges in the frequency domain to do a rotational analysis of the molecules that astrophysics could use to reproduce the spectrum with the ISM conditions and compare with the surveys for possible identification. Two types of frequency domain spectrometers have been used in our group to pursue the possible identification of the molecules candidates to be in the ISM: Stark modulation and frequency modulation (FM) spectrometers. Both spectrometers work at room temperature, which enables the identification of not only the ground state of a molecule but even excited vibrational states. The millimeter and sub-millimeter wave spectrometers cover from 50-1080 GHz within the single pass and double pass configurations. The Stark spectrometer<sup>57</sup> covers the range 12 to 110GHz. It is very useful when it comes to assigning excited vibrational states of a molecule, i.e., aminoacetonitrile (see chapter XI), because these transitions have a characteristic shape that matches the ones of the ground state, due to the M-degeneracy of the rotational transitions when an electric field is applied.

In the frequency domain spectroscopy, we vary the frequency with a radiation source and measure simultaneously the power absorbed by the sample under study. In contrast to the time domain spectroscopy, in this kind of spectroscopy, the experiment takes place at room temperature, i.e., without supersonic expansion. The radiation is coming from the signal generator and passes through a gas cell filled with the sample. At the room temperature of the experiment, pure rotational spectra in excited vibrational states can be observed and measured. Frequency domain spectroscopies are the most suitable to study



molecules of astrophysical interest. It allows the direct comparison between the laboratory data and the astrophysical observations obtained from radio telescopes, allowing the identifications of new molecules present in the interstellar medium.

### **2.1. Frequency Modulation Millimeter and Submillimeter-wave spectroscopies.**

Two configurations of the millimeter and submillimeter wave spectrometer have been built in our laboratory at the University of Valladolid and published elsewhere.<sup>58</sup> A single pass configuration which covers a range from 50 to 170 GHz and a double pass configuration which covers a range from 170 to 1080 GHz. The microwave source is a frequency modulated signal generator (Agilent E8257D) operating from 250 kHz to 20 GHz, phase locked to a Rubidium standard. In the double pass configuration (Fig. 3a), the microwave frequency is multiplied by 4, 6 or 9 using amplifier multiplier chains (VDI, Inc.), to reach the frequency ranges from 50 to 170 GHz. The optical path length of the free space cell of 3.6 m is doubled using a polarization grid (Millitech, Inc.) and a home-made rooftop mirror. Solid-state Schottky diodes detectors detect the output signal.

Rotational spectra above 170 GHz are measured in a single pass mode configuration shown in Fig. 3b using parabolic metal mirrors (Edmund Optics, Inc.) as focusing optical elements. An active VDI sextupler AMC WR9.0 (average power of 25 mW) is initially used to produce a suitable frequency input for additional active and passive multipliers (VDI, Inc.). Using combinations of these multipliers, frequencies up to 1080 GHz can be reached. A broadband Quasi-Optical Detector (QOD) from VDI, Inc. and liquid helium cooled silicon bolometer (Infrared Laboratories, Inc.) is used as the detection elements. For both configurations, the detected frequency-modulated signal is amplified and sent to the lock-in amplifier (SR510, Stanford Research Systems, Inc.) where  $2f$  detection is applied, where  $f$  is the modulation frequency, to increase the sensitivity of the measurements. The modulation frequency of 10.2 kHz is used for the non-cooled (room temperature) detectors while 90 Hz for the cryogenic detector and the modulation depth is determined to give the

Doppler line width. Standard GPIB connects the generator and the lock-in amplifier to the computer and controlled by a laboratory developed LabVIEW program.

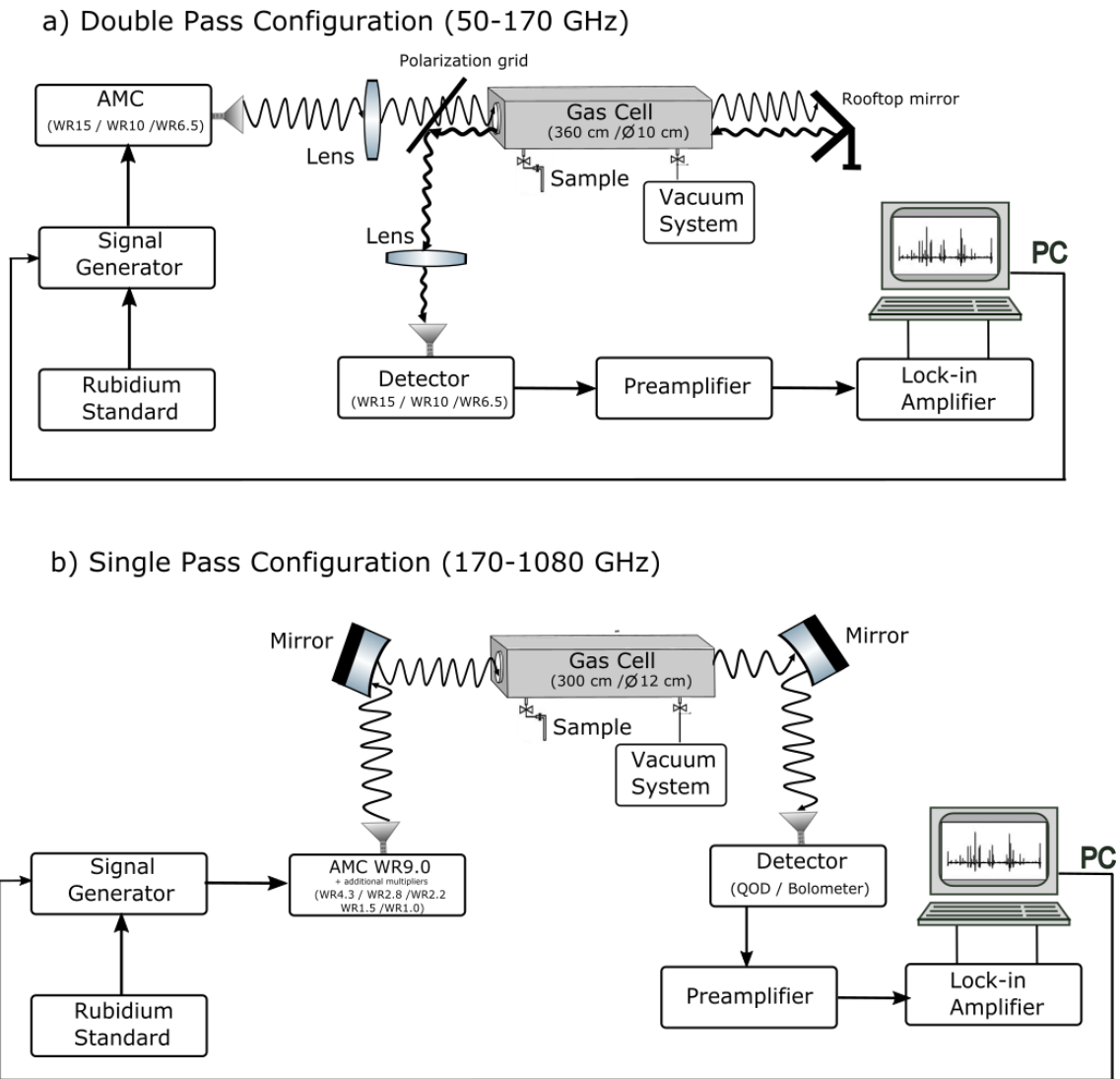


**Figure 3.** Schemes of the double (a) and single path (b) configurations of the millimeter- and submillimeter wave spectrometer at the University of Valladolid.

**2.2 Stark-Modulation Microwave and Millimeter-Wave Spectrometers.**

A scheme of our upgraded Stark-modulation spectrometer used in the present investigation is shown in Figure 4. The spectrometer covers the frequency range from 12 to 110 GHz using either backward wave oscillators (BWOs) or an Agilent synthesizer as microwave sources. In the first case, three BWOs are available, providing the following frequency outputs: 12.5-18GHz, 18-26.5GHz, and 26.5-40 GHz (see Figure 4). The frequency stabilization of the BWOs is achieved using a phase-lock loop using an external frequency synthesizer, harmonic mixer, and signal synchronizer with a constant IF of 20MHz. The signal from stabilized

BWOs enters the 1.95m long X-band waveguide directly, or an additional passive multiplier V-2X (Spacek Labs) can be implemented to double the output of the highest-frequency BWO (see Figure 4). In the second case, an Agilent synthesizer (250 kHz–20 GHz) is used to drive the amplifier-multiplier chains WR15 and WR10 (VDI, Inc.) with multiplication factors

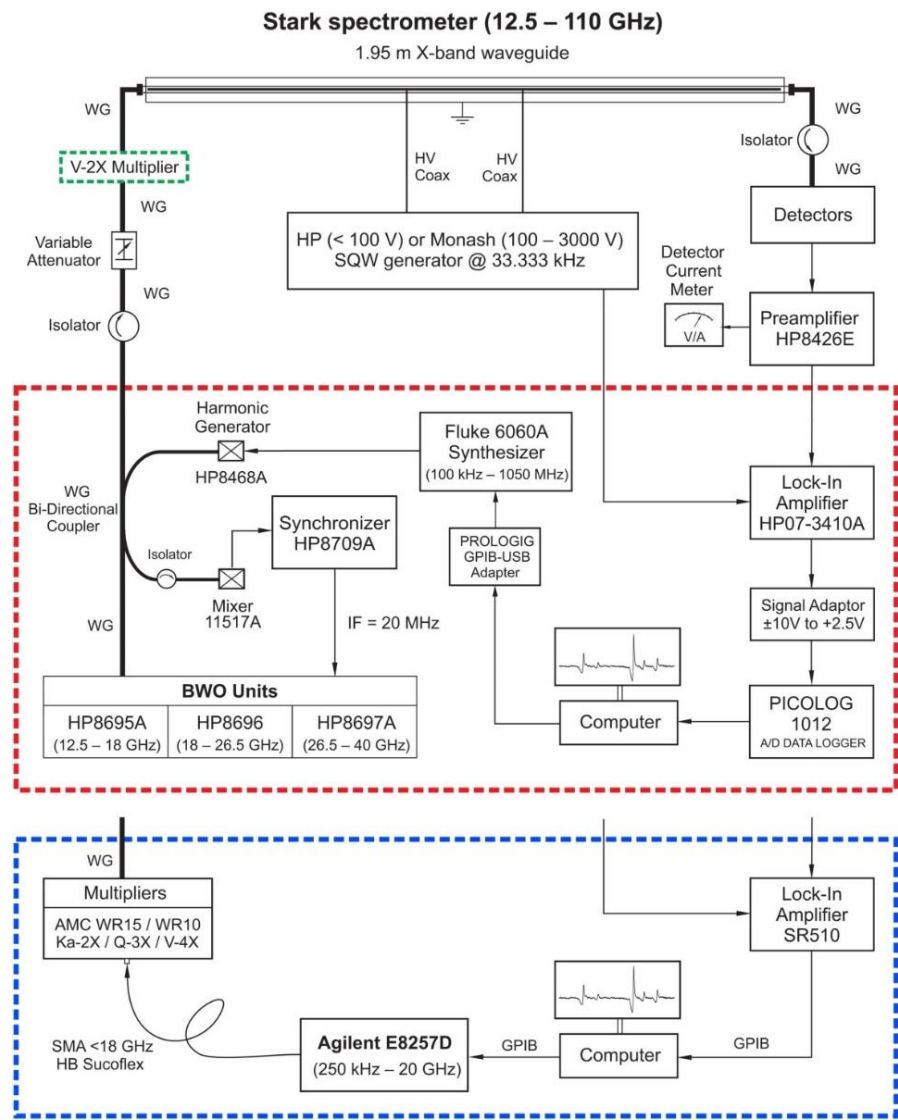


**Figure 4.** Stark-modulation spectrometer based on BWO (red rectangle) or Agilent microwave sources (blue rectangle).

of four and six to reach the frequency ranges of 50-75GHz and 75-110 GHz, respectively. Another option is to connect passive multipliers Ka-2X, Q-3X, and V-4X (Spacek Labs) that allow us to record the spectra in the 26-40GHz, 33-50GHz, and 50-75GHz regions, respectively. Modulation voltages up to 3000V with a 33.3 kHz modulation frequency can be applied to the septum of the waveguide. A Stark-modulated signal is detected by solid-state zero-bias Schottky-diode detectors (50-110 GHz) or HP crystal detectors (12.5-50GHz), pre-amplified and send to a lock-in amplifier where the phase-sensitive detection is applied.

### 3. COMPUTATIONAL METHODS

---

Although the research has been experimental, computational methods have also played an essential role in it. To obtain the structural information that the rotational spectroscopy gives us, the help provided by computational theory is precious due to the conformational mapping that we can obtain because of it when the complexity of the molecules does not allow the chemical intuition.

The standard procedure in the computational calculations using Gaussian 09<sup>59</sup> ran in my thesis is as follows:

A first conformational search is done using semi-empirical methods<sup>60,61</sup> like PM3 and AM1, low-cost methods that allow the search of the minima in the potential energy surface, obtaining a first conformational map of the molecule. The second round of computational calculations is run to optimize the structures of the conformers obtained in the semi-empirical calculations. Usually, this is done with a higher level of computational methods, DFT (B3LYP) and ab initio (MP2). To optimize the time of calculation a first B3LYP<sup>62</sup> method with the Pople basis set (6-31G(d,p) is used followed by a final MP2<sup>63</sup> with the standard Pople basis set 6-311++G(d,p). Recently, we have incorporated in DFT method a new term, the Grimme dispersion correction,<sup>64</sup> which gives us better performance in the calculations due to more precision in the dispersion forces.

## 4. REFERENCES

---

- <sup>1</sup> Structure data of free polyatomic molecules, vol 7 (1976), vol 15 (1987), vol 21 (1992), vol 23 (1995), vol 25A (1998), vol 25B (1999), vol 25C (2000), vol 25D (2003), vol 28A (2006), vol 28B (2006), vol 28C (2007), vol 28D (2007). Springer, Berlin.
- <sup>2</sup> Graner G, Hirota E, Iijima T, Kuchitsu K, Ramsay DA, Vogt J, Vogt N (1998) Structure data of free polyatomic molecules. Basic data. Springer, Berlin, 214 pp.
- <sup>3</sup> Gordy W, Cook RL (1984) Microwave molecular spectra. Wiley, New York.
- <sup>4</sup> Balle TJ, Flygare WH (1981) *Rev Sci Instrum* 52:33
- <sup>5</sup> Grabow J-U, Stahl W (1990) *Z Naturforsch A* 45:1043
- <sup>6</sup> Andresen U, Dreizler H, Grabow JU, Stahl W (1990) *Rev Sci Instrum* 61:3694
- <sup>7</sup> Brown GG, Dian BC, Douglass KO, Geyer SM, Shipman ST, Pate BH (2008) *Rev Sci Instrum* 79:053103
- <sup>8</sup> Grabow J-U, Mata S, Alonso JL, Peña I, Blanco S, López JC, Cabezas C (2011) *Phys Chem Chem Phys* 13:21063
- <sup>9</sup> Leopold KR, Fraser GT, Novick SE, Klemperer W (1994) *Chem Rev* 94:1807
- <sup>10</sup> Bauder A (1996) In: Fausto R (ed) *Low temperature molecular spectroscopy*. Kluwer, The Netherlands, pp 271–289
- <sup>11</sup> Legon AC, Millen DJ (1986) *Chem Rev* 86:635
- <sup>12</sup> Endo Y, Kohguchi H, Ohshima Y (1994) *Faraday Discuss* 97:341
- <sup>13</sup> McCarthy MC, Thaddeus P (2001) *Chem Soc Rev* 30:177
- <sup>14</sup> Sutter DH, Dreizler H (2001) *Z Naturforsch A Phys Sci* 56:425
- <sup>15</sup> Gerry MCL (1992) *Chem Phys Lett* 188:213
- <sup>16</sup> Brupbacher B, Brupbacher T (1999) *J Chem Phys* 111:6300
- <sup>17</sup> Antolínez S, López JC, Alonso JL (1999) *Angew Chem Int Ed* 38:1772
- <sup>18</sup> Sanz ME, López JC, Alonso JL (1999) *Chem Eur J* 5:3293
- <sup>19</sup> Sanz ME, Lesarri A, López JC, Alonso JL (2001) *Angew Chem Int Ed* 40:935
- <sup>20</sup> Antolínez S, López JC, Alonso JL (2001) *ChemPhysChem* 2:114
- <sup>21</sup> Alonso JL, Antolínez S, Blanco S, Lesarri A, López JC, Caminati W (2004) *J Am Chem Soc* 126:3244
- <sup>22</sup> Caminati W, López JC, Alonso JL, Grabow J-U (2005) *Angew Chem Int Ed* 44:2
- <sup>23</sup> Ottaviani P, Caminati W, Favero LB, Blanco S, López JC, Alonso JL (2006) *Chem Eur J* 12:915
- <sup>24</sup> López JC, Caminati W, Alonso JL (2006) *Angew Chem Int Ed* 45:290
- <sup>25</sup> Blanco S, Sanz ME, Mata S, Lesarri A, López JC, Dreizler H, Alonso JL (2003) *Chem Phys Lett* 375:355
- <sup>26</sup> Blanco S, Sanz ME, Lesarri A, López JC, Alonso JL (2004) *Chem Phys Lett* 397:379
- <sup>27</sup> Blanco S, López JC, Sanz ME, Lesarri A, Dreizler H, Alonso JL (2004) *J Mol Spectrosc* 227:202
- <sup>28</sup> Sanz ME, Alonso JL, Blanco S, Lesarri A, López JC (2004) *Astrophys J* 621:L157
- <sup>29</sup> Suenram RD, Lovas FJ, Fraser GT (1988) *J Mol Spectrosc* 127:472
- <sup>30</sup> Welzel A, Stahl W (1999) *Phys Chem Chem Phys* 1:5109
- <sup>31</sup> Blanco S, López JC, Alonso JL, Ottaviani P, Caminati W (2003) *J Chem Phys* 119:880
- <sup>32</sup> Brown RD, Godfrey PD, Storey JWV, Bassez MPJ (1978) *Chem Soc Chem Commun* 547–548
- <sup>33</sup> Suenram RD, Lovas FJ (1978) *J Mol Spectrosc* 72:372
- <sup>34</sup> Levis RJ (1994) *Annu Rev Phys Chem* 45:483
- <sup>35</sup> Simard B, Mitchell SA, Humphries MR, Hackett PA (1988) *J Mol Spectrosc* 129:186
- <sup>36</sup> Cable JR, Tubergen MJ, Levy DH (1989) *J Am Chem Soc* 111:9032
- <sup>37</sup> Barnes M, Fraser MM, Hajigeorgiou PG, Merer AJ, Rosner SD (1995) *J Mol Spectrosc* 170:449
- <sup>38</sup> Elam JW, Levy DH (1998) *J Phys Chem B* 102:8113
- <sup>39</sup> Suenram RD, Lovas FJ, Fraser GT, Matsumura K (1990) *J Chem Phys* 92:4724
- <sup>40</sup> Walker KA, Gerry MCL (1997) *J Mol Spectrosc* 182:178
- <sup>41</sup> Oshima Y, Endo Y (1993) *Chem Phys Lett* 213:95
- <sup>42</sup> Low RJ, Varberg TD, Sonnely JP, Auty AR, Howard BJ, Brown JM (1993) *J Mol Spectrosc* 161:499

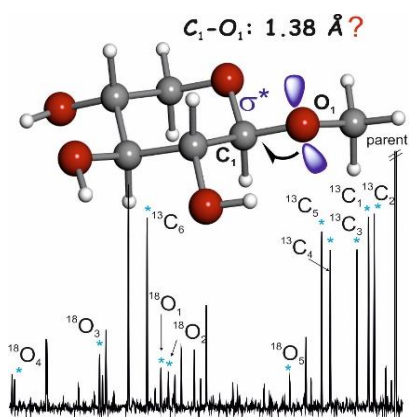
- 
- <sup>43</sup> Kretschmer U, Consalvo D, Knaack A, Schade W, Stahl W, Dreizler H (1996) *Mol Phys* 87:1159
- <sup>44</sup> Lovas FJ, Kawashima Y, Grabow J-U, Suenram RD, Fraser GT, Hirota E (1995) *Astrophys J Lett* 455:L201
- <sup>45</sup> Lesarri A, Mata S, López JC, Alonso JL (2003) *Rev Sci Instrum* 74:4799
- <sup>46</sup> Antolínez S, Lesarri A, Mata S, Blanco S, López JC, Alonso JL (2002) *J Mol Struct* 612:125
- <sup>47</sup> Lesarri A, Mata S, Blanco S, López JC, Alonso JL (2004) *J Chem Phys* 120:6191
- <sup>48</sup> Lesarri A, Mata S, Cocinero EJ, Blanco S, López JC, Alonso JL (2002) *Angew Chem Int Ed* 41:4673
- <sup>49</sup> Blanco S, Sanz ME, López JC, Alonso JL (2007) *Proc Natl Acad Sci U S A* 104:20183
- <sup>50</sup> a. Alonso JL, Pérez C, Sanz ME, López JC, Blanco S (2009). *Phys Chem Chem Phys* 11:617;  
b. Bermúdez C, Mata S, Cabezas C, Alonso J.L. (2014) *Angew. Chem. Int. Ed.* 53, 11015–11018
- <sup>51</sup> Cocinero EJ, Lesarri A, Ecija P, Basterretxea FJ, Grabow J-U, Fernández JA, Castaño F (2012) *Angew Chem Int Ed* 51:3119–3124
- <sup>52</sup> Mata S, Peña I, Cabezas C, López JC, Alonso JL (2012) *J Mol Spectrosc* 280:91–96
- <sup>53</sup> Peña I, Daly AM, Cabezas C, Mata S, Bermúdez C, Niño A, López JC, Grabow J-U, Alonso JL (2013) *J Phys Chem Lett* 4:65–69
- <sup>54</sup> Levy, D. H. (1981) *Science* 214, 263
- <sup>55</sup> Levy, D. H., Wharton, L. and Smalley, R. E. (1977) in *Chemical and Biochemical Applications of Lasers*, Vol. II (Moore, C. B., ed.), pp. 1–41, Academic Press, New York.
- <sup>56</sup> Hayes, J. M. and Small, G. J. (1983) *Anal. Chem.* 55, 565A.
- <sup>57</sup> Kolesniková, L., Alonso E.R., Mata S., Alonso J.L., (2017), *ApJS*, 229:26 (8pp)
- <sup>58</sup> Daly, A., Kolesniková, L., Mata, S., & Alonso, J.L. (2014), *J. Mol. Spectrosc.*, 306, 11
- <sup>59</sup> Gaussian 09, Revision A.02, M. J. Frisch, G. W. Trucks, H. B. Schlegel, G. E. Scuseria, M. A. Robb, J. R. Cheeseman, G. Scalmani, V. Barone, G. A. Petersson, H. Nakatsuji, X. Li, M. Caricato, A. Marenich, J. Bloino, B. G. Janesko, R. Gomperts, B. Mennucci, H. P. Hratchian, J. V. Ortiz, A. F. Izmaylov, J. L. Sonnenberg, D. Williams-Young, F. Ding, F. Lipparini, F. Egidi, J. Goings, B. Peng, A. Petrone, T. Henderson, D. Ranasinghe, V. G. Zakrzewski, J. Gao, N. Rega, G. Zheng, W. Liang, M. Hada, M. Ehara, K. Toyota, R. Fukuda, J. Hasegawa, M. Ishida, T. Nakajima, Y. Honda, O. Kitao, H. Nakai, T. Vreven, K. Throssell, J. A. Montgomery, Jr., J. E. Peralta, F. Ogliaro, M. Bearpark, J. J. Heyd, E. Brothers, K. N. Kudin, V. N. Staroverov, T. Keith, R. Kobayashi, J. Normand, K. Raghavachari, A. Rendell, J. C. Burant, S. S. Iyengar, J. Tomasi, M. Cossi, J. M. Millam, M. Klene, C. Adamo, R. Cammi, J. W. Ochterski, R. L. Martin, K. Morokuma, O. Farkas, J. B. Foresman, and D. J. Fox, Gaussian, Inc., Wallingford CT, 2016.
- <sup>60</sup> Stewart J. J. P., (1989) *Journal of Computational Chemistry*, 10, 209-220.
- <sup>61</sup> Dewar M. J. S., Zebisch E. G., Healy E. F., Stewart J. J. P., (1985) *Journal of the American Chemical Society*, 107, 3902-3909.
- <sup>62</sup> Stephens P. J., Devlin F. J., Chabalowski C. F., Frisch M. J., (1994) *The Journal of Physical Chemistry*, 98, 11623-11627(23)
- <sup>63</sup> Moller C., Plesset M. S., (1934) *Physical Review*, 46, 0618-0622.
- <sup>64</sup> Grimme S., Antony J., Ehrlich S., and Krieg H. (2010) *J. Chem. Phys.* , 132, 154104

# CHAPTER I.

## A Structural Expression of *Exo*-Anomeric Effect

---

Adapted from: *Journal of Physical Chemistry Letters*, 2016, 7, 845–850



Structural signatures for *exo*-anomeric effect have been extracted from the archetypal methyl- $\beta$ -D-xyloside using broadband Fourier transform microwave spectroscopy combined with laser ablation. Spectrum analysis allows the determination of a set of rotational constants, which has been unequivocally attributed to conformer  $cc$ - $\beta$ - $^4C_1$   $g$ -, corresponding to the global minimum of the potential energy surface, where the aglycon residue ( $CH_3$ ) orientation contributes towards maximization of the *exo*-anomeric effect. Further analysis allowed the determination of the  $r_s$  structure, based on the detection of eleven isotopologues – derived from the presence of six  $^{13}C$  and five  $^{18}O$  atoms - observed in their natural abundances. The observed glycosidic  $C_1-O_1$  bond length decrease ( $1.38 \text{ \AA}$ ) can be interpreted in terms of the *exo*-anomeric effect. As such, the *exo*-anomeric effect presents itself as one of the main driving forces controlling the shape of many biologically important oligosaccharides.





The anomeric effect refers to the propensity of polar substituents - bonded to an anomeric center - to occupy the axial ( $\alpha$ -anomer) position rather than the equatorial ( $\beta$ -anomer) as would normally be expected in a monosaccharide chair conformation.<sup>1-3</sup> Such effect is thought to arise from either molecular orbital interactions or electrostatic interactions.<sup>4-7</sup> The most favored and accepted molecular orbital framework revolves around an interaction between an axially-located lone pair of electron in a molecular orbital ( $n$ ) at the  $O_5$  atom and an unoccupied anti-bonding molecular orbital ( $\sigma^*$ ) of the  $C_1-O_1$  bond (see axial acetals in Fig.1). Such antiperiplanar arrangement for the axial orientation favors this  $n \rightarrow \sigma^*$  hyperconjugative interaction (back-bonding effect). Furthermore, if the axial exocyclic alkoxy -O-R group (aglycon) adopts the appropriate conformation, there is again an antiperiplanar arrangement of a molecular orbital ( $n$ ) on  $O_1$  and an unoccupied  $\sigma^*$  molecular orbital along the  $C_1-O_5$  bond giving rise also to an extra anomeric effect<sup>8</sup> (see Fig. 1). Although no physical difference exists between both anomeric effects, two different terms, *endo*-and *exo*-anomeric, were introduced.<sup>2,8</sup> The standard *endo*-anomeric provides a driving force for the preference for the axial orientation of the aglycon in the six-membered glycopyranosides whereas the *exo*-anomeric effect influences the configuration adopted by the aglycon of the glycoside.

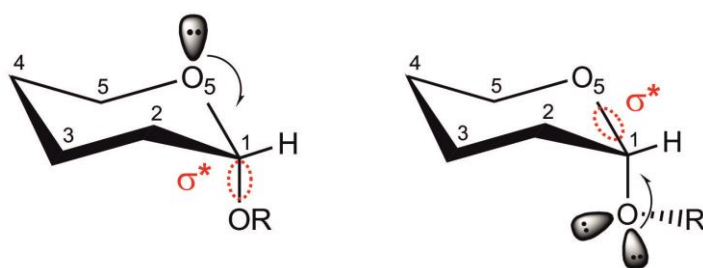


**Figure 1.** Axial acetals showing the *endo*-anomeric effect (left) which stabilizes the axial anomer and the antiperiplanar arrangement of the *exo*-cyclic alkoxy group for the *exo*-anomeric effect (right).

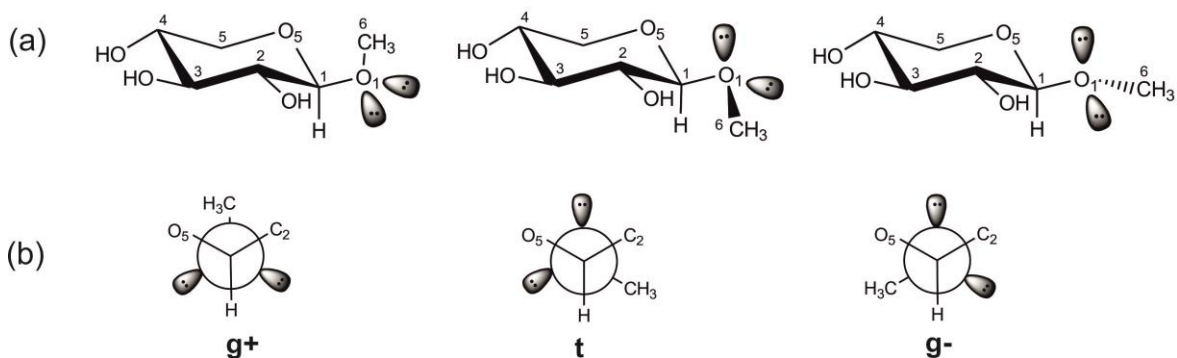


**Figure 2.** (a) The three plausible conformations of the aglycon in methyl β-D-xyloside with a <sup>4</sup>C<sub>1</sub> chair configuration (C<sub>4</sub> carbon is above the reference plane C<sub>2</sub>C<sub>3</sub>C<sub>5</sub>O<sub>5</sub> and C<sub>1</sub> carbon is found below it); the lone pair electrons on O<sub>1</sub> are shown as in sp<sup>3</sup> orbitals. (b) Newman projections along C<sub>1</sub>-O<sub>1</sub> bond; the symbols g<sup>+</sup> (+60°), t (180°) and g<sup>-</sup> (-60°) have been used to denote the values of the torsion angle φ = C<sub>6</sub>-O<sub>1</sub>-C<sub>1</sub>-O<sub>5</sub>.

Oppositely, in an equatorial acetal (see Fig. 2) -where no contribution from the *endo*-anomeric effect exists-, it is the *exo*-anomeric effect that prevails and thus dictates the preferred conformation of the alkoxy group at the anomeric C<sub>1</sub> carbon atom, seemingly being responsible for the conformational preferences around glycopyranoside linkages as well as the helical shape of various polysaccharide chains. Thus, any considerations on the conformational properties of glycopyranosides would require the determination of the torsional angle φ = C<sub>6</sub>-O<sub>1</sub>-C<sub>1</sub>-O<sub>5</sub> defined by the aglyconic carbon and the oxygen atom of pyranose ring (Fig. 2b). This is of paramount importance for shape determination of many biologically important oligosaccharides.<sup>9</sup>

A large volume of experimental results on glycosides, dating back to those obtained in condensed phases by NMR<sup>10</sup> and X-ray investigations,<sup>11,12</sup> already pointed towards the existence of *endo*- and *exo*-anomeric effects in the observed conformational preferences. Conversely, the existence of an *exo*-anomeric effect was later brought into question in the literature through a series of studies on C-glycosides -where the glycosidic oxygen atom had been replaced by a methylene group-<sup>13,14</sup> and were found to exhibit the same preferred conformations as their O-glycosides analogues, despite the inexistence of the lone pair effects.

It is generally accepted that all above-mentioned results in condensed phases are strongly influenced by environmental effects<sup>15</sup> associated with the solvent or crystal lattice interactions that may subtly mask the anomeric effect. As such, investigations have been recently conducted in isolation conditions of the gas phase, in order to overcome such shortcomings. The presence of the anomeric effect has been probed *via* “ion-dip” vibrational spectroscopy (IRID) of the doubly and triply hydrated  $\alpha$  and  $\beta$  anomers of phenyl D-mannopyranoside isolated under molecular beam conditions.<sup>16</sup> Subtle differences in the vibrational signatures of both hydrated  $\alpha$  and  $\beta$  anomers were interpreted by complementary theoretical calculations and ascribed to the anomeric effect. In the same context, complexes formed between the N-Acetyl-L-phenylalanine methylamide and the  $\alpha$  or  $\beta$ -anomers of D-galactose isolated in the gas phase were used to sense the *exo*- and *endo*-anomeric effect using a combination of laser spectroscopy and computational analysis.<sup>17</sup> Surprisingly, these results were recently brought into question by Wang et al.,<sup>18</sup> who provided strong computational evidence showing that the observed spectral changes attributed to the anomeric effect simply come from the conformational differences between the  $\alpha$ - and  $\beta$ -anomers.

The above scenario highlights the importance of a benchmark investigation on glycosides to determine its intrinsic conformational and structural properties, thus avoiding intricate and rather speculative spectroscopic interpretations. In the present work, we report the first experimental investigation of the archetypal acetal methyl- $\beta$ -D-xyloside ( $C_6H_{12}O_5$ , Fig.2) isolated in gas phase, probing for convincing structural evidences of the *exo*-anomeric effect. The major problem of working with gas-phase carbohydrates due to the labile nature of their solid samples and inherent vaporization difficulties has been overcome. Indeed, in latest years, a number of powerful strategies have been established in our lab, involving the use of laser ablation for vaporizing intact molecules of solid samples of a biomolecule into gas phase, followed swiftly by a rapid cooling in a free jet expansion, thus stabilize their conformational panorama, and highly selective Fourier-transform microwave spectroscopy to allow probing of such structures.<sup>19</sup> Such

methodology constitutes a powerful tool in gas phase studies of isolated sugars, as it has been recently shown for the representative D-glucose<sup>20</sup> and many other monosaccharides.<sup>21-26</sup> The combination of broadband chirped pulse Fourier-transform microwave techniques<sup>27</sup> (CP-FTMW) and picosecond laser ablation (LA),<sup>28</sup> has allowed the conformational study of methyl  $\beta$ -D-xyloside. The broadband rotational spectrum of laser ablated methyl  $\beta$ -D-xyloside comprehended within the 6-12 GHz region is shown in Figure 3. Apart from known photofragmentation lines common to other carbohydrates, the spectrum is dominated by intense  $\mu_a$ -type R-branch progressions belonging to a rotamer exhibiting a characteristic pattern of a nearly prolate asymmetric rotor. Much weaker  $\mu_b$ - and  $\mu_c$ -type transitions were also assigned and measured. A total of 64 transitions (Table S1 in the Supporting Information) were included in a rigid rotor analysis<sup>29</sup> to give the set of experimental rotational constants collected in the first column of Table 1.

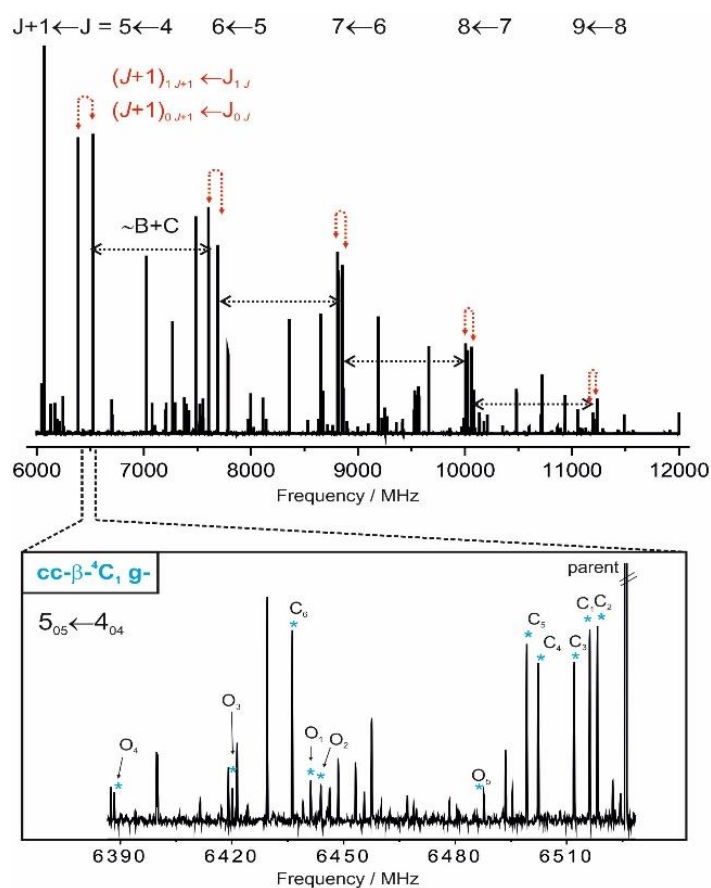
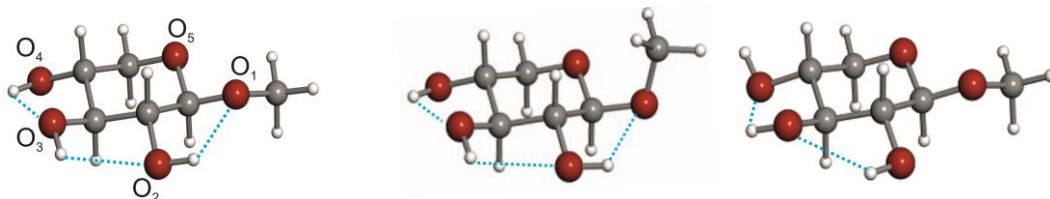


**Figure 3.** Broadband spectrum of methyl  $\beta$ -D-xyloside from 6 to 12 GHz (110000 fids) showing the intense sets of  $\mu_a$ -type R-branch transitions separated approximately  $B + C$  with  $J$  ranging from 4 to 8, belonging to the observed rotamer. a-type  $(J+1)_{1,J+1} \leftarrow J_{1,J}$  and  $(J+1)_{0,J+1} \leftarrow J_{0,J}$  pairs of rotational progressions (becoming degenerated with increasing  $J$ ) are indicated. The photofragmentation products have been discarded in the analysis. Inset: the  $5_{05} \leftarrow 4_{04}$  rotational transition for the six  $^{13}\text{C}$  and five  $^{18}\text{O}$  isotopologues of the observed cc- $\beta$ - $^4\text{C}_1$  g- conformer.

**Table 1.** Experimental Rotational Parameters for the Observed Rotamer of Methyl  $\beta$ -D-xyloside in Comparison with Those Predicted *Ab Initio*<sup>a</sup> for the Most Stable Conformers (within 1400 cm<sup>-1</sup>).

	Experimental	cc- $\beta$ - <sup>4</sup> C <sub>1</sub> g- <sup>g</sup>	cc- $\beta$ - <sup>4</sup> C <sub>1</sub> g+	c- $\beta$ - <sup>4</sup> C <sub>1</sub> g-
A <sup>b</sup>	1766.25692 (72) <sup>e</sup>	1771.6	1713.1	1774.5
B	829.25439 (24)	833.0	868.7	829.1
C	592.91443 (17)	595.4	638.0	595.3
\mu <sub>a</sub>	Intense <sup>f</sup>	2.1	1.4	2.0
\mu <sub>b</sub>	Weak	0.5	0.9	2.9
\mu <sub>c</sub>	Weak	0.8	0.9	0.5
$\Delta E^c$	-	0	1106	1448
$\Delta G^d$	-	0	1069	1230



<sup>a</sup> MP2/6-311++G(d,p) level of theory. <sup>b</sup> A, B, and C represent the rotational constants (in MHz); |\mu<sub>a</sub>|, |\mu<sub>b</sub>| and |\mu<sub>c</sub>| are the absolute values of electric dipole moment components (in D). <sup>c</sup> Relative electronic energies (in cm<sup>-1</sup>). <sup>d</sup> Gibbs energies calculated at 298 K (in cm<sup>-1</sup>). <sup>e</sup> Standard error in parentheses in the units of the last digit. <sup>f</sup> Qualitative intensity of the type of spectrum observed. <sup>g</sup> The notation used to label the different conformers include the symbols “c” or “cc” to indicate a clockwise or counterclockwise configuration of the adjacent OH bonds, respectively, “ $\beta$ ” to label the anomer type, “<sup>4</sup>C<sub>1</sub>” to denote the pyranose chair form and “g+” or “g-” to label the torsion angle  $\varphi = C_6-O_1-C_1-O_5$ .

In the identification of the observed rotamer as a particular conformer of methyl  $\beta$ -D-xyloside, structures exhibiting the most stable <sup>4</sup>C<sub>1</sub> chair configuration, with all substituents in the equatorial orientation, were considered first. *Ab initio* calculations (MP2/6-311++G(d,p)),<sup>30</sup> were carried out on the three plausible configurations of the aglycon defined through the torsion angle  $\varphi$  (see Fig.2). The theoretical requirement for a maximum *exo*-anomeric effect corresponds to that where the aglycon is oriented in such a way that the O<sub>1</sub> sp<sup>3</sup> (n) orbital is in an anti-periplanar orientation with regard to the O<sub>5</sub>-C<sub>1</sub> bond, thus maximizing the overlap with the  $\sigma^*$  orbital. Two such orientations are possible, displayed in the g+ ( $\varphi \sim 60^\circ$ ) and g- ( $\varphi \sim -60^\circ$ ) configurations. Configuration t ( $\varphi \sim 180^\circ$ ) is *a priori* disfavored by ordinary steric interactions and it is not comprised in the three pyranose forms cc- $\beta$ -<sup>4</sup>C<sub>1</sub> g-, cc- $\beta$ -<sup>4</sup>C<sub>1</sub> g+ and c- $\beta$ -<sup>4</sup>C<sub>1</sub> g- shown in Table 1 predicted in

an energy window of  $1400\text{ cm}^{-1}$ . A first comparison between experimental and theoretical rotational constants values collected in Table 1 clearly indicates that the experimental rotational constants values are consistent with those predicted for conformers **cc- $\beta$ - $^4\text{C}_1$  g-** and **c- $\beta$ - $^4\text{C}_1$  g-**. Both conformers present the same aglycon “g-” configuration stabilized by the *exo*-anomeric effect but differ in the intramolecular H-bond networks that take place for each configuration, which are strongly reinforced by  $\sigma$ -hydrogen-bond cooperativity.<sup>31</sup> Thus, the conformational analysis of methyl  $\beta$ -D-xyloside requires the consideration of the subtle variation in hydroxyl arrangement which is relevant to distinguish between different conformations. Hence, the most stable form **cc- $\beta$ - $^4\text{C}_1$  g-** presents a counter-clockwise (*cc*) arrangement of three intramolecular hydrogen bonds  $\text{O}_4\text{H}\cdots\text{O}_3\text{H}\cdots\text{O}_2\text{H}\cdots\text{O}_1\text{CH}_3$ , while the less stable **c- $\beta$ - $^4\text{C}_1$  g-** shows a chain of two cooperative hydrogen bonds  $\text{O}_2\text{H}\cdots\text{O}_3\text{H}\cdots\text{O}_4\text{H}$  orientated clockwise (*c*). This does not, however, significantly affect their rotational constants values and, as such, discrimination based solely on the values of the experimental rotational constants values is not possible. Yet, the *cc* and *c* arrangements do drastically alter  $\mu_b$  dipole moment component value, changing from 0.5 D to 2.9 D when passing from the **cc- $\beta$ - $^4\text{C}_1$  g-** conformer to **c- $\beta$ - $^4\text{C}_1$  g-** and, consequently, affect the intensity of observable type of transitions. Table 1 documents that the observed rotamer shows intense  $\mu_a$ -type transitions and weak  $\mu_b$ - and  $\mu_c$ -type transitions. Therefore, conformer **c- $\beta$ - $^4\text{C}_1$  g-** should be excluded due to the large predicted value for the b dipole moment component. Thus, the observed rotamer can only be ascribed as **cc- $\beta$ - $^4\text{C}_1$  g-** conformer. This is in good agreement with the predicted *ab initio* relative energies, which point out conformer **cc- $\beta$ - $^4\text{C}_1$  g-** as the global minimum.

**Table 2.** Experimental Rotational Parameters for the Observed  $^{13}\text{C}$  Isotopologues of Methyl  $\beta$ -D-xyloside.

Parameter	C <sub>1</sub>	C <sub>2</sub>	C <sub>3</sub>	C <sub>4</sub>	C <sub>5</sub>	C <sub>6</sub>
A <sup>a</sup>	1765.9994 ( 66) <sup>b</sup>	1760.1576 (87)	1763.7850 (65)	1762.1361 ( 53)	1747.032 (10)	1763.9109 ( 55)
B	827.44527 ( 35)	829.16223 ( 25)	827.18114 ( 25)	825.74089 ( 22)	828.88609 ( 48)	813.35867 ( 27)
C	592.01546 (30)	592.26157 ( 32)	591.64010 ( 20)	590.75622 (18)	590.58159 ( 38)	584.53354 (22)
$\sigma^c$	6.8	6.2	4.0	3.7	7.6	5.7
N <sup>d</sup>	23	18	16	18	19	25

<sup>a</sup>A, B and C are the rotational constants in MHz. <sup>b</sup>Standard error in parentheses in units of the last digit. <sup>c</sup>rms deviation of the fit in kHz. <sup>d</sup>Number of measured transitions.

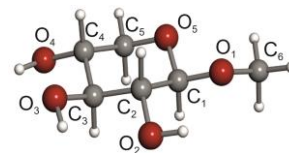
**Table 3.** Experimental Rotational Parameters for the Observed  $^{18}\text{O}$  Isotopologues of Methyl  $\beta$ -D-xyloside.

Parameter	O <sub>1</sub>	O <sub>2</sub>	O <sub>3</sub>	O <sub>4</sub>	O <sub>5</sub>
A <sup>a</sup>	1764.640 (16) <sup>b</sup>	1706.411 (35)	1738.630 (14)	1748.195 (18)	1742.544 (14)
B	813.81270 (70)	828.31433 (98)	816.0187 (22)	808.02371 (66)	827.4055 (10)
C	585.02862 (51)	585.79520 (97)	583.2463 (10)	580.19362 (57)	589.59210 (43)
$\sigma^c$	5.6	8.9	5.7	7.6	6.2
N <sup>d</sup>	8	10	7	9	9

<sup>a</sup>A, B and C are the rotational constants in MHz. <sup>b</sup>Standard error in parentheses in units of the last digit. <sup>c</sup>rms deviation of the fit in kHz. <sup>d</sup>Number of measured transitions.

**Table 4.** Substitution ( $r_s$ ) Structure for Conformer cc- $\beta$ - $^4\text{C}_1$  g- of Methyl  $\beta$ -D-xyloside and Comparison with *Ab Initio* Calculations. Distances in Å and Angles in Degrees.

Bond distances	Gas phase <sup>a</sup>	MP2/ M06. <sup>b</sup>	Angles	Gas phase <sup>a</sup>	Theory <sup>b</sup>
C <sub>5</sub> -O <sub>5</sub>	1.4047 (52) <sup>c</sup>	1.426/ 1.416	C <sub>1</sub> -O <sub>5</sub> -C <sub>5</sub>	110.93 (34) <sup>c</sup>	110.71/ 112.09
O <sub>5</sub> -C <sub>1</sub>	1.477 (31)	1.416/ 1.409	C <sub>1</sub> -C <sub>2</sub> -C <sub>3</sub>	111.06 (78)	109.29/ 109.27
C <sub>1</sub> -C <sub>2</sub>	1.526 (26)	1.522/ 1.520	C <sub>2</sub> -C <sub>3</sub> -C <sub>4</sub>	110.45 (34)	110.06/ 109.90
C <sub>2</sub> -C <sub>3</sub>	1.435 (17)	1.515/ 1.513	C <sub>3</sub> -C <sub>4</sub> -C <sub>5</sub>	108.64(29)	109.17/ 109.29
C <sub>3</sub> -C <sub>4</sub>	1.5072 (43)	1.517/ 1.516	C <sub>6</sub> -O <sub>1</sub> -C <sub>1</sub>	116.0 (12)	112.72/ 113.83
C <sub>4</sub> -C <sub>5</sub>	1.5434(43)	1.524/ 1.521	O <sub>1</sub> -C <sub>1</sub> -O <sub>5</sub>	106.1 (14)	109.50/ 109.62
<b>C<sub>1</sub>-O<sub>1</sub></b>	<b>1.3816 (77)</b>	<b>1.387/ 1.381</b>	C <sub>5</sub> -O <sub>5</sub> -C <sub>1</sub> -C <sub>2</sub>	-61.90 (92)	-63.57/ -62.46
O <sub>1</sub> -C <sub>6</sub>	1.4209 (54)	1.427/ 1.417	O <sub>5</sub> -C <sub>1</sub> -C <sub>2</sub> -C <sub>3</sub>	59.33 (65)	58.62/ 58.24
C <sub>2</sub> -O <sub>2</sub>	1.4435 (63)	1.421/ 1.411	C <sub>1</sub> -C <sub>2</sub> -C <sub>3</sub> -C <sub>4</sub>	-58.0 (10)	-54.17/ -54.81
C <sub>3</sub> -O <sub>3</sub>	1.4327 (39)	1.422/ 1.412	C <sub>2</sub> -C <sub>3</sub> -C <sub>4</sub> -C <sub>5</sub>	55.82 (73)	53.89/ 54.09
C <sub>4</sub> -O <sub>4</sub>	1.4190(34)	1.418/ 1.408	C <sub>3</sub> -C <sub>4</sub> -C <sub>5</sub> -O <sub>5</sub>	-57.99 (71)	-57.94/ -56.81
			C <sub>4</sub> -C <sub>5</sub> -O <sub>5</sub> -C <sub>1</sub>	62.45 (94)	63.36/ 61.92
			O <sub>1</sub> -C <sub>1</sub> -O <sub>5</sub> -C <sub>5</sub>	176.78 (78)	178.64/ 179.39
			<b>C<sub>6</sub>-O<sub>1</sub>-C<sub>1</sub>-O<sub>5</sub></b>	<b>-68.45 (75)</b>	<b>-67.76/-66.67</b>



<sup>a</sup>This work. <sup>b</sup>MP2/6-311++G(d,p) and M06-2X/aug-cc-pVTZ levels of calculation, respectively. <sup>c</sup> Derived errors in parentheses in units of the last digit following reference 32

A closer inspection into the low intensity background of the spectrum did not reveal the existence of spectral signatures attributable to the **cc- $\beta$ - $^4$ C $_1$  g+**. However, on the low frequency side of each intense  $\mu_a$ -type R-branch transition of the observed **cc- $\beta$ - $^4$ C $_1$  g-** conformer, very weak sets of the same R-branch progressions could be identified and were indeed ascribed to six monosubstituted  $^{13}\text{C}$  and five  $^{18}\text{O}$  species of the parent molecule observed in their natural abundance of 1.1% and 0.2%, respectively. Isotopic progressions for the  $5_{05}\leftarrow 4_{04}$  rotational transition are shown in the inset of Fig. 3. Predicted frequency shifts for the **cc- $\beta$ - $^4$ C $_1$  g-** conformer were found to be consistent with those observed experimentally, further supporting the identification of this conformer in the supersonic expansion. More than 150 rotational transitions were measured (Tables S5-S15) for the eleven isotopic species and used in a rigid rotor analysis<sup>28</sup> to give the experimental rotational constants collected in Tables 2 and 3. The isotopic information was then used to derive the substitution structure<sup>32,33</sup> shown in Table 4 (atomic coordinates in Table S16 in the Supporting Information).

The *exo*-anomeric effect and hydrogen bonding are the main factors controlling the conformational behavior of the archetypal methyl  $\beta$ -D-xyloside, represented by conformer **cc- $\beta$ - $^4$ C $_1$  g-**, where hydroxyl groups are preferentially orientated in such way as to yield cooperative hydrogen bonding as efficiently as possible. The highly detailed picture obtained for this conformer provides new insights into the *exo*-anomeric effect, which is particularly expressed in the determined glycosidic structure. Hence, the determined value for the torsion angle  $\varphi$  ( $= \text{C}_6\text{-O}_1\text{-C}_1\text{-O}_5$ ) of  $-68^\circ$  in the observed conformer is consistent with a “g-” conformation of the aglycon that maximizes the *exo*-anomeric effect. Thus, the importance of the *exo*-anomeric effect is unchallenged, and it may be seen as the main driving force influencing the aglycon structure, dominating over all other factors that are likely to. Nonetheless, the most important feature of the structural data presented in Table 4 is the fact that the determined value for the glycosidic  $\text{C}_1\text{-O}_1$  bond (1.38 Å) is shown to be substantially shorter than the normal C-O bonds, typically ranging between 1.42-1.44 Å.<sup>34,35</sup> The observed shortening of the  $\text{C}_1\text{-O}_1$



bond can be interpreted in light of the currently popular hyperconjugative explanation or interpreted in terms of electrostatic interactions.

Further calculations<sup>30</sup> were carried out in order to evaluate the level of theory and basis set which better reproduce the rotational constants and the C<sub>1</sub>-O<sub>1</sub> bond distance. We compared initially the pure *ab initio* method (MP2) with three density-functional-theory procedures (B3LYP, M05-2X and M06-2X) using the Pople's 6-311++G(d,p). Later, the global minimum was further investigated using the triple- $\zeta$  Dunning's correlation-consistent cc-pVTZ and the augmented aug-cc-pVTZ basis sets. MP2/6-311++G(d,p) method was proved to give the best results for the calculation of the rotational constants.<sup>36,20</sup> Also, the B3LYP hybrid functional with the cc-pVTZ basis set has performed well in predicting rotational constants. Conversely, the M06HF and M06-2X methods provided good results in predicting the C<sub>1</sub>-O<sub>1</sub> bond distance. The structure at the M06-2X/aug-cc-pVTZ level of theory, collected in Table 4, is in excellent accordance with our experimental results. Our experimental results provide an invaluable benchmark to validate *ab initio* computations collected in Table S17 of the Supporting Information

Given the great sensitivity reached with our LA-CP-FTMW technique and the relevance of glycosidic linkages in biology, further investigation on other biologically relevant glycosides has been undertaken to improve our understanding of the key roles that anomeric and *exo*-anomeric effects play in current organic chemistry.

## 1. EXPERIMENTAL SECTION

---

A sample of methyl  $\beta$ -D-xyloside (m.p. 155–158 °C) was used without further purification, and prepared by mixing the compound powder with a commercial binder. The mixture was pressed to form cylindrical rods, which were placed in a laser ablation nozzle<sup>28</sup> to be vaporized using a 20 ps Nd:YAG laser (12 mJ/pulse). The vaporized sample was then seeded in the Ne carrier gas at backing pressure of 18 bar, to expand

adiabatically into the vacuum chamber, and probed by broadband CP-FTMW spectroscopy.<sup>28</sup> Up to 110 000 individual free induction decays at a 2 Hz repetition rate were averaged in the time domain and Fourier transformed to obtain the broadband frequency domain spectrum from 6 to 12 GHz.

## 2. REFERENCES

---

- <sup>1</sup> Edward, J.T. Stability of Glycosides to Acid Hydrolysis. *Chem. Ind. (Lond.)* 1955, 36, 1102-1104.
- <sup>2</sup> Lemieux, R. U.; Chü, P. in *133rd National Meeting of the American Chemical Society* 31N [American Chemical Society, 1958].
- <sup>3</sup> Lemieux, R.U. *Molecular Rearrangements*. John Wiley and Sons, New York, 1964, p.709.
- <sup>4</sup> Juaristi, E.; Cuevas, G. Recent Studies of the Anomeric Effect. *Tetrahedron* 1992, 48, 5019-5087.
- <sup>5</sup> Perrin, C. L.; Armstrong, K. B.; Fabian, M. A. The Origin of the Anomeric Effect: Conformational Analysis of 2-Methoxy-1,3-dimethylhexahydropyrimidine. *J. Am. Chem. Soc.* 1994, 116, 715-722.
- <sup>6</sup> Juaristi, E.; Cuevas, G. *The Anomeric Effect*. CRC Press, 1995.
- <sup>7</sup> Tvaroska, I. & Bleha, T. Anomeric and Exoanomeric Effects in Carbohydrate Chemistry. *Adv. Carbohydr. Chem. Biochem.* 1989, 47, 45-123.
- <sup>8</sup> Lemieux, R. U.; Koto, S.; Voisin, D. The Exo-Anomeric Effect. *ACS Symposium Series*, 1979, 87, Chapter 2, 17-29.
- <sup>9</sup> Meyer, B. Conformational Aspects of Oligosaccharides. *Topics Curr. Chem.* 1990, 154, 141-208.
- <sup>10</sup> Lemieux, R.U.; Koto, S. Conformational Properties of Glycosidic Linkages. *Tetrahedron* 1974, 30, 1933-44.
- <sup>11</sup> Berman, H. M.; Chu, S.S.C.; Jeffrey, G. A. Anomeric Bond-Character in the Pyranose Sugars. *Science* 1967, 157, 1576-1577.
- <sup>12</sup> Brown, C. J.; Cox, G.; Llewellyn, F. J. The Crystalline Structure of the Sugars. Part V. A Three-dimensional Analysis of Methyl  $\beta$ -Xyloside. *J. Chem. Soc. (A)* 1966, 922-927.
- <sup>13</sup> Goekjian, P. G.; Wu, T.-C.; Kishi, Y. Preferred Conformation of C-Glycosides. 6. Conformational Similarity of Glycosides and Corresponding C-Glycosides. *J. Org. Chem.* 1991, 56, 6412-6422.
- <sup>14</sup> Goekjian, P. G.; Wu, T.-C.; Kang, H.-Y.; Kishi, Y. Preferred Conformation of C-Glycosides. 7. Preferred Conformation of Carbon Analogues of Isomaltose and Gentiobiose. *J. Org. Chem.* 1991, 56, 6422-6434.
- <sup>15</sup> Lemieux, R.U. Newer Developments in the Conformational Analysis of Carbohydrates. *Pure Appl. Chem.* 1971, 27, 527-548.
- <sup>16</sup> Mayorkas, N.; Rudic, S.; Davis, B.G.; Simons, J. P. Heavy Water Hydration of Mannose: the Anomeric Effect in Solvation, Laid Bare. *Chem.Sci.* 2011, 2, 1128-1134.
- <sup>17</sup> Cocinero, E. J.; Çarçabal, P.; Vaden, T. D.; Simons, J. P.; Davis, B. G. Sensing the Anomeric Effect in a Solvent-Free Environment. *Nature* 2011, 469, 76-79.
- <sup>18</sup> Wang, C.; Ying, F.; Wu, W.; Mo, Y. Sensing or No Sensing: Can the Anomeric Effect Be Probed by a Sensing Molecule?. *J. Am. Chem. Soc.* 2011, 133, 13731-13736.
- <sup>19</sup> Alonso, J. L.; López, J. C. "Microwave Spectroscopy of Biomolecular Building Blocks" *Top. Curr. Chem.* 2015, 364, 335-402, Springer International Publishing Switzerland.
- <sup>20</sup> Alonso, J. L.; Lozoya, M. A.; Peña, I.; López, J. C.; Cabezas, C.; Mata, S.; Blanco, S. The Conformational Behaviour of Free D-Glucose-at Last. *Chem. Sci.* 2014, 5, 515-522.

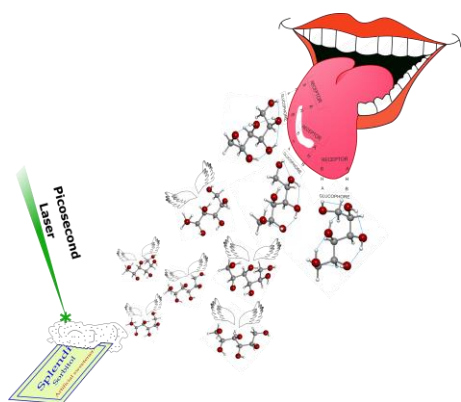
- <sup>21</sup> Peña, I.; Cabezas, C.; Alonso, J. L. Unveiling Epimerization Effects: a Rotational Study of  $\alpha$ -D-Galactose. *Chem. Commun.* 2015, *51*, 10115-10118.
- <sup>22</sup> Peña, I.; Mata, S.; Martín, A.; Cabezas, C.; Daly, A. M.; Alonso, J. L. Conformations of D-Xylose: the Pivotal Role of the Intramolecular Hydrogen-Bonding. *Phys. Chem. Chem. Phys.* 2013, *15*, 18243-18248.
- <sup>23</sup> Bermúdez, C.; Peña, I.; Cabezas, C.; Daly, A. M.; Alonso, J. L. Unveiling the Sweet Conformations of D-Fructopyranose. *ChemPhysChem* 2013, *14*, 893-895.
- <sup>24</sup> Peña, I.; Cocinero, E. J.; Cabezas, C.; Lesarri, A.; Mata, S.; Écija, P.; Daly, A.M.; Cimas, A.; Bermúdez, C.; Basterretxea, F. J.; Blanco, S.; Fernández, J. A.; López, J. C.; Castaño, F.; Alonso, J. L. Six Pyranoside Forms of Free 2-Deoxy-D-ribose. *Angew. Chem. Int. Ed.* 2013, *52*, 11840-11845.
- <sup>25</sup> Cabezas, C.; Peña, I.; Daly, A. M.; Alonso, J. L. Erythrose Revealed as Furanose Forms. *Chem. Commun.* 2013, *49*, 10826-10828.
- <sup>26</sup> Cocinero, E. J.; Lesarri, A.; Écija, P.; Basterretxea, F. J.; Grabow, J.-U.; Fernández, J. A.; Castaño, F. Ribose Found in the Gas Phase. *Angew. Chem. Int. Ed.* 2012, *51*, 3119–3124.
- <sup>27</sup> Brown, G. G.; Dian, B. C.; Douglass, K. O.; Geyer, S. M.; Shipman, S. T.; Pate, B. H. A Broadband Fourier Transform Microwave Spectrometer Based on Chirped Pulse Excitation. *Rev. Sci. Instrum.* 2008, *79*, 053103.
- <sup>28</sup> Mata, S.; Peña, I.; Cabezas, C.; López, J. C.; Alonso, J. L. A Broadband Fourier-Transform Microwave Spectrometer with Laser Ablation Source: The Rotational Spectrum of Nicotinic Acid. *J. Mol. Spectrosc.* 2012, *280*, 91-96.
- <sup>29</sup> Gordy, W.; Cook, R. L. *Microwave Molecular Spectroscopy*; John Wiley & Sons, New York, 1984.
- <sup>30</sup> Frisch, M. J.; et al., *Gaussian 09*, revision B.01; Gaussian, Inc., Wallingford, CT, 2009; Calculations carried out at our 'Olimpo' Beowulf Cluster facility, recently installed in our laboratory.
- <sup>31</sup> Jeffrey, G. A.; Saenger, W. *Hydrogen Bonding in Biological Structures*, Springer, New York, 1991.
- <sup>32</sup> Kraitchman, J. Determination of Molecular Structure from Microwave Spectroscopic Data. *Am. J. Phys.* 1953, *21*, 17-24.
- <sup>33</sup> Van Eijck, B. P. Influence of Molecular Vibrations on Substitution Coordinates. *J. Mol. Spectrosc.* 1982, *91*, 348-362.
- <sup>34</sup> Kuchitsu, K. "Structure of Free Poliatomic Molecules", Springer-Verlag Berlin Heidelberg New York, 1998.
- <sup>35</sup> Anslyn, E.V.; Dougherty, D. A. "Modern Physical Organic Chemistry" University Science Book, Sausalito, 2006.
- <sup>36</sup> Zhang, D.; Bocklitz, S.; Zwier, T. S. Broadband Microwave Spectroscopy of Prototypical Amino Alcohols and Polyamines: Competition Between H-Bonded Cycles and Chains. *J. Phys. Chem. A* 2016, *120*, 55–67.



## CHAPTER II.

# The Sweet Structures of D-Sorbitol

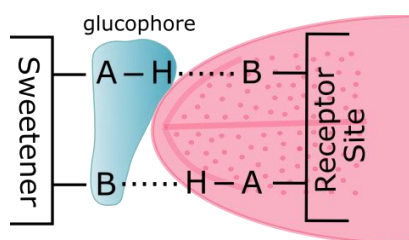
---



*In the gas phase isolation conditions of a supersonic expansion, three different conformers have been revealed for the artificial sweetener D-sorbitol, investigated for the first time using a combination of chirped pulse Fourier transform microwave spectroscopy (CP-FTMW) coupled with a laser ablation (LA) source. All conformers are over-stabilized by a network of five-cooperative intramolecular hydrogen bonds between vicinal hydroxyl groups in clockwise or counterclockwise arrangements. They all share a common structural signature: the  $O_1H\cdots O_2$  intramolecular hydrogen bond that fulfills the requirements of the glucophore proposed by Shallenberger's molecular theory of sweet taste. Present results provide the first linkage between sweetness and structure in sugar alcohols.*



It is noteworthy that the sweet taste comes from compounds with diverse chemical function. To explain that, abundant research has addressed in the last century the link between the sweetness and the structure of sweeteners.<sup>1-3</sup> None of these studies were able to offer a unified explanation regarding the sweetness-structure relation until Shallenberger and Acree's molecular theory of sweet taste.<sup>4,5</sup> It established that all sweeteners contain an AH-B moiety of two functional groups, one acting as the proton donor (A-H) and the other as the proton acceptor (B) which is called glucophore. These interact in a complementary way by a hydrogen bond with two similar points of a sweet receptor placed on our tongue. A and B are electronegative atoms separated from 2.5 to 4 Å (see Scheme 1). A third binding  $\gamma$ -site capable of enhancing the sweet flavor which interacts with receptor via hydrophobic or van der Waals' interaction was later proposed by Kier forming the "sweetness triangle".<sup>6-8</sup> New theories that provide new models have also been developed<sup>9,10</sup> but all of them agree in need of the presence of a glucophore to own sweet properties.<sup>11,12</sup>



**Scheme 1.** Glucophore structure proposed by Shallenberger and Acree

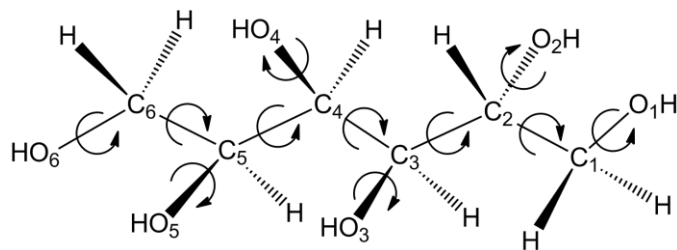
Unfortunately, at the time all these theories were formulated, structural data of sweeteners were restricted to condensed phases which were unable to offer much detail concerning the spatial distribution of the atoms and, consequently, to explain the relation of molecular structure to the sweetness. However, nowadays Fourier transform microwave spectroscopy techniques coupled with laser ablation sources under the isolation conditions of a supersonic expansion has emerged as a definitive tool in the structural analysis of solid organic compounds.<sup>13</sup> Hence, a first step forward in the structure-activity of natural sweeteners was given in the study of D-Fructose<sup>14</sup> and very recently confirmed in the other

ketohehexoses<sup>15</sup> using laser ablation chirped pulse Fourier transform microwave (LA-CP-FTMW) spectroscopy.<sup>16</sup> The presence of a common structural signature involving the hydroxyl groups in the small network  $\text{OH}_2 \cdots \text{OH}_1 \cdots \text{O}_{\text{ring}}$  unveiled in the most abundant observed conformers indicate the presence of the glucophore responsible for the sweet taste of these natural sweeteners.

All the above highlights the importance of revealing the structure of artificial sweeteners. Nowadays, the food industry has responded people's demand by producing various artificial sweeteners considered helpful in the control of calories intake. These are used in replacement of natural sugars, being responsible for the sweet perception in our mouth. Hence, it is rare not to see a sugar substitute as an ingredient in the label of foodstuffs. There are no previous structural data on artificial sweeteners so its relation between chemical structure and sweet sensation it is not yet adequately resolved. Hence, it is not surprising at all that many of them have been casually discovered.<sup>11</sup> Therefore, it is of utmost importance to know their structure-sweetness relation to guide the synthesis of new artificial sweeteners.

Here we report on the structural behavior of D-sorbitol (2S,3R,4R,5R)-hexane-1,2,3,4,5,6 hexol, one of the most renowned sugar alcohols belonging to the  $\text{C}_6$  polyalcohol family ( $\text{C}_6\text{H}_{14}\text{O}_6$ ). It is the chosen molecule to open our structural investigation of the artificial sweeteners. We can anticipate the formation of intricate networks of intramolecular hydrogen bonds considering the number of hydroxyl groups and the vast number of internal torsions (see scheme 2). The tremendous conformational diversity could lead to low-energy conformations with the appropriate disposition of the atoms to form the glucophore moiety AH-B that could explain the sweetness of this artificial sweetener.





**Scheme 2.** A zig-zag molecular model of (2S,3R,4R,5R)-hexane-1,2,3,4,5,6 hexol (sorbitol).

D-sorbitol (2S,3R,4R,5R)-hexane-1,2,3,4,5,6 hexol, is a solid (m.p. 95°C) which decomposes, as the natural sweeteners, using the standard heating methods of vaporization. We address this issue using picosecond pulses from the fourth harmonic (266nm) of a Nd-YAG laser which has resulted in being the key to get to fly the sorbitol molecules. They are seeded in Neon as a carrier gas, supersonically expanded and probed in the cold and efficiently isolated conditions of a supersonic expansion by broadband chirp pulsed Fourier transform microwave spectroscopy (CP-FTMW).<sup>17</sup> The congested broadband rotational spectrum from 6 to 12 GHz shown in Fig.1 is full of unwanted photofragmentation lines and not straightforward to assign. Once these signals were identified and removed from the spectrum, a progression of  $\mu_{\sigma}$ -type R-branch transitions corresponding to a first rotamer, denoted as I was assigned and measured. Also,  $\mu_{\sigma}$ -type R-branch transitions were observed. Hence, a total of 59 experimental lines reported in table S4 of the Supporting Information were analyzed<sup>18</sup> using a Watson's A-reduced semirigid rotor Hamiltonian.<sup>19</sup> The determined rotational constants from the fit are collected in Table 1. The subtraction of these lines from the spectrum facilitates the identification of degeneracy pairs of  $\mu_{\sigma}$ -type R-branch transitions (see inset of Figure 1) as belonging to other two rotamers, II and III, of sorbitol.  $\mu_{\sigma}$ -type R-branch transitions were also observed for rotamer III. The 26 and 48 transition lines measured for rotamers II and III respectively are reported in tables S5 and S6 of the Supporting Information. The spectroscopic constants obtained from the semirigid rotor analysis are given in the second and third column of Table 1.

**Table 1.** Experimental rotational parameters for the three observed conformers of sorbitol.

	Rotamer I	Rotamer II	Rotamer III
A <sup>[a]</sup>	1685.6613(21)	1737.12866(68)	1511.27412(53)
B	507.41631(27)	495.31233(24)	593.30388(29)
C	458.66973((30)	455.50293(20)	513.91589(35)
$\Delta J$	0.0000175(12)	-	0.0000214(18)
$\Delta JK$	-0.0000779(72)	-	-
$\Delta K$	0.00109(19)	-	-
a/b/c	obs./ - /obs	- / - / obs.	obs./ - / obs.
N	59	26	48
$\sigma$	7.2	8.8	7.4

[a] A, B, and C represent the rotational constants (in MHz);  $\Delta J$ ,  $\Delta JK$ , and  $\Delta K$  represent the determined centrifugal distortion constants (in MHz); a, b and c are the observed selection rules; N is the Number of measured transitions and  $\sigma$  is the rms deviation of the fit (in kHz).

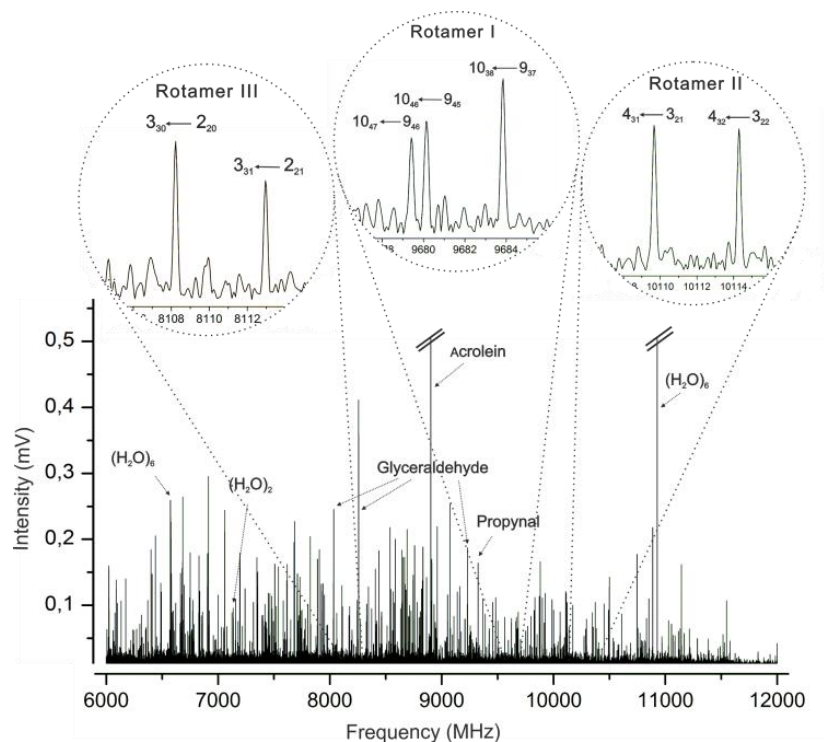


**Figure 1.** Broadband rotational spectrum of D-sorbitol indicating some lines of the unwanted photofragmentation products and water complexes. Top inset: details of the spectrum showing the identification of degeneracy pairs of  $\mu_c$ -type R-branch transitions ascribed to the three detected conformers. The observed signal-to-noise ratios reflect their similar abundance in the supersonic expansion.

A distinguishing feature of rotational spectra is the ability to generate very accurate spectroscopic parameters directly comparable with *in vacuo* theoretical predictions. On this basis, the conformational space of D-sorbitol was explored to relate each set of experimental rotational constants of Table 1 with those predicted theoretically for the lower-energy conformers of sorbitol. The eleven hindered rotations around the single bonds generate a plethora of conformational species, confirming the conformational richness of D-sorbitol. Thus, up to 20 possible conformers were localized in the potential energy surface with relative energies below  $1500\text{ cm}^{-1}$  using *ab initio* methods at the MP2/6-311G++(d,p) level of the theory.<sup>20</sup> Each conformer was confirmed to be a local minimum by checking that its Hessian matrix did not have imaginary values. They are grouped in three families G-TT, G+TT and TTT in Tables S1, S2 and S3 of the Supporting Information according to the carbon skeletal configuration defined by the three dihedral angles  $\angle\text{C}_1\text{-C}_2\text{-C}_3\text{-C}_4$ ,  $\angle\text{C}_2\text{-C}_3\text{-C}_4\text{-C}_5$  and  $\angle\text{C}_3\text{-C}_4\text{-C}_5\text{-C}_6$ . The labels T, G+, and G- are being used to denote values of dihedral angles close to  $180^\circ$ ,  $+60^\circ$  and  $-60^\circ$ , respectively. Within each family of conformers, the two terminal hydroxymethyl groups can generate three staggered conformations denoted by two letters, associated to the  $\angle\text{O1-C1-C2-C3}$  and  $\angle\text{O6-C6-C5-C4}$  dihedral angles of  $60^\circ$ ,  $-60^\circ$  or  $180^\circ$ , designated as G+, G- and T, respectively. Finally, the labels (c) and (cc) indicate the clockwise or counterclockwise arrangement of the intramolecular hydrogen bonding networks. If needed, a number is added to provide the MP2 energy ordering within the same family. The predicted rotational constants together with the electric dipole moment components for the lower-energy conformers (below  $500\text{ cm}^{-1}$ ) of sorbitol are shown in Table 2 and Figure S1 of the Supporting Information.

**Table 2.** Predicted spectroscopic rotational parameters and relative energies for the six lower energy conformers of D-sorbitol.

	G-TT/TG-/cc	G-TT/TG-/c	G-TT/G+G-/c
A/B/C <sup>[a]</sup>	1687/512/ 462	1749/498/ 458	1519/597/518
$ \mu_a  /  \mu_b  /  \mu_c $ <sup>[b]</sup>	1.8/0.5/1.4	0.3/ 0.4/1.1	2.0/0.3/1.4
$\Delta E/ \Delta G$ <sup>[c]</sup>	0/0	41/-25	87/-29
	G+TT/G+G-/cc	TTT/G+G-/c	G-TT/G+G-/cc
A/B/C <sup>[a]</sup>	1745/554/504	1940/478/449	1475/606/521
$ \mu_a / \mu_b / \mu_c $	2.1/0.0/2.1	0.6/0.8/0.5	0.5/0.2/1.6
$\Delta E/ \Delta G$	396/470	405/170	413/243

[a] A, B, and C represent the rotational constants (in MHz); [b]  $|\mu_a|$ ,  $|\mu_b|$  and  $|\mu_c|$  are the absolute values of the electric dipole moment components (in D); [c]  $\Delta E$  and  $\Delta G$  are the relative and Gibbs energies (in  $\text{cm}^{-1}$ ) at 298 K with respect to the global minimum calculated at the MP2/6-311++G(d,p) level of theory.

Promptly, it was easy to realize the experimental values of the rotational constants of rotamers I, II and III in Table 1, match nicely with that predicted *ab initio* in Table 2 for conformers G-TT/TG-/cc, G-TT/TG-/c, and G-TT/G+G-/c respectively. The observed selection rules in Table 1 ( $\mu_a$  - and  $\mu_c$ -type for rotamers I and III, and  $\mu_c$ -type for conformer II), which are consistent with the predicted values of the electric dipole moment components in Table 2, served as a further support to this identification. A final piece of evidence comes from the fact that a scale factor ranging from 0.990 to 0.999 brings the *ab initio* values of the rotational constants for the TT/TG-/cc, G-TT/TG-/c and G-TT/G+G-/c conformers nearly into coincidence with the experimental values of rotamers I, II, and III. It proves the global consistency of the conformational assignment. Furthermore, the observed conformers show similar abundance in the supersonic expansion as roughly estimated from relative intensity measurements.<sup>21</sup> It is in agreement with the predicted  $\Delta E$  or  $\Delta G$  values for the third ree lowest energy G-TT conformers in Table 2. Further searches using predicted

rotational constants corrected by the above scale factor failed to observe any spectroscopic signatures belonging to higher-energy conformers.

The revealed conformers of D-sorbitol depicted in Fig. 2, are stabilized by intramolecular hydrogen bonds between vicinal hydroxyl groups forming a network of five-cooperative intramolecular hydrogen bonds involving the O<sub>6</sub>H, O<sub>5</sub>H, O<sub>3</sub>H, O<sub>2</sub>H and O<sub>4</sub>H hydroxyl groups strongly reinforced by sigma-hydrogen bond cooperativity.<sup>22</sup> From the excellent agreement between the experimental and predicted spectroscopic constants we can infer that the actual geometries should be very close to that calculated *ab initio* given in Tables S5 to S7 of Supporting Information. The G-TT/TG-/cc and G-TT/TG-/c conformers present the same skeletal framework but opposite clockwise (cl) or counterclockwise (cc) network arrangements. It not significantly affects the values of the rotational constants but does drastically alter the  $\mu_a$  dipole moment component, which changes from 1.8 to 0.3 D. Hence,  $\mu_a$ -type transitions of G-TT/TG-/c are not observed. G-TT/G+G-/c conformer differs from the G-TT/TG-/c in the gauche disposition of the terminal hydroxymethyl group.

The notion that  $\alpha$ -glycol groups with the staggered configuration were the AH,B unit has been well established in the studies of sugars.<sup>12</sup> A priori, any vicinal hydroxyl pairs in the most abundant conformers of sorbitol show hydrogen-bond interactions that could easily be adapted to the linkage to the receptor forming the AH-B glucophore. Notice that for sorbitol, the orientation of O<sub>1</sub>H hydroxyl group in the three conformers disrupt any plausible hydrogen bond network over the entire molecule. They share a characteristic structural signature: the O<sub>1</sub>H hydroxyl group is always pointing to O<sub>2</sub> to form an O<sub>1</sub>H...O<sub>2</sub> intramolecular hydrogen bond with distances ranging 2.39-2.41Å (see Fig.2). This feature may fulfill the requirements of the glucophore; O<sub>1</sub>H could act as the proton donor (AH) and O<sub>2</sub>H as the proton acceptor (B) sites of the Shallenberger's proposal. Also, the distances between the proton donor (O<sub>1</sub>) and proton acceptor (O<sub>2</sub>) ranging from 2.7 to 2.9 Å satisfy the requirements of the molecular theory of sweet taste.<sup>4,5</sup> Just like natural sugars, these "sweet structures" present a common surrounding of the C<sub>6</sub> (see Fig.2) free of any

hydrophilic group that could be considered the third  $\gamma$ -site involved in the sweetness triangle AH-B- $\gamma$  of the Kier's proposal.<sup>6-8</sup> It was stated that it merely enhances the sweet flavor.<sup>23</sup>

The presence of other hydroxyl groups in sorbitol might allow additional assignments to the AH, B glucophore unit. However, if the glycol hydroxyl groups are too strongly bonded intramolecularly, their ability to act as a glucophore is restricted. Therefore, according to the intramolecular hydrogen bond distances ranging 2.2-2.3 Å, the  $\alpha$ -glycol unit O<sub>2</sub>H...O<sub>3</sub>H of the G-TT/TG-/c and G-TT/G+G-/c conformers, and the O<sub>6</sub>H...O<sub>5</sub>H one of the G-TT/TG-/cc conformer could also be attributed as the glucophore sites responsible for the sweet flavour. Owing to their spatial disposition, O<sub>2</sub>H and O<sub>6</sub>H act as proton donor (AH) and O<sub>3</sub>H and O<sub>5</sub>H as acceptor (B).

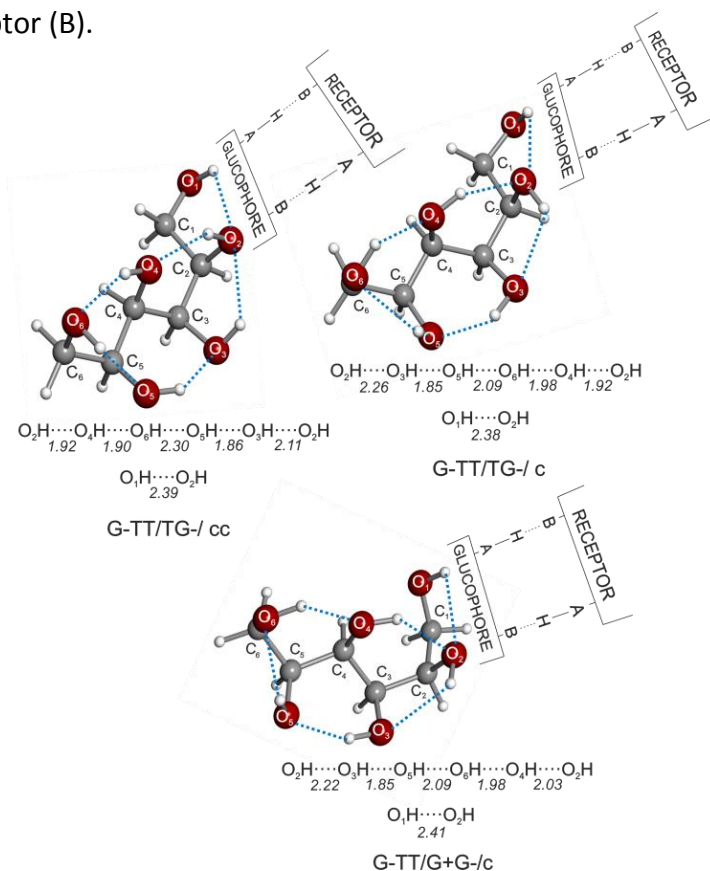


**Figure 2.** The geometries calculated for the three observed conformers of sorbitol. The intramolecular hydrogen bond distances in Å.

In summary, the ability of our LA-CP-FTMW technique to provide high-quality spectroscopic information directly comparable with *ab initio* computations provides an unmatched means to extract from D-sorbitol structural signatures related to the sweetness. The detected conformers of D-sorbitol adapt their molecular shapes to optimize the sequence of intramolecular hydrogen bonds to increase their strength by cooperativity<sup>22</sup>. Although the conformational behavior in the gas phase is only an approximation to the actual physiological in aqueous solution, they are precious information since the conformational behavior in solution should fluctuate between the most stable structures found in the isolation conditions of the gas phase. To stimulate the sensation of sweet taste, at least one “sweet structure” should be present.

Despite being an alicyclic molecule, the hydrogen bonding in D-sorbitol acts as a driving force that produces a sort of cyclisation forming a crown of intramolecular hydrogen bonds that simulates the cyclic structures of the natural sweeteners of ketohexoses. These results lead us to the question; does the sorbitol mimic the shape of the natural sweeteners of ketohexoses? Preliminary results already obtained in the related dulcitol point to this conclusion.

## REFERENCES

---

- <sup>1</sup> G. Cohn, *Die organischen Geschmacksstoffe*, F. Siemenroth, 1914.
- <sup>2</sup> E. Oertly and R. G. Myers, *J. Am. Chem. Soc.*, 1919, 41, 855-867.
- <sup>3</sup> T. Kaneko, *J. Chem. Soc. (Japan)*, 1938, 29, 433-439
- <sup>4</sup> R. S. Shallenberger and T. E. Acree, *Nature*, 1967, 216, 480-482.
- <sup>5</sup> R. S. Shallenberger, T.E. Acree and C. Y. Lee, *Nature*, 1969, 221, 555-556.
- <sup>6</sup> L. B. Kier, *J. Pharm. Sci.*, 1972, 61, 1394-1397.
- <sup>7</sup> A. van der Heijden, L. B. P. Brussel and H. G. Peer, *Food Chem.*, 1978, 3, 207-211.
- <sup>8</sup> T. Yamazaki, E. Benedetti, D. Kent and M. Goodman, *Angew. Chem. Int. Ed.*, 1994, 33, 1437-1451.
- <sup>9</sup> C. Nofre and J.M. Tinti, *Food Chemistry*, 1996, 56, 263-274.
- <sup>10</sup> *Sweet-Taste Chemoreception* M.Mathlouthi and J.A.Kanters in, Chapman and Hall, 1993.
- <sup>11</sup> R. S. Shallenberger, *Food Chemistry*, 1996, 56, 209-214.
- <sup>12</sup> R.S.Shallenberger, “*Taste Chemistry*.” Springer-Verlag New York 2012.
- <sup>13</sup> J.L. Alonso, J.C.López, “*Microwave Spectroscopy of Biomolecular Building Blocks*” *Topics in Current Chemistry*, Vol. 364 Springer, Heidelberg, 2015, pp.335–402.
- <sup>14</sup> (a) C. Bermúdez, I. Peña, C. Cabezas, A. M. Daly, J. L. Alonso, *ChemPhysChem*. 2013, 14, 893– 895. (b) E. J. Cocinero, A. Lesarri, P. Écija, A. Cimas, G. Davis, F.J. Basterretxea, J.A. Fernández, F. Castaño, *J. Am. Chem. Soc.*, 2013, 135, 2845–2852

- <sup>15</sup> C. Bermúdez, I. Peña, S. Mata, J. L. Alonso, *Chem. Eur. J.* 2016, 22, 16829.
- <sup>16</sup> a) S.Mata, I.Peña, C.Cabezas, J.C.López and J.LAlonso, *J. Mol. Spectrosc.* 2012, 280, 91 –96. (b) I. Peña, S. Mata, A.Martín, C. Cabezas, A.M.Daly, J.L.Alonso, *Phys. Chem. Chem. Phys.* 2013, 15, 18243 –18248.
- <sup>17</sup> G.G. Brown, B.C. Dian, K.O. Douglass, S.M. Geyer, S.T. Shipman, B.H. Pate, *Rev. Sci. Instrum.* 2008, 79, 053103
- <sup>18</sup> H. M. Pickett, *J. Mol. Spectrosc.*, 1991, 148, 371.
- <sup>19</sup> (a) J. K. G. Watson, in *Vibrational Spectra and Structure*, Vol. 6 (Ed.: J. R.Durig), Elsevier, New York, 1977, pp. 1– 78.
- <sup>20</sup> Gaussian 09, Revision B.01, M. J. Frisch et al., Gaussian Inc., G Wallingford CT, 2010.
- <sup>21</sup> a) G. T. Fraser, R. D. Suenram, C. L. Lugez, *J. Phys. Chem. A* 2000, 104,1141–1146; b) S. Blanco, A. Lesarri, J. C.López, J. L. Alonso, *J. Am. Chem. Soc.* 2004, 126, 11675–11683.
- <sup>22</sup> G. A. Jeffrey. W. Saenger, *Hydrogen Bonding in Biological Structures*, Springer, New York. 1991
- <sup>23</sup> S. C. Ebeling, *Food Chem.* 1998, 61, 107 – 112.



## CHAPTER III.

# The rotational spectrum of artificial sweetener saccharine

---

*A significant step forward in the structure-activity relationships of sweeteners was the assignment of the AH-B- $\gamma$  tripartite in sweeteners by Shallenberger-Acree-Kier. They proposed that all sweeteners contain an AH-B moiety, known as glucophore, in which A and B are electronegative atoms separated by a distance between 2.5 to 4 Å. H is a hydrogen atom attached to one of the electronegative atom by a covalent bond. A third hydrophobic point,  $\gamma$ , suggested by Kier. For saccharine, one of the oldest artificial sweeteners widely used in food and drinks, two possible B moieties exist, the carbonyl oxygen atom and the sulfoxide oxygen atom although there is a consensus of opinion among scientists over the assignment of AH-B moieties to HN-SO. In the present work, the solid of saccharine (m.p. 220°C) has been vaporized by laser ablation (LA) and its rotational spectrum has been analyzed by broadband CP-FTMW and narrowband MB-FTMW Fourier transform microwave techniques. The detailed structural information extracted from the rotational constants and  $^{14}\text{N}$  nuclear quadrupole coupling constants provided enough information to ascribe the glucophore's AH, B and  $\gamma$  sites of saccharine.*



## 1. INTRODUCTION

---

Sweeteners can be found among a great variety of organic compounds, such as carbohydrates, amino acids, peptides, proteins, ureas and sulfamates. The potencies of the sweeteners are generally compared to that of sucrose (=1) on a molar basis, and can be as high as 100000. In the last years, the natural sugars have been replaced by artificial sweeteners in a large variety of foods, decreasing its calorie amount and also, in some cases, duplicating its sugar taste. According to the attempt of Shallenberger and Acree<sup>1</sup> to rationalize the sweet taste, all sweet compounds have a so-called AH-B moiety (glucophore). It consists of a proton donor (AH) and a proton acceptor (B) points in a correct spatial disposition in such a way that the distance between them is greater than 2.5 Å but less than 4 Å. However, there are also compounds having the same AH-B moieties, but they are not sweet; hence other structural requirements have to be fulfilled for sweet taste perception.

The significant observation that many D-amino acids are sweet while their L-isomers are not, led to Kier to suggest a stereo-selective receptor site with three components, by the existence of a third hydrophobic component, a dispersive bonding site  $\gamma$ , in addition to the AH/B unit. This binding  $\gamma$ -site capable of enhancing the sweet flavor interacting with receptor via hydrophobic or van der Waals' interaction forming the "sweetness triangle."<sup>2,3,4</sup> The sweet response is produced via the interaction with a complementary tripartite AH, B,  $\gamma$  site in the taste bud receptor.<sup>5</sup> At the present state of our knowledge, however, this "sweetness triangle" theory, appears much too simple to explain all of the observations, particularly when bearing in mind, that sweet-taste perception is mediated by a cascade of complex biochemical processes,<sup>6,7</sup> that is little understood at the cellular and molecular level.

The tripartite AH, B,  $\gamma$  glucophore concept has had its merits as a unifying criterion and proved useful. However, it neglects of a three-dimensional shape, in rationalizing structure-sweetness relationship in such diverse classes of compounds as amino acids, dipeptides, sulfimides (e.g., saccharin and acesulfame), and sugars, in particular, the natural

sweeteners. Nowadays, however, the availability of advanced experimental techniques<sup>8</sup> and their application to solid compounds have allowed the elucidation of the individual conformations of glucose,<sup>9</sup> galactose,<sup>10</sup> fructose<sup>11</sup> and ketohexoses<sup>12</sup> in isolation conditions of the gas-phase. Hence, the possibility of representing tridimensionally the contact surface of the sugars have added a new dimension to the visual perception of sweeteners. Incorporation of such results into structure-sweetness consideration, led to a new allocation of the Shallenberger-Acree-Kier tripartite AH, B,  $\gamma$  glucophore in several sweet substances. Hence, the AH, B,  $\gamma$  glucophore concept has not only been applied to sugars but to other non-carbohydrate sweeteners such sorbitol<sup>13</sup> (see Chapter II) and saccharine. In this context, it is of interest to extend the structural studies on ketohexoses and polyalcohols to a representative non-carbohydrate sweetener as saccharine.

Saccharine (2,3-dihydro-3-oxobenzisulgaole) was discovered by an accidental event in the course of organic synthesis.<sup>8</sup> It is a white crystalline substance that prevail as dimers formed by intermolecular hydrogen bonding formed between the imide hydrogen and the carbonyl oxygen atom. The pure acid is about twice as sweet as the commercial product, presumably sodium saccharate.<sup>14</sup> It has been considered to be about 200-700 times as sweet as sucrose. Everything points to the sulfonamide function as the possible glucophore, but so far there are no reports about the structure of saccharine in isolation conditions. This lack of information about the saccharine structure and its correlation with its sweetness property is the motivation of this work, in which we present the first microwave rotational study.

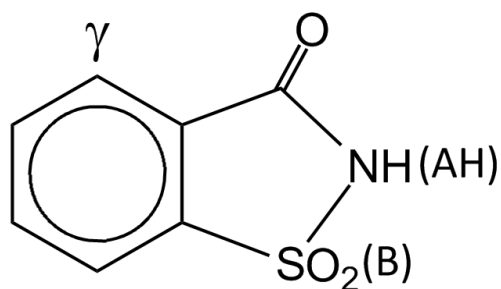


**Figure 1.** Scheme of saccharine showing the tripartite AH,B, $\gamma$  proposed by Kier.

## 2. METHODS

---

To bring the solid sample of saccharine (m.p. = 228.8 °C) into the gas-phase, and to obtain the rotational spectrum, a laser ablation source coupled with microwave Fourier transform microwave techniques are employed to study the saccharine. In a first step, the jet-cooled rotational spectrum of saccharine has been investigated by using our laser ablation (LA) chirped pulse Fourier transform microwave spectrometer (CP-FTMW), described in detail elsewhere.<sup>15</sup> Solid samples of saccharine (m.p. = 228.8 °C) were ground and mixed with a minimum amount of a commercial binder and pressed into cylindrical rods, which were placed in an ablation nozzle and vaporized using a Nd:YAG picosecond laser. Then, saccharine molecules were seeded in the carrier gas Ne at a backing pressure of 10 bar, to expand adiabatically into the vacuum chamber. An arbitrary waveform generator created a chirped pulse from 6.4 to 10.4 GHz, which was directly amplified by a 300 W TWT (travelling wave tube) amplifier. The conventional microwave horns have been replaced by the parabolic reflector system composed by dual ridge horns and two parabolic reflectors (40 cm diameter) separated 70 cm in a paraxial beam configuration.<sup>16</sup> The excitation pulse emerged from a horn antenna to polarize the molecules arising from the laser ablation nozzle located at the center of one of the parabolic reflectors. A second ridge horn antenna was used to detect the free induction decay signal (FID), which was finally amplified and digitized on a fast oscilloscope.

The LA-MB-FTMW spectrometer<sup>17</sup> was used to record the saccharine spectrum with the necessary resolution to analyze the hyperfine structure due to the presence of a <sup>14</sup>N nucleus. The optimal conditions to polarize the molecules in the jet correspond to molecular pulses of about 1.1 ms, followed by MW polarization pulses of 0.3 ms duration with powers of 1–40 mW. The microwave FID was recorded for 100 μs in the time domain at 40–100 ns sample intervals, and Fourier-transformed to the frequency domain. Due to the collinear disposition between the supersonic jet and the microwave resonator axis, all emission signals appeared to be split into Doppler doublets (Figure 2). The arithmetic mean of the doublets was taken as the rest frequency. The estimated accuracy of the frequency

measurements is greater than 3 kHz. From 50 to 250 averages were phase-coherently coadded to achieve reasonable signal-to-noise ratios.

The structure of saccharine was optimized by using Gaussian suite programs.<sup>18</sup> The model of choice was the Minnesota 06 (M06-2X) functional with the triple-zeta aug-cc-pVTZ basis set. The predicted rotational constants (A, B and C), quadrupole coupling constants ( $\chi_{aa}$ ,  $\chi_{bb}$  and  $\chi_{cc}$ ) and electric dipole moment components are collected in Table 1. The values obtained for other theoretical models can be found in the Supplementary Information (Appendix SI) for a comparison.

### 3. RESULTS AND DISCUSSION

---

#### 3.1 Rotational Spectrum

The broadband rotational spectrum of saccharine in the 6.4 to 10.4 GHz frequency range is shown in Fig.2. Two pairs of intense a-type R-branch  $(J+1)_{1,J+1} \leftarrow J_{1,J}$  and  $(J+1)_{0,J+1} \leftarrow J_{0,J}$  transitions with  $J=6$  and  $J=7$  were easily identified in the spectrum. A weaker pair of b-type R-branch transitions  $(J+1)_{0,J+1} \leftarrow J_{1,J}$  and  $(J+1)_{1,J+1} \leftarrow J_{0,J}$  were also assigned at each side of the intense a-type transition (see lower inset in figure 2). The saccharine molecule possesses a  $^{14}\text{N}$  nuclei with  $I = 1$  that originates a hyperfine structure in all the observed transitions. It arises from the interaction of the electric quadrupole moment of this nucleus with the electric field gradient created at the site of the nitrogen by the rest of the molecule. This interaction couples the  $^{14}\text{N}$  nuclear spin with the overall angular momentum, which results in a nuclear hyperfine structure in the rotational transitions. The LA-CP-FTMW spectrometer, used in this first stage of the investigation, does not have enough resolution to resolve the hyperfine structure. Only singular transitions as those of  $(J+1)_{2,J+1} \leftarrow J_{0,J}$  of  $J=2$  and  $J=3$  transitions, showed in the upper inset of Fig.2, are well resolved.

A more detailed inspection of the broadband spectrum, revealed the existence on the low frequency side of a weaker pair of the same a-type R-branch transitions (see inset of Figure 2). It has been assigned as corresponding to the  $^{34}\text{S}$  isotopologue of the parent

molecule observed in their natural abundance of 4,24%. A total 14 center of frequencies were fitted with a rigid rotor Hamiltonian to give the rotational constants collected in the second column of Table 1.

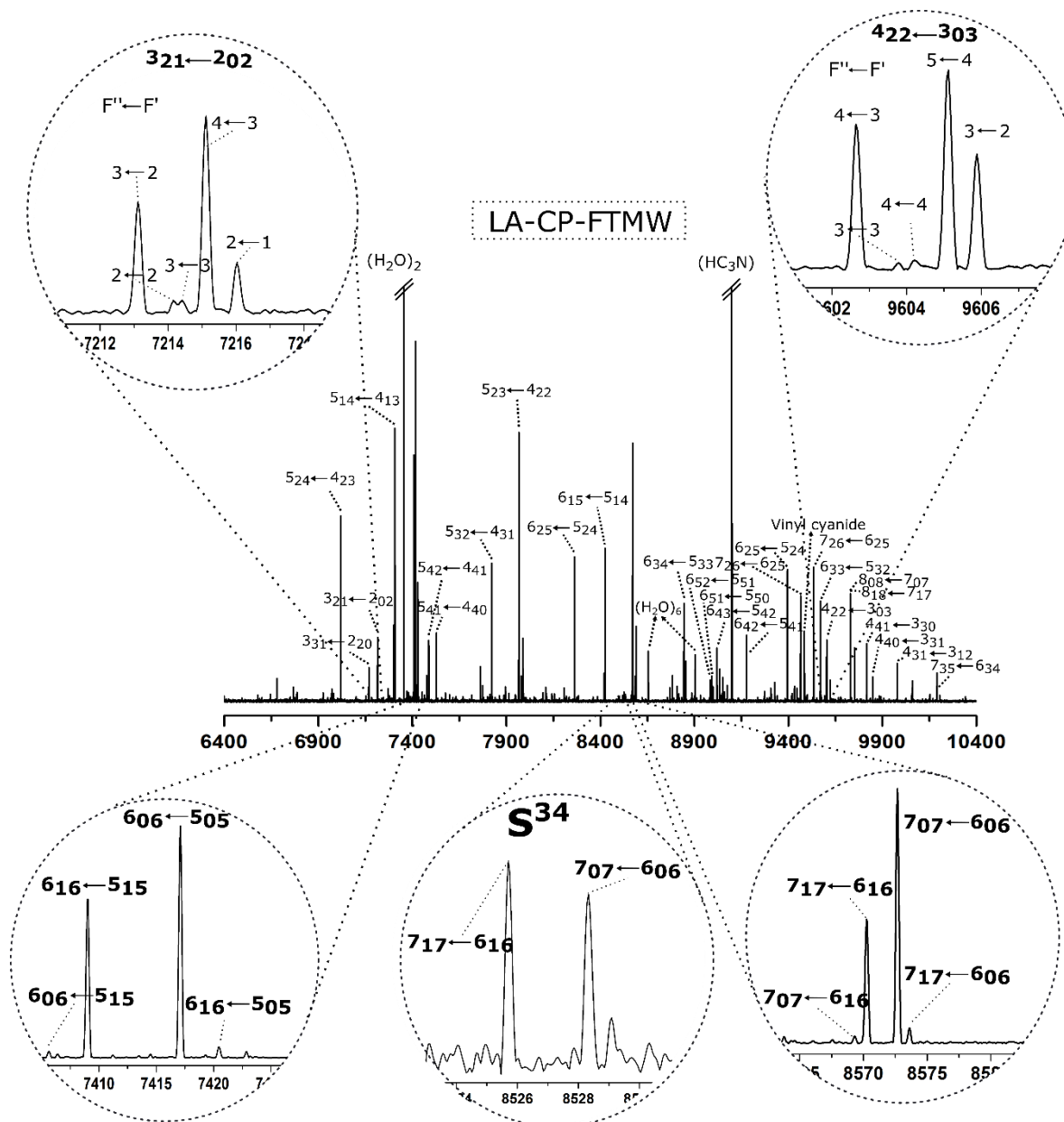


**Figure 2.** Broadband rotational spectrum of saccharine from 6.4 to 10.4 GHz (100.000 FID's). All the transitions corresponding to the saccharine are identified together with the photofragmentation lines. Extensions of the spectrum show the packages of strong pairs of a-type R-branch transitions  $(J+1)_{1J+1} \leftarrow J_{1J}$  and  $(J+1)_{0J+1} \leftarrow J_{0J}$  with  $J=6$  and  $J=7$  and two weaker b-type R-branch transitions  $(J+1)_{0J+1} \leftarrow J_{1J}$  and  $(J+1)_{1J+1} \leftarrow J_{0J}$ . Also, the satellites lines corresponding to  $(J+1)_{J+1} \leftarrow J_{1J}$  and  $(J+1)_{0J+1} \leftarrow J_{0J}$  with  $J=7$  transitions of the monosubstituted isotopologue of  $S^{34}$ .

In next stage of the investigation, the Laser Ablation Molecular Beam Fourier Transform (LA-MB-FTMW) spectrometer that provides sub-Doppler resolution was used to resolve the hyperfine structure of the transitions a high resolution spectroscopy is needed. that makes possible to resolve the hyperfine structure that the rotational transitions present due to the presence of a  $^{14}\text{N}$ . A total of 60 hyperfine components were measured in a range from 6-11GHz. They were fitted<sup>19</sup> using a rigid rotor Hamiltonian  $H_R^{(A)}$  supplemented with a  $H_Q$  term to account for the nuclear quadrupole coupling contribution.<sup>20</sup> The Hamiltonian was set up in the coupled basis set  $I + J = F$  and diagonalized in blocks of  $F$ .<sup>21</sup> The experimentally determined rotational constants  $A, B, C$  and the nuclear quadrupole coupling constants  $\chi_{aa}$ ,  $\chi_{bb}$ , and  $\chi_{cc}$  for the observed species are given in Table 1. All measured transitions for the parent and  $^{34}\text{S}$  species are collected in the Supplementary Information (see Appendix)

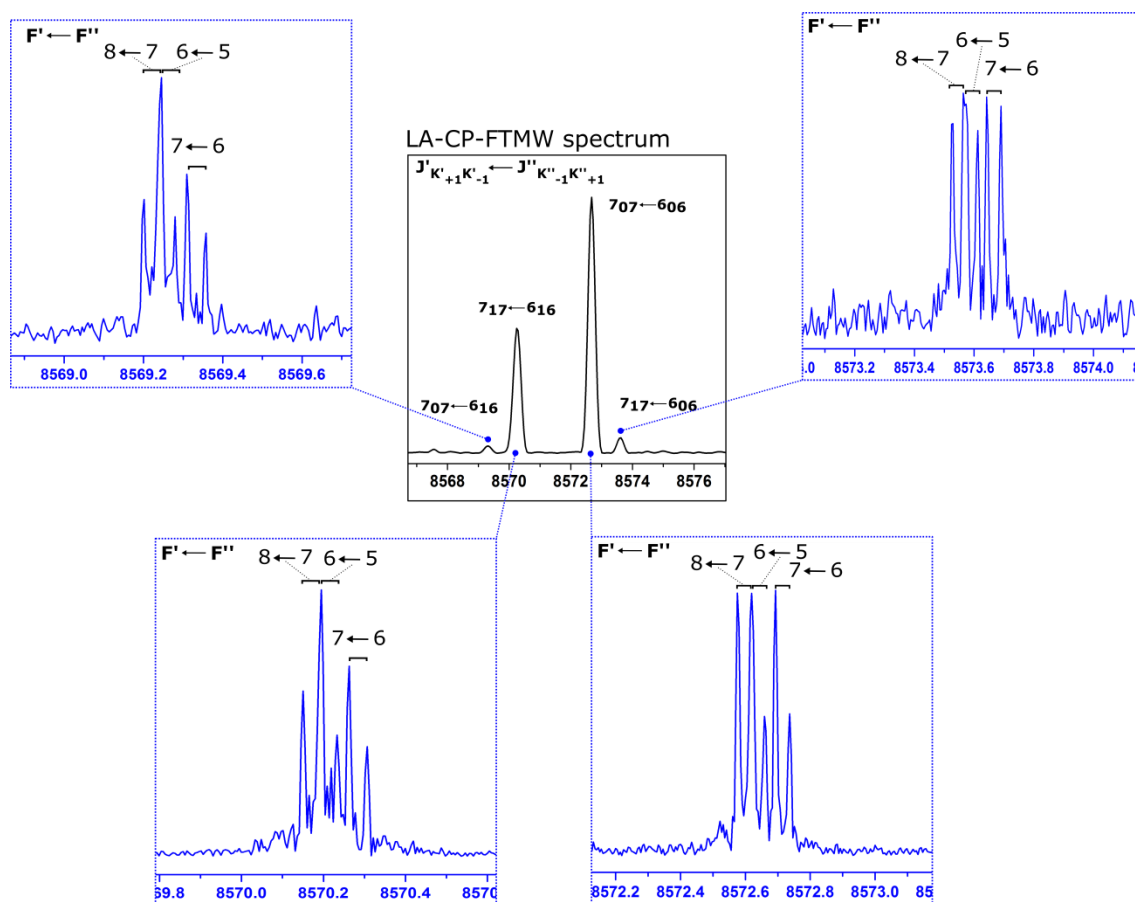


**Figure 3.** The rotational transitions using the LA-MB-FTMW spectrometer, showing the  $^{14}\text{N}$  quadrupole hyperfine structure. Since the molecular beam and the microwave radiation travel parallel to each other, each rotational transition appears as a doublet due to the Doppler effect.



**Table 1.** Experimental and theoretical rotational constants

	Experimental parent	Experimental <sup>34</sup> S	M062X/ cc-pTVZ
<b>A</b> <sup>a</sup>	1298.4982(44)	1296.907(29)	1301.0 (0.99)
<b>B</b>	871.2573(29)	865.282(18)	870.7 (1.00)
<b>C</b>	579.46230(20)	576.41970(94)	580.5 (0.99)
$\chi_a$ /MHz	1.84(17)	-	1.8
$\chi_b$ /MHz	2.502(82)	-	2.7
$\chi_c$ /MHz	-4.340(82)	-	-4.5
$\mu_a$ / $\mu_b$ / $\mu_c$ / D	intense/weak/---		4.0/0.9/0.0
<b>P<sub>cc</sub></b>	-97.1081(35)	-96.987(21)	-98.2

[a] A, B, and C represent the rotational constants (in MHz);  $P_c$  is the planar inertial moment (in  $\text{u}\text{\AA}^2$ ), conversion factor:  $505379.1 \text{ MHz}\cdot\text{u}\text{\AA}^2$ ;  $\mu_a$ ,  $\mu_b$  and  $\mu_c$  are the electric dipole moment components (in D);  $\chi_{aa}$ ,  $\chi_{bb}$  and  $\chi_{cc}$  are the diagonal elements of the  $^{14}\text{N}$  nuclear quadrupole coupling tensor (in MHz).

### 3.2 Discussion

The rotational constants obtained for the parent and the  $^{34}\text{S}$  isotopic species allowed to investigate the  $C_s$  symmetry of saccharine. The values of the planar moment  $P_{cc} = (I_a + I_b - I_c)/2 = \sum_i m_i c_i^2$  gives the mass extension out of the  $ab$  inertial plane. The very close values determined for the parent and the  $^{34}\text{S}$  isotopic species in table 1 indicates that the substituted atom is in the  $ab$  inertial plane and thus the  $ab$  plane is a plane of symmetry in saccharine. The sulfoxide oxygens are out of the plane in equivalent positions.

The AH, B,  $\gamma$  tripartite concept for sweetness has not only applied to sugars but also has been applied as the unifying criterion to saccharine. Following Shallenberger<sup>1</sup> and Kier<sup>2</sup>, the NH group acts as proton donor (AH), the oxygens of the sulfoxide group as proton acceptor (B) and the upper carbon of the benzene as the hydrophobic point  $\gamma$  (see figure 4). Due to the symmetry plane that makes both oxygens equivalent symmetrically, it can be said that the saccharine has a top and a bottom face, and it can interact by a slide operation and/or a rotation operation with the complementary tripartite in the receptor to produce the sweet response (see figure 5). This could explain the high sweet sensation that the saccharine produce respect to other sweeteners.

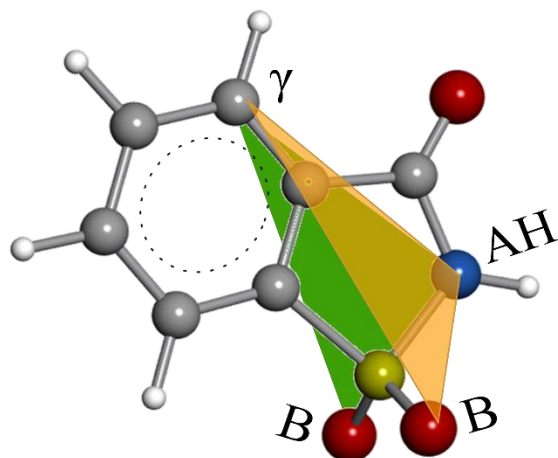


**Figure 4.** Planar structure of saccharine with the two possible tripartite AH, B,  $\gamma$  glucophore anchor points.

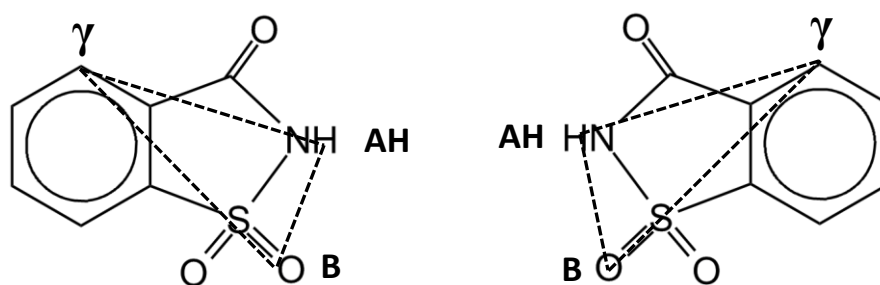


**Figure 5.** Specification of the chiral nature of the saccharine tripartite AH, B,  $\gamma$  glucophores for either side of the molecule

### 3.3 Conclusion

In summary, much remains to be learned about the intricacies of the mechanism involved in activation of sweet-sensitive receptors, and direct solid evidence is urgently required. Nevertheless, the incorporation of the three-dimensional shape of sweet molecules, of their contact surfaces, and, particularly, inclusion of their rotational studies, has provided this field with a new dynamic vision of the sweet molecule as such. This revelation of the three-dimensional structures, via microwave spectroscopy, may lead to more realistic structure-sweetness concepts than those heretofore developed.

## 4. REFERENCES

---

- <sup>1</sup> R. S. Shallenberger and T. E. Acree, *Nature*, 1967, 216, 480.
- <sup>2</sup> L. B. Kier, *J. Pharm. Sci.*, 1972, 61, 1394–1397.
- <sup>3</sup> A. van der Heijden, L. B. P. Brussel and H. G. Peer, *Food Chem.*, 1978, 3, 207–211.
- <sup>4</sup> T. Yamazaki, E. Benedetti, D. Kent and M. Goodman, *Angew. Chemie Int. Ed. English*, 1994, 33, 1437–1451.
- <sup>5</sup> C.K. Lee, *Adv Carbohydr Chem Biochem*. 1987, 45, 199-351.
- <sup>6</sup> G.E. Dubois, D.E. Walters, M.S. Kellog, *Sweet-taste Chemoreception*, Ed. M. Mathlouth.
- <sup>7</sup> G.G. Birch, Elsevier Applied Science 1993, London/New York
- <sup>8</sup> J.L. Alonso, J.C.López, “*Microwave Spectroscopy of Biomolecular Building Blocks*” *Topics in Current Chemistry*, Vol. 364 Springer, Heidelberg, 2015, pp.335–402.
- <sup>9</sup> J. L. Alonso, M. A. Lozoya, I. Peña, J. C. López, C. Cabezas, S. Mata, S. Blanco, *Chem. Sci.*, 2014, 5, 515-522
- <sup>10</sup> I. Peña, C. Cabezas, J. L. Alonso, *Chem. Commun.*, 2015, 51, 10115
- <sup>11</sup> C. Bermúdez, I. Peña, C. Cabezas, A. M. Daly and J. L. Alonso, *ChemPhysChem*, 2013, 14, 893.
- <sup>12</sup> C. Bermúdez, I. Peña, S. Mata and J. L. Alonso, *Chem. - A Eur. J.*, 2016, 22, 17047–17047.
- <sup>13</sup> E.R. Alonso, L. Kolesniková, S. Mata, C. Cabezas, I. Peña, J.L. Alonso. H-bonding network in sugar alcohols. The 24<sup>TH</sup> International Conference on High Resolution Molecular Spectroscopy, Praha, 2016.
- <sup>14</sup> Moncrieff, R.V. “*The Chemical Senses*” 1967, Leonard Hill, London.
- <sup>15</sup> S. Mata, I. Peña, C. Cabezas, J.C. López, J.L. Alonso, *J. Mol. Spectrosc.* 180 (2012)91.
- <sup>16</sup> I. Peña, S. Mata, A. Martín, C. Cabezas, A. M. Daly, J. L. Alonso, *Phys. Chem. Chem. Phys.*, 2013, 15, 18243-18248
- <sup>17</sup> J.L. Alonso, C. Pérez, M.E. Sanz, J.C. López, S. Blanco, *Phys. Chem. Chem. Phys.* 11(2009) 617.
- <sup>18</sup> M. J. Frisch, G. W. Trucks, H. B. Schlegel, G. E. Scuseria, M. A. Robb, J. R. Cheeseman, G. Scalmani, V. Barone, B. Mennucci, G. A. Petersson, H. Nakatsuji, M. Caricato, X. Li, H. P. Hratchian, A. F. Izmaylov, J. Bloino, G. Zheng, J. L. Sonnenberg, M. Hada, M. Ehara, K. Toyota, R. Fukuda, J. Hasegawa, M. Ishida, T. Nakajima, Y. Honda, O. Kitao, H. Nakai, T. Vreven, J. A. Montgomery, Jr., J. E. Peralta, F. Ogliaro, M. Bearpark, J. J. Heyd, E. Brothers, K. N. Kudin, V. N. Staroverov, R. Kobayashi, J. Normand, K. Raghavachari, A. P. Rendell, J. C. Burant, S. S. Iyengar, J. Tomasi, M. Cossi, N. Rega, M. J. Millam, M. Klene, J. E. Knox, J. B. Cross, V. Bakken, C. Adamo, J. Jaramillo, R. Gomperts, R. E. Stratmann, O. Yazyev, A. J. Austin, R. Cammi, C. Pomelli, J. W. Ochterski, R. L. Martin, K. Morokuma, V. G. Zakrzewski, G. A. Voth, P. Salvador, J. J. Dannenberg, S. Dapprich, A. D. Daniels, O. Farkas, J. B. Foresman, J. V. Ortiz, J. Cioslowski and D. J. Fox, *Gaussian*, Gaussian 09 Rev. D01., Gaussian, Inc., Wallingford, CT, 2012, see also: <http://www.gaussian.com>.
- <sup>19</sup> H.M. Pickett, *J. Mol. Spectrosc.* 148 (1991) 371.
- <sup>20</sup> W. Gordy, R.L. Cook, *Microwave Molecular Spectra*, third edn., Wiley, New York, 1984.
- <sup>21</sup> H.M. Foley, *Phys. Rev.* 71 (1947) 747.

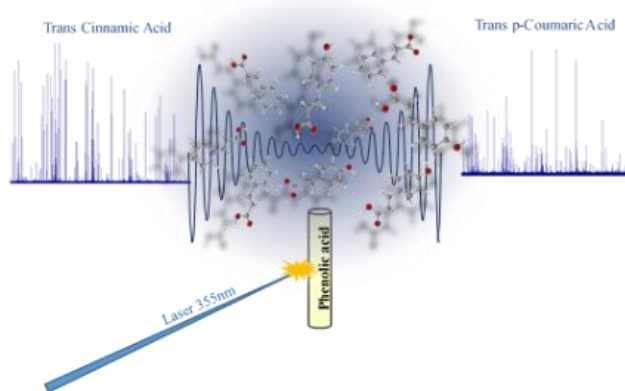


# CHAPTER IV.

## The Conformational Map of Phenolic Acids.

---

*Adapted from: J. Phys. Chem. A. 2018; 122(2): 646-651.*



*The benefits of vaporization by laser ablation and the high resolution and sensitivity attained by the chirped pulse Fourier transform microwave spectroscopy CP-FTMW have provided the first conformational map of the simplest phenolic acids of trans-cinnamic and p-coumaric. Two*

*conformers of trans-cinnamic acid and four conformers of trans-p-coumaric acid have been characterized under the isolation conditions of a supersonic expansion. The spectroscopic constants derived from the analysis of the rotational spectra compared with those predicted theoretically provide an unmatched means to achieve an unambiguous identification of the observed species.*



## 1. INTRODUCTION

---

The phenolic acids are natural bioactive compounds<sup>1</sup> present in fruits, vegetables, medicinal plants and aromatics among others<sup>2</sup> and play a vital role in pharmaceutical industry.<sup>3,4</sup> These compounds have aroused great medicinal<sup>5</sup> and pharmacological<sup>6</sup> interest in the last years due to the health benefits provided by their consumption. Although their antioxidant<sup>7</sup> and anticancer<sup>8,9</sup> properties, among others,<sup>10-14</sup> have been widely reported, little is known about the detailed mechanism of action of these class of compounds. As some studies have revealed,<sup>15,16</sup> their biological and pharmacological properties rely on the corresponding structure-activity relationships. Thus, a detailed exploration at the molecular level of the conformational preferences of these bioactive systems is of interest.

In nature, two of the most important phenolic acids are the *trans*-cinnamic and *p*-coumaric acids. *Trans*-cinnamic acid (from now tCA) is the simplest unit present in all hydroxycinnamic acids. It could exist in two *s-cis* and *s-trans* configurations (see Figure 1a) arising from the corresponding arrangement of the carboxylic group. *Trans*-*p*-coumaric acid (from now tpCA) derives from the *trans*-cinnamic acid by attaching an OH group at the *para* position in the phenyl ring. Hence, two additional configurations due to the *syn* (*s*) or *anti* (*a*) disposition of the OH group could emerge for each *s-cis* and *s-trans* configurations of tCA. All the plausible configurations are labeled accordingly in Figure 1b.

Experimental studies in condensed phases on tCA and tpCA do not provide very precise structural information. Only centrosymmetric dimers have been characterized for both phenolic acids by X-Ray, Raman, NMR and FTIR spectroscopy.<sup>17,18,19,20,21,22</sup> Taking advantage of the chromophoric character, electronic spectroscopic techniques have been used in combination with supersonic expansion to investigate tpCA in the isolated conditions of the gas phase. In a first instance, two different conformers were reported by Ryan *et al*<sup>23</sup> using fluorescence excitation and dispersed emission methods but a subsequent study<sup>24</sup> using MR-RE2PI spectroscopy showed that the recorded spectrum really corresponds to the *p*-vinyl phenol, the thermal decarboxylation product of tpCA.<sup>25</sup> More recently, Buma *et al*<sup>26</sup>

have proposed the existence of two *cis* and one *trans* conformers for tpCA by comparison of its experimental absorption spectroscopy data with those obtained for the *related* methyl-4-Hydroxycinnamate.<sup>27</sup> The case of the tCA, the simplest phenolic acid, is remarkable as to date no experimental investigations have been carried out to elucidate its conformational landscape. Thus, the conformational panorama of phenolic acids remains unknown, and their investigation has been, until now, restricted solely to theoretical studies.<sup>28-30</sup>

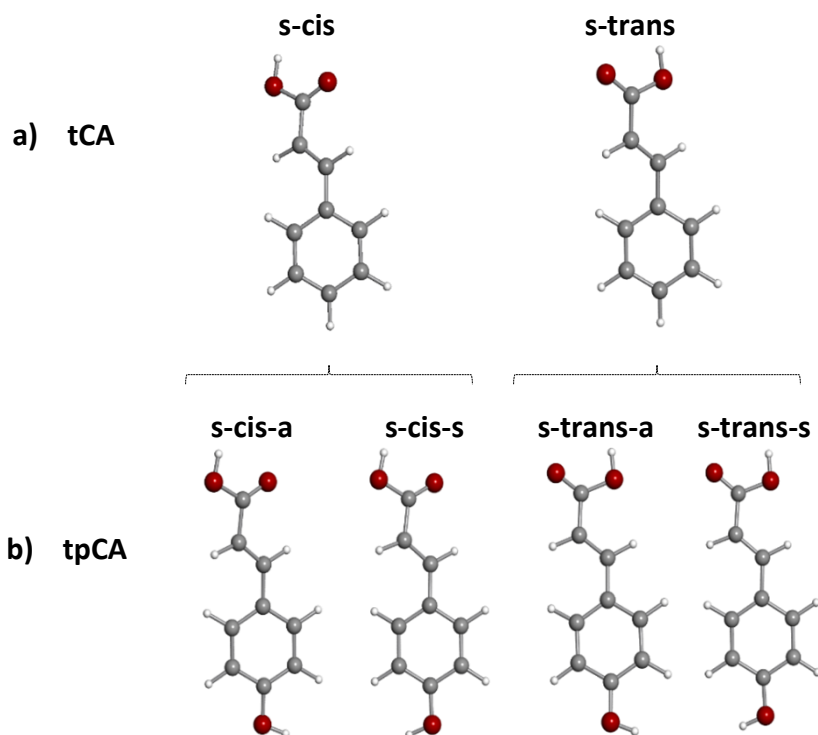


**Figure 1.** (a) *trans*-cinnamic acid configurations *s-cis* and *s-trans* arising from the corresponding arrangement of the carboxylic group. (b) *trans*-*p*-coumaric acid configurations attending to the *anti* (*a*) or *syn* (*s*) disposition of the OH group.

Phenolic tCA and tpCA acids are solid with high melting point of 134,5°C and 214°C respectively and low vapor pressure. Rotational studies using heating methods have been hampered by their thermal instability, preventing easy measurement of its gas-phase rotational spectra. Laser ablation techniques are being used in our research group at Valladolid to transfer solid biomolecules into the gas phase allowing to probe them by the



latest broadband and narrowband Fourier transform microwave spectroscopic techniques.<sup>31</sup> Excellent results have been recently achieved on many biologically relevant solid biomolecules as nucleosides,<sup>32</sup> sugars<sup>33,34</sup> and dipeptides,<sup>35</sup> unveiling for the first time their conformational preferences in the gas phase. We have applied this experimental approach to unveiling the conformational panorama of tCA and tpCA using our LA-CP-FTMW<sup>36</sup> technique. Two conformers of tCA and the four conformers of tpCA have been unequivocally identified through the analysis of their rotational spectra. Details of the investigation are presented in the next sections.

## 2. EXPERIMENTAL DETAILS

---

Samples of tCA acid and tpCA were obtained commercially and used without further purification. In the experiment, solid cylindrical rod targets prepared by pressing the compound's fine powder mixed with a small amount of commercial binder, were vaporized by the third harmonic (355 nm) of a Nd:YAG picosecond laser. The ablation products, seeded in a flow of Neon at 15 bar of stagnation pressure, were supersonically expanded and characterized by chirped pulse Fourier transform microwave spectroscopy<sup>37</sup> in the frequency range 2 to 8 GHz. Up to 75000 individual free induction decays at 2 Hz repetition rate (4 FID emission decays per gas pulse) were averaged in the time domain and Fourier transformed to obtain the frequency domain rotational spectrum of tCA and tpCA. The accuracy of frequency measurements is estimated to be better than 10 kHz.

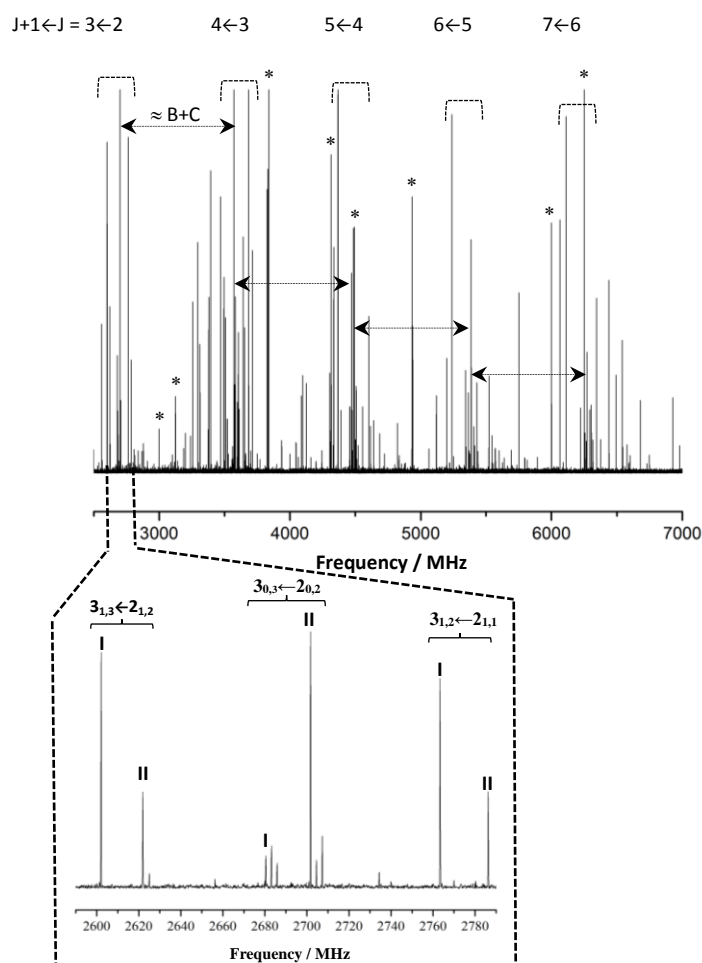
## 3. RESULTS AND DISCUSSION

---

### ***3.1. Rotational Spectrum of trans-cinnamic acid.***

The broadband rotational spectrum of laser ablated tCA in the 2.5-7 GHz region is shown in Figure 2. It exhibits the characteristic pattern of the nearly prolate asymmetric rotor with  $\mu_a$ -type R-branch transitions appearing to form regularly spaced bands at  $B+C$  intervals. A

more detailed inspection into the  $J = 3 \leftarrow 2$  band structure (see inset of Figure 2), reveals the existence of two separate sets of  $\mu_a$ -type R-branch transitions  $3_{1,3} \leftarrow 2_{1,2}$ ,  $3_{0,3} \leftarrow 2_{0,2}$ ,  $3_{1,2} \leftarrow 2_{1,1}$ . They correspond to two different rotameric species, which were labeled as I and II. Similar patterns were found for other bands (from  $J=2$  to  $J=6$ ) that appeared in the recorded frequency range. Following an iterative process of fitting and prediction,<sup>38</sup>  $\mu_b$ -type R-branch rotational transitions were also identified and measured for both rotamers.  $\mu_c$ -type lines were predicted but not found. A total of 52 transitions, collected in Tables S1-S2 of the Supporting Information, were measured for each rotamer. They were analyzed using a rigid rotor Hamiltonian<sup>39</sup> to give the sets of rotational constants listed in the first section of Table 1. The two observed rotamers exhibit similar values of their experimental rotational constants (see Table 1), as belonging to conformers with the same skeletal frame but different orientation of their functional groups. The small negative values of the inertial defect<sup>40</sup>  $\Delta = I_c - I_a - I_b$  of  $-1.10 \text{ u}\text{\AA}^2$  for rotamer I and  $-1.18 \text{ u}\text{\AA}^2$  for rotamer II, along with the



non-observation of  $\mu_c$ -type rotational transitions allow us to conclude that both rotameric species have planar or nearly planar structures. They can be initially ascribed to the *s-cis* and *s-trans* forms of tCA depicted in Figure 1a.

**Figure 2.** A section of the broadband rotational spectrum of tCA from 2.5 to 7 GHz obtained by LA-CP-FTMW technique after 75000 FIDS showing rotational bands of  $\mu_a$  type R-branch transitions separated approximately  $B+C$  ranging from  $J = 2$  to  $J = 6$ . Common photofragmentation lines have been marked with the symbol \*. Inset: Small section of the spectrum showing the  $3_{1,3} \leftarrow 2_{1,2}$ ,  $3_{0,3} \leftarrow 2_{0,2}$ ,  $3_{1,2} \leftarrow 2_{1,1}$  rotational transitions of the two observed rotamers of tCA.

To discriminate between them, DFT calculations at B3LYP/6-311++G(d,p) were performed on these configurations to estimate energies and rotational constants values assuming planar configurations. Results are collected in the second section of Table 1 for comparison. *s-cis* and *s-trans* forms differ only in the opposite arrangement of the carboxylic group (see Figure 1a) that induces minor changes in the absolute values of the rotational constants. Therefore, it is not possible to carry out an unequivocal identification of the observed rotamers on this basis. Fortunately, the change in orientation of the carboxylic group in the *s-cis* and *s-trans* conformations causes distinctive shifts in the inertial moments which are translated to the rotational constants in Table 1. Thus, the small shifts in the rotational constants between rotamers I and II of  $\Delta A \approx -14.6$  MHz,  $\Delta B \approx 4.1$  MHz and  $\Delta C \approx 3.0$  MHz are in good agreement with the predicted changes  $\Delta A \approx -13.7$  MHz,  $\Delta B \approx 4.1$  MHz and  $\Delta C \approx 3.0$  MHz going from conformer *s-cis* to *s-trans*. This fact allows us to a conclusive identification of rotamer I as conformers *s-cis* and rotamer II as conformer *s-trans*. Relative intensity measurements carried out on selected  $\mu_a$ -type lines of both conformers yield to a population ratio of  $N_{s-cis} : N_{s-trans} \approx 1 : 0.7$ , in agreement with DFT calculations which predict the *s-cis* conformer as the global minimum with the *s-trans* conformer  $195 \text{ cm}^{-1}$  higher in energy.

**Table 1.** Theoretical and experimental spectroscopic parameters for the conformers of tCA.

	Experimental		Theory <sup>a</sup>	
	I	II	s-cis	s-trans
$A^b$	3677.7943(15)	3663.1408(11)	3689.0	3675.3
$B$	474.059177( 89)	478.146097(62)	472.1	476.2
$C$	420.315661( 91)	423.358479(72)	418.6	421.6
$\Delta$	-1.1013(5)	-1.1807 (4)	0.0 <sup>g</sup>	0.0 <sup>g</sup>
$ \mu_a $	Observed	Observed	2.3	3.0
$ \mu_b $	Observed	Observed	1.3	1.4
$ \mu_c $			0.0	0.0
$\Delta E^c$			0	195
$N^d$	52	52		
$\sigma^e$	5.4	3.9		

<sup>a</sup>DFT computations at B3LYP/6-311++G(d,p) level of theory. <sup>b</sup>A, B and C represent the rotational constants in MHz;  $\Delta = I_c - I_a - I_b$  in  $\text{u}\text{\AA}^2$ . <sup>c</sup>Relative energies with respect to the global minimum in  $\text{cm}^{-1}$ . <sup>d</sup>Number of fitted transitions. <sup>e</sup>RMS deviation of the fit. <sup>f</sup>Observation of a-, b- and c-type transitions for each structure. <sup>g</sup>Fixed to zero for planar structures.

### 3.2. Rotational Spectrum of *trans-p-coumaric acid*.

A model based on the structures obtained above for tCA conformers predicts the four plausible configurations of tpCA of Figure 1b to be near prolate asymmetric rotors with the electric dipole moment mainly oriented along the principal  $a$  inertial axis. The 2.5-5 GHz section of the LA-CP-FTMW spectrum in Figure 3 indicates the expected  $\mu_a$ -type R-branch band structure. The assignment of individual  $\mu_a$ -type R-branch lines was straightforward. Each band from (from  $J = 3$  to  $J = 6$ ) shows four different sets of  $\mu_a$ -type R-branch rotational transitions ( $J+1$ ) $_1$ ,  $J+1 \leftarrow J$ ,  $J$ , ( $J+1$ ) $_0$ ,  $J+1 \leftarrow J$ ,  $J$  and ( $J+1$ ) $_1$ ,  $J \leftarrow J$ ,  $J-1$  belonging to four different rotamers. They have labeled as I, II, III and IV, as exhibited the inset of Figure 3 for the  $J=4 \leftarrow 3$  rotational transitions.

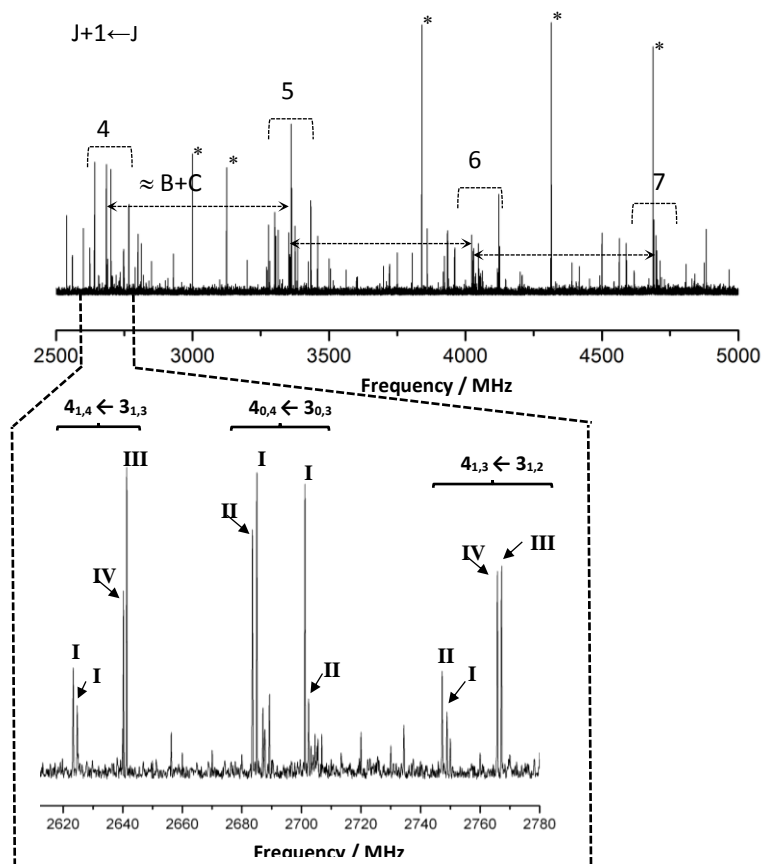


**Figure 3.** A section of the broadband rotational spectrum of tpCA from 2.5 to 5 GHz obtained by LA-CP-FTMW technique (75000 fids) showing four bands of  $\mu_a$ -type R-branch transitions separated approximately  $B+C$  with  $J$  ranging from 3 to 6. Common photofragmentation lines have been marked with the symbol \*. Inset: small section of the spectrum showing the  $4_{1,4} \leftarrow 3_{1,3}$ ,  $4_{0,4} \leftarrow 3_{0,3}$ ,  $4_{1,3} \leftarrow 3_{1,2}$  rotational transitions of the four observed rotamers of *p-coumaric acid* denoted as I, II, III and IV.

Like for tCA,  $\mu_c$ -type rotational transitions were absent in all rotamers, as a first indication of planarity. However,  $\mu_b$ -type R-branch transitions were observed and measured for the II

and III rotamers. A total of 32, 32, 29 and 18 rotational transitions, corresponding to I, II, III and IV rotamers respectively, were fitted<sup>38</sup> using a rigid rotor Hamiltonian.<sup>39</sup> They are listed in Tables S3-S6 of Supporting Information. The derived spectroscopic parameters have been collected in the first section of Table 2. The values of the inertial defects, ranging from -1.03 to -1.21 uÅ<sup>2</sup> strongly indicate that the four observed rotamers adopt planar or nearly planar structures and they should be ascribed to the two *s-cis* and the two *s-trans* forms of tpCA depicted in Figure 1b. As for tCA, DFT calculation assuming planar structures were carried out on these four plausible configurations, and the results have been collected in the second section of Table 2. The comparison between the experimental rotational constants of the four observed rotamers and those predicted for the *s-cis-a*, *s-cis-s*, *s-trans-a* and *s-trans-s* configurations does not allow any conclusive discrimination between them.

**Table 2.** Theoretical and experimental spectroscopic parameters for the conformers of tpCA.

	Experimental				Theory <sup>a</sup>			
	I	II	III	IV	<i>s-cis-a</i>	<i>s-cis-s</i>	<i>s-trans-a</i>	<i>s-trans-s</i>
$A^b$	3600.07( 75)	3602.8448(20)	3595.8205(21)	3599.64( 50)	3613.3	3617.8	3611.1	3615.1
$B$	351.42397(27)	351.20353(12)	353.81899(11)	353.62618( 46)	349.9	349.7	352.3	352.1
$C$	320.37778(28)	320.23615(15)	322.35751(12)	322.23754( 63)	319.0	318.9	321.0	320.9
$\Delta$	-1.02 (3)	-1.1192 (13)	-1.1415 (11)	-1.19 (2)	0.0 <sup>g</sup>	0.0 <sup>g</sup>	0.0 <sup>g</sup>	0.0 <sup>g</sup>
$\mu_a$	Observed <sup>f</sup>	Observed	Observed	Observed	3.1	2.7	3.7	3.3
$\mu_b$	-----	Observed	Observed	-----	0.2	2.6	2.9	0.1
$\mu_c$	-----	-----	-----	-----	0.0	0.0	0.0	0.0
$\Delta E^c$					0	38	215	229
$N^d$	32	32	29	18				
$\sigma^e$	5.0	6.8	5.7	7.4				

<sup>a</sup> DFT computations at B3LYP/6-311++G(d,p) level of theory. <sup>b</sup>  $A$ ,  $B$  and  $C$  represent the rotational constants in MHz;  $\Delta = |c-a-b|$  in uÅ<sup>2</sup>. Conversion factor: 505379,07uÅ<sup>2</sup>MHz<sup>c</sup> Relative energies in cm<sup>-1</sup>. <sup>d</sup> Number of fitted transitions. <sup>e</sup> RMS deviation of the fit in KHz. <sup>f</sup> Observation of a-, b- and c-type transitions for each structure. <sup>g</sup> Fixed to zero for planar structures.

The values of the dipole moment components that control the microwave selection rules, can be used in favorable cases as a definitive tool in the conformational assignment. Although the specific values of the dipole moment components cannot be obtained from our experiment, it is possible to check whether the observed selection rules of a rotamer is in accordance with the predicted ones for a particular conformer. Hence, while the change in the orientations of the carboxylic and hydroxyl groups induces small variations in the

values of the rotational constants, the change in the orientation of the hydroxyl group (*syn/anti* forms) dramatically affect the predicted values of the  $\mu_b$  dipole moment component within each *s-cis* or *s-trans* configurations (see Table 2). On the basis of the observed selection rules, the pair of rotamers I and IV should be related to the pair of *s-cis-a* and *s-trans-s* conformers and the II and III rotamers to the *s-cis-s* and *s-trans-a* pair. Within each pair however, the distinctions are not so easily made based on the absolute values of the rotational constants. Once again, the small shifts in the rotational constants allow us to carry out a conclusive assignment of the observed rotamers. Thus, the changes in the experimental values of the rotational constants in going from rotamer I to rotamer IV of  $\Delta A \approx -0.4$  MHz,  $\Delta B \approx 2.2$  MHz and  $\Delta C \approx 1.9$  MHz, are only consistent with the predicted changes  $\Delta A \approx 1.8$  MHz,  $\Delta B \approx 2.2$  MHz and  $\Delta C \approx 1.9$  MHz going from conformer *s-cis-a* to *s-trans-s*, allowing us to assign unambiguously rotamer I as conformer *s-cis-a* and rotamer IV as conformer *s-trans-s*. In the same manner, the shifts  $\Delta A \approx -6.7$  MHz,  $\Delta B \approx 2.6$  MHz and  $\Delta C \approx 2.1$  MHz in going from rotamer II to rotamer III, are in perfect agreement with the predicted changes  $\Delta A \approx -6.7$  MHz,  $\Delta B \approx 2.6$  MHz and  $\Delta C \approx 2.1$  MHz going from conformer *s-cis-s* to *s-trans-a*, allowing us to conclusively assign rotamer II to conformer *s-cis-s* and rotamer III to conformer *s-trans-a*. By measuring the relative intensities of different  $\mu_a$ -type rotational transitions a population ratio  $N_{s-cis-a} : N_{s-cis-s} : N_{s-trans-a} : N_{s-trans-s} \approx 0.6 : 1 : 0.2 : 0.3$  was obtained which is in reasonable agreement with the predicted relative energies in Table 2.

#### 4. CONCLUSIONS

---

The present study provides the first experimental information on *trans*-cinnamic tCA and *trans*-p-coumaric tpCA phenolic acids which led to the determination of their intrinsic conformational landscape. Two conformers have been detected for tCA and four tpCA for which the rotational parameters and relative abundances have been determined. The solids of these phenolic acids have been brought into the gas phase by laser ablation LA and their rotational spectra investigated in the isolated condition of a supersonic expansion by chirp pulsed Fourier transform microwave spectroscopy CP-FTMW. The spectroscopic data provided and the fact that they are directly compared with those predicted theoretically

constitute an unmatched tool to discriminate and identify conformers which possess the same skeletal mass distribution. The most abundant species of tCA and tpCA exhibit the same *s-cis* arrangement of the carboxylic group. This conformational behavior has been also observed in the related nicotinic acid.<sup>36</sup>

The negative values of inertial defects of about  $\Delta = -1,1 \text{ u\AA}^2$ , obtained in the jet expansion in the vibrational ground states, are typical of planar molecules with low -frequency out-of-plane motions and compatible with the existence of two out-of-plane low-energy C-C<sub>carb</sub> and C<sub>arom</sub>-C torsions in the phenolic acids. These values are consistent with those of nicotinic acid ( $\Delta = -0,35 \text{ u\AA}^2$ ),<sup>36</sup> benzoic acid ( $\Delta = -0,36 \text{ u\AA}^2$ ),<sup>41</sup> and salicylic acid ( $\Delta = -0,25 \text{ u\AA}^2$ )<sup>42</sup> with only one out of-plane torsional motion.

## 5. REFERENCES

- <sup>1</sup> Vogt, T. Phenylpropanoid Biosynthesis. *Mol. Plant.* 2010, 3, 2-20. DOI: 10.1093/mp/ssp106.
- <sup>2</sup> Dixon, R. A. Natural Products and Plant Disease Resistance. *Nature.* 2001, 411, 843–847. DOI: 10.1038/35081178
- <sup>3</sup> Sharma, P. Cinnamic Acid Derivatives: A New Chapter of Various Pharmacological Activities. *J. Chem. Pharm. Res.* 2011, 3, 403-423.
- <sup>4</sup> Ashton, A.Q. Ph.D. *Cinnamates-Advances in Research and Applications.* Ed. Scholarly Brief. 2013
- <sup>5</sup> Roy, A. J.; Prince P. S. Preventive Effects of p-Coumaric Acid on Lysosomal Dysfunction and Myocardial Infarct Size in eExperimentally Induced Myocardial Infarction. *Eur. J. Pharmacol.* 2013, 699, 33–39.
- <sup>6</sup> Amalan, V.; Vijayakumar, N.; Ramakrishnan A. P-Coumaric Acid Regulates Blood Glucose and Antioxidant Levels in Streptozotocin Induced Diabetic Rats. *J. Chem. Pharm. Res.* 2015, 7, 831-839.
- <sup>7</sup> Shang Y.-J.; Liu B.-Y.; Zhao M.-M. Details of the Antioxidant Mechanism of Hydroxycinnamic Acids. *Czech J. Food Sci.* 2015, 33, 210-216.
- <sup>8</sup> De P.; Baltas M.; Bedos-Belval, F. Cinnamic Acid Derivatives as Anticancer Agents-A Review. *Curr. Med. Chem.* 2011, 18, 1672-1703.
- <sup>9</sup> Liu, L.; Hudgins, W. R.; Shack, S.; Yin, M. Q.; Samid, D. Cinnamic Acid: a Natural Product with Potential Use in Cancer Intervention. *Int. J. Cancer.* 1995, 62, 345-350.
- <sup>10</sup> Guzman, J. D. Natural Cinnamic Acids, Synthetic Derivatives and Hybrids with Antimicrobial Activity. *Molecules.* 2014, 19, 19292-19349. DOI: 10.3390/molecules191219292.
- <sup>11</sup> Jitareanu, A.; Tataranga, G.; Zbancioc, A. M.; Tuchilus, C.; Stanescu, U. Antimicrobial Activity of Some Cinnamic Acid Derivatives. *Rev. Med. Chir. Soc. Med. Nat. Iasi.* 2011, 115, 965–971.
- <sup>12</sup> Korošec, B.; Sova, M.; Turk, S.; Kraševac, N.; Novak, M.; Lah, L.; Stojan, J.; Podobnik, B.; Berne, S.; Zupanec, N. et al. Antifungal Activity of Cinnamic Acid Derivatives Involves Inhibition of Benzoate 4-Hydroxylase (CYP53). *J. Appl. Microbiol.* 2014, 116, 955–966S.
- <sup>13</sup> Pragasam, S. J.; Venkatesan, V.; Rasool, M. Immunomodulatory and Anti-Inflammatory Effect of p-Coumaric Acid, A Common Dietary Polyphenol on Experimental Inflammation in Rats. *Inflammation.* 2013, 36, 169-176. DOI: 10.1007/s10753-012-9532-8.
- <sup>14</sup> Guven, M.; Aras, A. B.; Akman, T.; Sen, H. M.; Ozkan, A.; Salis, O.; Sehitoglu, I.; Kalkan, Y.; Silan, C.; Deniz, M.; et al. Neuroprotective Effect of p-Coumaric Acid in Rat Model of Embolic Cerebral Ischemia. *Iran J. Basic Med. Sci.* 2015, 18, 356-363.

- <sup>15</sup> Chen, Y.; Xiao, H.; Zheng, J.; Liang, G. Structure-Thermodynamics-Antioxidant Activity Relationships of Selected Natural Phenolic Acids and Derivatives: An Experimental and Theoretical Evaluation. *PLOS ONE*, 2015, *10*, e0121276. and references therein. DOI: 10.1371/journal.pone.0121276
- <sup>16</sup> Rice-Evans, C. A.; Miller, N. J.; Paganda, G. Structure-Antioxidant Activity Relationships of Flavonoids and Phenolic Acids. *Free Radic. Biol. Med.* 1996, *20*, 933-956, and references therein.
- <sup>17</sup> Mc Donald, J. Ladell, T. R. R. and Schmidt, G. M. J. The Crystal Structure of  $\square$ -trans-Cinnamic Acid. *Acta Cryst.* 1956, *9*, 195. DOI: 10.1107/S0365110X56000474
- <sup>18</sup> Wierda, D. A.; Feng, T. L.; Barron, A. R. Structure of trans-Cinnamic Acid. *Acta Cryst.* 1989, *C45*, 338-339.
- <sup>19</sup> Utsumi, H.; Fujii, K.; Irie, H.; Furusaki, A. and Nitta, I. The Crystal Structure of p-Coumaric Acid. *Bull. Chem. Soc. Jap.* 1966, *40*, 426.
- <sup>20</sup> Nolasco, M. M.; Amado, A. M.; Ribeiro-Claro, P. J. A. Effect of Hydrogen Bonding in the Vibrational Spectra of trans-Cinnamic Acid. *J. Raman Spectrosc.* 2009, *40*, 394-400.
- <sup>21</sup> Vinod, K. S.; Periandt, S.; Govindarajan, M. Spectroscopic Analysis of Cinnamic Acid Using Quantum Chemical Calculations. *Spectrochim. Acta A*, 2015, *136*, 808-817.
- <sup>22</sup> Kumar, N.; Pruthy, V.; Goel, N. Structural, Thermal and Quantum Chemical Studies of p-Coumaric and Caffeic acids. *J. Mol. Struct.* 2015, *1085*, 242-248.
- <sup>23</sup> Ryan, W. L.; Gordon, D. J.; Levy, D. H. Gas-phase Photochemistry of the Photoactive Yellow Protein Chromophore trans-p-Coumaric acid. *J. Am. Chem. Soc.*, 2002, *124*, 6194-6201.
- <sup>24</sup> De Groot, M.; Buma, W. J. Comment on "Gas-phase Photochemistry of the Photoactive Yellow Protein Chromophore trans-p-Coumaric Acid". *J. Phys. Chem. A*. 2005, *109*, 6135-6136.
- <sup>25</sup> Morgan, P. J.; Mitchell, D. M.; Pratt, D. W. High-Resolution Electronic Dpctroscopy of p-Vinylphenol in the Gas Phase. *J. Chem. Phys.* 2008, *347*, 340-345.
- <sup>26</sup> Smolarek, S.; Vdovin, A.; Perrier, D. L.; Smit, J. P.; Drabbels, M.; Buma, W. J. High-resolution Excitation and Sbsorption Spectroscopy of Gas Phases p-Coumaric Acid: Unveiling an Elusive Chromophore. *J. Am. Chem. Soc.* 2010, *132*, 6315-6317.
- <sup>27</sup> De Groot, M.; Gromov, Evgeniy V.; Köppel, H.; Buma, W. J. High-resolution Spectroscopy of Methyl-4-hydroxycinnamate and its Hydrogen-bonded Water Complex. *J. Phys. Chem. B*. 2008, *112*, 4427-4434.
- <sup>28</sup> Bakalbassisa, E. G.; Chatzopoulou, A.; Melissas, V. S.; Tsimidou, M.; Tsolaki, M.; Vafiadis, A. Ab Initio and Density Functional Theory Studies for the Explanation of the Antioxidant Activity of Certain Phenolic Acids. *Lipids*. 2001, *36*, 181-191.
- <sup>29</sup> Urbaniak, A.; Molski, M.; Szeląg, M. Quantum-chemical Calculations of the Antioxidant Properties of trans-p-Coumaric Acid and trans-Sinapinic Acid. *Comp. Meth. Sci. Tech.* 2012, *18*, 117-128.
- <sup>30</sup> Dávalos, J. Z.; Herrero, R.; Chana, A.; Guerrero, A.; Jiménez, P.; Santiuste, J. M. Energetics and Structural Properties in the Gas Phase, of trans-Hydroxycinnamic Acids. *J. Phys. Chem. A*, 2012, *116*, 2261-2267.
- <sup>31</sup> Alonso, J. L.; López, J. C. Microwave Spectroscopy of Biomolecular Building Blocks. *Top. Curr. Chem.* 2014, *364*, 3358-3401, and references therein.
- <sup>32</sup> Peña, I.; Cabezas, C.; Alonso, J. L. The Nucleoside Uridine Isolated in the Gas Phase. *Angew. Chem. Int. Ed.* 2015, *54*, 2991-2994, and references therein.
- <sup>33</sup> Bermúdez, C.; Peña, I.; Mata, S.; Alonso, J. L. Sweet Structural Signatures Unveiled in Ketohexoses. *Chem. Eur. J.* 2016, *47*, 17047 (cover) and references therein. DOI: 10.1002/chem.201604041
- <sup>34</sup> Alonso, E. R.; Peña, I.; Cabezas, C.; Alonso, J.L. Structural Expression of Exo-anomeric Effect. *J. Phys. Chem. Lett.* 2016, *7*, 845-850 and references therein.
- <sup>35</sup> Cabezas, C.; Varela, M.; Alonso, J. L. The Structure of the Elusive Simplest Dipeptide Gly-Gly. *Angew. Chem. Int. Ed.* 2017, *56*, 6420-6425 and references therein.
- <sup>36</sup> Mata, S.; Peña, I.; Cabezas, C.; López, Juan C.; Alonso, J. L. A Broadband Fourier Transform Microwave Spectrometer with Laser Ablation Source: The Rotational Spectrum of Nicotinic acid. *J. Mol. Spectrosc.* 2012, *280*, 91-96.
- <sup>37</sup> Brown, G. G.; Dian, B. C.; Douglass, K. O.; Geyer, S. M.; Shipman, S. T.; Pate, B. H. A broadband Fourier Transform Microwave Spectrometer Based on Chirped Pulse Excitation. *Rev. Sci. Instrum.* 2008, *79*, 053103.
- <sup>38</sup> Pickett, H. M. The Fitting and Prediction of Vibration-rotation Spectra with Spin Interactions. *J. Mol. Spectrosc.* 1991, *148*, 371-377.
- <sup>39</sup> Gordy, W.; Cook, R. L. *Microwave Molecular Spectroscopy*. John Wiley & Sons, New York, 1984.
- <sup>40</sup> Oka, T. On Negative Inertial Defect. *J. Mol. Struct.* 1995, *352/353*, 225-233.
- <sup>41</sup> Onda, M.; Asai, M.; Takise, K.; Kuwae, K.; Hayami, K.; Kuroe, A.; Mori, M.; Miyazaki, M.; Suzuki, N.; Yamaguchi, I. Microwave Spectrum of Benzoic Acid. *J. Mol. Struct.* 1999, *482-483*, 301-303.
- <sup>42</sup> Evangelisti, L.; Tang, S.; Velino, B.; Caminati, W. Microwave Spectrum of Salicylic Acid ; *J. Mol. Struct.* 2009, *921*, 285-288



## CHAPTER V.

# The role of amino acid side chains in stabilizing dipeptides: The laser ablation Fourier transform microwave spectrum of Ac-Val-NH<sub>2</sub>

---

*Adapted from: Phys. Chem. Chem. Phys., 2017, 19, 24985-24990*

*The steric effects imposed by the isopropyl group of valine in the conformational stabilization of the capped dipeptide N-acetyl-L-valinamide (Ac-Val-NH<sub>2</sub>) have been studied by laser ablation molecular beam Fourier transform microwave (LA-MB-FTMW) spectroscopy. The rotational and quadrupole coupling constants of the two <sup>14</sup>N nuclei determined in this work show that this dipeptide exists as a mixture of C7 and C5 conformers in the supersonic expansion. The conformers are stabilized by a C=O...H-N intramolecular hydrogen bond closing a seven- or a five-membered ring respectively. The observation of both conformers is in good agreement with previous results on the related dipeptides containing different residues, confirming that the polarity/non-polarity of the side chains of the amino acid is the responsible of the conformational locking/unlocking. The voluminous isopropyl group is not able to prevent the less stable C5 conformer to be formed but it destabilizes the C=O...H-N interaction.*



## 1. INTRODUCTION

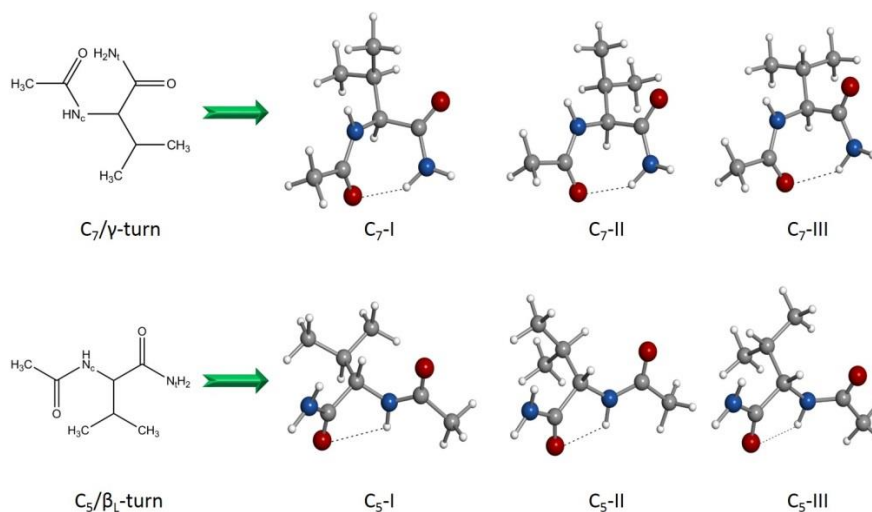
---

Proteins are some of the most versatile macromolecules in living systems that serve crucial functions in most of the biological processes.<sup>1</sup> There is a direct relationship between the protein's structure and its particular function or properties.<sup>1,2</sup> Therefore, an understanding of the functional architecture of these macromolecules, which is the result of a complex and subtle balance of different interactions, is fundamental not only as a whole, but also at a molecular level. To understand how these building blocks are organized, an accurate methodology is offered by studying the interactions in aminoacids or peptides. Dipeptide analogues containing two peptide linkages (-CO-NH-) are realistic systems in order to understand the basic conformational effects in peptides, aminoacids or proteins. In solution or solid states, the structures are the result not only of the number and type of the interactions in their building blocks, but also with the surrounding media. For example, A. B. Mandal et. al had synthesized and characterized several di, tri, and tetra-peptides demonstrating the aggregation, inter and intra molecular hydrogen bonding, monolayers, thermodynamics and conformational studies on these small peptides in aqueous (polar) and non-polar media.<sup>3,4</sup> On the other hand, gas phase experiments provide a unique and ideal medium to study, understand and model the interactions between small molecules free from any external interaction.<sup>5-8</sup>

In this line, aside from several theoretical studies,<sup>9-14</sup> there are several works focused on the study of dipeptide conformations in gas phase. Most of these works were done using double resonance laser spectroscopy techniques,<sup>6,15-21</sup> which entails the requirement of the introduction of an aromatic molecule in the system, creating the possibility of having some influence on the conformational preferences. On the other hand, microwave spectroscopy is one of the most powerful techniques that allows an unambiguous identification of the molecular structure, and hence the structural arrangement of the system under study. Lavrich et al.<sup>22</sup> investigated the alanine dipeptide N-acetyl-alanine N'-methyamide (Ac-Ala-NHMe) and observed only a C<sub>7</sub><sup>eq</sup> conformation.

Microwave spectra have also been recently measured by our group for several dipeptides: N-acetyl-glycinamide (Ac-Gly-NH<sub>2</sub>),<sup>23</sup> N-acetyl-alaninamide (Ac-Ala-NH<sub>2</sub>),<sup>24</sup> N-acetyl-prolinamide (Ac-Pro-NH<sub>2</sub>)<sup>25</sup> and N-acetyl-serinamide (Ac-Ser-NH<sub>2</sub>).<sup>26</sup> Ac-Gly-NH<sub>2</sub> and Ac-Ala-NH<sub>2</sub> dipeptides were found in both, C<sub>5</sub> (β-turn) and C<sub>7</sub> (γ-turn) conformations, in which the backbones are stabilized by a C=O•••H-N intramolecular hydrogen bond closing a five- or seven-membered rings, respectively. On the other hand, Ac-Pro-NH<sub>2</sub> showed only the C<sub>7</sub> conformer; the pyrrolidine ring avoids the formation of other configurations. Despite that Ac-Ala-NH<sub>2</sub> differs from Ac-Gly-NH<sub>2</sub> in the substitution of hydrogen by a CH<sub>3</sub> group, it is not large enough to avoid any conformational blocking. Additionally, Ac-Ser-NH<sub>2</sub> differs from the previous dipeptides as it has a polar side chain. We showed how the presence of a polar group was responsible of restricting the number of conformers and only the C<sub>7</sub> species was observed.<sup>26</sup>

N-acetyl-valinamide (Ac-Val-NH<sub>2</sub>) dipeptide has a non-polar and voluminous isopropyl moiety in the centre of the dipeptide, which could influence the C<sub>5</sub> Vs C<sub>7</sub> conformational landscape. The replacement of a H by a CH<sub>3</sub> group from Ac-Gly-NH<sub>2</sub> to Ac-Ala-NH<sub>2</sub> increases the number of conformers.<sup>27</sup> Similarly, Ac-Val-NH<sub>2</sub> shows a complex conformational landscape due to the rotation of the isopropyl group and, for example, several conformers based on each type, C<sub>5</sub> and C<sub>7</sub>, are possible. Some of the lowest energy conformers in this work are shown in scheme 1. Therefore, it presents to be an interesting system to be undertaken. In this work, we combine the benefits of molecular-beam Fourier-transform MW spectroscopy with that of vaporization by laser ablation (LA-MB-FTMW)<sup>28-31</sup> to study the conformational preferences of Ac-Val-NH<sub>2</sub> dipeptide molecule. The results presented in this work provide interesting conclusions on how the steric effects could affect the conformational behaviour in dipeptides.



**Scheme 1.** Chemical structures of the  $\text{C}_7$  (top) and  $\text{C}_5$  (bottom) configurations for Ac-Val-NH<sub>2</sub>. Each type gives rise to three different conformers, labelled from I to III.

## 2. METHODS

---

### 2.1. EXPERIMENTAL DETAILS

A commercial sample of Ac-Val-NH<sub>2</sub> (Bachem, ~99%) was used without any further purification. A solid rod was prepared by pressing the compound's fine powder mixed with a small amount of commercial binder and was placed in the ablation nozzle. A picosecond Nd:YAG laser (20 mJ per pulse, 20 ps pulse width) was used as a vaporization tool. Products of the laser ablation were supersonically expanded using the flow of carrier gas (Ne, 10 bar) and characterized by molecular beam Fourier transform microwave spectroscopy (LA-MB-FTMW), using a recent constructed instrument<sup>32</sup> dedicated to maximize its performance from 2 to 8 GHz. It is ideal to record the rotational spectrum of large molecules such as Ac-Val-NH<sub>2</sub> providing the high-resolution necessary to analyze the hyperfine structure due to the presence of several <sup>14</sup>N nuclei in the molecule.

Very recently, a pulse sequence that allows for multiple FID collection was implemented. At a flight time of about 1 ms for the jet propagating along the resonator's

axis, about 4 FIDs can be recorded per gas pulse without compromising the resolution while an S/N improvement of x2 is achieved. The number of FIDs could be increased up to 8 FIDs, with the corresponding increase in the S/N ratio, but at the cost of lowering the resolution. For this work, four FIDs per gas pulse were recorded. The pulse sequence is depicted in detail in Figure S01 of the Electronic Supplementary Information (ESI). Vice versa, with the fourfold FID collection the same signal to noise ratio is obtained four times faster than before implementation of the multiple FID collection on a single gas pulse. Therefore, this method is particularly highly convenient for the experiments conducted with laser ablation as it minimizes considerably the degradation of the sample.

**Table 1.** Experimental and calculated spectroscopic parameters for the Ac-Val-NH<sub>2</sub> conformers together with the *ab initio* energies at the MP2/6-311++G(d,p) theory.

	Experimental		Calculated MP2/6-311++G(d,p)					
	Rotamer I	Rotamer II	C <sub>7</sub> -I	C <sub>7</sub> -II	C <sub>7</sub> -III	C <sub>5</sub> -I	C <sub>5</sub> -II	C <sub>5</sub> -III
A <sup>a</sup>	1388.6071(22) <sup>g</sup>	1353.8151(58)	1268	1535	1385	1348	1460	1366
B	840.91159(42)	826.98719(28)	887	774	838	806	763	823
C	619.86354(17)	657.16182(21)	645	636	626	627	644	657
μ <sub>a</sub>			1.1	1.3	1.2	0.7	2.1	2.2
μ <sub>b</sub>			2.4	2.4	1.9	0.6	0.7	0.0
μ <sub>c</sub>			1.3	0.4	0.8	0.1	0.5	0.4
N <sub>c</sub> /χ <sub>aa</sub>	2.024(5)	2.170(11)	2.05	2.10	2.06	2.28	2.32	2.21
N <sub>c</sub> /χ <sub>bb</sub>	-2.987(11)	-2.286(14)	-2.40	-1.27	3.22	-3.46	-0.58	-2.29
N <sub>c</sub> /χ <sub>cc</sub>	0.962(11)	0.116(14)	0.36	-0.84	1.16	1.18	-1.74	0.08
N <sub>t</sub> /χ <sub>aa</sub>	-0.769(7)	0.613(12)	0.83	-0.05	-1.04	-2.11	0.14	0.38
N <sub>t</sub> /χ <sub>bb</sub>	1.902(13)	-0.925(15)	1.83	1.58	1.95	0.07	-0.37	-1.23
N <sub>t</sub> /χ <sub>cc</sub>	-1.133(13)	0.312(15)	-2.67	-1.52	-0.91	2.05	0.23	0.84
σ <sup>b</sup>	2.2	2.7						
N <sup>c</sup>	28	29						
ΔE <sup>d</sup>			440	588	0	403	342	83
ΔE <sub>ZPE</sub> <sup>e</sup>			429	629	0	267	272	45
ΔG <sup>f</sup>			602	811	113	0	351	154

<sup>a</sup>A, B, and C represent the rotational constants (in MHz); μ<sub>a</sub>, μ<sub>b</sub>, and μ<sub>c</sub> are the electric dipole moment components (in D); χ<sub>aa</sub>, χ<sub>bb</sub>, and χ<sub>cc</sub> are the diagonal elements of the <sup>14</sup>N nuclear quadrupole coupling tensor (in MHz); N<sub>c</sub> and N<sub>t</sub> correspond to the central and terminal <sup>14</sup>N nuclei, respectively <sup>b</sup>RMS deviation of the fit (in kHz). <sup>c</sup>Number of measures transitions. <sup>d</sup>Relative energies (in cm<sup>-1</sup>) with respect to the global minimum calculated at MP2/6-311++G(d,p) level of theory. <sup>e</sup>Relative energies (in cm<sup>-1</sup>) with respect to the global minimum, taking into account the zero point energy (ZPE), calculated at MP2/6-311++G(d,p) level of theory. <sup>f</sup>Gibbs energies (in cm<sup>-1</sup>) calculated at 298 K at the MP2/6-311++G(d,p) level of theory. <sup>g</sup>Standard error in parentheses in units of the last digit.

All the transitions shown in this work appeared as Doppler doublets due to the parallel configuration of the molecular beam and the microwave radiation. The resonance frequency was determined as the arithmetic mean of the two Doppler components.

## 2.2. THEORETICAL MODELING

To ensure that no important structures were left out, an automated exploration of the intermolecular potential energy surface was carried out using fast molecular mechanics methods (MMFFs) and two search algorithms: the “Large scales Low Mode” (which uses frequency modes to create new structures) and a Monte Carlo-based search, as implemented in Macromodel ([www.schrodinger.com](http://www.schrodinger.com)). In a second stage, geometry optimizations of the lower-energy conformers of Ac-Val-NH<sub>2</sub> were done using Gaussian suite programs.<sup>33</sup> The model of choice was the Møller-Plesset (MP2) perturbation theory in the frozen core approximation with the Pople’s 6-311++G(d,p) basis set. The predicted rotational constants (A, B and C), quadrupole coupling constants ( $\chi_{aa}$ ,  $\chi_{bb}$  and  $\chi_{cc}$ ) and electric dipole moment components are collected in Table 1. The values obtained for other theoretical models can be found in the Electronic Supplementary Information (ESI) for a comparison. The relative energies and ZPE-corrected energies are also shown. Finally, frequency calculations were also computed to ensure that the optimized geometries are true minima and to calculate the Gibbs free energies. Among the possible configurations, theoretical calculations predict several low-lying energetic conformers which could be populated enough in the supersonic expansion. The structure of these conformers, are based on the C<sub>5</sub> and C<sub>7</sub> conformations and differ on the orientation of the isopropyl group. The different conformers of each type have been labelled from I to III for an easier comparison along this work (see scheme 1). According to the calculations, and based on energetic considerations the most likely candidates are the C<sub>7</sub>-III conformer followed by the C<sub>5</sub>-III structure, although the rest of the conformers cannot be ruled out, particularly because the close proximity both in energetic terms and based on entropic considerations.

### 3. RESULTS AND DISCUSSION

Guided by the predicted spectroscopic constants and selection rules, several frequency regions of the rotational spectrum of Ac-Val-NH<sub>2</sub> dipeptide were explored. At first, a set of  $\mu$ a type R-branch transitions were first assigned to a first rotamer I. They all present a very complex and compact hyperfine structure spread about 0.2-0.5 MHz (see Figure 1a). The Ac-Val-NH<sub>2</sub> dipeptide presents two <sup>14</sup>N nuclei. The <sup>14</sup>N nuclei have a non-zero quadrupole moment ( $I=1$ ) owing to a non-spherical distribution of the nuclear-charge, which interacts with the electric field gradient created by the rest of the molecule at the site of these nuclei. The nuclear spin of <sup>14</sup>N nuclei couples to the rotational angular momentum resulting in a hyperfine structure in the rotational spectrum.<sup>34</sup> In a first approach, the centre frequencies of a total of 37 observed transitions corresponding to  $\mu$ a- and  $\mu$ b-type R-branch progressions were fitted to an asymmetric rigid rotor Hamiltonian.

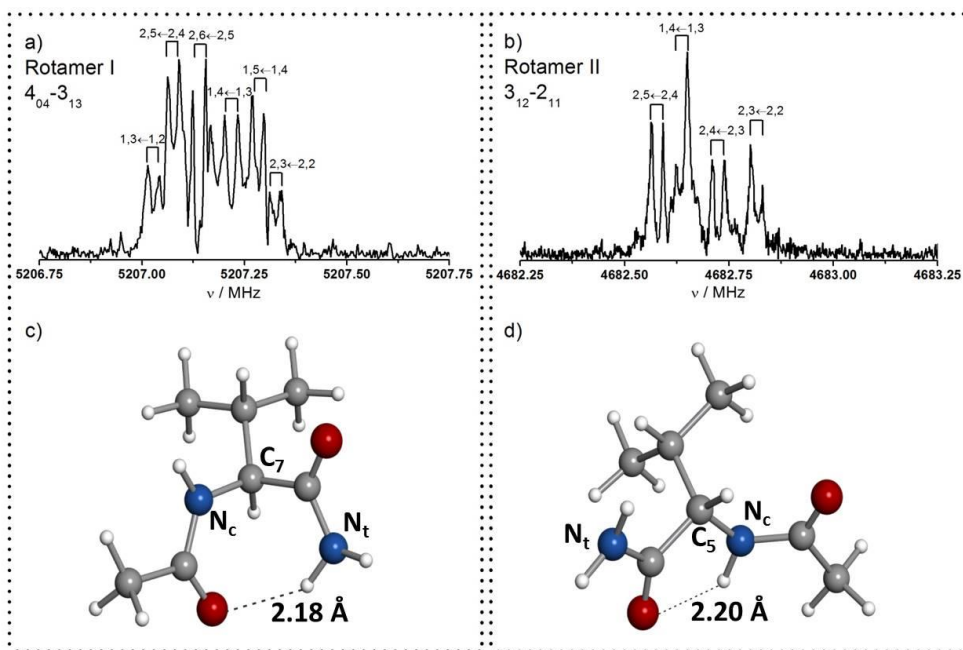


**Figure 1.** a)  $4_{04}-3_{13}$  and (b)  $3_{12}-2_{11}$  rotational transitions of conformers C<sub>7</sub> and C<sub>5</sub> of Ac-Val-NH<sub>2</sub> respectively, showing their hyperfine structure completely resolved using LA-MB-FTMW spectrometer. Each hyperfine component labelled with the corresponding values of  $l'$ ,  $F' \leftarrow l''$ , and  $F''$  quantum numbers is split by the Doppler effect. (c and d) Structures of the two rotamers detected in this work.



The calculated rotational constants  $A=1389$ ,  $B=841$  and  $C=620$  MHz are in good agreement with those predicted for the  $C_7$ -III conformer in Table 1. Once the lines assigned to this first rotamer were discarded from the records, a second set of weaker of  $\mu_a$  type R-branch transitions were identified as belonging to a second rotamer II. Following the same procedure mentioned above, a second set of experimental rotational constants  $A=1354$ ,  $B=827$  and  $C=657$  MHz were derived from a rigid rotor analysis of 18 of  $\mu_a$ -type transitions. These values are in close agreement with those theoretically calculated for  $C_5$ -III conformer in Table 1, but other conformers cannot be safely ruled out.

A more straightforward way to obtain an unambiguous identification is to take into account the information extracted from the nuclear quadrupole hyperfine structure of rotational transitions. The  $^{14}\text{N}$  nuclei introduce hyperfine rotational probes at defined sites of Ac-Val-NH<sub>2</sub> and act as a reporter of the interactions involving  $N_c$  and  $N_t$  quadrupolar nuclei. At this point, we took advantage of the high resolution reached with our narrowband LA-MB-FTMW<sup>32</sup> technique to fully resolve the  $^{14}\text{N}$  nuclear quadrupole hyperfine structure, as shown in Figures 1a and 1b. A closer view into the hyperfine structure shows the high resolution and sensibility capabilities of our instrument, highlighting the benefits of the recently implemented multifid procedure. The hyperfine pattern for all  $C_7$  and  $C_5$  low energy conformers was modelled and contrasted with experimental ones. As shown in Fig. 1, only those of  $C_7$ -III and  $C_5$ -III nicely juxtapose with the experimental patterns confirming the presence of these conformers in the supersonic expansion. 28 and 29 nuclear quadrupole hyperfine components for the  $C_7$ -III and  $C_5$ -III conformers respectively (see Tables S02 and S03 of the Supporting Information) were analysed using a Watson's A-reduced rigid rotor Hamiltonian in the  $I_r$ -representation<sup>35</sup> supplemented with a term to account for the nuclear quadrupole coupling contribution.<sup>34</sup> The quadrupole coupling Hamiltonian was set up in the coupled basis set  $(I_1 I_2 J F)$ ,  $I_1 + I_2 = I$ ,  $I + J = F$ . The energy levels involved in each transition are thus labeled with the quantum numbers  $J$ ,  $K_{-1}$ ,  $K_{+1}$ ,  $I$ ,  $F$ . The rotational constants  $A$ ,  $B$ ,  $C$  and the diagonal elements of the nuclear quadrupole coupling tensor ( $\chi_{aa}$ ,  $\chi_{bb}$ , and  $\chi_{cc}$ ) for the two  $^{14}\text{N}$  nuclei are accurately

determined and summarized in the first section of Table 1. The experimentally determined diagonal elements of the nuclear quadrupole coupling tensor for the  $^{14}\text{N}_c$  and  $^{14}\text{N}_t$  are sensitive to the chemical environment around the  $^{14}\text{N}$  nuclei and to the relative orientation of the amino terminal group. It is therefore a precious tool in conformational identification since the experimental values are only consistent with those predicted for  $\text{C}_7\text{-III}$  and  $\text{C}_5\text{-III}$  conformers, which are thus conclusively identified in our experiment. Additionally, the observation of both *a*- and *b*-types for  $\text{C}_7\text{-III}$  and only the *a*-type spectra for  $\text{C}_5\text{-III}$ , together with the corresponding intensities of the rotational transitions, are in accordance with the predicted dipole moment components for these conformers.

Both conformers contain one methyl top which implies low torsional barriers (in the 50-100  $\text{cm}^{-1}$  range for the  $\text{C}_7$  and  $\text{C}_5$  conformers), which results in a large *A-E* splitting of the spectra. Their assignment is not straightforward and no attempt was made to assign *E* component lines in the rotational spectra. Therefore, all the present assignments correspond to the unperturbed *A* states of the  $\text{C}_7$  and  $\text{C}_5$  conformers, which is the state that can be used for deriving structural considerations.

Despite that other low energy conformers are good candidates to survive the supersonic expansion, new attempts failed when assigning lines attributable to other species. Its absence could be either because of their weak populations in the expansion or either because of a weak dipole moment. Another possible explanation is that they may collisionally relax, or at least partially, during the supersonic expansion. In this contest, we estimated the conformational barrier height between different conformers, as the interconversion barrier comes by a simple rotation of the isopropyl group. Figure S03 in the ESI shows the calculated potential energy surface (PES) which predicts barriers in the 700-1200  $\text{cm}^{-1}$  range. This may indicate a possible partial isomerization supporting their non-observation.

The observation of both  $C_5$  and  $C_7$  types, similar to what it was observed for Ac-Gly-NH<sub>2</sub> and Ac-Ala-NH<sub>2</sub>, indicates that the introduction of a larger voluminous group such as the isopropyl, does not prevent the less stable conformer, i.e. the  $C_5$ -type, to be formed. In order to estimate the influence of the voluminous isopropyl group, we evaluated the relative intensities. Both conformers present similar dipole moments in their stronger lines and so, the measured intensities between the rotational lines should give an estimation on their relative abundances. The  $C_5/C_7$  population ratio of the Ac-Gly-NH<sub>2</sub> conformers was estimated to be 0.32 and that of Ac-Ala-NH<sub>2</sub> was 0.5. For Ac-Val-NH<sub>2</sub>, conformer  $C_7$  presents stronger lines than those of conformer  $C_5$ . Considering the same transitions and taking into account the difference in the transition probability due to the dipole moments, a  $C_5/C_7$  ratio of approximately 0.4 was found. Hence, the more compact  $C_7$  conformer is more abundant than the more extended  $C_5$  conformer. Interestingly, the steric effects introduced by the isopropyl group are not enough to cause a substantial modification of the conformational  $C_5/C_7$  ratio. The results are revealing: in contrast to Ac-Ser-NH<sub>2</sub>, which presented only one conformer based on the  $C_7$  configuration, the observation of both  $C_5$  and  $C_7$  types in Ac-Gly-NH<sub>2</sub>, Ac-Ala-NH<sub>2</sub> and Ac-Val-NH<sub>2</sub> indicates that a neutral lateral chain does not affect the  $C_5/C_7$  ratio. It would be interesting to explore new dipeptides with different lateral chains to test whether this assumption remains true.

## 4. CONCLUSIONS

---

Fourier transform microwave technique has been applied to Ac-Val-NH<sub>2</sub> to understand the structural arrangement of this dipeptide. Our results show that there are two conformations,  $C_5$  and  $C_7$  species, in gas phase. Thus, non-polar side chain dipeptides Ac-Gly-NH<sub>2</sub>, Ac-Ala-NH<sub>2</sub>, and Ac-Val-NH<sub>2</sub> show the presence of both seven- and five-membered rings. The observation of both conformers despite the spatial restrictions imposed by the isopropyl group, reinforces our initial assessment in that the polar side chain of the Ac-Ser-NH<sub>2</sub> dipeptide is the responsible of the conformational locking

reducing the conformational landscape down to a single C<sub>7</sub> species. Furthermore, a non-polar lateral chain does not affect the C<sub>5</sub>/C<sub>7</sub> ratio in dipeptides.

## 5. REFERENCES

---

- <sup>1</sup> H. A. Lehninger, D. Nelson and M. Cox, *Lehninger Principles of Biochemistry*, W. H. Freeman, 2008.
- <sup>2</sup> Y. Park and V. Helms, *Bioinformatics*, 2007, 23, 701–708.
- <sup>3</sup> A. B. Mandal, A. Dhathathreyan, R. Jayakumar and T. Ramasami, *J. Chem. Soc. Faraday Trans.*, 1993, 89, 3075–3079.
- <sup>4</sup> J. James and A. B. Mandal, *J. Colloid Interface Sci.*, 2011, 360, 600–605.
- <sup>5</sup> E. G. Robertson and J. P. Simons, *Phys. Chem. Chem. Phys.*, 2001, 3, 1–18.
- <sup>6</sup> M. S. De Vries and P. Hobza, *Annu. Rev. Phys. Chem.*, 2007, 58, 585–612.
- <sup>7</sup> J. Oomens, J. D. Steill and B. Redlich, 2009, 131, 4310–4319.
- <sup>8</sup> W. Caminati, *Angew. Chemie - Int. Ed.*, 2009, 48, 9030–9033.
- <sup>9</sup> A. Perczel, J. Angyan and M. Kajtar, *J. Am. Chem. Soc.*, 1991, 113, 6256–6265.
- <sup>10</sup> I. R. Gould, W. D. Cornell and I. H. Hillier, *J. Am. Chem. Soc.*, 1994, 116, 9250–9256
- <sup>11</sup> T. Head-Gordon, M. Head-Gordon, M. J. Frisch, C. L. Brooks III and J. A. Pople, *J. Am. Chem. Soc.*, 1991, 113, 5989–5997.
- <sup>12</sup> R. Improta and V. Barone, *J. Comput. Chem.*, 2004, 25, 1333–1341.
- <sup>13</sup> P. Echenique and J. L. Alonso, *J. Comput. Chem.*, 2008, 29, 1408–1422.
- <sup>14</sup> A. D. Mackerell, M. Feig and C. L. Brooks, *J. Comput. Chem.*, 2004, 25, 1400–1415.
- <sup>15</sup> W. Chin, F. Piuze, I. Dimicoli and M. Mons, *Phys. Chem. Chem. Phys.*, 2006, 8, 1033–1048.
- <sup>16</sup> H. S. Biswal, Y. Loquais, B. Tardivel, E. Gloaguen and M. Mons, *J. Am. Chem. Soc.*, 2011, 133, 3931–3942.
- <sup>17</sup> M. Gerhards, C. Unterberg, A. Gerlach and A. Jansen, *Phys. Chem. Chem. Phys.*, 2004, 6, 2682–2690.
- <sup>18</sup> B. C. Dian, A. Longarte, S. Mercier, D. A. Evans, D. J. Wales and T. S. Zwier, *J. Chem. Phys.*, 2002, 117, 10688–10702.
- <sup>19</sup> E. Gloaguen, B. De Courcy, J. P. Piquemal, J. Pilmé, O. Parisel, R. Pollet, H. S. Biswal, F. Piuze, B. Tardivel, M. Broquier and M. Mons, *J. Am. Chem. Soc.*, 2010, 132, 11860–11863.
- <sup>20</sup> W. H. James III, E. E. Baquero, V. A. Shubert, S. H. Choi, S. H. Gellman and T. S. Zwier, *J. Am. Chem. Soc.*, 2009, 131, 6574–6590.
- <sup>21</sup> V. Brenner, F. Piuze, I. Dimicoli, B. Tardivel and M. Mons, *Angew. Chemie - Int. Ed.*, 2007, 46, 2463–2466.
- <sup>22</sup> R. J. Lavrich, D. F. Plusquellic, R. D. Suenram, G. T. Fraser, A. R. Hight Walker and M. J. Tubergen, *J. Chem. Phys.*, 2003, 118, 1253–1265.
- <sup>23</sup> C. Puzzarini, M. Biczysko, V. Barone, L. Largo, I. Peña, C. Cabezas and J. L. Alonso, *J. Phys. Chem. Lett.*, 2014, 5, 534–540.
- <sup>24</sup> C. Cabezas, M. Varela, V. Cortijo, A. I. Jiménez, I. Peña, A. M. Daly, J. C. López, C. Cativiela and J. L. Alonso, *Phys. Chem. Chem. Phys.*, 2013, 15, 2580.
- <sup>25</sup> C. Cabezas, M. Varela and J. L. Alonso, *ChemPhysChem*, 2013, 14, 2539–2543.
- <sup>26</sup> C. Cabezas, M. A. T. Robben, A. M. Rijs, I. Peña and J. L. Alonso, *Phys. Chem. Chem. Phys.*, 2015, 17, 20274–20280.
- <sup>27</sup> R. Vargas, J. Garza, B. P. Hay and D. A. Dixon, *J. Phys. Chem. A*, 2002, 106, 3213–3218.
- <sup>28</sup> J. L. Alonso and J. C. López, in *Gas-Phase IR Spectroscopy and Structure of Biological Molecules*, eds. A. M. Rijs and J. Oomens, *Topics in*, 2015, vol. 364, pp. 335–402.
- <sup>29</sup> J. L. Alonso, C. Pérez, M. E. Sanz, J. C. López and S. Blanco, *Phys. Chem. Chem. Phys.*, 2009, 11, 617–627.
- <sup>30</sup> I. Peña, M. E. Sanz, J. C. López and J. L. Alonso, *J. Am. Chem. Soc.*, 2012, 134, 2305–2312.
- <sup>31</sup> C. Cabezas, M. Varela, I. Pena, S. Mata, J. C. Lopez and J. L. Alonso, *Chem. Commun.*, 2012, 48, 5934–

5936.

<sup>32</sup>C. Bermúdez, S. Mata, C. Cabezas and J. L. Alonso, *Angew. Chemie - Int. Ed.*, 2014, 53, 11015–11018.

<sup>33</sup>M. J. Frisch, G. W. Trucks, H. B. Schlegel, G. E. Scuseria, M. A. Robb, J. R. Cheeseman, G. Scalmani, V. Barone, B. Mennucci, G. A. Petersson, H. Nakatsuji, M. Caricato, X. Li, H. P. Hratchian, A. F. Izmaylov, J. Bloino, G. Zheng, J. L. Sonnenberg, M. Hada, M. Ehara, K. Toyota, R. Fukuda, J. Hasegawa, M. Ishida, T. Nakajima, Y. Honda, O. Kitao, H. Nakai, T. Vreven, J. A. Montgomery, Jr., J. E. Peralta, F. Ogliaro, M. Bearpark, J. J. Heyd, E. Brothers, K. N. Kudin, V. N. Staroverov, R. Kobayashi, J. Normand, K. Raghavachari, A. P. Rendell, J. C. Burant, S. S. Iyengar, J. Tomasi, M. Cossi, N. Rega, M. J. Millam, M. Klene, J. E. Knox, J. B. Cross, V. Bakken, C. Adamo, J. Jaramillo, R. Gomperts, R. E. Stratmann, O. Yazyev, A. J. Austin, R. Cammi, C. Pomelli, J. W. Ochterski, R. L. Martin, K. Morokuma, V. G. Zakrzewski, G. A. Voth, P. Salvador, J. J. Dannenberg, S. Dapprich, A. D. Daniels, Ö. Farkas, J. B. Foresman, J. V. Ortiz, J. Cioslowski and D. J. Fox, *Gaussian, Gaussian 09 Rev. D01.*, Gaussian, Inc., Wallingford, CT, 2012, see also: <http://www.gaussian.com>.

<sup>34</sup>W. Gordy and R. L. Cook, *Microwave molecular spectra*, Wiley, New York, 1984.

<sup>35</sup>J. K. G. Watson, *Vibrational Spectra and Structure*, Elsevier, Amsterdam, 1977.

<sup>36</sup>A. Li, H. S. Muddana and M. K. Gilson, *J. Chem. Theory Comput.*, 2014, 10, 1563–1575.



## CHAPTER VI.

# The millimeter wave spectrum of *s-cis* and *s-trans* acrylic acid in its ground vibrational state

---

*Adapted from: Journal of Molecular Spectroscopy 316 (2015) 84–89.*

*The millimeter wave spectrum of acrylic acid ( $\text{CH}_2=\text{CH}-\text{COOH}$ ), the simplest unsaturated carboxylic acid, was measured and analyzed from 130 to 360 GHz. Additional measurements from 18 to 26.5 GHz were also made using a waveguide CP-FTMW spectrometer. More than 4000 rotational lines were assigned to *s-cis*- and *s-trans*-acrylic acid in their ground vibrational states leading to precise determination of rotational, quartic and first complete set of sextic centrifugal distortion constants. New laboratory data of acrylic acid were then used to search for its spectral features in Orion KL, Sgr B2, and W51 molecular clouds. An upper limit to the column density of acrylic acid in Orion KL is provided.*





## 1. INTRODUCTION

---

Active regions of high-mass star formations, such as the Orion KL and Sgr B2 molecular clouds, show incredibly rich chemistry as a result of the interaction of the newly formed stars with their environment and are the prime targets of several current astrochemical investigations. The search for complex organic molecules (COMs) undoubtedly belongs among them. In the context of astrochemistry, COMs are defined as organic molecules with six or more atoms<sup>1</sup> and are considered crucial molecules due to their connection with organic and biochemical processes occurring on the Earth. One of the most important techniques for studying these molecular clouds and searching for COMs is mm/submm astronomy, which probes the rotational spectra of gas phase molecules and, in addition to the characterization of the species, provides valuable information about the physical conditions of the gas. Although a large variety of simpler molecules as well as COMs have been found in these sources,<sup>2,3</sup> thousands of spectral features are still observed in the line surveys captured by numerous observational facilities working on the ground (e.g. IRAM, ALMA, GBT, NRAO, BIMA, CARMA, CSO, SEST) or in space (Herschel/HIFI). The new generation of telescopes, especially such as the ALMA project, is bringing scientifically very important data, since the sensitivity and angular resolution are substantially improved in comparison with other currently used single-dish telescopes. These capabilities open more possibilities toward detections of interstellar molecules in smaller abundances than before. The frequency coverage of the ALMA interferometer from 84 to 720 GHz thus motivates laboratory spectroscopists to record and analyze the rotational spectra in the millimeter and sub-millimeter wave region and to gather an atlas of line positions and intensities for potentially detectable molecules. Acrylic acid (prop-2-enoic acid,  $\text{CH}_2=\text{CH}-\text{COOH}$ ) is the simplest unsaturated carboxylic acid and seems to be a logical molecule to search for since it shares the carboxyl ( $-\text{COOH}$ ) and vinyl ( $-\text{CH}=\text{CH}_2$ ) functional groups with other already detected interstellar and circumstellar molecules: formic acid ( $\text{H}-\text{COOH}$ ),<sup>4-8</sup> acetic acid ( $\text{CH}_3-\text{COOH}$ ),<sup>6,9-12</sup> vinyl alcohol ( $\text{CH}_2=\text{CH}-\text{OH}$ ),<sup>13</sup> vinyl cyanide ( $\text{CH}_2=\text{CH}-\text{CN}$ ),<sup>7,14-17</sup> propenal ( $\text{CH}_2=\text{CH}-\text{CHO}$ ),<sup>18,19</sup> and propylene ( $\text{CH}_2=\text{CH}-\text{CH}_3$ ).<sup>20</sup> Tentative detection of another complex vinyl containing species, vinyl acetate, has been discussed recently.<sup>21</sup>

Acrylic acid exists in two stable planar forms, *s-cis* and *s-trans* (IUPAC nomenclature), defined by the arrangement of two double bonds about the single C–C bond (see Fig. 1). The *s-cis* structure has been established to be the more stable one by only  $58 \pm 20 \text{ cm}^{-1}$ .<sup>22</sup> Rotational spectra of both isomeric forms were measured for the first time by Bolton et. al.<sup>22</sup> from 18 to 40 GHz by a conventional Stark-modulated spectrometer. Later on, Calabrese et. al.<sup>23</sup> used the supersonic-jet Fourier transform microwave and Stark-modulated free-jet techniques to record the spectra in the frequency ranges 6 – 18.5 and 52 – 74.4 GHz. Very recently, during the course of this study, another work in several narrow frequency windows was performed: 95.7 – 104, 108.7 – 109.2, 289.4 – 294, and 391.3 – 397.3 GHz.<sup>24</sup> Authors assigned almost 600 new lines and improved the determination of spectroscopic constants for both isomers. Predicted transitions of acrylic acid at frequencies above 480 GHz were then searched for towards the star forming region DR21(OH) using the Herschel Science Archive data with negative results.

The aim of this work was similar to those of Calabrese et. al.,<sup>24</sup> i.e. extension of the measurements of the acrylic acid rotational spectrum to higher frequencies that may facilitate its detection in the interstellar medium. The continuous broadband spectrum measured from 130 to 360 GHz allowed to assign more than 4000 lines and to derive the spectroscopic constants for both *s-cis* and *s-trans* isomers up to the sixth order. In comparison with previous work, direct laboratory data obtained in this study were used to search for the acrylic acid in several more sensitive surveys. Orion KL, Sgr B2, and W51 molecular clouds, which are known for their rich organic chemistry, were chosen and results are discussed in section 4.

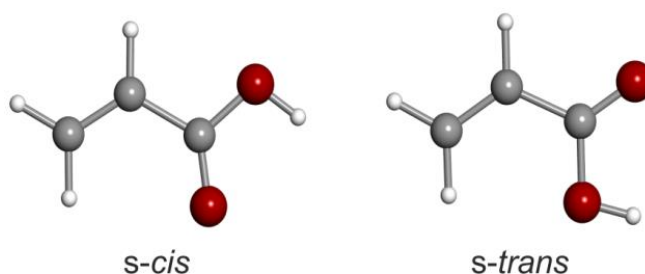


**Figure 1:** Two planar isomeric forms of acrylic acid.

## 2. EXPERIMENTAL DETAILS

---

A commercial sample of acrylic acid (b.p. 139 °C) was used without any further purification. Rotational spectra measurements were carried out on two different spectrometers. A waveguide chirped-pulse Fourier transform microwave spectrometer at New College of Florida was used to record the spectrum in the 18 – 26.5 GHz region at a temperature of –15 °C and a pressure of 3 mTorr. Details about the spectrometer can be found elsewhere.<sup>25</sup> In each spectrum, 100 million free induction decays of 4  $\mu$ s duration were averaged and Fourier transformed using a Kaiser–Bessel window function. The frequency accuracy was set to 50 kHz.

Rotational spectra from 130 to 360 GHz were taken at room temperature and a pressure of approximately 15 mTorr by the millimeter wave spectrometer at the University of Valladolid. Information concerning the synthesizer, cascade frequency multipliers as well as detectors can be found in Daly et. al.<sup>26</sup> All spectra were recorded in 1 GHz scans using the frequency modulation technique with  $2f$  lock-in detection, where  $f = 10.2$  kHz is the modulation frequency, and modulation depth of 30 kHz. Frequency accuracy of isolated well-developed lines was estimated to be better than 50 kHz.

## 3. ANALYSIS OF THE SPECTRA

---

Previous Stark measurements provided the dipole moment components of  $|\mu_a^{s-cis}| = 0.56$  (10) D,  $|\mu_b^{s-cis}| = 1.35$  (5) D,  $|\mu_a^{s-trans}| = 1.70$  (4) D, and  $|\mu_b^{s-trans}| = 1.10$  (5) D<sup>22</sup> indicating that both  $a$ -type and  $b$ -type transitions are relevant for both isomers. Predictions based on previous work of Calabrese et. al.<sup>23</sup> significantly facilitated the assignments at lower frequencies as well as their extension into the millimeter wave range. A section of the rotational spectrum at the millimeter wavelengths is shown in Fig. 2.  $a$ -type and  $b$ -type  $R$ -branch transitions between near degenerate pairs of levels for low values of  $K_a$  quantum number form the most intense lines of the acrylic acid rotational spectrum (see Fig. 2, upper panel). For  $K_a = 0$  and 1, these transitions are overlapped and one absorption line, repeating with a period of  $\approx 2C$ ,

thus corresponds to a pair of  $a$ -type and a pair of  $b$ -type transitions. In such cases, four transitions were assigned to one experimental frequency and were fitted to their intensity weighted averages. With increasing  $K_a$ , these transitions form quartets (see Fig. 2, lower panels) which become degenerate as  $J$  increases. For the *s-cis* isomer, a total of 2381 distinct frequency lines were newly assigned in this work to 3107  $a$ -type and  $b$ -type  $Q$ - and  $R$ -branch transitions and several  $b$ -type  $P$ -branch transitions ( $2 \leq J \leq 74$ ,  $0 \leq K_a \leq 24$ ). These data were collected into a single data set with 24 lines from Bolton et. al. <sup>22</sup> and 76 lines from Calabrese et. al. <sup>23</sup> and were least-squares fitted using the Watson's semi-rigid Hamiltonian in  $S$ -reduction and  $I'$ -representation <sup>27</sup>. For the *s-trans* isomer, 1697 distinct frequency lines were assigned to 2323  $a$ -type and  $b$ -type  $Q$ - and  $R$ -branch transitions and a few  $b$ -type  $P$ -branch transitions ( $2 \leq J \leq 76$ ,  $0 \leq K_a \leq 24$ ). These transition lines were combined with 28 lines from Bolton et. al. <sup>22</sup> and 73 lines from Calabrese et. al. <sup>23</sup> and were analyzed in the same way as the *s-cis* isomer data. The resulting spectroscopic constants for both isomers of acrylic acid are listed in Table 1 and the complete lists of the rotational transitions included in the fits are given in Tables S1 and S2 of the electronic Supplementary material (<http://dx.doi.org/10.1016/j.jms.2015.08.002>). The present data sets improve the determination of quartic centrifugal distortion constants and allowed for the derivation of a complete set of sextic ones leading to stronger predictive power of many additional lines for both *s-cis* and *s-trans* isomer at higher frequencies if necessary. After having assigned the ground state spectra of both isomeric forms, many lines remained unassigned in the experimental spectrum. These lines probably originate from excited vibrational states associated with low-lying vibrations such as C-C torsional and C=C-C bending modes as well as from <sup>13</sup>C isotopic species. Analysis of these lines, however, was not the subject of the present work.

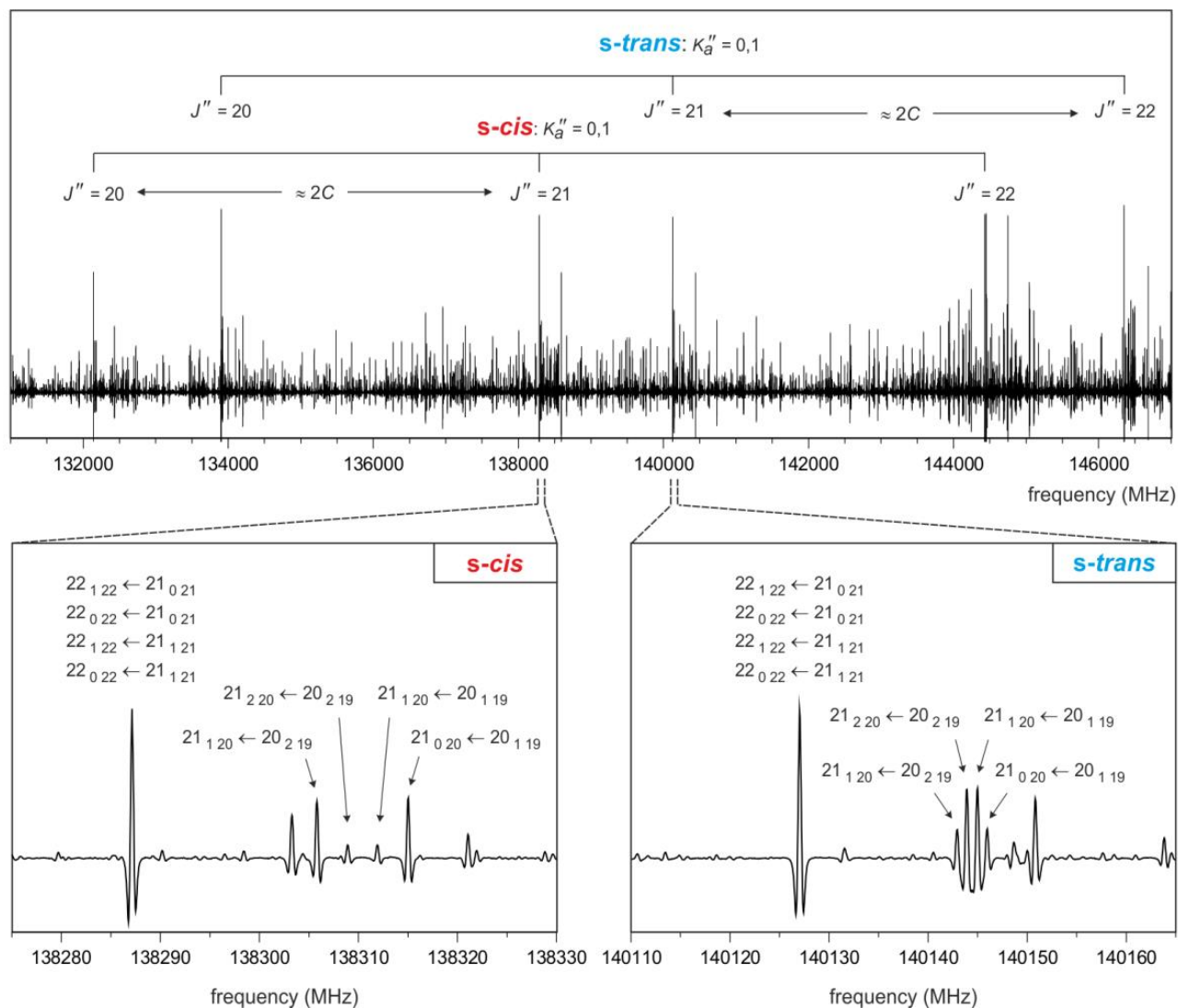


**Figure 2:** Upper panel: section of the acrylic acid rotational spectrum with assignment of the strongest spectral features for the *s-cis* and *s-trans* isomers. Lower panels: quartets of *a*-type and *b*-type *R*-branch rotational transitions between nearly degenerate pairs of levels with lowest values of  $K_a$  quantum number.

**Table 1:** Spectroscopic constants of *s-cis* and *s-trans* acrylic acid (*S*-reduction, *I'* representation)<sup>a</sup>.

Constant	Unit	<i>s-cis</i>	<i>s-trans</i>
<i>A</i>	MHz	11078.87327 (19)	10716.20452 (45)
<i>B</i>	MHz	4251.971260 (81)	4388.30110 (13)
<i>C</i>	MHz	3073.397662 (83)	3114.31077 (10)
<i>D<sub>J</sub></i>	kHz	0.662086 (58)	0.683756 (71)
<i>D<sub>JK</sub></i>	kHz	5.20116 (16)	5.42718 (82)
<i>D<sub>K</sub></i>	kHz	4.70200 (73)	3.9778 (44)
<i>d<sub>1</sub></i>	kHz	−0.2248528 (98)	−0.244260 (28)
<i>d<sub>2</sub></i>	kHz	−0.0731989 (40)	−0.084519 (12)
<i>H<sub>J</sub></i>	mHz	0.107 (12)	−0.102 (18)
<i>H<sub>JK</sub></i>	mHz	−4.723 (33)	−6.89 (37)
<i>H<sub>KJ</sub></i>	mHz	−2.95 (19)	−11.0 (32)
<i>H<sub>K</sub></i>	mHz	32.53 (89)	184 (14)
<i>h<sub>1</sub></i>	mHz	0.0535 (17)	−0.0126 (69)
<i>h<sub>2</sub></i>	mHz	0.0511 (11)	−0.0147 (56)
<i>h<sub>3</sub></i>	mHz	0.04074 (20)	0.0390 (12)
<i>N<sub>lines</sub></i> <sup>b</sup>		2381	1697
<i>σ<sub>fit</sub></i> <sup>c</sup>	kHz	38	49

<sup>a</sup> The numbers in parentheses are  $1\sigma$  uncertainties in the units of the last decimal digit.

<sup>b</sup> Number of the distinct frequency lines in the fit.

<sup>c</sup> Root mean square deviation of the fit.

## 4. SEARCH FOR ACRYLIC ACID IN SPACE

The spectroscopic data of acrylic acid ( $\text{CH}_2\text{CHCOOH}$ ) from Table 1 allow us to search for this species in space. Acrylic acid is an isomer of vinyl formate ( $\text{CH}_2\text{CHOCOH}$ ). Methyl formate ( $\text{CH}_3\text{OCOH}$ ) is a very abundant species in the ISM and its isomer, acetic acid ( $\text{CH}_3\text{COOH}$ ), has been detected in several interstellar clouds (see below). Hence, hot molecular clouds (HMCs) in which acetic acid has been detected seem the best places to find out this species. Acetic acid was discovered toward Sgr B2(N) by Mehringer et al.<sup>9</sup> After this detection, acetic acid has been

identified in other HMCs (w51e2,<sup>10</sup> G34.3+0.15,<sup>11</sup> and G19.61–0.23<sup>12</sup>) and in low mass star-forming regions (IRAS 16293–2422<sup>6</sup>). Moreover, the survey of acetic acid in different sources carried out by Remijan et al.<sup>11</sup> pointed out that this species seems to appear in regions where the emission from O- and N-containing species is co-spatial, while in sources for which we know that there is a spatial separation between these species, acetic acid has not been detected (see Ref. <sup>28</sup> for further discussion). However, using the available ALMA data, we have detected acetic acid towards the South hot core of Orion KL.<sup>29</sup> For the search of acrylic acid, we use several public data sets (see Table 2) of Sgr B2(N), W51, and Orion KL. We did not find acrylic acid in any of these sources above the detection limit of the data. Figure 3 shows the lack of positive detection of lines of *cis*-CH<sub>2</sub>CHCOOH (the most stable conformer) towards Sgr B2(N) and Orion KL. Several lines corresponding to *b*-type transitions ( $\mu_b$  is the largest dipole moment component) with high line strength ( $S_{ij}$ ) and in a large variety of upper level energies ( $E_u$ ) (see Table 3) have been selected according to the typical physical conditions of each source. For panels showing the Sgr B2(N) data, the red vertical line marks the expected rest frequency of the selected transition. For Orion KL, the panels between 214 – 244 GHz show two different positions of the ALMA SV data: the compact ridge (region rich in organic O-bearing species, blue line connecting dots) and the acetic acid peak (from Ref.29<sup>29</sup>, black histogram spectra). Using MADEx<sup>30</sup>, LTE approximation, and assuming these physical and line parameters: source size 3'' (telescope dilution is considered),  $T_K = 110$  K,  $v_{LSR} = 7.5$  km s<sup>-1</sup>,  $v = 1.5$  km s<sup>-1</sup>, we derive an upper limit to the column density of *cis*-acrylic acid in Orion KL of  $(3 \pm 1) \times 10^{15}$  cm<sup>-2</sup> and of  $(5 \pm 2) \times 10^{14}$  cm<sup>-2</sup> for the IRAM 30m data and the ALMA SV data, respectively. The thin red curve in Fig. 3 shows the synthetic spectrum of *cis*-acrylic acid for the adopted physical parameters.

The abundance ratio between acetic acid ( $N = 3 \times 10^{15}$  cm<sup>2</sup>)<sup>29</sup> and acrylic acid in Orion is >6. The upper limit on the column density of CH<sub>2</sub>CHCOOH puts strong constraints to the production mechanisms of this vinyl derivative. It is curious that vinyl species in Orion are associated with CN groups rather than with OH or COOH. A detailed study of the abundances of methyl and vinyl species in the different sources where these molecules have been detected could provide insights on the chemical paths leading to their production and to the physical conditions

controlling their abundances. From the abundance ratio of 6 found above for acetic and acrylic acids, and assuming that it will be maintained for their isomers methyl and vinyl formate, we could estimate an upper limit to the column density of vinyl formate of  $1.5 \times 10^{16} \text{ cm}^2$  (adopting  $N(\text{CH}_3\text{COOH}) = 1 \times 10^{17} \text{ cm}^{-2}$ ).<sup>29</sup> With such a column density, vinyl formate could be detected with ALMA. A detailed spectroscopic study on vinyl formate will be published elsewhere to allow for its search in space and to study the chemistry of  $\text{CH}_3\text{COOH}/\text{CH}_3\text{COOH}$  and  $\text{CH}_2\text{CHOCO}/\text{CH}_2\text{CHCOOH}$ .

**Table 2:** Data sets used to search for the acrylic acid rotational transitions.

Frequency (GHz)	Telescope	Source	Reference
7.7 – 10.7, 11.4 – 15.6, 17.6 – 26.4	GBT <sup>a</sup>	Sgr B2(N)	31 <sup>g</sup>
30.0 – 41.7, 42.4 – 49.3			
130 – 171	NRAO <sup>b</sup> 12m	Sgr B2(N)	32 <sup>g, h</sup>
218 – 264	SEST <sup>c</sup>	Sgr B2(N)	33
260 – 286	CSO <sup>d</sup>	Sgr B2(N)	34
18 – 26	GBT	W51	35 <sup>g</sup>
130 – 171	NRAO 12m	W51 M	32 <sup>g, h</sup>
80 – 115.5, 123.5 – 176, 196.7 – 307	IRAM <sup>e</sup> 30m	Orion KL	17, 36
213.71 – 246.63	ALMA <sup>f</sup>	Orion KL	37

<sup>a</sup> Green Bank Telescope.

<sup>b</sup> National Radio Astronomy Observatory.

<sup>c</sup> Swedish-ESO Submillimetre Telescope.

<sup>d</sup> Caltech Submillimeter Observatory.

<sup>e</sup> Institut de Radioastronomie Millimétrique.

<sup>f</sup> Atacama Large Millimeter/submillimeter Array.

<sup>g</sup> See this reference for full observational details, data reduction procedures, and analysis.

<sup>h</sup> These observations are a part of the “Barry E. Turner Legacy Survey”.



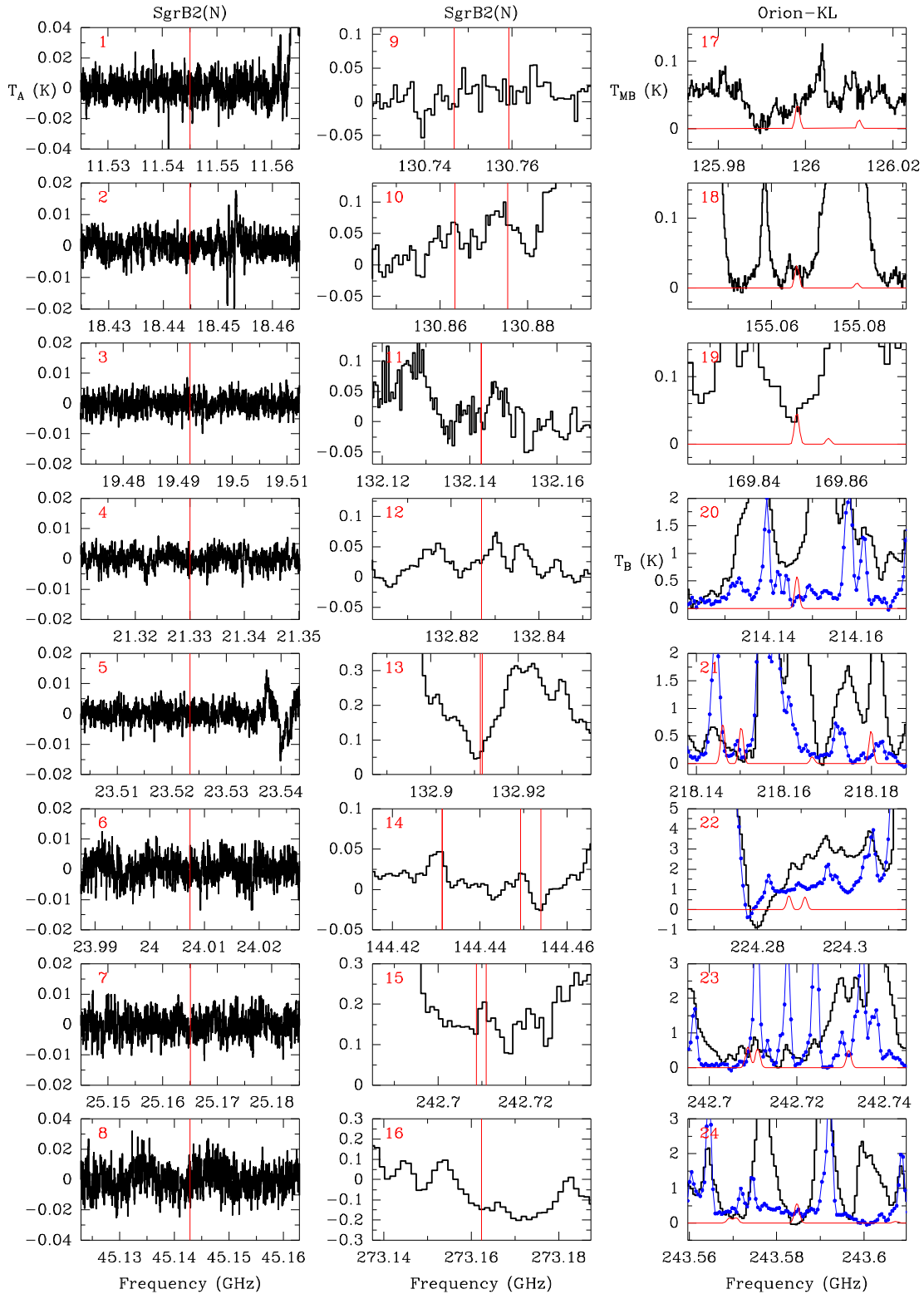


**Figure 3:** Negative detection of *cis*-CH<sub>2</sub>CHCOOH towards Sgr B2(N) ( $v_{\text{LSR}} = 64 \text{ km s}^{-1}$  is assumed) and Orion-KL ( $v_{\text{LSR}} = 7.5 \text{ km s}^{-1}$  is assumed), see the text.

**Table 3:** Selected transitions of cis-CH<sub>2</sub>CHCOOH.

Panel <sup>a</sup>	$J'$	$K_a'$	$K_c'$	$J''$	$K_a''$	$K_c''$	Frequency (MHz) <sup>b</sup>	$E_u$ (K) <sup>c</sup>	$S_{ij}$ <sup>d</sup>
1	3	1	2	3	0	3	11545.083	2.6	2.8
2	5	2	3	5	1	4	18444.902	6.9	4.32
3	3	2	1	3	1	2	19492.290	3.6	2.05
4	7	2	5	7	1	6	21330.072	11.8	5.83
5	4	0	4	3	1	3	23523.363	3.4	2.32
6	12	4	9	11	5	6	24007.389	33.5	1.15
7	6	1	5	6	0	6	25165.034	8.2	2.82
8	7	0	7	6	1	6	45142.910	9.2	5.49
9	24	2	22	24	1	23	130746.753	105	5.15
	24	3	22	24	2	23	130759.296	105	5.15
10	27	10	17	27	9	18	130863.491	170.5	15
	28	10	19	28	9	20	130875.507	180.6	15.8
11	21	0	21	20	1	20	132142.620	71.2	19.7
	21	1	21	20	0	20	132142.771	71.2	19.7
12	9	5	4	8	4	5	132826.894	24.8	4.5
13	7	6	2	6	5	1	132911.383	22.7	5.43
13	7	6	1	6	5	2	132911.805	22.7	5.43
14	23	0	23	22	1	22	144431.393	84.8	21.7
	23	1	23	22	0	22	144431.427	84.8	21.7
	22	1	21	21	2	20	144449.277	84	18
	21	2	19	20	3	18	144449.320	82.5	14.1
	22	2	21	21	1	20	144453.949	84	18
15	39	0	39	38	1	38	242708.781	235.8	37.7
	39	1	39	38	0	38	242708.781	235.8	37.7
	38	1	37	37	2	36	242711.01	235	34
	38	2	37	37	1	36	242711.01	235	34
16	14	12	3	13	11	2	273162.328	88.2	11.4
	14	12	2	13	11	3	273162.328	88.2	11.4
17	20	0	20	19	1	19	125997.968	64.9	18.7
	20	1	20	19	1	19	125998.070	64.9	19.8
	20	0	20	19	0	19	125998.179	64.9	19.8
	20	1	20	19	0	19	125998.281	64.9	18.7
18	8	7	2	7	6	1	155065.783	30.1	6.43
	8	7	1	7	6	2	155065.809	30.1	6.43
19	8	8	1	7	7	0	169849.934	35.4	7.46
	8	8	0	7	7	1	169849.934	35.4	7.46

20	10	10	1	9	9	0	214146.459	54.9	9.46
	10	10	0	9	9	1	214146.459	54.9	9.46
21	35	0	35	34	1	34	218146.019	191	33.7
	35	1	35	34	0	34	218146.019	191	33.7
	34	1	33	33	2	32	218150.228	190.2	30
	34	2	33	33	1	32	218150.228	190.2	30
	18	6	12	17	5	13	218166.531	74.2	4.63
	33	2	31	32	3	30	218179.902	188.7	26.3
	33	3	31	32	2	30	218179.995	188.7	26.3
22	36	0	36	35	1	35	224287.182	201.7	34.7
	36	1	36	35	0	35	224287.182	201.7	34.7
	35	1	34	34	2	33	224290.825	201	31
	35	2	34	34	1	33	224290.825	201	31
23	39	0	39	38	1	38	242708.781	235.8	37.7
	39	1	39	38	0	38	242708.781	235.8	37.7
	38	1	37	37	2	36	242711.010	235	34
	38	2	37	37	1	36	242711.010	235	34
24	14	10	5	13	9	4	243584.624	72.7	9.42
	14	10	4	13	9	5	243584.626	72.7	9.42

<sup>a</sup> Number of each panel given in Figure 1.

<sup>b</sup> Rest frequency.

<sup>c</sup> Upper level energy.

<sup>d</sup> Line strength.

## 5. CONCLUSIONS

Precise ground state spectroscopic constants including the first complete set of the sextic centrifugal distortion constants for both *s*-cis and *s*-trans acrylic acid are provided in the present work. New direct laboratory data allowed to search for the acrylic acid in the interstellar medium, namely in the regions of Orion KL, Sgr B2, and W51 molecular clouds, using the publically available spectral surveys captured by GBT, NRAO, SEST, CSO, IRAM, and ALMA telescopes. Although no spectral features of acrylic acid were found toward these clouds, present data can be used with confidence in future searches for acrylic acid in other interstellar sources.

## 6. REFERENCES

---

- <sup>1</sup> E. Herbst, E.F. van Dishoeck, *Annual Review of Astronomy and Astrophysics* 47 (2009) 427-480.
- <sup>2</sup> D.E. Woon, <http://www.astrochymist.org/> (2015).
- <sup>3</sup> A. Belloche, H.S.P. Müller, K.M. Menten, P. Schilke, C. Comito, 559 (2013).
- <sup>4</sup> B. Zuckerman, J.A. Ball, C.A. Gottlieb, *The Astrophysical Journal* 163 (1971) L41.
- <sup>5</sup> G. Winnewisser, E. Churchwell, *The Astrophysical Journal* 200 (1975) L33-L36.
- <sup>6</sup> S. Cazaux, A.G.G.M. Tielens, C. Ceccarelli, A. Castets, V. Wakelam, E. Caux, B. Parise, D. Teyssier, *The Astrophysical Journal Letters* 593 (2003) L51.
- <sup>7</sup> P. Schilke, T.D. Groesbeck, G.A. Blake, T.G.P. and, *The Astrophysical Journal Supplement Series* 108 (1997) 301.
- <sup>8</sup> S.-Y. Liu, J.M. Girart, A. Remijan, L.E. Snyder, *The Astrophysical Journal* 576 (2002) 255.
- <sup>9</sup> D.M. Mehringer, L.E. Snyder, Y. Miao, F.J. Lovas, *The Astrophysical Journal Letters* 480 (1997) L71.
- <sup>10</sup> A. Remijan, L.E. Snyder, S.Y. Liu, D. Mehringer, Y.J. Kuan, *The Astrophysical Journal* 576 (2002) 264.
- <sup>11</sup> A. Remijan, L.E. Snyder, D.N. Friedel, S.Y. Liu, R.Y. Shah, *The Astrophysical Journal* 590 (2003) 314.
- <sup>12</sup> Y.S.J. Shiao, L.W. Looney, A. Remijan, L.E. Snyder, D.N. Friedel, *The Astrophysical Journal* 716 (2010) 286.
- <sup>13</sup> B.E. Turner, A.J. Apponi, *The Astrophysical Journal* 561 (2001) L207-L210.
- <sup>14</sup> F.F. Gardner, G. Winnewisser, *The Astrophysical Journal* 195 (1975) L127-L130.
- <sup>15</sup> M. Agúndez, J.P. Fonfría, J. Cernicharo, J.R. Pardo, M. Guélin, *A&A* 479 (2008) 493-501.
- <sup>16</sup> A. Nummelin, P. Bergman, *A&A* 341 (1999) L59-L62.
- <sup>17</sup> A. López, B. Tercero, Z. Kisiel, A.M. Daly, C. Bermúdez, H. Calcutt, N. Marcelino, S. Viti, B.J. Drouin, I.R. Medvedev, C.F. Neese, L. Pszczolkowski, J.L. Alonso, J. Cernicharo, *Astronomy & Astrophysics* (2014).
- <sup>18</sup> J.M. Hollis, P.R. Jewell, F.J. Lovas, A. Remijan, H. Mollendal, *Astrophysical Journal* 610 (2004) L21-L24.
- <sup>19</sup> M.A. Requena-Torres, J. Martín-Pintado, S. Martín, M.R. Morris, *The Astrophysical Journal* 672 (2008) 352.
- <sup>20</sup> N. Marcelino, J. Cernicharo, M. Agúndez, E. Roueff, M. Gerin, J. Martín-Pintado, R. Mauersberger, C. Thum, *The Astrophysical Journal Letters* 665 (2007) L127.
- <sup>21</sup> L. Kolesníková, I. Peña, J.L. Alonso, J. Cernicharo, B. Tercero, I. Kleiner, *A&A* 577 (2015) A91.
- <sup>22</sup> K. Bolton, D.G. Lister, J. Sheridan, *Journal of the Chemical Society, Faraday Transactions 2: Molecular and Chemical Physics* 70 (1974) 113-123.
- <sup>23</sup> C. Calabrese, A. Vigorito, G. Feng, L.B. Favero, A. Maris, S. Melandri, W.D. Geppert, W. Caminati, *Journal of Molecular Spectroscopy* 295 (2014) 37-43.
- <sup>24</sup> C. Calabrese, A. Maris, L. Dore, W.D. Geppert, P. Fathi, S. Melandri, *Molecular Physics* (2015) 1-6.
- <sup>25</sup> B. Reinhold, I.A. Finneran, S.T. Shipman, *Journal of Molecular Spectroscopy* 270 (2011) 89-97.
- <sup>26</sup> A.M. Daly, L. Kolesníková, S. Mata, J.L. Alonso, *Journal of Molecular Spectroscopy* 306 (2014) 11-18.
- <sup>27</sup> J.K.G. Watson, in: J.R. Durig, (Ed.), Elsevier, Amsterdam, 1977, pp 1-89.
- <sup>28</sup> A. Remijan, Y.S. Shiao, D.N. Friedel, D.S. Meier, L.E. Snyder, *The Astrophysical Journal* 617 (2004) 384.
- <sup>29</sup> A. López, (2015).
- <sup>30</sup> J. Cernicharo, *EAS Publications Series* 58 (2012) 251-261.
- <sup>31</sup> J. Neill, L. , M. Muckle, T. , D. Zaleski, P. , A. Steber, L. , B. Pate, H. , V. Lattanzi, S. Spezzano, M. McCarthy, C., A. Remijan, J. , *The Astrophysical Journal* 755 (2012) 153.
- <sup>32</sup> R. Pulliam, L., B.A. McGuire, A.J. Remijan, *The Astrophysical Journal* 751 (2012) 1.
- <sup>33</sup> A. Nummelin, P. Bergman, H. Å, P. Friberg, W.M. Irvine, T.J. Millar, M. Ohishi, S. Saito, *The Astrophysical Journal Supplement Series* 117 (1998) 427.
- <sup>34</sup> B.A. McGuire, P.B. Carrol, A. Remijan, *arXiv: 1306.0927* (2013).
- <sup>35</sup> J.L. Neill, E.A. Bergin, D.C. Lis, T.G. Phillips, M. Emprechtinger, P. Schilke, *Journal of Molecular Spectroscopy* 280 (2012) 150-154.
- <sup>36</sup> B. Tercero, J. Cernicharo, J.R. Pardo, J.R. Goicoechea, *A&A* 517 (2010).
- <sup>37</sup> Project, 2011.0.00009.SV.

# CHAPTER VII.

## Millimeter Wave Spectrum and Astronomical Search for Vinyl Formate

---

*Adapted from: The Astrophysical Journal, 2016, 832:42 (5pp)*

*Previous detections of methyl and ethyl formate make other small substituted formates potential candidates for observation in the interstellar medium. Among them, vinyl formate is one of the simplest unsaturated carboxylic ester. The aim of this work is to provide direct experimental frequencies of the ground vibrational state of vinyl formate in a large spectral range for astrophysical use. The room-temperature rotational spectrum of vinyl formate has been measured from 80 to 360 GHz and analyzed in terms of Watson's semirigid rotor Hamiltonian. Two thousand six hundred transitions within  $J=3-88$  and  $K_a=0-28$  were assigned to the most stable conformer of vinyl formate and a new set of spectroscopic constants was accurately determined. Spectral features of vinyl formate were then searched for in Orion KL, Sgr B2(N), B1-b, and TMC-1 molecular clouds. Upper limits to the column density of vinyl formate are provided.*



## 1. INTRODUCTION

---

Methyl formate ( $\text{CH}_3\text{OCOH}$ ) is one of the most abundant complex organic molecules in the interstellar medium (ISM). Ever since its first detection in Sgr B2,<sup>1,2</sup> a large number of lines originating from the ground and torsionally excited vibrational states<sup>3,4,5</sup> as well as mono-deuterated,  $^{13}\text{C}$  and  $^{18}\text{O}$  isotopic species<sup>6,7,8,9,10</sup> have been found in different molecular clouds. The choice of new candidates to be searched for is usually justified by analogy with already detected molecules and based on a plausible chemistry occurring in the ISM. Thus, substituted formates could be present and, rather recently, the presence of the ethyl derivative ( $\text{CH}_3\text{CH}_2\text{OCOH}$ ) has been evidenced in Sgr B2(N)<sup>11,12</sup> and Orion KL.<sup>13</sup> Several species containing the vinyl functional group have been observed in the ISM: vinyl cyanide ( $\text{CH}_2=\text{CHCN}$ ),<sup>14,15,16,17</sup> vinyl alcohol ( $\text{CH}_2=\text{CHOH}$ ),<sup>18</sup> propenal ( $\text{CH}_2=\text{CHCHO}$ ),<sup>19,20</sup> and propylene ( $\text{CH}_2=\text{CHCH}_3$ ),<sup>21</sup> leading vinyl formate ( $\text{CH}_2=\text{CHOCHO}$ ) to be considered as a good candidate. It could be formed starting from vinyl alcohol and carbon monoxide or from formic acid and acetylene all possible precursors already detected in the ISM.

While vinyl acetate, one of the simplest unsaturated carboxylic ester after vinyl formate, has been recently searched for in Orion KL,<sup>22</sup> no such trials have been conducted for vinyl formate. Detection of new complex molecules, such as vinyl formate, by millimeter and sub-millimeter wave astronomy is usually hampered by several difficulties, such as low fractional abundances with respect to  $\text{H}_2$ , large partition functions, and presence of multiple conformations, but also, to a large extent, a lack of reference laboratory spectra. Prior to this work, vinyl formate has been studied in the gas phase using conventional Stark-modulation spectroscopy,<sup>23,24</sup> electron diffraction, and infrared spectroscopy.<sup>25</sup> All of those studies indicate that the cis–trans structure, presented in Figure 1, is the most stable conformer of gaseous vinyl formate at room temperature, in agreement with ab initio calculations.<sup>26,25</sup> Although previous microwave data (10–20 GHz,  $J''$  8 and  $K_a''$  2) provided the first rotational constants of this conformer, they cannot be used to accurately predict its frequencies in the millimeter wave domain. Large

frequency uncertainties resulting from extrapolation outside the experimentally known data region prevent the confident analysis of astronomical survey of interstellar molecular clouds. The absence of accurate laboratory millimeter wave data thus stimulated new spectroscopic measurements up to 360 GHz.

The precise set of spectroscopic constants is provided and has been used to search for this species in the ISM.

## **2. EXPERIMENTAL DETAILS**

---

### **2.1. CHEMICAL SYNTHESIS**

Vinyl formate is a colorless liquid compound with a boiling point of 46°C<sup>27</sup> and was synthesized as follows. Gaseous acetylene (C<sub>2</sub>H<sub>2</sub>) was bubbled for 2 hr into 100 g of 100% formic acid (HCOOH) and 4% Mercury phosphate (Hg<sub>3</sub>(PO<sub>4</sub>)<sub>2</sub>), giving vinyl formate (CH<sub>2</sub>CHOCHO) and 1,1-ethanediol diformate (CH<sub>3</sub>CH(OC(O)H)<sub>2</sub>). The temperature was maintained at 50°C–55°C during the reaction. The crude mixture was then fitted on a vacuum line (0.1 mbar) and the low boiling compounds were distilled. A first trap at –65°C selectively condensed high boiling compounds while vinyl formate was selectively trapped in a second trap cooled at –120°C. A second purification by distillation in vacuum was performed to obtain a pure compound. Yield: 45%.

### **2.2. ROTATIONAL SPECTRA MEASUREMENTS**

The room-temperature rotational spectra were recorded at the pressure of approximately 20 μbar using the Valladolid millimeter wave absorption spectrometer.<sup>28</sup> A sequential multiplication of the basic synthesizer frequency (20 GHz) by a set of active and passive multipliers (6×, 9×, 12×, and 18× multiplication factors; VDI, Inc.) allowed the frequency region from 80 to 360 GHz to be covered. The synthesizer output was frequency modulated at the modulation frequency  $f = 10.2$  kHz and modulation depth between 30 and



40 kHz. The signal was detected by solid-state zero-bias detectors (VDI, Inc.) and further processed by a lock-in amplifier using  $2f$  detection. The second derivative shape of the lines was fit to the Gaussian profile function. The uncertainty of the line center frequency is estimated to be better than 50 kHz.

### 3. ANALYSIS OF THE SPECTRA

---

The molecular structure of the cis–trans conformer of vinyl formate is shown in Figure 1. It is a planar near prolate asymmetric rotor ( $\kappa = -0.95$ ) of Cs symmetry with electric dipole moment oriented in the  $ab$  inertial plane. Two nonzero dipole moment components were determined by Rao & Curl (1964)<sup>23</sup> to  $|\mu_a| = 1.1$  (1) D and  $|\mu_b| = 1.0$  (1) D. A portion of the room-temperature millimeter wave spectrum is illustrated in Figure 2(a). Groups of a-type R-branch transitions dominate the millimeter wave spectrum and can be easily identified due to their typical  $(B + C)$  periodicity (see Figure 2(a)). These groups are interspersed by b-type R-branch transitions which do not cluster into any characteristic pattern. However, as  $J$  increases, the rotational energy levels with the lowest  $K_a$  quantum numbers become near-degenerate, and pairs of b-type transitions involving these energy levels form quartets of similar intensity with corresponding pairs of a-type transitions before they coalesce into one quadruply degenerate line. A good visualization of this progressive line blending with the use of a graphical Loomis–Wood-type plot (AABS package<sup>29</sup>) is shown in Figure 2(b). Finally, bands of b-type Q-branch transitions form another easily recognizable feature of the millimeter wave spectrum of vinyl formate. The typical contour and properties of the Q-branch series can be displayed in the Fortrat diagram, demonstrated in Figure 2(c), which plots the individual transition frequencies versus  $J$  quantum number.

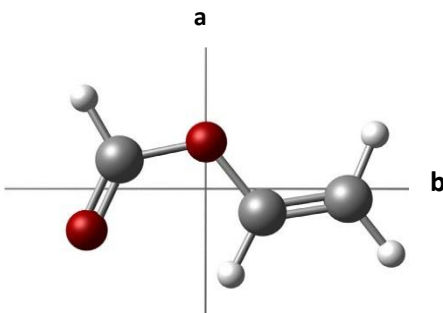


**Figure 1.** Most stable cis–trans conformer of vinyl formate, defined by two dihedral angles  $f_1(\text{O}=\text{C}-\text{O}-\text{C}) = 0^\circ$  and  $f_2(\text{C}-\text{O}-\text{C}=\text{C}) = 180^\circ$ .

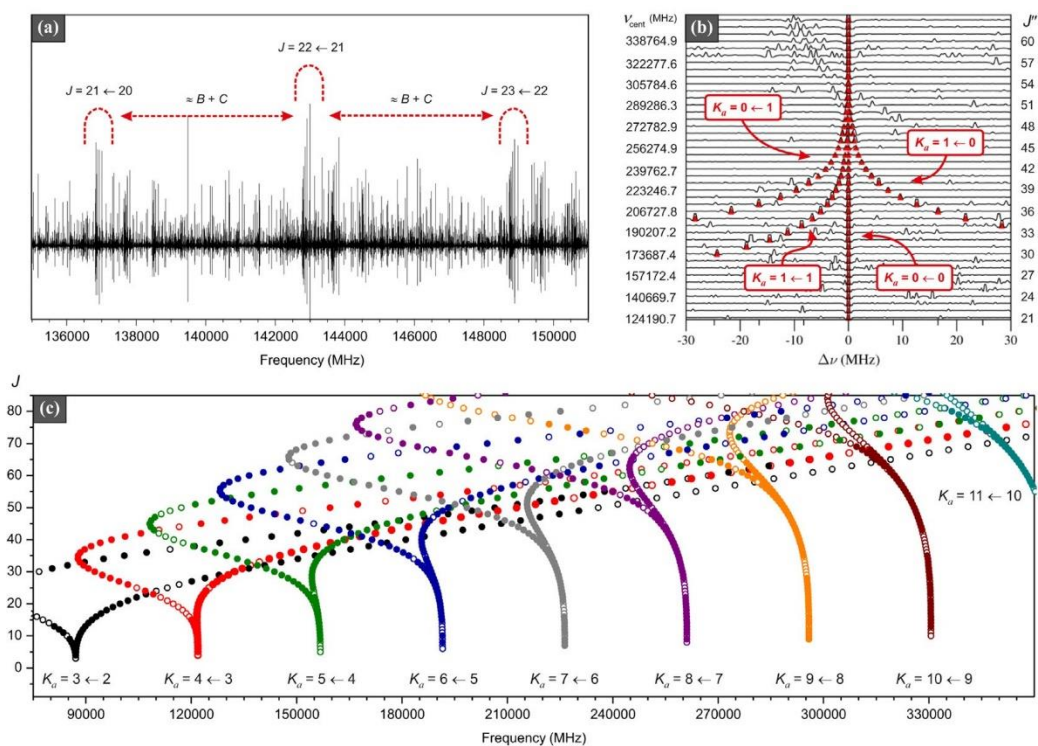


**Figure 2.** (a): A 16 GHz section of the room-temperature rotational spectrum of vinyl formate. Groups of the ground state a-type R-branch transitions and their approximate separations are indicated. (b): Loomis–Wood-type plot illustrating a convergence of the a-type and b-type R-branch transitions with the lowest values of the  $K_a$  quantum numbers. Four different line sequences corresponding to  $K_a = 0 \leftarrow 0$ ,  $1 \leftarrow 1$ ,  $1 \leftarrow 0$ , and  $0 \leftarrow 1$  can be found up to  $J'' \approx 45$ . At  $J'' > 50$ , only one strong line can be observed. Rotational transitions are lined up to the central frequencies  $\nu_{\text{cent}}$  of the  $K_a = 0 \leftarrow 0$  transitions with frequencies and  $J''$  quantum numbers indicated on the left and right sides of the diagram, respectively. A frequency distance from the central stripe is given by the  $\Delta\nu$  quantity. (c): Fortrat diagram of the b-type Q-branch series of transitions analyzed in this work. The filled circles represent the experimentally measured data while the opened circles come from predictions from the final fit. All Q-branches with  $K_a > 0$  are divided into two sub-branches. The lower-frequency sub-branch, which conspicuously doubles back on itself in frequency, corresponds to transitions fulfilling the  $K_a + K_c = J$  condition. On the other hand, the higher-frequency sub-branch belongs to the  $K_a + K_c = J + 1$  transitions.

At the initial stage of the line assignment, predictions based on the spectroscopic constants from Rao & Curl (1964)<sup>23</sup> were used. Intense R-branch transitions involving  $K_a=0, 1$  energy levels were searched for at first. Subsequently, higher  $K_a$  R-branch transitions together with several Q-branch and some P-branch transitions were assigned. Finally, 2600 transition lines were measured and the ranges of J and  $K_a$  quantum numbers were extended up to 88 and 28, respectively. The fits and predictions were made in terms of Watson's S-reduced Hamiltonian in I<sup>r</sup>-representation<sup>30</sup> with the Pickett's SPFIT/SPCAT program suite.<sup>31</sup> The present data allowed determination of the rotational constants and the full set of quartic and sextic centrifugal distortion constants. Three octic constants were necessary to fit the  $K_a \geq 18$  transitions within the experimental uncertainty. The spectroscopic constants are collected in Table 1, and the measured transitions are reported in Table 2.

**Table 1.** Ground State Spectroscopic Constants of Vinyl Formate (S-Reduction, I<sup>r</sup>-Representation)

Constant	Unit	Value <sup>a</sup>
A	MHz	20391.47934 (25)
B	MHz	3184.151243 (37)
C	MHz	2757.735370 (37)
D <sub>J</sub>	kHz	0.717093 (18)
D <sub>JK</sub>	kHz	-8.82527 (25)
D <sub>K</sub>	kHz	118.0508 (36)
d <sub>1</sub>	kHz	-0.1379641 (20)
d <sub>2</sub>	kHz	-0.00877161 (90)
H <sub>J</sub>	Hz	0.0003413 (28)
H <sub>JK</sub>	Hz	-0.008785 (93)
H <sub>KJ</sub>	Hz	0.05985 (66)
H <sub>K</sub>	Hz	-2.099 (16)
h <sub>1</sub>	mHz	0.00513 (30)
h <sub>2</sub>	mHz	0.02057 (20)
h <sub>3</sub>	mHz	0.003154 (53)
L <sub>JK</sub>	mHz	0.0001869 (97)
L <sub>JK</sub>	mHz	-0.005498 (81)
L <sub>KKJ</sub>	mHz	0.08838 (74)
$\sigma_{\text{fit}}^{\text{b}}$	kHz	24

<sup>a</sup> The numbers in parentheses are 1 $\sigma$  uncertainties in units of the last decimal digit.  
<sup>b</sup> Root mean square deviation of the fit.

**Table 2.** List of the Assigned Transitions to the Ground State Rotational Spectrum of Vinyl Formate.

$J'$	$K'_a$	$K'_c$	$J''$	$K''_a$	$K''_c$	$\nu_{\text{obs}}^{\text{a,b}}$	$\nu_{\text{obs}} - \nu_{\text{calc}}^{\text{c}}$
14	0	14	13	0	13	80380.074 (50)	0.008
15	0	15	14	0	14	85861.916 (50)	0.011
30	6	25	29	6	24	179245.443 (50)	-0.008
31	6	26	30	6	25	185284.508 (50)	0.010
56	10	46	55	10	45	334748.164 (50)	-0.021
57	10	47	56	10	46	340796.726 (50)	-0.012
23	4	19	23	3	20	109175.845 (50)	-0.007
24	4	20	24	3	21	106882.004 (50)	-0.001
37	9	28	37	8	29	293853.995 (50)	0.010
38	9	29	38	8	30	293617.252 (50)	-0.007
36	2	34	35	3	33	201778.534 (50)	-0.010
37	2	35	36	3	34	209007.174 (50)	0.004
56	5	51	55	6	50	260889.572 (50)	-0.007
57	5	52	56	6	51	273516.082 (50)	0.027

<sup>a</sup> Observed frequency. Spectral lines containing two or more unresolved transitions were excluded from the fit if the difference of predicted frequencies of individual transitions is larger than 30 kHz. If their difference is less than 30 kHz, only one transition was assigned to the observed line.

<sup>b</sup> Values in parentheses are the uncertainties of the observed frequency in kHz.

<sup>c</sup> Observed minus calculated frequency.

#### 4. SEARCHING FOR VINYL FORMATE IN SPACE

The new spectroscopic results presented in this work allow us to carry out a rigorous search for vinyl formate in space. High-mass star-forming regions are the best candidates for this search: on the one hand, both methyl and ethyl formate ( $\text{CH}_3\text{COOH}$  and  $\text{CH}_3\text{CH}_2\text{COOH}$ ) have been detected in Orion KL<sup>13</sup> and Sgr B2<sup>11,12</sup>, with the former species one of the most abundant molecules in these regions. On the other hand, vinyl cyanide ( $\text{CH}_2\text{CHCN}$ ) is another one of the most abundant species in those sources<sup>17,12</sup> and also is related to its extremely abundant methyl and ethyl counterparts. Therefore, we mainly focused on the available astronomical data of Orion KL and Sgr B2.

#### 4.1. ORION KL

Combining the IRAM 30 m survey<sup>32,33</sup> and the ALMA Science Verification (SV) data of this source we could analyze a wide frequency band (80–306 GHz) and focus on the different positions characterized by a typical chemistry: the compact ridge where the emission peak of methyl and ethyl formate is located<sup>34,33</sup> (see Favre et al. 2011a; Tercero et al. 2015) and a position in the middle of the hot core clumpy structure<sup>34</sup> (see, e.g., Favre et al. 2011b) that corresponds to the emission peak of ethylene glycol (HOCH<sub>2</sub>CH<sub>2</sub>OH;<sup>35</sup> Brouillet et al. 2015) and methyl isocyanate (CH<sub>3</sub>NCO).<sup>36</sup> Vinyl formate was implemented in the MADEX code<sup>37</sup> to obtain a synthetic spectrum of this species according to the typical physical parameters of the source (see Table 3 and, e.g., Tercero et al. 2015;<sup>33</sup> Cernicharo et al. 2016<sup>36</sup>). As Figure 3 shows, we did not detect vinyl formate above the confusion limit of these data. Hence, we can only estimate upper limits to its column density, which are shown in Table 3. In Figure 3 the model is shown by the red curve superimposed on the IRAM 30 m and ALMA SV data at selected frequencies and positions. Above the limit established by these models, we see that most of the vinyl formate lines are missing. We found that in the compact ridge of Orion KL, vinyl formate is, at the maximum, 240 and 2 times less abundant than methyl formate and ethyl formate, respectively (see Tercero et al. 2015<sup>33</sup> for the derived column densities of methyl and ethyl formate).

#### 4.2. SGR B2

We continued the search for vinyl formate in space by checking public data of Sgr B2. As in the Orion case, we did not find this species above the detection limit of the data, either in the PRIMOS survey at low frequencies from 7 to 50 GHz<sup>38</sup> or in the IRAM 30 m data at 3 mm (80–115 GHz) of Sgr B2(N) provided by Belloche et al. (2013).<sup>12</sup> According to the physical parameters derived for methyl formate in the source by Belloche et al. (2013),<sup>12</sup> we provide upper limits to the vinyl formate column density in these cloud components (see Table 3, Sgr B2(N), warm gas) and a N(CH<sub>3</sub>OCOH)/N(CH<sub>2</sub>CHOCOH) ratio ~10. In addition, we also derived upper limits to the column density for the cold gas of the region by adopting the

physical parameters derived by Brünken et al. (2010)<sup>39</sup> for HOCN (see Table 3, Sgr B2(N), cold gas).

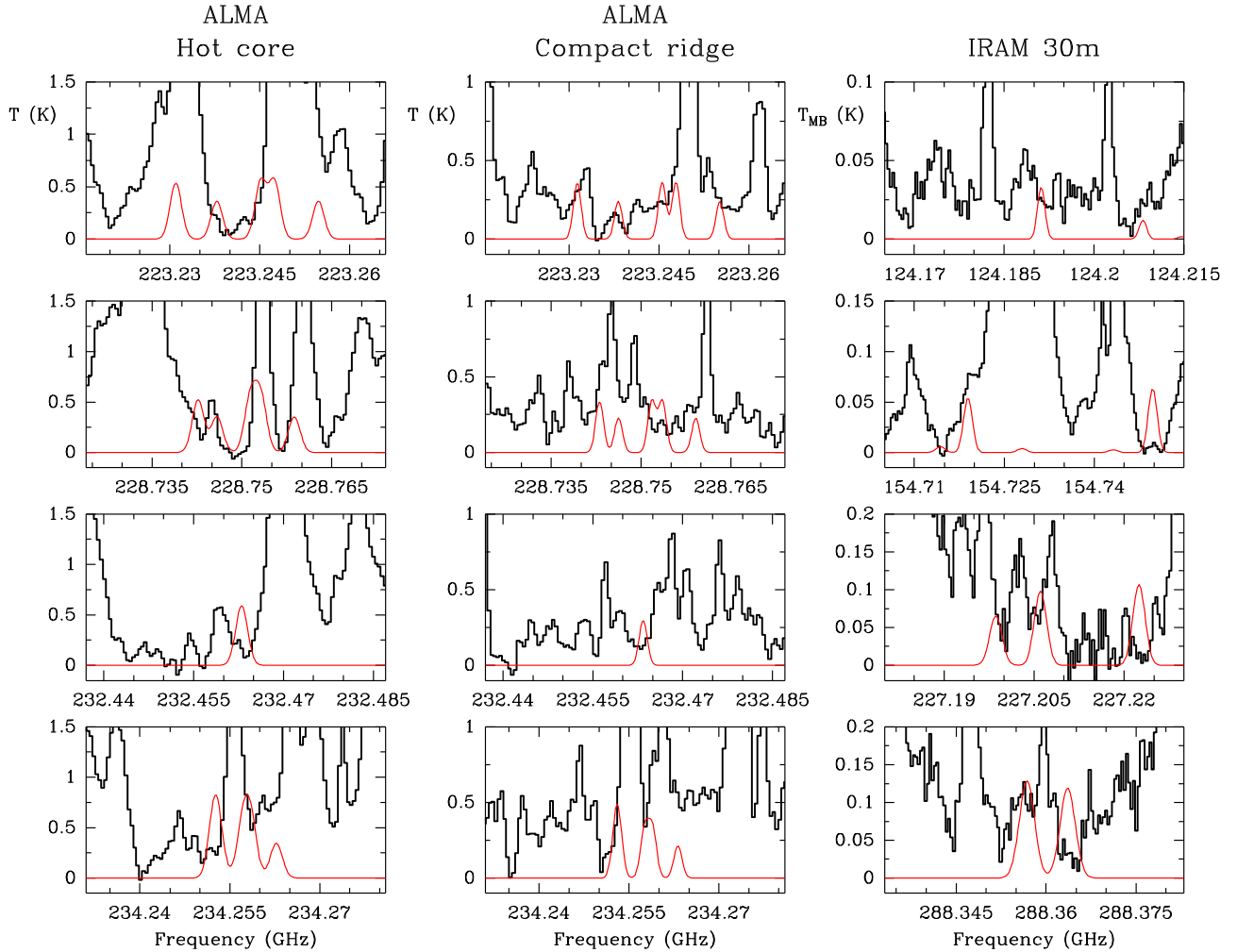


**Figure 3.** ALMA SV data of two different positions and IRAM 30 m data at selected frequencies together with the synthetic spectra of vinyl formate obtained using the column densities shown in Table 3. A  $v_{\text{LSR}}$  of +9.0 km s<sup>-1</sup> is assumed.

**Table 3.** Physical Parameters of the Considered Cloud Cores

Source	$v_{\text{LSR}}$ ( $\text{km s}^{-1}$ )	$\Delta v_{\text{FWHM}}$ ( $\text{km s}^{-1}$ )	$d_{\text{sou}}$ (")	Trot (K)	$N(\text{CH}_2\text{CHOCO}) \times 10^{15}$ ( $\text{cm}^{-2}$ )
Orion KL (IRAM 30 m)	8	3	5	150	$\leq (4.0 \pm 1.2)$
Orion KL (ALMA SV) Hot core	8	3	3	150	$\leq (2.0 \pm 0.6)$
Orion KL (ALMA SV) Compact Ridge	7.5	2	3	100	$\leq (1.0 \pm 0.3)$
Sgr B2(N)(IRAM 30 m) Warm gas	63.5	7	4	80	$\leq (50 \pm 15)$
	73.5	7	4	80	$\leq (20 \pm 6)$
Sgr B2(N)(IRAM 30 m) Cold gas	64	9	60	14	$\leq (0.5 \pm 0.2)$
	75	12	60	14	$\leq (0.5 \pm 0.2)$
B1-b (IRAM 30 m)	6.7	0.7	60	12	$\leq (0.005 \pm 0.002)$
TMC-1 (IRAM 30 m)	6.0	0.7	60	10	$\leq (0.005 \pm 0.002)$

### 4.3. DARK CLOUDS

Finally, although we mainly expected vinyl formate in the warm gas, we explored the IRAM 30 m surveys of B1-b and TMC-1<sup>40</sup> to derive new constraints to the chemistry of these objects. The upper limits to the  $\text{CH}_2\text{CHOCO}$  column density in these dark clouds are shown in Table 3.

### 4.4. VINYL SPECIES IN ORION

Using the results of acrylic acid ( $\text{CH}_2\text{CHCOOH}$ ),<sup>41</sup> we estimated an upper limit to the column density of vinyl formate of  $1.5 \times 10^{16} \text{ cm}^{-2}$  in Orion. In this work, we find a lower upper limit for the abundance of this molecule in the source. As we discussed in Alonso et al. (2015),<sup>41</sup> the upper limit on the column density of vinyl derivatives such as vinyl formate or acrylic acid puts strong constraints on the production mechanisms of vinyl species. These species in Orion are associated with cyanide groups rather than with alcohols, formates, or acetates. Interestingly, emission from vinyl and ethyl cyanide is strongly concentrated in a hot (Trot; 350 K) region of Orion KL (see Daly et al. 2013;<sup>42</sup> López et al. 2014;<sup>17</sup> Cernicharo et al. 2016<sup>36</sup>). Neither ethyl alcohol nor methyl and ethyl formate are associated with components at this high temperature, with the warm gas ( $\sim 150$  K) being responsible for the bulk of the emission of these later species. Therefore, in addition to possible different

mechanisms to produce the vinyl derivatives for each functional group, small differences in the gas temperature may play an important role in the production of the vinyl species.

Although we do not detect vinyl formate in this work, the search for this species should be considered in future spectroscopic analysis of star-forming regions where the gas temperatures are high and large abundances of methyl formate are found. The present data can be used with confidence in future searches for vinyl formate in space.

## 5. REFERENCES

---

- <sup>1</sup> Brown, R. D., Crofts, J. G., Godfrey, P. D., et al. 1975, *ApJL*, 197, L29
- <sup>2</sup> Churchwell, E., & Winnewisser, G. 1975, *A&A*, 45, 229
- <sup>3</sup> Kobayashi, K., Ogata, K., Tsunekawa, S., & Takano, S. 2007, *ApJL*, 657, L17
- <sup>4</sup> Demyk, K., Wlodarczak, G., & Carvajal, M. 2008, *A&A*, 489, 589
- <sup>5</sup> Lovas, F. J. 2004, *JPCRD*, 33, 177
- <sup>6</sup> Carvajal, M., Margulès, L., Tercero, B., et al. 2009, *A&A*, 500, 1109
- <sup>7</sup> Margulès, L., Huet, T. R., Demaison, J., et al. 2010, *ApJ*, 714, 1120
- <sup>8</sup> Tercero, B., Margulès, L., Carvajal, M., et al. 2012, *A&A*, 538, A119
- <sup>9</sup> Coudert, L. H., Drouin, B. J., Tercero, B., et al. 2013, *ApJ*, 779, 119
- <sup>10</sup> Haykal, I., Carvajal, M., Tercero, B., et al. 2014, *A&A*, 568, A58
- <sup>11</sup> Belloche, A., Garrod, R. T., Müller, H. S. P., et al. 2009, *A&A*, 499, 215
- <sup>12</sup> Belloche, A., Müller, H. S. P., Menten, K. M., Schilke, P., & Comito, C. 2013, *A&A*, 559, A4
- <sup>13</sup> Tercero, B., Kleiner, I., Cernicharo, J., et al. 2013, *ApJL*, 770, L13
- <sup>14</sup> Gardner, F. F., & Winnewisser, G. 1975, *ApJL*, 195, L127
- <sup>15</sup> Schilke, P., Groesbeck, T. D., Blake, G. A., & Phillips, T. G. 1997, *ApJS*,
- <sup>16</sup> Nummelin, A., & Bergman, P. 1999, *A&A*, 341, L59
- <sup>17</sup> López, A., Tercero, B., Kisiel, Z., et al. 2014, *A&A*, 572, A44
- <sup>18</sup> Turner, B. E., & Apponi, A. J. 2001, *ApJL*, 561, L207
- <sup>19</sup> Hollis, J. M., Jewell, P. R., Lovas, F. J., Remijan, A., & Møllendal, H. 2004, *ApJL*, 610, L21
- <sup>20</sup> Requena-Torres, M. A., Martín-Pintado, J., Martín, S., & Morris, M. R. 2008, *ApJ*, 672, 352
- <sup>21</sup> Marcelino, N., Cernicharo, J., Agúndez, M., et al. 2007, *ApJL*, 665, L127
- <sup>22</sup> Kolesníková, L., Pena, I., Alonso, J. L., et al. 2015, *A&A*, 577, A91
- <sup>23</sup> Rao, V. M., & Curl, R. F. 1964, *JChPh*, 40, 3688
- <sup>24</sup> Voss, H. L., Krajnovich, D., Hoke, W. E., & Flygare, W. H. 1978, *JChPh*, 68, 1439
- <sup>25</sup> Pyckhout, W., Alsenoy, C. V., Geise, H., et al. 1986, *JMoSt*, 147, 85
- <sup>26</sup> Aroney, M., Bruce, E., John, I., Radom, L., & Ritchie, G. 1976, *AJCh*, 29, 581
- <sup>27</sup> Rostovskii, E., & Barinova, A. 1963, *Zhurnal Obshechi Khimii*, 33, 828
- <sup>28</sup> Daly, A., Kolesníková, L., Mata, S., & Alonso, J. 2014, *JMoSp*, 306, 11
- <sup>29</sup> Kisiel, Z., Pszczółkowski, L., Medvedev, I. R., et al. 2005, *JMoSp*, 233, 231
- <sup>30</sup> Watson, J. K. G. 1977, in *Vibrational Spectra and Structure*, Vol. 6, ed. J. R. Durig (Amsterdam: Elsevier), 1
- <sup>31</sup> Pickett, H. M. 1991, *JMoSp*, 148, 371
- <sup>32</sup> Tercero, B., Cernicharo, J., Pardo, J. R., & Goicoechea, J. R. 2010, *A&A*, 517, A96
- <sup>33</sup> Tercero, B., Cernicharo, J., López, A., et al. 2015, *A&A*, 582, L1
- <sup>34</sup> Favre, C., Wootten, H. A., Remijan, A. J., et al. 2011b, *ApJL*, 739, L12
- <sup>35</sup> Brouillet, N., et al. 2011a, *A&A*, 532, A32
- <sup>36</sup> Cernicharo, J., Kisiel, Z., Tercero, B., et al. 2016, *A&A*, 587, L4
- <sup>37</sup> Cernicharo, J., Marcelino, N., Roueff, E., et al. 2012, *ApJL*, 759, L43



- 
- <sup>38</sup> Neill, J. L., Muckle, M. T., Zaleski, D. P., et al. 2012, *ApJ*, 755, 153
- <sup>39</sup> Brünken, S., Belloche, A., Martín, S., Verheyen, L., & Menten, K. M. 2010, *A&A*, 516, A109
- <sup>40</sup> Cernicharo, J. 2012, in *EAS Publ. Ser. 58, ECLA-European Conference on Laboratory Astrophysics*, ed. C. Stehlé, C. Joblin, & L. d’Hendecourt (Les Ulis: EDP Sciences), 251
- <sup>41</sup> Alonso, E. R., Kolesníková, L., Peña, I., et al. 2015, *JMoSp*, 316, 84
- <sup>42</sup> Daly, A. M., Bermúdez, C., López, A., et al. 2013, *ApJ*, 768, 81



## CHAPTER VIII.

# The rotational spectrum of methoxyamine up to 480 GHz: a laboratory study and astronomical search

---

***Adapted from: Astronomy & Astrophysics, 609, A24 (2018)***

*Aims. Methoxyamine is a potential interstellar amine predicted by gas-grain chemical models for formation of complex molecules. The aim of this work is to provide direct experimental frequencies of its ground vibrational state in the millimeter and submillimeter wave regions to achieve its detection in the interstellar medium.*

*Methods. Methoxyamine was chemically liberated from its hydrochloride salt and its rotational spectrum was recorded at room temperature from 75 to 480 GHz using the millimeter wave spectrometer in Valladolid. Many observed transitions revealed A-E splitting due to the methyl group internal rotation and had to be treated with a specific internal rotation code.*

*Results. Over 400 lines were newly assigned for the most stable conformer of methoxyamine and a precise set of spectroscopic constants was obtained. Spectral features of methoxyamine were then searched for in Orion KL, Sgr B2, B1-b, and TMC-1 molecular clouds. Upper limits to the column density of methoxyamine were derived.*



## 1. INTRODUCTION

---

Molecular line surveys of massive star-forming regions such as the Orion KL hot core or the Galactic-center hot cores Sgr B2(N) and (M) have shown very complex chemistry through the detection of a large variety of molecule.<sup>1,2</sup> Of these molecules, amines have received particular attention because they participate in the synthesis of amino acids, the basic units of proteins. Although the original interstellar detection of glycine,<sup>3</sup> the simplest amino acid, has been called into doubt,<sup>4,5,6</sup> the discovery of glycine in dust samples from comet Wild 2<sup>7</sup> and in the coma of 67P/Churyumov-Gerasimenko<sup>8</sup> shows that these types of biomolecules can be formed under cosmic conditions. In addition, several laboratory experiments of the interstellar icy grains analogs have demonstrated that formation of diverse amines and amino acids in the interstellar medium (ISM) is possible.<sup>9,10,11,12</sup> Spectroscopic characterization and subsequent search for chemically similar species or their possible pre-cursors thus create an important target for astrochemistry.

To the best of our knowledge, only a few molecules containing the  $-NH_2$  group have been confidently detected in the ISM: formamide ( $NH_2CHO$ ),<sup>13</sup> methylamine ( $CH_3NH_2$ ),<sup>14,15</sup> cyanamide ( $NH_2CN$ ),<sup>16</sup> acetamide ( $CH_3CONH_2$ ),<sup>17</sup> and aminoacetonitrile ( $NH_2CH_2CN$ ).<sup>18</sup> Urea ( $(NH_2)_2CO$ ), a molecule with two  $-NH_2$  groups, has been detected only tentatively.<sup>19</sup> Of these detected molecules, only two belong to the category of amines; nevertheless, the gas-grain chemical model for the formation of complex molecules predicts that more interstellar amines, such as methoxyamine ( $CH_3ONH_2$ ), hydroxylamine ( $NH_2OH$ ) or hydroxymethylamine ( $HOCH_2NH_2$ ), can be generated with significant abundances<sup>20</sup>. The interstellar formation of methoxyamine is proposed through a direct reaction between  $CH_3O$  and  $NH_2$  radicals on the grains at temperatures around 50 K.<sup>20</sup> It is predicted to remain on the grains until the temperature of  $\sim 100$  K is reached, when it starts to desorb into the gas phase. The peak gas-phase abundance of methoxyamine in the star-forming regions is then predicted at the approximate temperature of 120 K.<sup>20</sup>

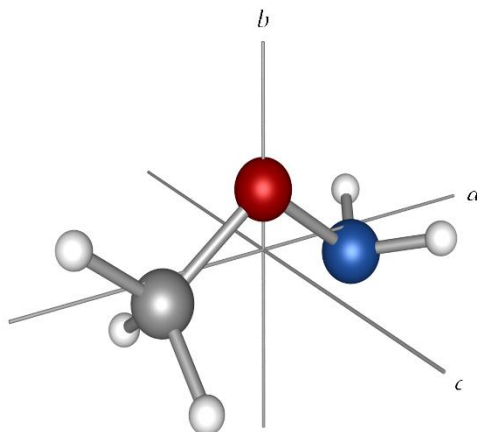


**Figure 1.** Equilibrium Cs symmetry structure of the most stable form of methoxyamine.

While hydroxylamine has been actively searched for toward several interstellar sources,<sup>21,22</sup> no such trials have been conducted for methoxyamine, probably because we have only insufficient laboratory information. The most stable conformation of methoxyamine has the  $\text{-NH}_2$  group in the trans-position with respect to the  $\text{-CH}_3$  group (see Fig. 1) and was studied in the gas phase from 8 to 39.5 GHz by Stark-modulation spectroscopy.<sup>23</sup> Since the rotational constants were obtained from the least-squares fit of four hyperfine-free  $a$ -type  $R$ -branch transitions with  $J''$  and  $k''_a \leq 1$ , they do not provide accurate predictions for the rotational spectrum at higher  $J$  and  $K_a$  values. At the 67% confidence level, uncertainties of up to 3, 8, and 13 MHz can be estimated for  $a$ -type  $R$ -branch transitions with  $J'' = 6, 12, \text{ and } 18$ , respectively. These transitions at the temperature of 120 K fall exactly into the range of millimeter-wave surveys that are provided by several astrophysical instruments, as shown in Fig. 2, and with these uncertainties, it is not possible to confidently search for methoxyamine. Lack of the accurate laboratory millimeter-wave data thus prompted new spectroscopic studies of methoxyamine over the frequency range from 75 to 480 GHz. More than 400 spectral features were newly assigned, which significantly extended the range of  $J$  and  $K_a$  quantum numbers, and the features were used to search for methoxyamine in Orion KL and Sgr B2 molecular clouds.

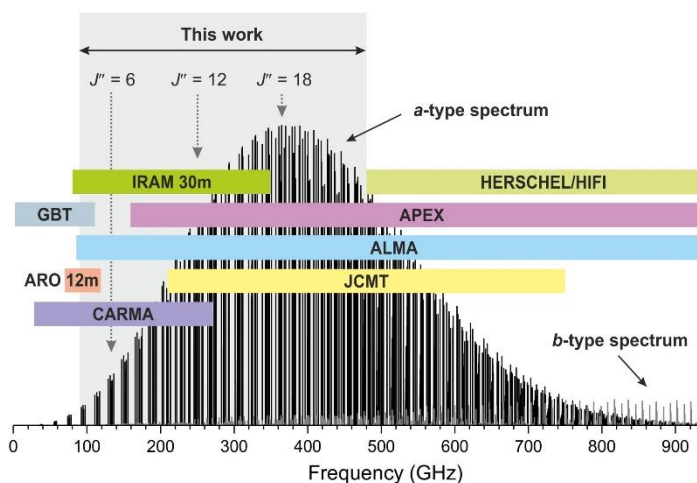


**Figure 2.** Predicted rotational spectrum of methoxyamine at the temperature of 120 K and its overlap with approximate frequency coverage of several astrophysical facilities (IRAM: Institut de Radioastronomie Millimétrique; HERSCHEL/HIFI: Herschel-Heterodyne Instrument for the Far-Infrared; GBT: Green Bank Telescope; APEX: Atacama Pathfinder Experiment telescope; ALMA: Atacama Large Millimeter/submillimeter Array; ARO: Arizona Radio Observatory; JCMT: James Clerk Maxwell Telescope; CARMA: Combined Array for Research in Millimeter-wave Astronomy). The frequency region studied in this work is highlighted in gray.

## 2. EXPERIMENTAL DETAILS

Methoxyamine is a colorless liquid with a boiling point at 48.1 °C,<sup>24</sup> and it was synthesized by reaction of liquid 1,8-diazabicyclo[5.4.0]undec-7-ene injected in excess (1.5 equivalent) through a septum in a two-necked flask containing solid methoxyamine hydrochloride and fitted on a vacuum line. The reaction product was collected in a U-tube trap cooled by liquid nitrogen and was used without any further purification. Methoxyamine was thus obtained in a 70% yield.

The room-temperature rotational spectrum was measured from 75 to 480 GHz using the millimeter-wave spectrometer at the University of Valladolid, which generates the millimeter-wave radiation by multiplying the fundamental synthesizer frequency ( $\leq 20$  GHz) by amplifier-multiplier chains (multiplication factors of 6, 9, 12, 18, and 24 in this case). A detailed description of the experimental setup has been given elsewhere.<sup>25</sup> The synthesizer

output was frequency modulated at a modulation frequency of 10.2 kHz and a modulation depth of between 10 and 30 kHz. After passing the radiation through the free-space cell (see the single- and double-pass configurations in Daly et al. 2014),<sup>25</sup> the signal was detected by zero-bias detectors and was demodulated by a lock-in amplifier tuned to twice the modulation frequency. This demodulation process gives rise to a shape of the lines that approximates the second derivative of a Gaussian function. The experimental uncertainty of the isolated symmetric lines is estimated to be better than 50 kHz.

### 3. ROTATIONAL SPECTRA ANALYSIS

---

Supporting ab initio calculations were performed at the beginning of the analysis using the Gaussian09 package.<sup>26</sup> The Møller–Plesset second-order method (MP2) and the aug-cc-pVTZ basis set were used to geometrically optimize the structure of methoxyamine, to estimate electric dipole moment components along the principal axis, and to obtain the information on equilibrium quartic centrifugal distortion constants. Methoxyamine possesses a plane of symmetry, and its optimized geometry is illustrated in Fig. 1 (a similar geometry has been calculated by Hays & Widicus Weaver 2013).<sup>27</sup> Equilibrium spectroscopic constants are given in the last column of Table 1. The calculated dipole moment components of  $|\mu_a| = 0.5$  D,  $|\mu_b| = 0.1$  D, and  $|\mu_c| = 0.0$  D are in agreement with the fact that only *a*-type transitions were observed in the previous microwave work of Fong et al. (1974).<sup>23</sup>

Groups of *a*-type *R*-branch transitions repeating approximately every 19 GHz were easily identified in the broadband rotational spectrum. Figure 3 shows one of these groups for  $J \leftarrow J'' = 10 \leftarrow 9$  with typical arrangement of individual  $K_a$  transitions common for a near-prolate asymmetric top ( $\kappa = -0.93$  in this case). A few *a*-type transitions with  $K_a = 1, 3, 4, 5,$  and  $6$  were found as doublets situated closely around the semi-rigid rotor pattern. This doublet structure originates from internal rotation of the methyl group and agrees with the relatively high barrier to internal rotation of  $V_3 = 873 \pm 15$  cm<sup>-1</sup> determined by Fong et al. (1974).<sup>23</sup> After we assigned the *a*-type transitions, we attempted to locate *b*-type



transitions, although the value of  $\mu_b$  predicted by *ab initio* calculations is very low. Surprisingly, many *b*-type *R*-branch and *Q*-branch transitions were successfully identified. While only a few *a*-type transitions were found to be subject to the *A–E* splitting, almost all *b*-type transitions appeared as doublets, and the separation of the two lines of the doublets was less than 10 MHz. Additionally, weak forbidden *x*-type and *c*-type transitions between the *E*-levels,<sup>28</sup> which borrow intensity from allowed *a*-type and *b*-type transitions, respectively, could occasionally be observed (see the middle part of Fig. 3) in situations where the asymmetry splitting became comparable in magnitude with the internal rotation splitting,<sup>29,30</sup> More than 400 distinct frequency lines were finally assigned to the ground torsional state of methoxyamine. More than 100 lines correspond to *A*-symmetry species, more than 100 lines to *E*-symmetry species, and over 200 lines reveal unresolved *A–E* splitting. The <sup>14</sup>N nuclear quadrupole hyperfine structure could be partly resolved for transitions where the value of  $K_a$  approaches the value of  $J$  and corresponding transitions were not taken into consideration. These transitions are expected to be weak and are not interesting for a possible detection in the ISM.

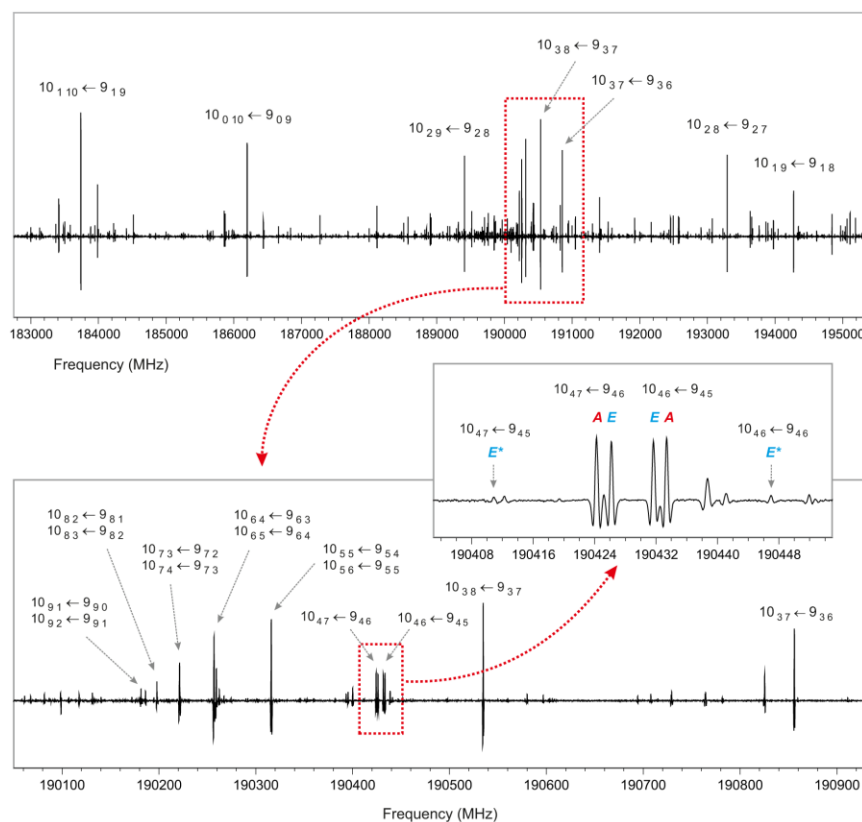


**Figure 3.** Portion of the room-temperature millimeter-wave spectrum of methoxyamine showing a group of *a*-type *R*-branch transitions for  $J'' \leftarrow J' = 10 \leftarrow 9$ . The asymmetry splitting for the  $K_a = 1$  transitions in this case reaches almost 11 GHz and decreases rapidly with increasing  $K_a$  until it is completely unresolved for  $K_a \geq 5$ . Small internal rotation *A–E* splitting can be seen for two  $K_a = 4$  rotational transitions. Forbidden *x*-type transitions ( $\Delta K_a = 0, \pm 2, \dots$ ,  $\Delta K_c = 0, \pm 2, \dots$ ) that gain intensity through the so-called intensity borrowing from allowed *a*-type transitions between the same pairs of levels are situated outside the *A* lines and are labeled with an *E\**.

Initially, *A* and *E* transitions were analyzed separately using the SPFIT/SPCAT programs.<sup>31</sup> The effective rotational and centrifugal distortion constants for the *A* sublevels were obtained by fitting the standard Watson *S*-reduced Hamiltonian in *I'* representation.<sup>32</sup> In determining the *E* sublevel constants, Watson's semirigid Hamiltonian was extended by the linear terms  $D_a J_a$  and  $D_b J_b$ .<sup>33,34</sup> Finally, only  $D_a$  parameter and its centrifugal distortion corrections were determinable. The results of both fits are collected in the first two columns of Table 1. The same sets of *A* and *E* transitions were subsequently fitted using the XIAM program<sup>35</sup> in order to obtain the barrier to the internal rotation  $V_3$  of the methyl group. As shown in Table 1, its value compares well with that from the microwave study of Fong et al. (1974).<sup>23</sup> Although the effective fits for the two internal rotation sublevels as well as the XIAM fit are able to reproduce the *A*-*E* split transitions near the experimental accuracy, it has to be noted that around 50% from the observed lines were not included in these fits because of the unresolved *A*-*E* splitting. Therefore, another fit using the ERHAM program,<sup>36</sup> which allows proper weighting of blended transitions, was performed in this work. In this way, it was possible to encompass all the measured *a*-type transitions with  $J'' = 3-24$  and  $K_a'' = 0-13$  and *b*-type transitions with  $J'' = 4-35$  and  $K_a'' = 0-5$ . This coverage of the rotational quantum numbers extends well beyond the absorption maximum at 120 K (see Fig. 2), so that the lines most likely to be detected toward the interstellar clouds are now well characterized. Table 1 presents the resulting set of 18 adjusted spectroscopic parameters, while the experimental frequencies are collected in Table 3. Among the floated parameters are rotational constants, centrifugal distortion constants up to the sixth order, internal rotation parameters  $\rho$  and  $\beta$ , and the first energy tunneling parameter  $\epsilon_1$ . Because about 50% of the assigned lines belong to the *b*-type transitions, which were not found in the previous work of Fong et al. (1974),<sup>23</sup> the value of the *A* rotational constant has been significantly improved (see Table 1). The derived spectroscopic constants are in good agreement with those predicted by ab initio calculations.

**Table 1.** Ground-state spectroscopic constants of methoxyamine.

	SPFIT		XIAM	ERHAM	Fong et al. (1974) <sup>23</sup>	Ab initio <sup>d</sup>
	A species <sup>a</sup>	E species <sup>a</sup>	A + E <sup>b</sup>	A + E <sup>c</sup>		
A / MHz	42487.2256 (67) <sup>e</sup>	42485.5971(51)	42 486.1426 (34)	42 486.1402 (30)	42 488 (150)	42 457
B / MHz	10 049.6972 (13)	10 049.6652 (11)	10 051.6212 (33)	10 049.67650 (39)	10 049.59 (3)	10 137
C / MHz	8962.8910 (14)	8962.8895 (12)	8960.9454 (33)	8962.89087 (32)	8962.85 (3)	9038
D <sub>J</sub> / kHz	9.7862 (55)	9.7854 (48)	9.7862 (25)	9.78791 (72)	...	9.72
D <sub>JK</sub> / kHz	3.575 (20)	1.967 (17)	2.492 (10)	2.4821 (46)	...	2.66
D <sub>K</sub> / kHz	471.46 (38)	443.32 (29)	452.94 (18)	452.89 (14)	...	443.97
d <sub>1</sub> / kHz	-1.5834 (15)	-1.5876 (11)	-1.59121 (76)	-1.58560 (41)	...	-1.57
d <sub>2</sub> / kHz	0.33027 (33)	0.33762 (29)	0.33992 (19)	0.33504 (12)	...	0.34
H <sub>J</sub> / Hz	0.0200 (78)	0.0168 (67)	0.0178 (40)	0.02053 (69)	...	...
H <sub>JK</sub> / Hz	-0.163 (35)	-0.132 (26)	-0.155 (17)	-0.1751 (35)	...	...
H <sub>KJ</sub> / Hz	1.88 (88)	-17.77 (70)	-11.23 (43)	-11.001 (27)	...	...
H <sub>K</sub> / Hz	124.4 (92)	-19.9 (73)	32.1(44)	29.4 (23)	...	...
h <sub>1</sub> / Hz	0.0030 (15)	0.0091 (11)	0.00622 (74)	0.00572 (35)	...	...
h <sub>2</sub> / Hz	-0.0039 (11)	-0.00786 (87)	-0.00625 (55)	-0.00571(15)	...	...
h <sub>3</sub> / Hz	-0.00153 (33)	-0.00181 (26)	-0.00191 (17)	-0.001988 (34)	...	...
D <sub>a</sub> / MHz	...	-4.074 (35)	...	...	...	...
D <sub>a</sub> <sup>J</sup> / MHz	...	0.001595 (56)	...	...	...	...
D <sub>a</sub> <sup>k</sup> / MHz	...	0.1711 (27)	...	...	...	...
D <sub>a</sub> <sup>kk</sup> / MHz	...	-0.002096 (61)	...	...	...	...
ρ/Unitless	...	...	0.23864 (19)	0.23869 (15)	...	0.23
β/ <sup>o</sup>	...	...	8.256 (13)	8.322 (12)	...	9.5
ε <sub>1</sub> / MHz	...	...	...	-4.7796 (53)	...	...
V <sub>3</sub> / cm <sup>-1</sup>	...	...	855.66 (52)	...	873 (15) <sup>f</sup>	...
σ <sub>fit</sub> <sup>g</sup> kHz	49	35	33	46	...	...
N <sup>h</sup>	119	108	227	434	4	...

**Notes.** <sup>(a)</sup> These constants are contaminated by contribution of the internal rotation. Unperturbed values that can be compared with those from the global A + E fits or from ab initio calculations can be obtained, for example, using the approximate expression  $(X_A + 2X_E)/3$ <sup>37</sup>(Gordy & Cook 1984), where X substitutes the rotational and centrifugal distortion constants. <sup>(b)</sup> Additionally derived internal rotation parameters: angles between the internal rotation axis *i* and the principal axis  $\angle(i, a) = 31.522 (42)^\circ$ ,  $\angle(i, b) = 58.478 (42)^\circ$ ,  $\angle(i, c) = 90^\circ$  (fixed value), moment of inertia of the methyl top  $I_\alpha = 3.2956 (40) \text{ u}\text{\AA}^2$ . <sup>(c)</sup> Additionally derived internal rotation parameters: torsional energy difference  $\Delta E_{E-A} = 14.339 (16) \text{ MHz}$ ,  $\angle(i, a) = 31.735 (38)^\circ$ ,  $\angle(i, b) = 58.265 (38)^\circ$ ,  $\angle(i, c) = 90^\circ$  (fixed value),  $I_\alpha = 3.3032 (18) \text{ u}\text{\AA}^2$ , reduced rotational constant  $F = 6.5347 (27) \text{ cm}^{-1}$ . <sup>(d)</sup> Equilibrium values at the MP2/aug-cc-pVTZ level of the theory. <sup>(e)</sup> The numbers in parentheses are 1σ uncertainties (67% confidence level) in units of the last decimal digit. <sup>(f)</sup> Average value obtained from three isotopic species. <sup>(g)</sup> Root mean square deviation of the fit. <sup>(h)</sup> Number of distinct frequency-fitted lines.

## 4. RADIOASTRONOMICAL OBSERVATIONS

---

Methoxyamine is a complex organic molecule (COM; carbon- based molecular species with more than six atoms, see, e.g., Herbst & van Dishoeck 2009)<sup>38</sup> containing hydrogen, carbon, oxygen, and nitrogen together. COMs have mostly been detected toward hot cores of high-mass star-forming regions<sup>39,40,41,53</sup> and the inner regions of low-mass protostars, that is, of hot corinos.<sup>42,43</sup> Nevertheless, N-bearing compounds are typically found in the former regions, whereas hot corinos are richer in O-bearing molecules like methyl formate ( $\text{CH}_3\text{OCOH}$ ). Three COMs have been identified in the ISM so far that contain H, C, O, and N:  $\text{NH}_2\text{CHO}$ ,  $\text{CH}_3\text{NCO}$ , and  $\text{CH}_3\text{CONH}_2$  (see, e.g., the CDMS database 1). Although formamide ( $\text{NH}_2\text{CHO}$ ) and methyl isocyanate ( $\text{CH}_3\text{NCO}$ ) have both been detected in hot corinos,<sup>44,45,46</sup> these three species together have only been detected in the hot core of Sgr B2 at the Galactic center<sup>13,47,17,48</sup> and in Orion KL,<sup>49,50,1</sup> the nearest hot core at  $414 \pm 7$  pc.<sup>51</sup> In addition,  $\text{CH}_3\text{NHCHO}$  has recently been tentatively detected in Sgr B2.<sup>48</sup> On the other hand, another possible related species of methoxyamine, methylamine  $\text{CH}_3\text{NH}_2$ , has been detected in the two high-mass star-forming regions mentioned above.<sup>14,1</sup> Therefore, we focused the search for  $\text{CH}_3\text{ONH}_2$  toward these high-mass star-forming regions.

Orion KL: two sets of data were used to seek for methoxyamine in this region. On the one hand, we explored the wide frequency band (80–306 GHz) of the IRAM 30 m survey of Orion KL.<sup>52,53</sup> On the other hand, we focused the search on different positions of this complex source using the ALMA Science Verification (SV) data that cover frequencies between 213.7 and 246.6 GHz. Cernicharo et al. (2016)<sup>1</sup> provided the spatial distribution of several molecular species in the source. The rather similar spatial distribution of the three more abundant species containing N, O, H, and C simultaneously is remarkable:  $\text{HNCO}$ ,  $\text{NH}_2\text{CHO}$ , and  $\text{CH}_3\text{NCO}$ . Moreover, these authors provided column densities for  $\text{CH}_3\text{NH}_2$  and  $\text{CH}_3\text{CONH}_2$ . To determine the suitable position within the source for the search for methoxyamine, we created maps of the spatial distribution of methylamine using two lines that were free of blending that arise in the ALMA SV band (see Fig. 4). Unfortunately, this was not possible for acetamide,  $\text{CH}_3\text{CONH}_2$ , because of the large uncertainty of the rest

frequencies at the ALMA SV frequency range (see Halfen et al. 2011,<sup>54</sup> and references therein).

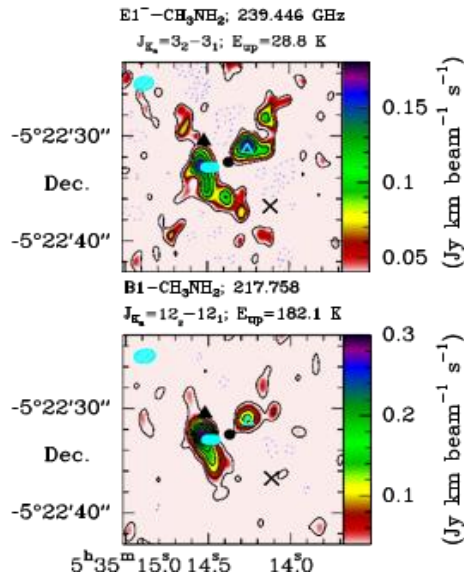


**Figure 4.** Spatial distribution of CH<sub>3</sub>NH<sub>2</sub> in Orion KL. The data are from ALMA SV observations. The interval of contours in black is 0.03 Jy beam<sup>-1</sup> km s<sup>-1</sup>, and the minimum contour is 0.03 Jy beam<sup>-1</sup> km s<sup>-1</sup>. Negative flux is represented by the blue dashed contours: the minimum contour is -0.05 Jy beam<sup>-1</sup> km s<sup>-1</sup> and the interval is -0.03 Jy beam<sup>-1</sup> km s<sup>-1</sup>. The cyan ellipse in the top left corner of the maps represents the synthetic beam. The black triangle shows source l, the black circle shows source n, the cross represents the compact ridge, and the cyan unfilled square and triangle indicate Positions A and B (see Sect. 4).

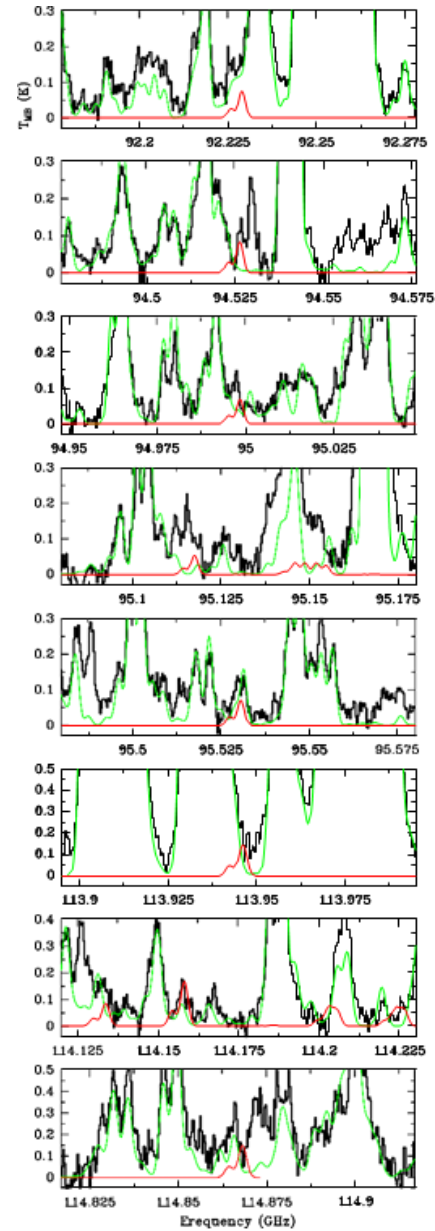


**Figure 5.** Lines partially free of blending of CH<sub>3</sub>ONH<sub>2</sub> in Sgr B2 (N) at 3 mm. The observed data (black histogram spectrum) and total model of the source (green curve) are taken from Belloche et al. (2013)<sup>2</sup>. The synthetic spectrum for methoxyamine corresponding to the upper limit reported in Table 2 is given by the red line. A  $v_{\text{LSR}}$  of +64.0 km s<sup>-1</sup> is assumed.

The main emission peaks for all the species discussed above coincide with a component in the middle of the hot core clumpy structure<sup>55</sup> and the millimeter continuum source MM4<sup>56</sup>. These positions are described in Cernicharo et al. (2016)<sup>1</sup> as positions A and B. We therefore concentrated on these two components and on the compact ridge (rich in CH<sub>3</sub>-O bearing molecules, see, e.g., Favre et al. 2011a<sup>57</sup>; Brouillet et al. 2013<sup>58</sup>; López et al., in prep.). We used MADEX<sup>59</sup> to implement the spectroscopy of CH<sub>3</sub>ONH<sub>2</sub> provided in the Col. 4 of Table 1 and to derive the synthetic spectrum according to the physical parameters shown in Table 2. We did not detect methoxyamine above the detection limit of the data, hence only upper limits to the column density could be derived.

Sgr B2: we also searched for CH<sub>3</sub>ONH<sub>2</sub> in public data available for Sgr B2. We did not find this species above the detection limit of the data, either in the PRIMOS survey<sup>60</sup> or in the IRAM 30 m data at 3 mm provided by Belloche et al. (2013)<sup>2</sup>. To estimate upper limits to the CH<sub>3</sub>ONH<sub>2</sub> column density in the region, we adopted the physical parameters derived by Belloche et al. (2013)<sup>2</sup> for formamide (see Table 2). Figure 5 shows the model provided by MADEX (red line) together with the IRAM 30 m data Sgr B2(N). Interestingly, this model is consistent with the lack of methoxyamine lines above the detection limit of the PRIMOS data.

Although we cannot claim detection, some U lines that are partially free of blending in the 30 m data agree with the modeled spectrum of this species. In addition, according to this model, we did not find missing lines. Nevertheless, this is not a strong constraint

because most of the  $\text{CH}_3\text{ONH}_2$  lines are fully blended with more abundant species in these data.

Finally, we used the data presented in Cernicharo et al. (2012)<sup>61</sup> to derived upper limits to the methoxyamine column density in dark clouds and at different evolutionary stages (B1-b and TMC-1 clouds; see Table 2).

**Table 2.** Physical parameters of the considered cloud cores.

Source	Coordinates J2000.0	HPBW <sup>†</sup> ( $''$ )	Frequencies <sup>††</sup> GHz	$v_{\text{LSR}}$ ( $\text{km s}^{-1}$ )	$\Delta v_{\text{FWHM}}$ ( $\text{km s}^{-1}$ )	$d_{\text{sou}}$ ( $''$ )	$T_{\text{rot}}$ (K)	$N(\text{CH}_3\text{ONH}_2)$ $\times 10^{15} (\text{cm}^{-2})$
Orion KL (IRAM 30 m)	$\alpha = 5^{\text{h}}35^{\text{m}}14^{\text{s}}.5$ $\delta = -05^{\circ}22'30.''0$	30–8	80–307	8.0	3.0	10	150	$\leq (1.0 \pm 0.3)$
Orion KL (ALMASV) Hot core	$\alpha = 05^{\text{h}}35^{\text{m}}14^{\text{s}}.5$ $\delta = -05^{\circ}22'32.''5$	$\sim 1.9 \times 1.4$	213.7–246.7	8.0	3.0	3.0	150	$\leq (3.0 \pm 1.0)$
Orion KL (ALMASV) Compact ridge	$\alpha = 05^{\text{h}}35^{\text{m}}14^{\text{s}}.1$ $\delta = -05^{\circ}22'36.''9$	$\sim 1.9 \times 1.4$	213.7–246.7	7.5	2.0	3.0	100	$\leq (2.0 \pm 0.6)$
Orion KL (ALMASV) MM4	$\alpha = 05^{\text{h}}35^{\text{m}}14^{\text{s}}.2$ $\delta = -05^{\circ}22'31.''1$	$\sim 1.9 \times 1.4$	213.7–246.7	8.0 5.0	3.0 3.0	3.0 3.0	150 150	$\leq (2.0 \pm 0.6)$
Sgr B2	(IRAM 30 m) $\alpha = 17^{\text{h}}47^{\text{m}}20^{\text{s}}.0$ $\delta = -28^{\circ}22'19.''0$	30–21	80–115.5	63	7.0	2.4	180	$\leq (1000 \pm 60)$
	$\alpha = 17^{\text{h}}47^{\text{m}}19^{\text{s}}.8$ $\delta = -28^{\circ}22'17.''0$	80–15	7–50	73	7.0	1.4	180	$\leq (1000 \pm 60)$
				83	8.0	60	2.7	$\leq (1000 \pm 60)$
B1-b (IRAM 30 m)	$\alpha = 03^{\text{h}}33^{\text{m}}20^{\text{s}}.8$ $\delta = 31^{\circ}07'34.''0$	30–21	80–115.5	6.7	0.7	60	12	$\leq (0.0020 \pm 0.0006)$
TMC-1 (IRAM 30 m)	$\alpha = 04^{\text{h}}41^{\text{m}}41^{\text{s}}.88$ $\delta = 25^{\circ}41'27.''0$	30–21	80–115.5	6.0	0.7	60	10	$\leq (0.0020 \pm 0.0006)$

**Notes.** <sup>(†)</sup> Half-power beam width (HPBW) for observations with single-dish telescopes (IRAM 30 m and GBT 100 m) and synthetic beam for the ALMA SV observations. <sup>(††)</sup> Range of frequencies considered in the analysis.

## 5. DISCUSSION

To compare the results for the search for methoxyamine to the chemical model predictions provided by Garrod et al. (2008)<sup>20</sup>, we derived upper limits to the molecular abundance of this species in the hot core of Orion KL and Sgr B2(N). Tercero et al. (2010)<sup>52</sup>

obtained a source-averaged  $N(\text{H}_2)$  of  $4.2 \times 10^{23} \text{ cm}^{-2}$  for the hot core of Orion KL by means of the  $\text{C}^{18}\text{O}$  column density, assuming that the  $\text{CO}/\text{H}_2$  abundance ratio is roughly constant ( $2 \times 10^{-4}$  in warm regions) and adopting a source diameter of  $10''$  for the hot core. To obtain a value for the molecular abundance, we also have to assume that the  $\text{H}_2$  column density spatially coincides with the emission from the species considered. We derived an upper limit to the  $\text{CH}_3\text{ONH}_2$  abundance of  $2 \times 10^{-9}$  using the upper limit for the column density obtained for Orion KL with the IRAM 30 m data. A large uncertainty should be associated with this value (at least a factor of 2) because of the mentioned assumptions.

On the other hand, Belloche et al. (2008)<sup>18</sup> derived an  $N(\text{H}_2)$  of  $1.3 \times 10^{25} \text{ cm}^{-2}$  in the inner region ( $2''$ ) of Sgr B2(N) using the continuum emission detected with the Plateau de Bure Interferometer (PdBI) and assuming that this continuum emission at 3.7 mm is dominated by thermal dust emission (optically thin and a dust temperature of 100 K). Further assumptions related to the dust mass opacity and the dust emissivity exponent have to be made to obtain this  $N(\text{H}_2)$  value (see Belloche et al. 2008<sup>18</sup>, for details). We derive an upper limit to the  $\text{CH}_3\text{ONH}_2$  abundance of  $(7-8) \times 10^{-8}$  using the upper limit for the column density obtained for the  $63 \text{ km s}^{-1}$  component of Sgr B2(N). Once again, an uncertainty of at least a factor of 2 is associated with this value<sup>18</sup>.

Like Garrod et al. (2008)<sup>20</sup>, we note a reasonable match in the comparison of the derived upper limit abundances (and the assumed rotational temperatures) and the results of the “reduced ice composition” chemical model provided by these authors. In this model, the initial ice composition (standard) was adjusted to agree with infrared observations of protostellar envelopes, reducing the amount of the ices available for primary-radical production<sup>20</sup>. Abundances of methoxyamine in the fast ( $5 \times 10^4 \text{ yr}$ ) and slow ( $1 \times 10^6 \text{ yr}$ ) warm-up timescales are  $3.7 \times 10^{-9}$  and  $6.4 \times 10^{-8}$ , respectively (the rotational temperature derived is around 120 K in both models). These timescales are identified with high- and low-mass star formation, respectively<sup>20</sup>. It is worth noting that Aikawa et al. (2008)<sup>62</sup> proposed a different relation between mass and warm-up timescale. They



suggested that the warm-up timescale is dependent on the ratio of the size of the warm region to the infall speed, rather than on the overall speed of star formation. The abundances predicted by the model are on the same order (within the uncertainties) as the upper limits derived observationally. However, because we study two high-mass star-forming regions, these differences may indicate different initial ice compositions and/or evolutionary stages.

To check these results and to avoid the large uncertainties introduced by the estimation of the  $\text{CH}_3\text{ONH}_2$  abundances, we also compared the observed and predicted  $\text{NH}_2\text{CHO}/\text{CH}_3\text{ONH}_2$  abundance ratios. The  $\text{NH}_2\text{CHO}$  column density has been derived by Motiyenko et al. (2012)<sup>50</sup> and Belloche et al. (2013)<sup>2</sup> for Orion KL and Sgr B2, respectively, using similar physical parameters and the same observational data (IRAM 30 m data) as those used in this work to derive the  $\text{CH}_3\text{ONH}_2$  column density. The derived lower limit ratios are  $\geq 0.6$  and  $\geq 1.35$  for Orion KL and the  $63 \text{ km s}^{-1}$  component of Sgr B2. The predicted results provided by the “reduced ice composition” chemical model of Garrod et al. (2008)<sup>20</sup> are 27, 12, and 2 for the fast, medium, and slow warm-up timescales. The predictions of all three models are consistent with the derived lower limit ratios. Hence, by means of these ratios and according to this model, we cannot constraint the relation between mass and warm-up timescale.

## 6. CONCLUSION

---

The rotational spectrum of methoxyamine has been recorded from 75 to 480 GHz and over 400 lines were newly assigned for the most stable conformer. Methoxyamine has not been identified above the detection limit of various sets of data of the well-known high-mass star-forming regions Orion KL and Sgr B2. Nevertheless, the upper limits to the methoxyamine abundance in these regions agree with the  $\text{CH}_3\text{ONH}_2$  abundances derived in chemical models. This suggests a possible positive detection of methoxyamine in the near

future using high-sensitivity data of hot cores and hot corinos and the accurate spectroscopic data of this work.

\* Table 3 is only available at the CDS via anonymous ftp to [cdsarc.u-strasbg.fr](ftp://cdsarc.u-strasbg.fr) (130.79.128.5) or via <http://cdsarc.u-strasbg.fr/viz-bin/qcat?J/A+A/609/A24>

## 7. REFERENCES

---

- <sup>1</sup> Cernicharo, J., Kisiel, Z., Tercero, B., et al. 2016, *A&A*, 587, L4
- <sup>2</sup> Belloche, A., Müller, H. S. P., Menten, K. M., Schilke, P., & Comito, C. 2013, *A&A*, 559, A47
- <sup>3</sup> Kuan, Y.-J., Charnley, S. B., Huang, H.-C., Tseng, W.-L., & Kisiel, Z. 2003, *ApJ*, 593, 848
- <sup>4</sup> Snyder, L. E., Lovas, F. J., Hollis, J. M., et al. 2005, *ApJ*, 619, 914
- <sup>5</sup> Jones, P. A., Cunningham, M. R., Godfrey, P. D., & Cragg, D. M. 2007, *MNRAS*, 374, 579
- <sup>6</sup> Cunningham, M. R., Jones, P. A., Godfrey, P. D., et al. 2007, *MNRAS*, 376, 1201
- <sup>7</sup> Elsila, J. E., Glavin, D. P., & Dworkin, J. P. 2009, *Meteor. Planet. Sci.*, 44, 1323
- <sup>8</sup> Altwegg, K., Balsiger, H., Bar-Nun, A., et al. 2016, *Sci. Adv.*, 2
- <sup>9</sup> Bernstein, M. P., Dworkin, J. P., Sandford, S. A., Cooper, G. W., & Allamandola, L. J. 2002, *Nature*, 416, 401
- <sup>10</sup> Caro, G. M., Meierhenrich, U., Schutte, W., et al. 2002, *Nature*, 416, 403
- <sup>11</sup> Zheng, W., & Kaiser, R. I. 2010, *J. Phys. Chem. A*, 114, 5251
- <sup>12</sup> Kim, Y. S., & Kaiser, R. I. 2011, *ApJ*, 729, 68
- <sup>13</sup> Rubin, R., G. W. Swenson, J., Benson, R., Tigelaar, H., & Flygare, W. 1971, *ApJ*, 169, L39
- <sup>14</sup> Kaifu, N., Morimoto, M., Nagane, K., et al. 1974, *ApJ*, 191, L135
- <sup>15</sup> Fourikis, N., Takagi, K., & Morimoto, M. 1974, *ApJ*, 191, L139
- <sup>16</sup> Turner, B., Liszt, H., Kaifu, N., & Kisliakov, A. 1975, *ApJ*, 201, L149
- <sup>17</sup> Hollis, J. M., Lovas, F. J., Remijan, A. J., et al. 2006, *ApJ*, 643, L25
- <sup>18</sup> Belloche, A., Menten, K. M., Comito, C., et al. 2008, *A&A*, 482, 179
- <sup>19</sup> Remijan, A. J., Snyder, L. E., McGuire, B. A., et al. 2014, *ApJ*, 783, 77
- <sup>20</sup> Garrod, R. T., Weaver, S. L. W., & Herbst, E. 2008, *ApJ*, 682, 283
- <sup>21</sup> Pulliam, R. L., McGuire, B. A., & Remijan, A. J. 2012, *ApJ*, 751, 1
- <sup>22</sup> McGuire, B. A., Carroll, P. B., Dollhopf, N. M., et al. 2015, *ApJ*, 812, 76
- <sup>23</sup> Fong, M. Y., Johnson, L. J., & Harmony, M. D. 1974, *J. Mol. Spectr.*, 53, 45
- <sup>24</sup> Bissot, T. C., Parry, R. W., & Campbell, D. H. 1957, *J. Am. Chem. Soc.*, 79, 796
- <sup>25</sup> Daly, A., Kolesniková, L., Mata, S., & Alonso, J. 2014, *J. Mol. Spectr.*, 306, 11
- <sup>26</sup> Frisch, M. J., Trucks, G. W., Schlegel, H. B., et al. 2009, Gaussian 09 Revision E.01 (Wallingford CT: Gaussian Inc.)
- <sup>27</sup> Hays, B. M., & Widicus Weaver, S. L. 2013, *J. Phys. Chem. A*, 117, 7142
- <sup>28</sup> Woods, R. 1966, *J. Mol. Spectr.*, 21, 4
- <sup>29</sup> Herschbach, D. R., & Swalen, J. D. 1958, *J. Chem. Phys.*, 29, 761
- <sup>30</sup> Plummer, G. M., Herbst, E., & De Lucia, F. C. 1987, *ApJ*, 318, 873
- <sup>31</sup> Pickett, H. M. 1991, *J. Mol. Spectr.*, 148, 371
- <sup>32</sup> Watson, J. K. G. 1977, in *Vibrational Spectra and Structure*, ed. J. R. Durig (Amsterdam: Elsevier), 6, 1
- <sup>33</sup> Lin, C. C., & Swalen, J. D. 1959, *Rev. Mod. Phys.*, 31, 841
- <sup>34</sup> Demaison, J., Margulès, L., Kleiner, I., & Császár, A. 2010, *J. Mol. Spectr.*, 259, 70
- <sup>35</sup> Hartwig, H., & Dreizler, H. 1996, *Z. Naturforsch. A*, 51, 923
- <sup>36</sup> Groner, P. 1997, *J. Chem. Phys.*, 107, 4483
- <sup>37</sup> Gordy, W., & Cook, R. L. 1984, *Microwave molecular spectra* (New York: Wiley Interscience)
- <sup>38</sup> Herbst, E., & van Dishoeck, E. F. 2009, *Ann. Rev. Astron. Astr.*, 47, 427
- <sup>39</sup> Belloche, A., Garrod, R. T., Müller, H. S. P., et al. 2009, *A&A*, 499, 215

- 
- <sup>40</sup> Belloche, A., Garrod, R. T., Müller, H. S. P., & Menten, K. M. 2014, *Science*, 345, 1584
- <sup>41</sup> Tercero, B., Kleiner, I., Cernicharo, J., et al. 2013, *ApJ*, 770, L13
- <sup>42</sup> Cazaux, S., Tielens, A. G. G. M., Ceccarelli, C., et al. 2003, *ApJ*, 593, L51
- <sup>43</sup> Jørgensen, J. K., van der Wiel, M. H. D., Coutens, A., et al. 2016, *A&A*, 595, A117
- <sup>44</sup> Martín-Doménech, R., Rivilla, V. M., Jiménez-Serra, I., et al. 2017, *MNRAS*, 469, 2230
- <sup>45</sup> Ligterink, N. F. W., Coutens, A., Kofman, V., et al. 2017, *MNRAS*, 469, 2219
- <sup>46</sup> Coutens, A., Jørgensen, J. K., van derWiel, M. H. D., et al. 2016, *A&A*, 590, L6
- <sup>47</sup> Halfen, D. T., Ilyushin, V. V., & Ziurys, L. M. 2015, *ApJ*, 812,
- <sup>48</sup> Belloche, A., Meshcheryakov, A. A., Garrod, R. T., et al. 2017, *A&A*, 601, A49
- <sup>49</sup> Turner, B. E. 1991, *ApJS*, 76, 617
- <sup>50</sup> Motiyenko, R. A., Tercero, B., Cernicharo, J., & Margulès, L. 2012, *A&A*, 548, A71
- <sup>51</sup> Menten, K. M., Reid, M. J., Forbrich, J., & Brunthaler, A. 2007, *A&A*, 474, 515
- <sup>52</sup> Tercero, B., Cernicharo, J., Pardo, J. R., & Goicoechea, J. R. 2010, *A&A*, 517, A96
- <sup>53</sup> Tercero, B., Cernicharo, J., López, A., et al. 2015, *A&A*, 582, L1
- <sup>54</sup> Halfen, D. T., Ilyushin, V., & Ziurys, L. M. 2011, *ApJ*, 743, 60
- <sup>55</sup> Favre, C., Wootten, H. A., Remijan, A. J., et al. 2011b, *ApJ*, 739, L12
- <sup>56</sup> Wu, Y., Liu, T., & Qin, S.-L. 2014, *ApJ*, 791, 123
- <sup>57</sup> Favre, C., Despois, D., Brouillet, N., et al. 2011a, *A&A*, 532, A32
- <sup>58</sup> Brouillet, N., Despois, D., Baudry, A., et al. 2013, *A&A*, 550, A46
- <sup>59</sup> Cernicharo, J. 2012, in *ECLA-2011: Proc. of the European Conf. on Laboratory Astrophysics, Laboratory Astrophysics and Astrochemistry in the Herschel/ALMA Era*, 58, 251
- <sup>60</sup> Neill, J. L., Muckle, M. T., Zaleski, D. P., et al. 2012, *ApJ*, 755, 153
- <sup>61</sup> Cernicharo, J., Marcelino, N., Roue, E., et al. 2012, *ApJ*, 759, L43
- <sup>62</sup> Aikawa, Y., Wakelam, V., Garrod, R. T., & Herbst, E. 2008, *ApJ*, 674, 984



## CHAPTER IX.

# Laboratory millimeter wave spectrum of N-methylhydroxylamine

---

*Adapted from: Journal of Molecular Spectroscopy, 335 (2017) 54–60*

*The pure rotational spectrum of N-methylhydroxylamine (CH<sub>3</sub>NHOH), a potential candidate in the interstellar medium, has been studied in the millimeter-wave region up to 360 GHz. The molecule was liberated from its hydrochloride salt and the ground and six lowest excited vibrational states of the most stable trans conformation as well as the <sup>13</sup>C isotopologue in natural abundance have been measured and analyzed. From the observed ground state A–E splittings, a barrier hindering the methyl internal rotation  $V_3 = 1245.8 (46) \text{ cm}^{-1}$  has been derived. The sub-Doppler Lamb-dip technique has been employed to resolve the <sup>14</sup>N hyperfine structure of strong transitions. The spectroscopic constants reported in the present study should constitute a solid set of laboratory data to support future searches of N-methylhydroxylamine in the interstellar medium.*

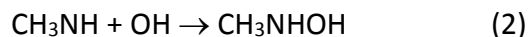
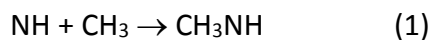


## 1. INTRODUCTION

---

Ever since the first polyatomic molecule, ammonia,<sup>1</sup> has been detected in the interstellar medium passed almost five decades and to date over 190 molecules have been unambiguously identified in the interstellar clouds or circumstellar envelopes<sup>2</sup> due to the ongoing astronomical observations complemented with elaborated laboratory studies. Many of these molecules are organic in nature and are found especially in the hot cores<sup>3-5</sup> (e.g. Sgr B2(N), Sgr B2(M), Orion KL, W51), i.e. in the regions of prolific star formation with temperatures higher than 100 K. More species are expected to be detected especially thanks to currently working ALMA interferometer that offer to astronomers orders of magnitude better resolution and excellent sensitivity in comparison with single-dish telescopes and opens more possibilities towards detections of molecules in smaller abundances than before. This vast amount of data prompts laboratory spectroscopists to record and analyze rotational spectra of potential interstellar molecules and to fulfill the first requirement for an unequivocal identification of new molecules in space, i.e. the availability of transition frequencies with high accuracy in a large spectral range.

N-methylhydroxylamine, CH<sub>3</sub>NHOH (NMH from now), is a derivative of interstellar methylamine, where one hydrogen from the amino group is substituted by the hydroxyl group. It is an isomeric form of aminomethanol (CH<sub>2</sub>(OH)NH<sub>2</sub>) and methoxyamine (CH<sub>3</sub>ONH<sub>2</sub>), which are predicted to occur with significant abundances in hot cores or corinos.<sup>6</sup> Although the chemistry of such regions is far from understood and NMH is not included directly into the modern chemical models of the star-forming regions,<sup>6,7</sup> a plausible formation pathway could be



where NH, CH<sub>3</sub>, and OH are primary grain-surface radicals formed by the cosmic-ray photodissociation of NH<sub>3</sub>, CH<sub>3</sub>OH, and H<sub>2</sub>O, respectively, which are present in the ice mantles

covering the interstellar grains.<sup>6</sup> Gradual heating of the grains during the star formation process makes the above radicals being mobile and may undergo association reactions to form more complex molecules, among them N-methylhydroxylamine. It could remain in the grain mantles and be evaporated when the temperature rises again. NMH may be thus considered as a potential candidate for observations in the interstellar medium and could be probed by millimeter and submillimeter wave astronomy. The previous microwave information provided by Sung and Harmony<sup>8</sup> up to 40 GHz is not, however, sufficient for an astrophysical investigation due to usual extrapolation problems outside the experimentally known data region.

In the present work, the millimeter wave spectrum of NMH has been studied up to 360 GHz to provide laboratory reference spectra that are needed to compare directly against the observational data. More than 2000 new rotational lines belonging to the ground vibrational state, six vibrationally excited states and the <sup>13</sup>C isotopologue in natural abundance (1.1%) have been assigned and measured. Moreover, a detailed analysis of the observed A–E splitting due to the coupling between the methyl torsion and overall rotation allowed the determination of the barrier to internal rotation of the methyl group. These results should provide sufficiently precise laboratory information for future search of NMH in the interstellar medium.

## 2. EXPERIMENTAL DETAILS

---

NMH is commercially available in its hydrochloride salt and was chemically liberated by reaction with 1,8-diazabicyclo[5.4.0] undec-7-ene and collected in a U-tube liquid nitrogen trap directly connected to the free-space cell of the spectrometer. The room temperature millimeter-wave spectrum was recorded at sample pressure of about 20 lbar employing the frequency-modulated spectrometer at the University of Valladolid described in detail elsewhere<sup>10</sup>. The millimeter wave region from 126 to 360 GHz was reached by active multiplier chains (WR6.5, WR9.0, VDI, Inc) additional frequency doubler and tripler (WR4.3, WR2.8, VDI, Inc.). All spectra were recorded in 1 GHz scans using the frequency modulation technique with



2f lock-in detection, where  $f=10.2$  kHz is the modulation frequency, and modulation depth of 30 kHz. Frequency accuracy of well-resolved lines was estimated to be better than 50 kHz. To record the spectrum at sub-Doppler resolution, the Lamb dip technique was used.<sup>11</sup> These measurements were performed using a free-space cell with a doubled-radiation path arrangement in order to increase both the sensitivity of the spectrometer as well as the Lamb-dip effect. Lower values of pressure and modulation depth were chosen to minimize the dip widths as much as possible and in this way to improve the resolution. Fig. 3d provides a typical example for the recorded spectra and demonstrates how the resolution is improved with the Lamb-dip technique.

### 3. ROTATIONAL SPECTRA ANALYSIS

#### 3.1. Ground state rotational spectra

NMH is a relatively small eight-atomic molecule that can present two stable configurations: *cis* and *trans* that differ by the value of the dihedral angles  $\tau$  (C-N-O-H). The *cis* conformer is predicted to be about  $1500\text{ cm}^{-1}$  higher in energy.<sup>12</sup> Only the *trans* conformer ( $\tau\approx 234^\circ$ ) shown in Fig. 1 was observed in the previous microwave work.<sup>8</sup> This is a near prolate asymmetric top with dipole moment components  $|\mu_a| = 0.611\text{ D}$  and  $|\mu_b| = 0.366\text{ D}$  along the a- and b-inertial axis. The millimeter wave spectrum is dominated by groups of a-type R-branch transitions separated by  $B + C$  value and weaker b-type R- and Q-branch lines which were easily identified based on predictions using the previous microwave spectroscopic constants from Sung and Harmony.<sup>8</sup>

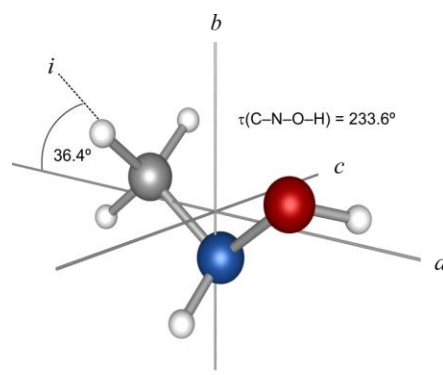


**Figure 1.** The *trans* conformation of N-methylhydroxylamine (NMH) depicted in the principal inertial axes system.

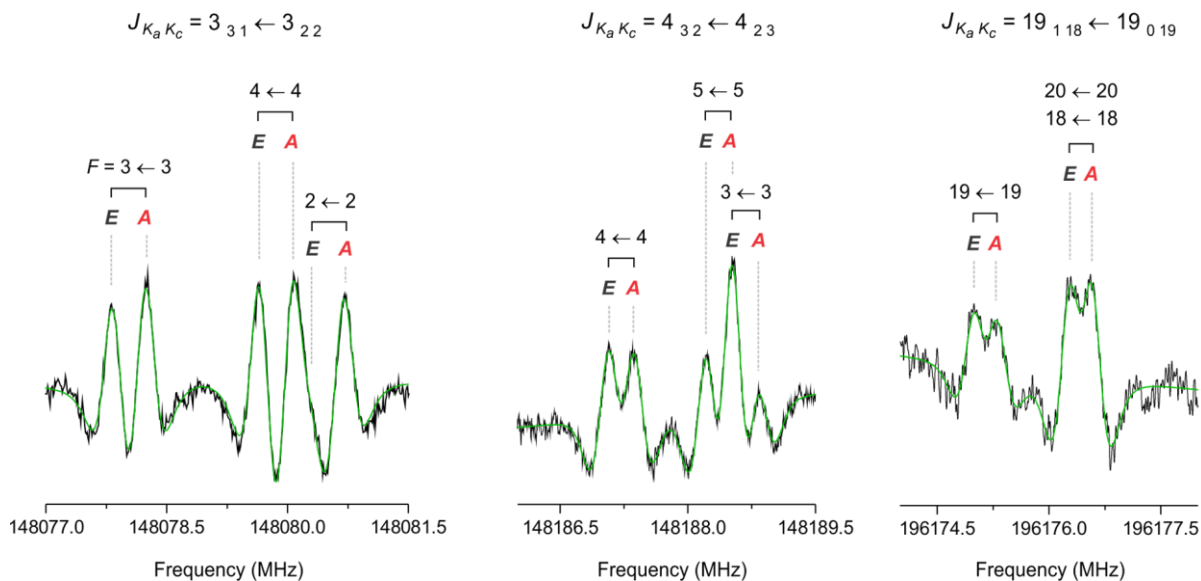


**Figure 2.** Some of the observed internal rotation A-E doublets in the ground vibrational state of N-methylhydroxylamine.

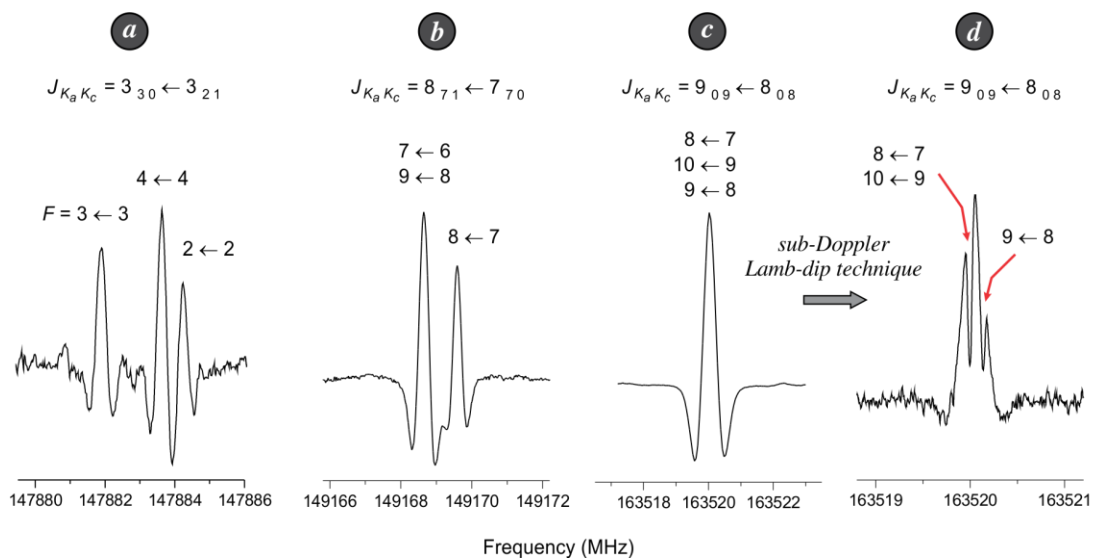


**Figure 3.** Examples of  $^{14}\text{N}$  hyperfine structures observed in the millimeter wave spectrum of N-methylhydroxylamine.

Many of the identified transitions were found split due to the nuclear quadrupole hyperfine interactions resulting from the presence of  $^{14}\text{N}$  nucleus with nuclear spin  $I_N = 1$ . For low J, b-type Q-branch transitions (see Fig. 2a), three  $\Delta F = \Delta J$  hyperfine components could be resolved

and assigned. For high  $J$ , a-type R-branch transitions, the  $F = J \pm 1$  components appeared overlapped while the  $F = J$  component could be fully or partly resolved (see Fig. 2b).

**Table 1.** Spectroscopic constants for the parent and the  $^{13}\text{C}$  isotopologue of N-methylhydroxylamine in its ground vibrational state.

Constant	Unit	Parent species	$^{13}\text{C}$ species
$A$	(MHz)	38930.75315 (58) <sup>a</sup>	38722.060 (21)
$B$	(MHz)	9939.618070 (99)	9665.5215 (11)
$C$	(MHz)	8690.696846 (90)	8470.2947 (10)
$\Delta J$	(kHz)	9.97346 (29)	9.5125 (10)
$\Delta_{JK}$	(kHz)	-30.8957 (13)	-31.1552 (52)
$\Delta_K$	(kHz)	379.356 (38)	360.9 (61)
$\delta J$	(kHz)	1.966429 (39)	1.8489 (10)
$\delta_K$	(kHz)	4.8354 (28)	4.8354 <sup>b</sup>
$\Phi_J$	(mHz)	14.28 (21)	14.28 <sup>b</sup>
$\Phi_{JK}$	(mHz)	-75.90 (93)	-75.90 <sup>b</sup>
$\Phi_{KJ}$	(Hz)	-2.3091 (77)	-2.3091 <sup>b</sup>
$\Phi_K$	(Hz)	10.89 (63)	10.89 <sup>b</sup>
$\phi_J$	(mHz)	5.987 (26)	5.987 <sup>b</sup>
$\phi_{JK}$	(mHz)	164.3 (25)	164.3 <sup>b</sup>
$\chi_{aa}$	(MHz)	4.3446 (92)	... <sup>c</sup>
$\chi_{bb}$	(MHz)	0.7123 (76)	... <sup>c</sup>
$\chi_{cc}$	(MHz)	-5.0569 (69)	... <sup>c</sup>
$J_{\min}/J_{\max}^d$		0/47	1/20
$K_{a, \min}/K_{a, \max}^d$		0/16	0/12
$N_{\text{lines}}^e$		597	92
$\sigma_{\text{fit}}^f$	(MHz)	0.021	0.032

<sup>a</sup> The numbers in parentheses are  $1\sigma$  uncertainties in units of the last decimal digit. <sup>b</sup> Fixed to the parent species value. <sup>c</sup> Hyperfine transitions too weak to be analyzed. <sup>d</sup> Minimum/maximum quantum number value included in the fit. <sup>e</sup> Number of distinct frequency lines in the fit. <sup>f</sup> Root mean square deviation of the fit. Different weights  $w_i = 1/\sigma_i^2$  were applied to various data sets in order to take into consideration the differences in measurement accuracies:  $\sigma_i = 15$  kHz was assigned to the data measured by the Lamb-dip technique,  $\sigma_i = 25$  kHz was estimated for transitions numerically treated by the above mentioned procedure,  $\sigma_i = 50$  kHz was given to the transitions from the previous work, and  $\sigma_i = 100$  kHz to the lines with unresolved hyperfine structure.

In the case of strong a-type R-branch transitions with unresolved hyperfine structure (see Fig. 2c) the sub-Doppler Lamb-dip technique was used to resolve the nuclear hyperfine structure (see Fig. 2c and d for the  $9_{09} \leftarrow 8_{08}$  transition). Partially resolved hyperfine features

were subjected to the numerical treatment where the overall line shapes were fitted to the sums of the second derivatives of the Voigt profile functions.<sup>13</sup> Over 200 distinct frequency hyperfine components and more than 300 hyperfine unresolved lines were assigned and measured for the ground vibrational state. A global fit, including the 25 hyperfine transitions from the microwave study,<sup>8</sup> was carried out using the effective Hamiltonian  $H = H_R + H_Q$  (A-reduction, I<sup>r</sup>-representation) in the SPFIT/SPCAT programs,<sup>14</sup> where  $H_R$  is the standard Watson's asymmetric semirigid-rotor Hamiltonian<sup>15</sup> up to the sixth order terms and  $H_Q$  is the nuclear quadrupole coupling Hamiltonian.<sup>16</sup> The coupling scheme  $F=J+I_N$  between the rotational angular momentum  $J$  and the <sup>14</sup>N nuclear spin angular momentum  $I_N$  was used. The rotational constants, quartic and sextic centrifugal distortion constants along with the diagonal elements of the nuclear quadrupole coupling tensor ( $\chi_{aa}$ ,  $\chi_{bb}$ ,  $\chi_{cc}$ ) determined in the fit are listed in Table 1.

The excellent signal to noise ratio observed for the parent species enabled to observe the <sup>13</sup>C isotopologue in natural abundance. Up to 92 unsplit a-type R-branch transitions were assigned and combined with 3 a-type and 3 b-type hyperfine-free transitions from the microwave study.<sup>8</sup> They were analyzed using the Watson's asymmetric semirigid-rotor Hamiltonian up to the sixth order terms. The final set of the spectroscopic constants is given in the second column of Table 1. All measured transitions are collected in Tables S1 and S2 of the supplementary content.

No evidence of the methyl top internal rotation splitting was found in the previous microwave study<sup>8</sup> and authors determined an internal rotation barrier of  $V_3 = 1243$  (12)  $\text{cm}^{-1}$  from the A–E splittings observed in the first excited state of the methyl torsion. On this basis, after detailed spectroscopic searches, A–E doublets attributable to internal rotation were found for few b-type Q-branch transitions with well resolved <sup>14</sup>N nuclear hyperfine structure (see Fig. 3). XIAM<sup>17</sup> program was used to fit the observed A–E splittings yielding to a barrier height of  $V_3 = 1245.8$  (46)  $\text{cm}^{-1}$  in the ground vibrational state. The internal rotation parameters are shown in the first column of Table 2.

**Table 2.** Internal rotation parameters of NMH

Parameter	G.S.	$\nu_{18} = 1$	$\nu_{18} = 2$
$V_3^a / \text{cm}^{-1}$	1245.8 (46)	1251.96 (34)	1271.9 (28)
$s^b$	85.9	86.5	86.8
$I_\alpha^c / \text{amu } \text{Å}^2$	3.195 <sup>e</sup>	3.23302 (79)	3.1814 (97)
$\angle(i, a)^{d/o}$	36.4 <sup>f</sup>	34.297 (21)	34.526 (67)
$\angle(i, b)^{d/o}$	53.6 <sup>f</sup>	55.857 (21)	55.509 (74)
$\angle(i, c)^{d/o}$	87.0 <sup>f</sup>	87.0 <sup>f</sup>	88.62 (14)

<sup>a</sup> Barrier height to the methyl group internal rotation. <sup>b</sup> Reduced barrier height  $s=4V_3/9F$  where  $F$  is the reduced rotational constant of the internal rotor. <sup>c</sup> Moment of inertia of the methyl top. <sup>d</sup>Angles between the internal rotor axis  $i$  and the principal axis  $a, b, c$ . <sup>e</sup>Assumed value. <sup>f</sup>Fixed to the value obtained from direction cosines of the internal rotor to the principal axis  $\lambda_a = 0.8042$ ,  $\lambda_b = 0.592$ , and  $\lambda_c = 0.0531$ .<sup>8</sup>

### 3.2. Rotational spectra in vibrationally excited states

Around each ground state line, many satellite lines attributable to pure rotational transitions in excited vibrational states were easily observed as shown in Fig. 4a for  $15_2\ 14 \leftarrow 14_2\ 13$  transition. In order to interpret the vibrational pattern, ab initio calculations at the MP2/aug-cc-pVTZ level of the theory (Gaussian09 package)<sup>18</sup> were carried out to estimate harmonic frequencies of the lowest normal vibrational modes and vibrational contributions to the rotational constants. Three lowest-frequency modes, schematically visualized in Fig. 4b, are predicted. They are associated with methyl torsion  $\nu_{18}$ , hydroxyl torsion  $\nu_{17}$ , and skeletal bending mode  $\nu_{16}$ . Up to six excited vibrational states arising from these modes are located below  $700\ \text{cm}^{-1}$  (see Fig. 4d). They should be enough populated to produce observable vibrational satellite spectrum.

Calculated first-order vibration-rotation constants made possible to estimate changes of rotational constants relative to the ground state values and to model the vibrational satellite pattern shown in Fig. 4c. The good matching of modeled positions with experimental lines in Fig. 4a is evident and allow the assignment of transitions in  $\nu_{18}=1$ ,  $\nu_{17}=1$ , and  $\nu_{16}=1$  excited states. The available long experimental scan, carried out in the present investigation, made possible to apply the well-known Loomis- Wood-type plots<sup>19</sup> from the AABS package<sup>20,21</sup> and to

follow individual J and  $K_a$  sequences for vibrational satellites (see Fig. S1 in the supplementary content).

Most of the assigned rotational transitions in  $v_{18}=1$  state showed characteristic A–E splittings with magnitude up to a few MHz as illustrated in Fig. 5a and e. Vast majority of the observed lines was assigned to a-type or b-type transitions, however, weak c-type transitions could be occasionally found in the E symmetry sub-state, despite almost zero component of the permanent dipole moment along the c axis. In this case, the c-type transitions may gain intensity from the accompanying b-type transitions through the so-called intensity borrowing that occurs in situations when the asymmetry splitting reaches the magnitude of the internal rotation splitting.<sup>22</sup> Simultaneous appearance of the c-type transitions and decrease of intensity of associated b-type transitions is demonstrated on example of Q-branch  $K_a=6\leftarrow 5$  transitions in Fig. 5e. Resolved A–E doublets were fitted using the XIAM<sup>17</sup> program and the internal rotation parameters are collected in the second column of Table 2. Internal rotation axis i lies close to the ab inertial plane (see Fig. 1) and the measured splittings were found to have only a poor dependence on  $\langle(i, c)$  so it was kept fixed to the value obtained from the experimental structure.<sup>8</sup> Finally, in order to derive rotational and centrifugal distortion constants from all the observed transitions, i.e. also from those where the A and E components were overlapped, another fit using the ERHAM program<sup>23</sup> was performed and the resulting spectroscopic constants are given in Table 3. Near harmonic progression of successive excitation of m18 could be then followed up to  $v_{18}=2$  as illustrated in Fig. 4a. As usual, the order of the A and E sublevels was found reversed in  $v_{18}=2$  with respect to  $v_{18}=1$  and observation of more than 20 times larger A–E splitting than for the same transition in  $v_{18} = 1$  state (see Fig. 5a and b) confirms the assignment of  $v_{18} = 2$ . As a consequence of significantly larger splitting, the observed data were more sensitive to the parameters associated with the methyl internal rotor. This is demonstrated by simultaneous determination of all three angles  $\langle(i, a)$ ,  $\langle(i, b)$ , and  $\langle(i, c)$  in Table 2 or  $\rho$ ,  $\beta$ , and  $\alpha$  parameters in Table 3.

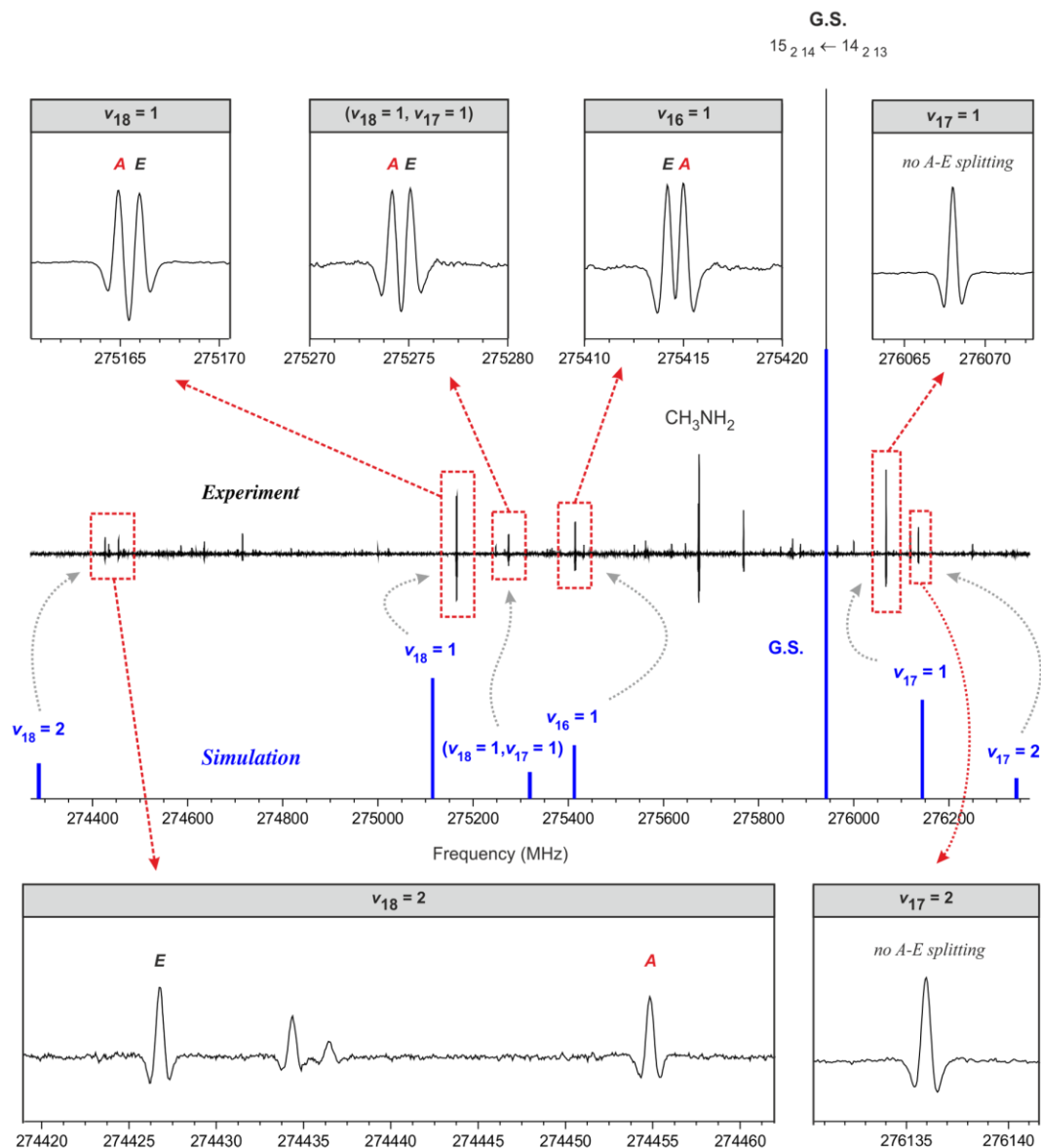


**Figure 4.** (a) A section of the experimental spectrum of N-methylhydroxylamine with assignment of six different excited vibrational states. The most intense ground state transition is intentionally off-scale. (b) Normal coordinate displacement vectors of three lowest-frequency normal vibrational modes  $\nu_{18}$ ,  $\nu_{17}$ , and  $\nu_{16}$  of N-methylhydroxylamine calculated at the MP2/aug-cc-pVTZ level. (c) Modeled vibrational satellite pattern around the ground state  $15_{2,14} \leftarrow 14_{2,13}$  transition of N-methylhydroxylamine arising from the first excited states of  $\nu_{18}$ ,  $\nu_{17}$ , and  $\nu_{16}$ . (d) Vibrational energy levels of N-methylhydroxylamine below  $700 \text{ cm}^{-1}$ .

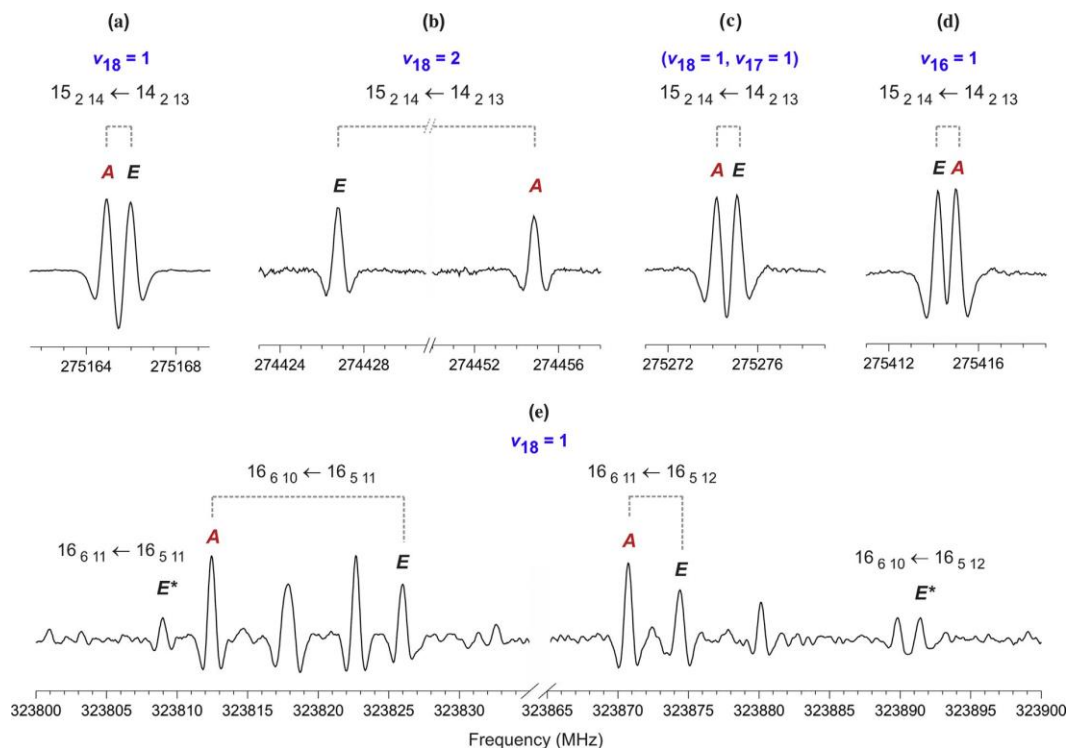


**Figure 5.** Internal rotation splitting in excited vibrational states of N-methylhydroxylamine. Weak c-type transitions observed in the degenerate sub-state are labeled by E\*.

No evidence of the A–E splitting in the measured range of J and  $K_a$  quantum numbers was found in  $v_{17} = 1$  and the spectroscopic constants were obtained simply from the fits to the Watson’s semirigid-rotor Hamiltonian. Knowledge of the rotational constant changes for  $v_{17} = 1$  with respect to the ground state values allowed to localize the rotational transitions in  $v_{17} = 2$  state (see Fig. 4a), where no A–E splitting was also observed. Results of fittings for  $v_{17} = 1$  and  $v_{17} = 2$  states are given in Table 3.

Combination state ( $v_{18}=1, v_{17}=1$ ) was easily identified (see Fig. 4a) by means of linear combination of changes of rotational constants already known for  $v_{18}=1$  and  $v_{17}=1$  states. More than 50% of the rotational transitions in this state were observed split into A and E components with separation similar to those for corresponding transitions in  $v_{18}=1$  state (see Fig. 4a and c). ( $v_{18}=1, v_{17}=1$ ) state was found to behave like  $v_{18}=1$ , i.e. the A and E sub-levels are inverted with respect to the ground state. Spectroscopic constants from the global fit of all the observed



transitions are listed in Table 3.

**Table 3.** Spectroscopic constants of N-methylhydroxylamine in six excited vibrational states (A-reduction, I<sup>r</sup>-representation).

Constant	$\nu_{18} = 1$	$\nu_{17} = 1$	$\nu_{16} = 1$	$\nu_{18} = 2$	$(\nu_{18} = 1, \nu_{17} = 1)$	$\nu_{17} = 2$
<b>A/MHz</b>	38887.9835 (37) <sup>a</sup>	38746.6364 (58)	39322.0704 (40)	38885.67 (14)	38711.490 (54)	38567.816 (78)
<b>B/MHz</b>	9899.93427 (48)	9959.12202 (81)	9931.53550 (58)	9861.3662 (23)	9921.0820 (14)	9972.4390 (12)
<b>C/MHz</b>	8671.58222 (45)	8688.58032 (70)	8666.28760 (58)	8654.1576 (20)	8667.6837 (13)	8686.6399 (10)
<b><math>\Delta J</math>/kHz</b>	9.72238 (62)	10.01005 (85)	9.88905 (56)	9.5279 (24)	9.7652 (13)	10.0118 (17)
<b><math>\Delta JK</math>/kHz</b>	-24.6123 (87)	-32.7944 (42)	-31.4496 (83)	-19.290 (28)	-23.886 (27)	-35.090 (21)
<b><math>\Delta K</math>/kHz</b>	363.346 (61)	361.871 (96)	416.742 (68)	330.6 (28)	354 (10)	379.356 <sup>b</sup>
<b><math>\delta J</math>/kHz</b>	1.89312 (31)	1.97305 (56)	1.96037 (49)	1.8400 (16)	1.9205 (11)	1.95616 (98)
<b><math>\delta J</math>/kHz</b>	-0.685 (21)	1.040 (43)	9.297 (25)	-8.45 (18)	-0.79 (18)	-3.70 (14)
<b><math>\rho^c</math></b>	0.20785 (10)	–	0.20218 (23)	0.205807 (33)	0.20117 <sup>b</sup>	–
<b><math>\beta^d</math></b>	9.809 (10)	–	10.615 (18)	9.7203 (72)	11.175 (58)	–
<b><math>\alpha^d</math></b>	4.492 <sup>e</sup>	–	4.492 <sup>e</sup>	2.268 (44)	4.492 <sup>e</sup>	–
<b><math>\epsilon_1^f</math></b>	14.331 (21)	–	-9.635 (19)	-401.70 (50)	10.586 (49)	–
<b><math>[A - (B + C)/2]_1^g</math>/kHz</b>	–	–	–	594 (31)	–	–
<b><math>[(B - C)/4]_1^g</math>/kHz</b>	–	–	–	12.91 (24)	–	–
<b><math>-\Delta JK]_1^g</math>/Hz</b>	–	–	–	-73.6 (79)	–	–
<b><math>J_{\min}/J_{\max}^h</math></b>	1/30	6/29	6/29	6/22	6/22	6/20
<b><math>K_{a,\min}/K_{a,\max}^h</math></b>	0/9	0/9	0/10	0/10	0/8	0/5
<b><math>N^i</math></b>	435	275	332	253	187	112
<b><math>r_{\text{fit}}^j</math>/MHz</b>	0.050	0.053	0.043	0.088	0.054	0.053

<sup>a</sup> The numbers in parentheses are 1 $\sigma$  uncertainties in units of the last decimal digit.

<sup>b</sup> Fixed to the ground state value.

<sup>c</sup> Magnitude of the  $\rho$ -vector:  $\rho = \sqrt{\rho_a^2 + \rho_b^2 + \rho_c^2}$  where  $\rho_k = I_\alpha \lambda_k / \lambda_k$  ( $k = a, b, c$ ).  $I_\alpha$  is the moment of inertia of the methyl top,  $\lambda_k$  is the direction cosine of the internal rotor to the principal axis and  $I_k$  is the principal moment of inertia.

<sup>d</sup> Angles between the  $\rho$ -vector and the principal axis:  $\beta = \arccos(\rho_a/\rho)$ ,  $\alpha = \arccos\sqrt{\rho_b^2 + \rho_c^2}$

<sup>e</sup> Fixed to the value derived from the structural data of Sung and Harmony<sup>8</sup>.

<sup>f</sup> First energy tunneling parameter.

<sup>g</sup> First tunneling component of the linear combination of the rotational constants and centrifugal distortion constant. Definitions of these parameters are given elsewhere<sup>23,24</sup>.

<sup>h</sup> Minimum/maximum quantum number value included in the fit.

<sup>i</sup> Number of transitions.

<sup>j</sup> Root mean square deviation of the fit.

As an unexpected feature, the rotational transitions in  $v_{16}=1$  state were also found split with separation of the two lines of the doublets slightly smaller than the A–E splitting in  $v_{18}=1$  state (see Fig. 4a and d). To analyze the transitions in this state, it was assumed that the splitting originates also from the methyl group internal rotation with positions of the A and E sublevels the same as for the ground state, i.e. the A sublevel has lower energy than the E sublevel. Results of the fittings are given in Tables 3. The complete lists of the experimental frequencies measured for  $v_{18}=1$ ,  $v_{18}=2$ ,  $v_{17}=1$ ,  $v_{17}=2$ , ( $v_{18}=1$ ,  $v_{17}=1$ ), and  $v_{16}=1$  states are provided in Tables S3–S8 of the supplementary content.

## 4. CONCLUSIONS

---

The present work provides the results of a comprehensive investigation of the rotational spectrum in the millimeter wave region for the most abundant *trans* isomer of N-methylhydroxylamine. Accurate ground state rotational constants, complete set of the quartic together with numerous sextic centrifugal distortion constants and  $^{14}\text{N}$  nuclear quadrupole coupling constants have been determined. In addition,  $^{13}\text{C}$  isotopic species was analyzed in natural abundance.

Six excited vibrational states of the parent species resulting from the methyl torsion, hydroxyl torsion and skeletal bending mode were unambiguously assigned. All the studied excited vibrational states were amenable to the single state fits in the measured range of rotational quantum numbers given in Table 3. Slight departures of  $D_{JK}$  and  $D_K$  values and change of sign of  $d_K$  constants can be noted when compared to the ground state values. This could be an indicative of interstate couplings whose evidence might become stronger at higher  $J$  and  $K_a$  values. Centrifugal distortion constants reported in Table 3 can be taken as effective parameters that together with the rotational constants reproduce the vibrational satellite spectrum near the experimental uncertainty.

The barrier height of NMH,  $V_3 = 1245.8 (46) \text{ cm}^{-1}$ , is determined in this work from the ground state splittings. It can be seen from Table 2 that the  $V_3$  values obtained independently from the analysis of  $v_{18}=1$  and  $v_{18}=2$  states are in good consistence with that of the ground state. High-barrier approximation<sup>16</sup> can be used to estimate a harmonic frequency for the methyl torsion of  $269 \text{ cm}^{-1}$  which is in excellent agreement with the theoretical value of  $272 \text{ cm}^{-1}$ .

The present work significantly extends the frequency coverage of the NMH rotational spectrum known up to now and newly derived spectroscopic constants of NMH obtained from the fits of more than 2000 transition lines are expected to provide confident spectral predictions for frequencies in the millimeter and submillimeter wave regions and are sufficient to guide future radioastronomical observational searches for this molecule.

## 5. REFERENCES

- 
- <sup>1</sup> A.C. Cheung, D.M. Rank, C.H. Townes, D.D. Thornton, W.J. Welch, *Phys. Rev.Lett.* 21 (1968) 1701–1705.
  - <sup>2</sup> D.E. Woon, 2017. <<http://www.astrochymist.org/>>.
  - <sup>3</sup> A. Belloche, H.S.P. Müller, K.M. Menten, P. Schilke, C. Comito, *Astron. Astrophys.* 559 (2013) A47.
  - <sup>4</sup> J. Cernicharo, Z. Kisiel, B. Tercero, L. Kolesníková, I.R. Medvedev, A. López, S. Fortman, M. Winnewisser, F.C. de Lucia, J.L. Alonso, J.-C. Guillemin, *Astron. Astrophys.* 587 (2016) L4.
  - <sup>5</sup> E. Herbst, E.F. van Dishoeck, *Ann. Rev. Astron. Astrophys.* 47 (2009) 427–480.
  - <sup>6</sup> R.T. Garrod, S.L.W. Weaver, E. Herbst, *Astrophys. J.* 682 (2008) 283–302.
  - <sup>7</sup> A.I. Vasyunin, H. Eric, *Astrophys. J.* 762 (2013) 86.
  - <sup>8</sup> E.-M. Sung, M.D. Harmony, *J. Mol. Spectrosc.* 74 (1979) 228–241.
  - <sup>10</sup> A.M. Daly, L. Kolesníková, S. Mata, J.L. Alonso, *J. Mol. Spectrosc.* 306 (2014) 11–18.
  - <sup>11</sup> G. Cazzoli, L. Dore, *J. Mol. Spectrosc.* 143 (1990) 231–236.
  - <sup>12</sup> B.M. Hays, S.L. Widicus Weaver, *J. Phys. Chem. A* 117 (2013) 7142–7148.
  - <sup>13</sup> L. Kolesníková, J. Varga, H. Beckers, M. Šimečková, Z. Zelinger, L.N. Střiteská, P. Kania, H. Willner, Š.Urban, *J. Chem. Phys.* 128 (2008) 224302.
  - <sup>14</sup> H.M. Pickett, *J. Mol. Spectrosc.* 148 (1991) 371–377.
  - <sup>15</sup> J.K.G. Watson, in: J.R. Durig (Ed.), *Vibrational Spectra and Structure*, Elsevier, Amsterdam, 1977, pp. 1–89.
  - <sup>16</sup> W. Gordy, R.L. Cook, *Microwave Molecular Spectra*, Interscience Publishers, 1970.
  - <sup>17</sup> H. Hartwig, H. Dreizler, *Z. Naturforsch. A* 51 (1996) 923–932.
  - <sup>18</sup> M.J. Frisch, G.W. Trucks, H.B. Schlegel, G.E. Scuseria, M.A. Robb, J.R. Cheeseman, G. Scalmani, V. Barone, B. Mennucci, G.A. Petersson, H. Nakatsuji, M. Caricato, X. Li, H.P. Hratchian, A.F. Izmaylov, J. Bloino, G. Zheng, J.L. Sonnenberg, M. Hada, M. Ehara, K. Toyota, R. Fukuda, J. Hasegawa, M. Ishida, T. Nakajima, Y. Honda, O. Kitao, H. Nakai, T. Vreven, J.A. Montgomery Jr., J.E. Peralta, F. Ogliaro, M.J. Bearpark, J. Heyd, E.N. Brothers, K.N. Kudin, V.N. Staroverov, R. Kobayashi, J. Normand, K. Raghavachari, A.P. Rendell, J.C. Burant, S.S. Iyengar, J. Tomasi, M. Cossi, N. Rega, N.J. Millam, M. Klene, J.E. Knox, J.B. Cross, V. Bakken, C. Adamo, J. Jaramillo, R. Gomperts, R.E. Stratmann, O. Yazyev, A.J. Austin, R. Cammi, C. Pomelli, J.W. Ochterski, R.L. Martin, K. Morokuma, V.G. Zakrzewski, G.A. Voth, P. Salvador, J.J. Dannenberg, S. Dapprich, A.D. Daniels, Ö. Farkas, J.B. Foresman, J.V. Ortiz, J. Cioslowski, D.J. Fox, GAUSSIAN09, Gaussian, Inc., Wallingford CT, USA, 2009.

- <sup>19</sup> B.P. Winnewisser, J. Reinstädler, K.M.T. Yamada, J. Behrend, *J. Mol. Spectrosc.* 136 (1989) 12–16.
- <sup>20</sup> Z. Kisiel, L. Pszczółkowski, I.R. Medvedev, M. Winnewisser, F.C. De Lucia, E. Herbst, *J. Mol. Spectrosc.* 233 (2005) 231–243.
- <sup>21</sup> Z. Kisiel, AABS package. <<http://www.ifpan.edu.pl/~kisiel/aabs/aabs.htm#aabs>>
- <sup>22</sup> R.C. Woods, *J. Mol. Spectrosc.* 21 (1966) 4–24.
- <sup>23</sup> P. Groner, *J. Chem. Phys.* 107 (1997) 4483–4498.
- <sup>24</sup> P. Groner, *J. Mol. Spectrosc.* 278 (2012) 52–67

## CHAPTER X.

# A Comprehensive Rotational Study of Interstellar *Iso-propyl Cyanide* up to 480 GHz.

---

***Adapted from: The Astrophysical Journal Supplement Series, 233, 24, (2017)***

*A detailed analysis of the rotational spectra of the interstellar iso-propyl cyanide has been carried out up to 480 GHz using three different high-resolution spectroscopic techniques. Jet-cooled broadband chirped pulse Fourier transform microwave spectroscopy from 6 to 18 GHz allowed us to measure and analyze the ground-state rotational transitions of all singly substituted  $^{13}\text{C}$  and  $^{15}\text{N}$  isotopic species in their natural abundances. The monohydrate of iso-propyl cyanide, in which the water molecule bounds through a stronger  $\text{O}-\text{H}\cdots\text{N}$  and weaker bifurcated  $(\text{C}-\text{H})_2\cdots\text{O}$  hydrogen bonds in a  $C_s$  configuration, has also been detected in the supersonic expansion. Stark-modulation spectroscopy in the microwave and millimeter wave range from 18 to 75 GHz allowed us to analyze the vibrational satellite pattern arising from pure rotational transitions in the low-lying vibrational excited states. Finally, assignments and measurements were extended through the millimeter and submillimeter wave region. The room temperature rotational spectra made possible the assignment and analysis of pure rotational transitions in 19 vibrationally excited states. Significant perturbations were found above 100 GHz in most of the observed excited states. Due to the complexity of the interactions and importance of this astrophysical region for future radioastronomical detection, both a graphical plot approach and a coupled fit have been used to assign and measure almost 10,000 new lines.*



## 1. INTRODUCTION

---

More than 30 molecules containing the cyano ( $-\text{CN}$ ) group have been detected so far in the interstellar medium (ISM) or circumstellar shells. Among them, four belong to alkyl cyanides, organic molecules with the general formula  $\text{R}-\text{CN}$ , where  $\text{R}=\text{C}_n\text{H}_{2n+1}$ . Methyl cyanide ( $\text{CH}_3\text{CN}$ ) and ethyl cyanide ( $\text{C}_2\text{H}_5\text{CN}$ ) are the simplest ones and were detected in the 1970's.<sup>1,2</sup> The next member, propyl cyanide ( $\text{C}_3\text{H}_7\text{CN}$ ), has two structural isomers: the straight-chain normal-propyl cyanide and branched iso-propyl cyanide; both were detected toward the Sgr B2(N) massive star-forming region.<sup>3,4</sup>

Interstellar detection of iso-propyl cyanide (hereafter i-PrCN) is particularly important for its branched carbon chain structure, which is a crucial characteristic of many molecules that are key to life, like amino acids. This detection suggests a connection between interstellar chemistry and the molecular composition of meteorites for which branched amino acids dominate over their straight-chain isomers,<sup>5</sup> and predicts the presence of amino acids in the ISM.<sup>4</sup> Additionally, the  $-\text{CN}$  group in i-PrCN is an excellent H-atom acceptor and can efficiently undergo hydrogen-bonding with proton donors to form molecular complexes. One of the most significant series of molecular complexes is that created by water, the small molecule with evident terrestrial importance. The chemistry of hydrogen bonded molecular complexes in the ISM is far from understood and no such cluster has been detected so far.

In the present work, broadband time-domain chirped pulse Fourier transform microwave spectroscopy (CP-FTMW)<sup>6</sup> at conditions of supersonic expansion was used to analyze the parent, the three  $^{13}\text{C}$  species, and the  $^{15}\text{N}$  isotopic species in their natural abundances. In addition, the complex i-PrCN-water has been observed and characterized for the first time, showing the nature of the intermolecular forces in play. Frequency-domain microwave Stark-modulation and frequency-modulation spectroscopy were used to record the room temperature spectrum of i-PrCN up to 480 GHz and to identify the pure rotational spectra

in 19 excited vibrational states. Plentiful perturbations that shift the rotational transitions beyond their expected region were observed and analyzed. The nearly 10,000 new accurately measured transition lines provided in this work should facilitate further astrophysical detections of *i*-PrCN in the ISM.

## 2. EXPERIMENTAL DETAILS

---

The sample of liquid *i*-PrCN (also known as isobutyronitrile) was obtained commercially and required no further purification. The jet-cooled rotational spectrum in the 6–18 GHz frequency range was investigated using a broadband CP-FTMW spectrometer.<sup>7</sup> Two pulsed nozzles were used to expand a gas mixture containing 0.3% of *i*-PrCN in neon from a backing pressure of 1.5 bar. Up to 112,000 individual free induction decays (four FIDs on each valve cycle) were averaged in the time domain and Fourier-transformed using a Kaiser–Bessel window function to obtain the frequency-domain spectrum. The uncertainty of the frequency measurements was estimated to be better than 10 kHz.

Room temperature rotational spectra were recorded from 26 to 480 GHz at a pressure of approximately 15  $\mu$ bar. An upgraded Stark-modulation spectrometer employing 33.3 kHz modulation frequency and phase-sensitive detection was used to acquire the rotational spectra up to 75 GHz, while the frequency-modulation millimeter and submillimeter wave spectrometer was used for measurements above 75 GHz. Both spectrometers are based on the harmonic multiplication of the synthesizer frequency by a set of active and passive multipliers (VDI, Inc.) and their detailed description can be found in Kolesníková et al. (2017)<sup>8</sup> and Daly et al. (2014).<sup>9</sup> For the frequency-modulation measurements, the synthesizer output was frequency-modulated at  $f=10.2$  kHz and at modulation depths between 20 and 40 kHz. A second derivative shape of the lines resulting from a  $2f$  lock-in detection was fitted to the Gaussian profile function and the uncertainty of the line center frequency was estimated to be better than 30 kHz.



### 3. RESULTS AND DISCUSSION

---

#### 3.1. JET-COOLED BROADBAND ROTATIONAL SPECTRUM

The recorded broadband CP-FTMW rotational spectrum of *i*-PrCN is shown in Figure 1(a). Strong a-type R-branch  $J = 1 \leftarrow 0$  and  $2 \leftarrow 1$  transitions, accompanied by several weaker a-type Q-branch, c-type R-branch, and c-type Q-branch transitions, were easily identified in the spectrum in accordance with two nonzero dipole moment components  $|\mu_a| = 4.0219$  (50) D and  $|\mu_c| = 0.619$  (27) D.<sup>10</sup> All the observed transitions exhibit nuclear quadrupole hyperfine structure owing to the presence of one <sup>14</sup>N nucleus with a nonzero quadrupole moment that interacts with the electric field gradient created at the <sup>14</sup>N nucleus by the rest of the molecule. Observed hyperfine patterns were in agreement with those predicted from previous Stark<sup>11</sup> and MB-FTMW<sup>10</sup> studies. At the low-frequency side of each a-type R-branch transition, several weaker lines with the same hyperfine pattern were found as shown for the  $2_{12} \leftarrow 1_{11}$  transition in Figure 1(b). They were attributed to rotational transitions of <sup>13</sup>C isotopologues in their natural abundances. The one with no quadrupole hyperfine structure was assigned to <sup>15</sup>N isotopic species (see Figure 1(b)). The observation of only three <sup>13</sup>C signals for the four carbon atoms of *i*-PrCN is consistent with the existence of a symmetry plane (see the *ac* inertial plane in Figure 2(a)) that makes the C(3) and C(4) atoms equivalent, giving rise to a single signal with approximate double intensity. The same sets of low-*J* rotational transitions for the parent and isotopic species were fitted to a rigid rotor Hamiltonian complemented with a nuclear quadrupole Hamiltonian term<sup>12</sup> with a coupling scheme  $\mathbf{F} = \mathbf{J} + \mathbf{I}_N$  between the rotational angular momentum  $\mathbf{J}$  and the <sup>14</sup>N nuclear spin angular momentum  $\mathbf{I}_N$ . The experimental spectroscopic constants in Table 1 provide definitive evidence of the existence of an *ac* symmetry plane in *i*-PrCN; the  $P_b$  values are nearly identical for all the isotopologues, except for the out-of-plane C(3) or C(4) species. Kraitchman's equations<sup>13,12</sup> were used to evaluate the structure of *i*-PrCN given in Figure 2(a).

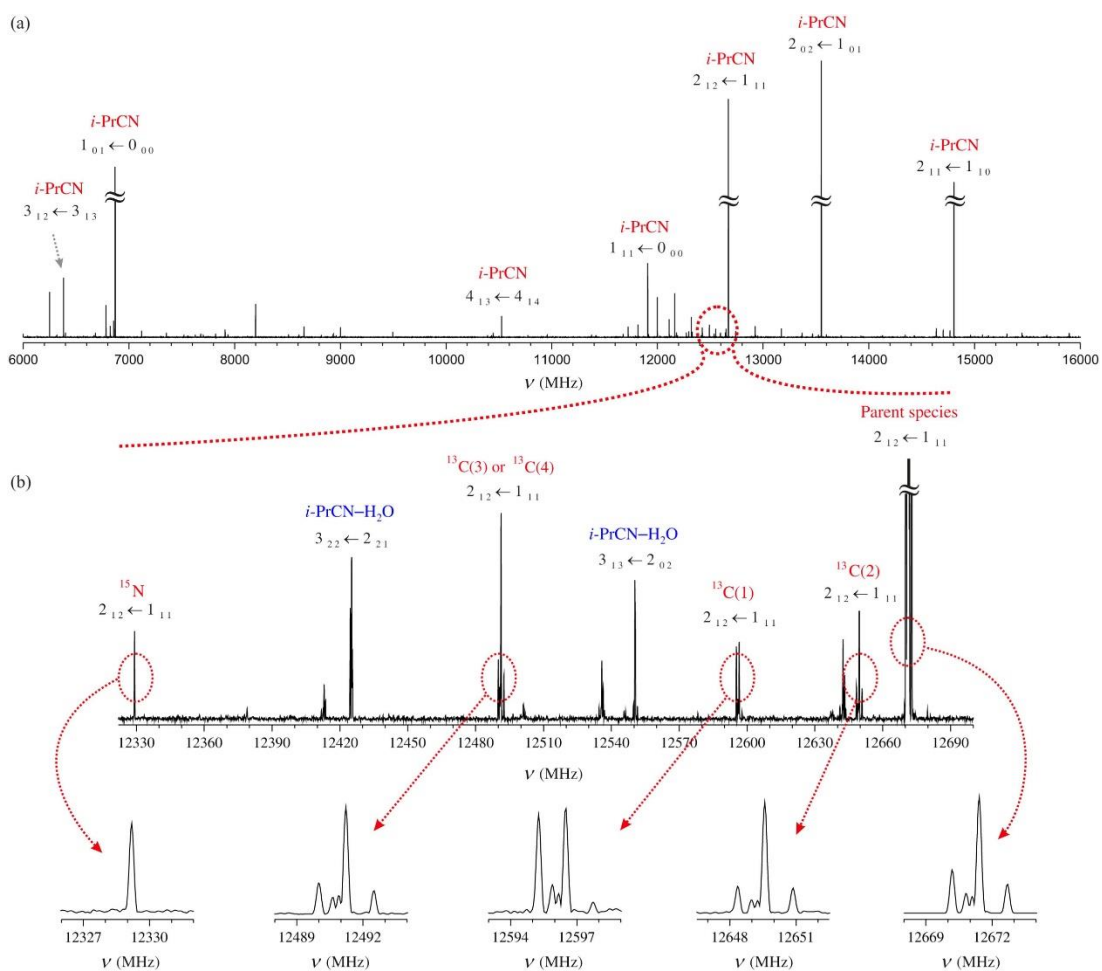


**Figure 1.** (a) Broadband CP-FTMW spectrum of iso-propyl cyanide with assignment of prominent features. (b) A section of the spectrum showing assignment of rotational transitions of the parent,  $^{13}\text{C}$ , and  $^{15}\text{N}$  species of iso-propyl cyanide and the monohydrate.

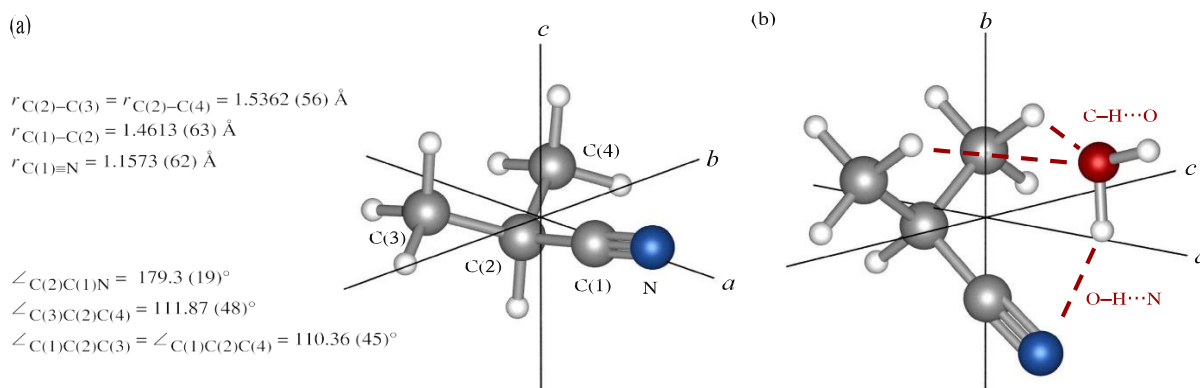


**Figure 2.** (a) Iso-propyl cyanide and its substitution  $r_s$  structure. (b) Monohydrate of iso-propyl cyanide.

**Table 1.** Spectroscopic Constants for the Parent and Isotopic Species of iso-propyl Cyanide and Its Monohydrate Derived from the Jet-cooled Measurements

Constant/Unit	i-PrCN					i-PrCN-H <sub>2</sub> O	
	Parent Species <sup>a</sup>	<sup>13</sup> C(1) <sup>a</sup>	<sup>13</sup> C(2) <sup>a</sup>	<sup>13</sup> C(3) or <sup>13</sup> C(4) <sup>a</sup>	<sup>15</sup> N <sup>a</sup>	Experiment <sup>b</sup>	Ab initio <sup>c</sup>
A/MHz	7941.78 (49) <sup>d</sup>	7940.29 (58)	7923.32 (53)	7747.66 (42)	7939.79 (81)	3279.4204 (73)	3324
B/MHz	3968.0684 (35)	3939.1001(40)	3956.5312 (37)	3927.9247 (32)	3837.1287 (90)	2257.5487 (27)	2351
C/MHz	2901.0366 (30)	2885.7173	2897.6034 (33)	2854.3535 (28)	2830.6890 (90)	1884.2656 (18)	1957
P <sub>a</sub> /uÅ <sup>2</sup>	118.9662 (20)	119.8909 (23)	119.1809 (21)	120.2444 (17)	123.2959 (32)	168.98285 (26)	160.58
P <sub>b</sub> /uÅ <sup>2</sup>	55.2401 (20)	55.2402 (23)	55.2318 (21)	56.8111 (17)	55.2398 (32)	99.22721 (26)	97.65
P <sub>c</sub> /uÅ <sup>2</sup>	8.3953 (20)	8.4072 (23)	8.5519 (21)	8.4187 (17)	8.4116 (32)	54.87898 (26)	54.38
χ <sub>aa</sub> /MHz	-3.955 (19)	-3.942 (22)	-3.957 (21)	-3.943 (18)	...	-1.8220 (81)	-1.97
χ <sub>bb</sub> /MHz	2.139 (25)	2.118 (29)	2.143 (27)	2.125 (24)	...	-0.239 (10)	0.17
χ <sub>cc</sub> /MHz	1.816 (26)	1.824 (30)	1.814 (28)	1.818 (24)	...	2.0606 (65)	1.80
σ <sub>fit</sub> <sup>e</sup> /MHz	0.014	0.016	0.015	0.013	0.016	0.008	...

<sup>a</sup> Rigid rotor Hamiltonian fit. Rotational transitions used for this fit are given in Table 4.

<sup>b</sup> Semi-rigid rotor Hamiltonian fit (S-reduction, I<sup>r</sup>-representation). The measured rotational transitions are provided in Table 4. Determined quartic centrifugal distortion constants are: DJ = 5.831 (90) kHz, DJK = -8.97 (36) kHz, DK = 8.6 (13) kHz, d<sub>1</sub> = -1.285 (77) kHz, and d<sub>2</sub> = 0.433 (44) kHz.

<sup>c</sup> MP2/aug-cc-pVTZ level of the theory, Gaussian 09 package<sup>14</sup> (Frisch et al. 2009).

<sup>d</sup> The numbers in parentheses are 1σ (67% confidence level) uncertainties in units of the last decimal digit.

<sup>e</sup> Root mean square deviation of the fit.

The observation of water dimer (H<sub>2</sub>O)<sub>2</sub> rotational transitions in the broadband spectrum may indicate the plausible formation of the i-PrCN monohydrate with the residual water. On this basis, the remaining unassigned lines with <sup>14</sup>N nuclear quadrupole hyperfine structure were initially ascribed to i-PrCN monohydrate. Hence, a new set of a-type R-branch transitions was identified as belonging to the monohydrate. Additional b-type R-branch transitions were also located, but c-type ones were not observed. Rotational constants, planar moments of inertia, and nuclear quadrupole coupling constants are collected in Table 1 along with the quartic centrifugal distortion constants given in the footnote. The nearly equal values of P<sub>b</sub> of the monomer and P<sub>c</sub> of the monohydrate listed in Table 1 indicate that the ac symmetry plane of the monomer (see Figure 2(a)) coincides with the ab symmetry plane of the monohydrate (see Figure 2(b)) where the water molecule is situated. This is consistent with the observation of the a-type and b-type spectra in the

monohydrate and the absence of c-type spectra. This structure of the monohydrate is definitely confirmed by comparisons of experimental spectroscopic constants with those that were ab initio predicted for the global minimum listed in the last column of Table 1. The observed configuration benefits not only from a strong O–H···N hydrogen bond but also from a bifurcated weaker (C–H)<sub>2</sub>···O hydrogen bond with the two methyl groups.<sup>15,16</sup>

### 3.2. MICROWAVE AND MILLIMETER WAVE STARK-MODULATION SPECTRA

The  $9_{18} \leftarrow 8_{17}$  transition in Figure 3(a) illustrates that each ground vibrational state line of the Stark spectrum was accompanied by many satellite lines attributable to pure rotational transitions in excited vibrational states. As shown in previous studies of aminoacetonitrile,<sup>8</sup> methyl isocyanate,<sup>17</sup> propenal,<sup>18</sup> vinyl cyanide,<sup>19</sup> and ethyl cyanide,<sup>20</sup> satellite lines with the same Stark pattern as the ground-state line can be ascribed to the same rotational transition in excited vibrational states. The five lowest normal modes,  $\nu_{30}$  (A''),  $\nu_{17}$  (A'),  $\nu_{29}$  (A''),  $\nu_{16}$  (A'), and  $\nu_{15}$  (A'), associated with C–C≡N and C–C–(CN) bending and CH<sub>3</sub> torsional motions (see Figure 3(c)), are expected to be the main contributors to the satellite lines in Figure 3(a). The satellite pattern arising from their first excited states was modeled on the basis of calculated first-order vibration-rotation constants  $a_i$  (Gaussian 09 package,<sup>14</sup> B3LYP/6-311++G(d,p) level of the theory) that define the well-known vibrational dependence of rotational constants  $B_v = B_e - \sum_i \alpha_i(v_i + \frac{1}{2})$ , where  $B_v$  and  $B_e$  substitute all three rotational constants in a given excited state and in equilibrium and  $v_i$  is the vibrational quantum number. The predicted pattern, shown in Figure 3(b), matches nicely in positions and intensities with that of the Stark spectrum, and provides definitive proof for the identification of rotational transitions in fundamental states. Successive higher excitations of  $n_{30}$ ,  $n_{29}$  could be also located. Finally, combination states ( $\nu_{30}=1$ ,  $\nu_{17}=1$ ), ( $\nu_{30}=1$ ,  $\nu_{29}=1$ ), ( $\nu_{30}=1$ ,  $\nu_{16}=1$ ), and ( $\nu_{17}=1$ ,  $\nu_{15}=1$ ) and four additional states, labeled  $\nu_a$ ,  $\nu_b$ ,  $\nu_c$ , and  $\nu_d$ , could also be assigned. From the 16 excited states identified in the Stark spectra, 3 coincide with those reported in the previous microwave study of Durig & Li (1974),<sup>21</sup> up to 40 GHz. The first set of spectroscopic constants obtained from the Stark measurements<sup>22</sup> was subsequently used to predict the

corresponding transitions in the higher-frequency region. Following this first assignment from Kolesniková et al. (2016),<sup>22</sup> measurements of 10 of the above 16 excited states have been reported<sup>23</sup> using a new commercial BrightSpec segmented chirped pulse spectrometer<sup>24</sup> working in the W-band (75–110 GHz).

### 3.3. FREQUENCY-MODULATED MILLIMETER AND SUBMILLIMETER WAVE SPECTRA

Starting from the previous Stark assignments, the well-known Loomis–Wood type plot technique<sup>25,26</sup> was applied to transfer the assignments for the 16 excited states up to 480 GHz. As an example, Figure 4 shows the  $K_a = 0 \leftarrow 0$  transition sequence. Stripes corresponding to the rotational transitions in excited vibrational states can be easily followed from  $J' = 9$  (Stark-modulation region) to  $J' = 71$ . Three new satellite progressions labeled  $v_e$ ,  $v_f$ ,  $v_g$  were discovered using this graphical procedure (see Figure 4), leading to the assignment of pure rotational spectra in 19 vibrationally excited states. As the ground vibrational state can in most cases be considered an unperturbed state, its rotational transitions were first measured and analyzed between 50 and 480 GHz in order to obtain a reference set of rotational and centrifugal distortion parameters that can be compared with those in excited states. Watson's S-reduced Hamiltonian<sup>27</sup> with centrifugal distortion terms up to the sixth order was used to fit more than 2300 a-type R-branch and Q-branch transitions (SPFIT/SPCAT package<sup>28</sup>), and the resulting constants are reported in the first column of Table 2. These constants are given for completeness reasons, as the quality of their values cannot compete with the values from Müller et al. (2011),<sup>10</sup> where transitions measured by the high-resolution jet-cooled MB-FTMW technique were used. For completeness, the assignment of  $^{13}\text{C}$  isotopic species in their natural abundances was also extended into the millimeter wave region and the obtained spectroscopic constants are given in Table 3. A list of the measured frequencies of both the parent and  $^{13}\text{C}$  species can be found in Table 4.

Once the Loomis–Wood assisted assignment was brought in, appreciable perturbations could be quickly spotted above 100 GHz in the majority of identified excited states lines and special attention to this aspect is dedicated in the following two sections.

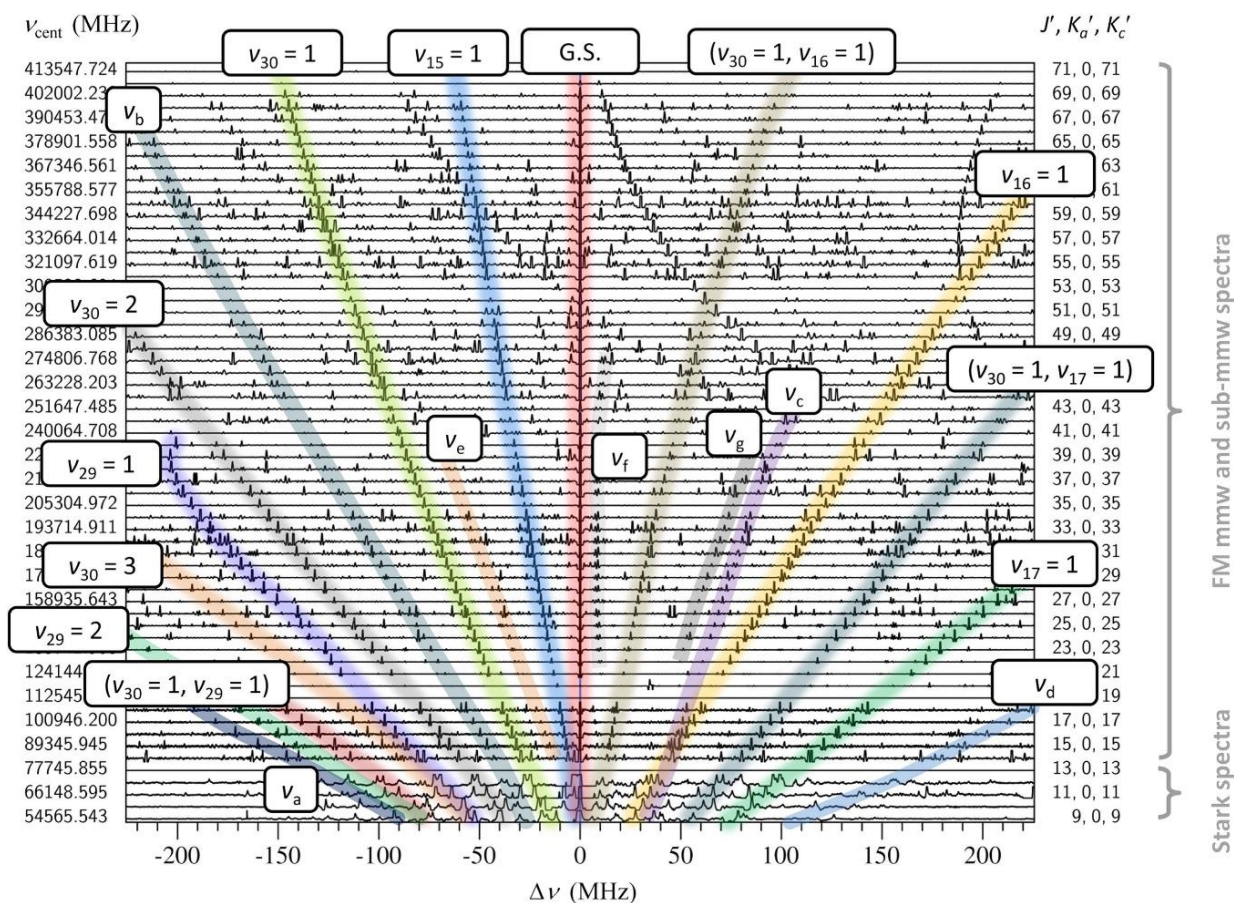


**Figure 3.** Loomis–Wood-type plot obtained from the AABS package<sup>26</sup>, showing the identification of lines corresponding to the ground-state and excited vibrational states of iso-propyl cyanide. Rotational transitions are lined up to the central frequencies  $\nu_{\text{cent}}$  of the ground-state  $K_a = 0 \leftarrow 0$  transition.  $\nu_{\text{cent}}$  and the upper level rotational quantum numbers  $J', K'_a, K'_c$  are indicated on the left and right sides of the diagram, respectively. The distance from the central frequency is given by  $\Delta\nu$ .

### 3.3.1. Excited States below 300 cm<sup>-1</sup>

Four excited vibrational states are predicted below 300 cm<sup>-1</sup>, as shown in Figure 3(d). Almost 1500 transition lines have been measured for the lowest  $\nu_{30} = 1$  excited state that fits the semi-rigid rotor Hamiltonian in a broad range of  $J$  and  $K_a$  quantum numbers. Only some transitions in limited  $J$  ranges showed anomalous deviations of their experimentally measured frequencies and were excluded. The resulting spectroscopic constants are given in the second column of Table 2. The  $K_a = 0$  and lower-frequency  $K_a = 1$  sequence of transitions originating from  $J_{0J}$  and  $J_{1J}$  energy levels were, on the other hand, the only ones in  $\nu_{17} = 1$  that could be encompassed within the semi-rigid rotor Hamiltonian up to the highest  $J$  values. Already, the upper frequency  $K_a = 1$  component, which is associated with  $J_{1J-1}$  levels, showed significant departures from their predicted positions in a wide range of  $J'$  quantum numbers (see  $J' = 30$ – $60$  in see Figure 5). Deviations similar in magnitude and different in sign could be recognized in the same range of  $J'$  in the lower-frequency  $K_a = 1$  sequence of transitions ( $J_{1J}$  levels) of  $\nu_{29} = 1$  (see Figure 5). This mirror image behavior is characteristic for mutually interacting states and is in accordance with the small energy difference between  $\nu_{17} = 1$  and  $\nu_{29} = 1$  in Figure 3(d). Since both states might be relevant for future astrophysical searches, a simultaneous analysis of  $\nu_{17} = 1$  and  $\nu_{29} = 1$  was carried out.

**Table 2.** Spectroscopic Constants in the Ground-state and Excited Vibrational States of iso-propyl Cyanide below 300 cm<sup>-1</sup> (S-reduction, I'-representation)

Constant/Unit	G.S.	$\nu_{30} = 1$	$\nu_{17} = 1$	$\nu_{29} = 1$	$\nu_{16} = 1$
A/MHz	7940.87823 (43) <sup>a</sup>	7896.80912 (77)	7995.5117 (22)	7930.9396 (20)	7923.1442 (15)
B/MHz	3968.087339 (56)	3980.03060 (11)	3971.85736 (20)	3964.95930 (17)	3970.26245 (15)
C/MHz	2901.052880 (43)	2899.857594 (77)	2904.8589 (10)	2898.0735 (10)	2902.83122 (13)
D <sub>J</sub> /kHz	0.609971 (16)	0.631009 (32)	0.611532 (44)	0.604695 (39)	0.604472 (27)
D <sub>JK</sub> /kHz	12.176382 (65)	11.52206 (17)	12.65453 (79)	12.16478 (67)	12.00451 (13)
D <sub>K</sub> /kHz	-5.2110 (11)	-7.3344 (19)	-2.6810 (63)	-5.2770 (59)	-5.3246 (29)
d <sub>1</sub> /kHz	-0.244012 (10)	-0.255115 (24)	-0.240432 (19)	-0.242324 (16)	-0.243118 (24)
d <sub>2</sub> /kHz	-0.1893655 (54)	-0.183894 (13)	-0.196335 (17)	-0.189434 (18)	-0.185858 (16)
H <sub>J</sub> /Hz	-0.0006330 (22)	-0.0006644 (63)	-0.0003203(59)	-0.0006950 (55)	-0.0005843 (39)
H <sub>JK</sub> /Hz	0.037319 (10)	0.033848 (38)	0.04040 (23)	0.03902 (16)	0.035446 (21)
H <sub>KJ</sub> /Hz	0.011908 (34)	-0.03718 (15)	0.011908 <sup>b</sup>	0.011908 <sup>b</sup>	0.017155 (90)
h <sub>1</sub> /Hz	0.0000440 (14)	0.0001210 (45)	0.0000440 <sup>b</sup>	0.0000440 <sup>b</sup>	0.0000515 (34)
h <sub>2</sub> /Hz	0.0008951 (13)	0.0008570 (33)	0.0008951 <sup>b</sup>	0.0008951 <sup>b</sup>	0.0008512 (29)
h <sub>3</sub> /Hz	0.00031802 (55)	0.0002386 (11)	0.0003714 (17)	0.0003232 (13)	0.0003001 (10)
ΔE/MHz	...	...	214803.02(14)	...	...
G <sub>a</sub> /MHz	....	...	574.735 (48)	...	...
G <sub>a</sub> <sup>2</sup> /MHz	...	...	0.016774 (14)	...	...
G <sub>a</sub> <sup>3</sup> /MHz	...	...	-0.05968 (14)	...	...



$G_a^{KK}/\text{MHz}$	...	...	-0.01455 (31)	...	...
$G_c/\text{MHz}$	...	...	175.80 (65)	...	...
$G_c^k/\text{MHz}$	...	...	-0.05363 (35)	...	...
$F_{ab}/\text{MHz}$	...	...	-6.482 (11)	...	...
$J_{\min}/J_{\max}$	6/82	6/81	6/79	6/79	6/75
$K_{a,\min}/K_{a,\max}$	0/46	0/37	0/19	0/19	0/40
$N_{\text{lines}}^c$	2355	1584	994	1065	1684
$\sigma_{\text{fit}}^d/\text{MHz}$	0.029	0.039	0.053	0.054	0.037

<sup>a</sup> The numbers in parentheses are  $1\sigma$  uncertainties in units of the last decimal digit.

<sup>b</sup> Fixed to the ground-state value.

<sup>c</sup> Number of distinct frequency lines in the fit.

<sup>d</sup> Root mean square deviation of the fit.

The two states in question,  $\nu_{17} = 1$  and  $\nu_{29} = 1$ , belong to different symmetries, therefore both a-type ( $\Delta K_a = \text{even}$ ,  $\Delta K_c = \text{odd}$ ) and c-type ( $\Delta K_a = \text{odd}$ ,  $\Delta K_c = \text{even}$ ) Coriolis interactions are allowed. On this basis, the large perturbations observed in Figure 5 for transitions between  $J' = 30$  and 60 are caused by a-type interaction between the  $J_{1J-1}$  levels of  $\nu_{17} = 1$  and  $J_{1J}$  levels of  $\nu_{29} = 1$ . In more detail, the levels involved in resonance are  $44_{143}$  of  $\nu_{17} = 1$  and  $44_{144}$  of  $\nu_{29} = 1$ , as can be seen in a part of the reduced energy level diagram in Figure 6(a). As a consequence of this resonance, the  $45_{144} \leftarrow 44_{143}$  transition of  $\nu_{17} = 1$  and the  $45_{145} \leftarrow 44_{144}$  transition of  $\nu_{29} = 1$  are shifted by more than 2 GHz from the main trend (see Figure 6(b)). An additional perturbation around  $J' = 25$  is observed in Figure 5 for the  $\nu_{29} = 1$  sequence results, on the other hand, from c-type interaction between the  $J_{1J}$  levels of  $\nu_{29} = 1$  and  $J_{2J-2}$  of  $\nu_{17} = 1$  (see Figures 6(a) and 6(b)). The most perturbed transitions, in this case, were found at a distance of approximately 80 MHz from the main trend (see Figure 6(b)). Many additional resonances obeying both a-type and c-type selection rules can be identified in Figure 6(a) for several adjacent  $K_a$  and are responsible for even larger perturbations than those mentioned above. Analysis of perturbations taking place for the lowest- $K_a$  transitions allowed first determination of the first-order Coriolis parameters  $G_a$  and  $G_c$ , the energy difference  $\Delta E$  between  $\nu_{17} = 1$  and  $\nu_{29} = 1$ , as well as the quadratic vibration-rotation parameter  $F_{ab}$ . As the assignment and fitting procedure proceeded, centrifugal distortion corrections related with  $G_a$  and  $G_c$  were also necessary to properly reproduce the perturbed transitions. The Coriolis analysis carried out in this study has made it possible to measure more than 2000 lines and to expand the assignments and the fit of



rotational transitions up to  $J=79$  and  $K_a = 19$  (see Table 4). The final set of spectroscopic parameters is collected in Table 2. It can be seen in Table 2 that the quartic centrifugal distortion constants of  $v_{29} = 1$  are very close to those from the ground state. Larger differences, however, take place for  $v_{17}=1$ , in particular for  $D_K$ . Its values probably encompass neglected interactions with  $v_{30}=1$ , the evidence for which was found at the advanced stage of the coupled analysis. Many trial fits considering three-state  $v_{30} = 1$ ,  $v_{17} = 1$ ,  $v_{29} = 1$  or two-state  $v_{30} = 1$ ,  $v_{17} = 1$  perturbations failed. However, an energy difference between  $v_{30} = 1$  and  $v_{17} = 1$  has been estimated to be about  $30 \text{ cm}^{-1}$  on the basis of the specific perturbations observed in the Loomis–Wood-type plots as shown in Figure 7. Since the most affected transitions in  $v_{17} = 1$ , as well as in  $v_{30} = 1$ , were excluded, the reader is referred to the electronically available material (<https://doi.org/10.3847/1538-4365/aa9614>), where Loomis–Wood-type plots similar to those of Figures 5 and 7 are presented, for deep insight into the reliability of predictions based on the present fits.

**Table 3.** Spectroscopic Constants of  $^{13}\text{C}$  Species of iso-propyl Cyanide Obtained from the Global Fits of Microwave and Millimeter Wave Data

Constant/Unit	$^{13}\text{C}(1)^a$	$^{13}\text{C}(2)^a$	$^{13}\text{C}(3)$ or $^{13}\text{C}(4)^a$
A/MHz	7939.346 (55) <sup>a</sup>	7922.258 (74)	7747.2999 (39)
B/MHz	3939.11746 (98)	3956.54960 (90)	3927.9414 (10)
C/MHz	2885.73189 (64)	2897.61731 (68)	2854.36709 (38)
D <sub>J</sub> /kHz	0.60667(43)	0.60171 (48)	0.5878 (15)
D <sub>JK</sub> /kHz	12.239 (30)	12.368 (51)	11.910 (52)
D <sub>K</sub> /kHz	-5.2110 <sup>b</sup>	-5.2110 <sup>b</sup>	-5.2110 <sup>b</sup>
d <sub>1</sub> /kHz	-0.244012 <sup>b</sup>	-0.244012 <sup>b</sup>	-0.244012 <sup>b</sup>
d <sub>2</sub> /kHz	-0.1893655 <sup>b</sup>	-0.1893655 <sup>b</sup>	-0.19198 (87)
$\chi_{aa}$ /MHz	-3.9331 (56)	-3.9492 (49)	-3.9253 (62)
$\chi_{bb}$ /MHz	2.1043 (85)	2.1315 (75)	2.1034 (84)
$\chi_{cc}$ /MHz	1.8288 (85)	1.8177 (75)	1.8219 (84)
$J_{\min} / J_{\max}$	0/33	0/31	0/36
$K_{a,\min} / K_{a,\max}$	0/3	0/2	0/4
$N_{\text{lines}}^c$	45	28	60
$\sigma_{\text{fit}}^d$ /MHz	0.022	0.017	0.026

<sup>a</sup> The numbers in parentheses are  $1\sigma$  (67% confidence level) uncertainties in units of the last decimal digit.

<sup>b</sup> Fixed to the parent species value.

<sup>c</sup> Number of distinct frequency lines in the fit.

<sup>d</sup> Root mean square deviation of the fit.

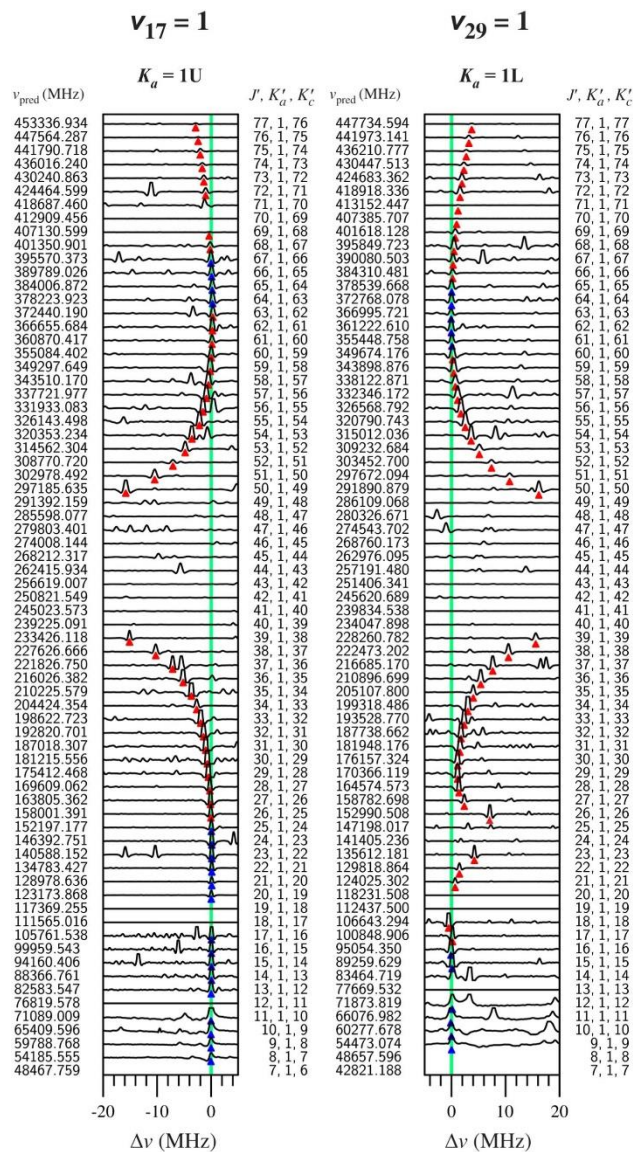


**Figure 5.** Loomis–Wood-type plot where sections of the experimental spectrum are plotted around the predicted positions (green vertical line, initial single-state fits) of the  $K_a = 1U$  sequence in  $v_{17} = 1$  and of  $K_a = 1L$  in  $v_{29} = 1$ . The predicted frequencies  $\nu_{\text{pred}}$  and the upper level rotational quantum numbers  $J'$ ,  $K'_a$ ,  $K'_c$  are indicated on the left and right side of each plot, respectively. A frequency distance from  $\nu_{\text{pred}}$  is given by  $\Delta\nu$ . Letters L and U distinguish between the lower and upper frequency components for the same value of  $K_a$  fulfilling the selection rules  $K_a + K_c = J + 1$  and  $K_a + K_c = J$ , respectively. The red triangles identify transitions with anomalous deviations from the predicted positions.

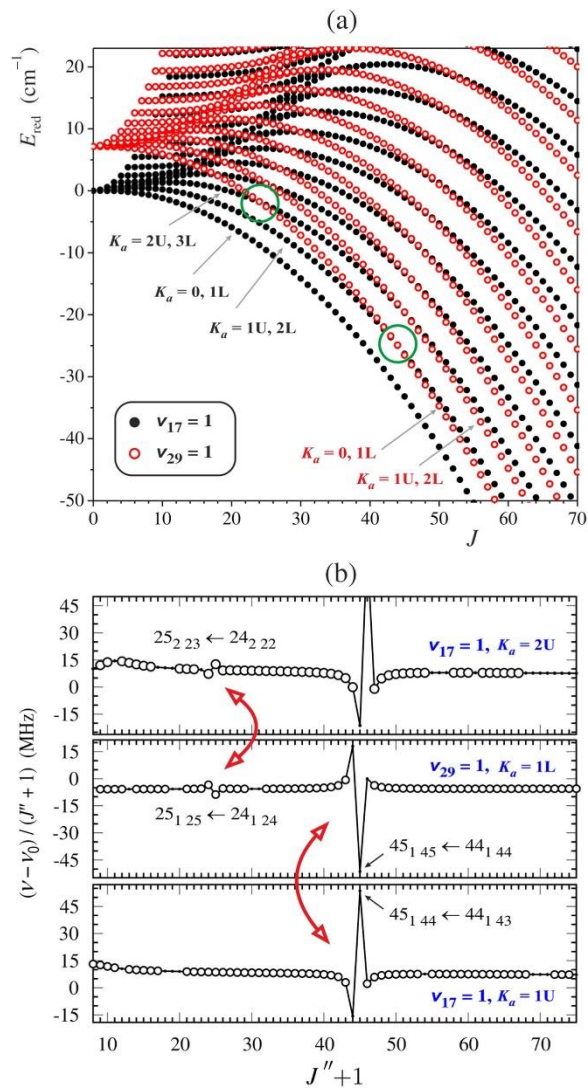


**Figure 6.** (a) Reduced energy level diagram for interacting  $v_{17} = 1$  and  $v_{29} = 1$  states. The reduced energies are calculated as  $E_{\text{red}} = E - E_{17} - J(J + 1)(B + C) / 2$ . The resonances at  $J = 24$  and  $44$  that are responsible for the perturbation maxima of  $K_a = 1$  transitions at  $J' = 25$  and  $J' = 45$  shown in Figure 5 are highlighted by the green circles. Resonances taking place for several adjacent  $K_a$  can be followed in the diagram. (b) Examples of perturbations in a-type R-branch transitions of  $v_{17} = 1$  and  $v_{29} = 1$  states visualized as scaled differences between the frequency of a transition in a given vibrational state and that of the same transition in the ground state vs.  $J'' + 1$ . The circles represent experimentally measured transitions and the continuous lines are predictions from the final fit. The quantum numbers of transitions involved in perturbation maxima are provided.

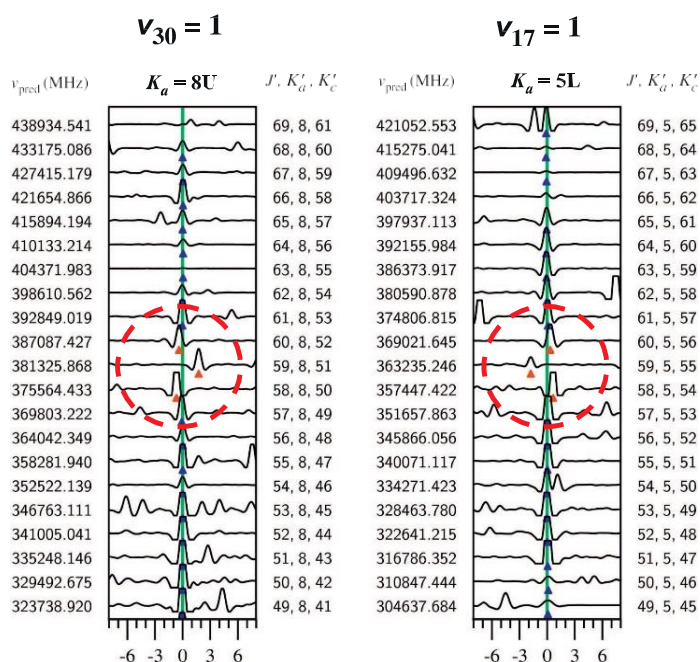


**Figure 7.** Perturbations observed in the Loomis–Wood-type plots for the  $K_a = 8U$  and  $K_a = 5L$  sequences of the  $v_{30} = 1$  and  $v_{17} = 1$ , respectively. The red triangles identify transitions with anomalous deviations from the predicted positions. It can be seen that the most perturbed transitions,  $59_{8\ 51} \leftarrow 58_{8\ 50}$  of  $v_{30} = 1$  and  $59_{5\ 55} \leftarrow 58_{5\ 54}$  of  $v_{17} = 1$ , are shifted by  $+1.77$  and  $-1.76$  MHz, respectively, from their predicted frequencies.

More than 1600 transition lines were measured in the higher energy  $v_{16} = 1$  state. This state has been found to be free of interactions and its spectroscopic constants, given in the last column of Table 2, show an excellent correspondence with those for the ground state.

### 3.3.2. Excited States above $300\text{ cm}^{-1}$

A plethora of excited vibrational states above  $300\text{ cm}^{-1}$  is apparent in Figure 3(d). A multitude of perturbations observed in the rotational spectra of these states obviously results from the proximity of individual vibrational energy levels and brings significant difficulties into their laboratory analysis. Simultaneous analysis of more than two states is generally far from trivial, as many coupling terms should be considered. Furthermore, it does not have to necessarily lead to a global solution with all perturbations taken into account.<sup>18</sup> Therefore, a new approach has been adopted in this work to provide a list of experimental frequencies in these states for astrophysical purposes. First, all measured transitions were submitted to a semi-rigid rotor analysis with centrifugal distortion constants up to the sixth-order terms. Only those that supported this treatment were retained and the obtained spectroscopic constants are summarized in Table 5. The measured frequencies can be found in Table 4. At this point, the deviation trends observed

in the Loomis–Wood type plots for  $v_{15} = 1$ ,  $v_{30} = 2$ , ( $v_{30} = 1$ ,  $v_{17} = 1$ ), ( $v_{30} = 1$ ,  $v_{29} = 1$ ), ( $v_{30} = 1$ ,  $v_{16} = 1$ ), ( $v_{17} = 1$ ,  $v_{15} = 1$ ),  $v_{30} = 2$ ,  $v_{30} = 3$ ,  $v_a$ ,  $v_b$ ,  $v_c$ ,  $v_d$ ,  $v_e$ ,  $v_f$ , and  $v_g$  states, like those in Figure 5, were advantageously followed to measure the frequencies of transitions that could not be encompassed in the semi-rigid rotor fits. The 70 images provided in the figure set show the assignment of these perturbed lines whose frequencies are collected in Table 4. At the same time, these images can serve as a handy tool to check the reliability of predictions using the constants from Table 5.

**Table 4.** List of the Measured Transitions in the Ground and 19 Excited Vibrational States, Three  $^{13}\text{C}$  and  $^{15}\text{N}$  Isotopologues, and the Monohydrate of Iso-propyl Cyanide

Specie	$J'$	$K'_a$	$K'_c$	$F'$	$J''$	$K''_a$	$K''_c$	$F''$	$\nu_{\text{obs}}$ (MHz) <sup>a</sup>	$u_{\text{obs}}$ (MHz) <sup>b</sup>	$\nu_{\text{obs}} - \nu_{\text{calc}}$ (MHz) <sup>c</sup>	Comment <sup>d</sup>
G.S.	2	1	1	2	1	1	0	1		0.010	-0.005	(1)
G.S.	19	3	16	...	18	3	15	...	12683	0.030	0.018	(2)
$^{13}\text{C}(1)$	2	1	1	2	1	1	0	1		0.010	0.005	(1,3)
i-PrCN–H <sub>2</sub> O	2	1	2	2	1	1	1	1		0.010	-0.004	(1)
$v_{30} = 1$	15	5	13	...	17	5	12	...	13313	0.030	0.013	(2)
( $v_{30} = 1$ , $v_{17} = 1$ )	25	2	23	...	24	2	22	...	15682	0.050	...	(4)
( $v_{30} = 1$ , $v_{29} = 1$ )	31	0	31	...	30	0	30	...	18187	0.050	...	(4)
$v_{15} = 1$	19	6	14	...	18	6	13	...	13430	0.050	-0.008	(5)
$v_{30} = 2$	23	8	15	...	22	8	14	...	16934	0.050	0.024	(5)

<sup>a</sup> Observed frequency.

<sup>b</sup> Uncertainty of the observed frequency.

<sup>c</sup> Observed minus calculated frequency.

<sup>d</sup> (1) Transition used to fit the constants from Table 1. (2) Transition used to fit the constants from Table 2. (3) Transition used to fit the constants from Table 3. (4) Perturbed transition, measured using the Loomis–Wood type plots. (5) Transition used to fit the constants from Table 5.

## 4. CONCLUSIONS

---

Equipped with the frequency and time-domain microwave, millimeter, and submillimeter wave techniques, a comprehensive rotational study of interstellar *i*-PrCN is reported. The almost 10,000 new lines for the ground state and 19 vibrationally excited states were assigned and measured. Several excited vibrational states of normal-propyl cyanide have been recently detected in the hot molecular core Sgr B2(N2) by Müller et al. (2016)<sup>29</sup> and *i*-PrCN seems to be a logical molecule to be searched for in excited vibrational states in the future when more sensitive observations are available. Due to the number and complexity of perturbations observed in the rotational spectra of *i*-PrCN, any extrapolation outside the experimentally analyzed region reported in this work (up to 480 GHz) is not recommended. All transitions to be used for interstellar identifications of excited vibrational states should be checked against experimentally measured frequencies. Those collected in this work, along with the extensive graphical material composed of Loomis–Wood type plots, constitute a solid base for such searches of *i*-PrCN.

Electronically available material at <https://doi.org/10.3847/1538-4365/aa9614>

**Table 5.** Spectroscopic Constants of iso-propyl Cyanide in Excited Vibrational States above 300 cm<sup>-1</sup> (S-reduction, I'-representation)

Constant/Unit	$\nu_{15} = 1$	$\nu_{30} = 2$	$(\nu_{30} = 1, \nu_{17} = 1)$	$(\nu_{30} = 1, \nu_{29} = 1)$	$(\nu_{30} = 1, \nu_{16} = 1)$	$\nu_{29} = 2$	$(\nu_{17} = 1, \nu_{15} = 1)$	$\nu_{30} = 3$
A/MHz	7928.4535 (52)	7853.1373 (58)	7945.6999 (89)	7879.382 (25)	7875.0540 (40)	7926.879 (24)	7987.362 (41)	7814.43 (19)
B/MHz	3978.71720 (48)	3991.94241 (48)	3983.3711 (27)	3976.6839 (57)	3981.96710 (48)	3963.9250 (30)	3982.1610 (22)	4003.076 (37)
C/MHz	2900.51184 (22)	2898.59970 (33)	2903.42410 (45)	2896.9684 (17)	2901.57367 (21)	2896.3670 (33)	2904.3498 (14)	2897.34181 (74)
D <sub>J</sub> /kHz	0.60641 (25)	0.65186 (30)	0.6447 (41)	0.6238 (15)	0.63248 (18)	0.5762 (45)	0.501 (12)	0.57561 (18)
D <sub>JK</sub> /kHz	12.2641 (19)	10.8195 (32)	13.211 (17)	10.06 (15)	11.3220 (21)	10.455 (89)	16.35 (39)	11.422 (67)
D <sub>K</sub> /kHz	-5.008 (46)	-9.217 (48)	-5.2110 <sup>b</sup>	-5.2110 <sup>b</sup>	-8.297 (22)	-5.2110 <sup>b</sup>	-5.2110 <sup>b</sup>	-5.2110 <sup>b</sup>
d <sub>1</sub> /kHz	-0.24861 (15)	-0.26720 (10)	-0.2569 (26)	-0.2554 (51)	-0.25355 (12)	-0.2490 (26)	-0.244012 <sup>b</sup>	-0.244012 <sup>b</sup>
d <sub>2</sub> /kHz	-0.192615 (74)	-0.17851 (13)	-0.19103 (80)	-0.1823 (35)	-0.175590 (65)	-0.1750 (20)	-0.2450 (62)	-0.1893655 <sup>b</sup>
H <sub>J</sub> /Hz	...	...	...	...	-0.000770 (35)	...	...	...
H <sub>JK</sub> /Hz	-0.00620 (72)	0.0229 (19)	0.1739 (38)	-0.315 (18)	0.0334 (12)	...	...	...
H <sub>KJ</sub> /Hz	...	...	...	...	-0.1048 (68)	...	...	...
h <sub>2</sub> /Hz	...	...	...	...	0.000538 (17)	...	...	...
J <sub>min</sub> J <sub>max</sub>	6/58	6/55	6/76	6/63	6/73	7/21	7/30	9/60
K <sub>a,min</sub> K <sub>a,max</sub>	0/15	0/12	0/10	0/7	0/20	0/5	0/3	0/3
N <sub>lines</sub> <sup>c</sup>	347	328	134	69	471	38	42	39
S <sub>fit</sub> <sup>d</sup> /MHz					0.044	0.054	0.051	0.058

Constant/Unit	$\nu_a^e$	$\nu_b$	$\nu_c^e$	$\nu_d^e$	$\nu_e$	$\nu_f$	$\nu_g$	...
A/MHz	7825.724 (24)	7850.8 (42)	7897.203 (16)	8004.7 (74)	7913.0 (17)	8232 (51)	8253 (37)	...
B/MHz	3988.3186 (78)	3990.15 (90)	3994.8264 (37)	3982.2 (15)	3989.92 (38)	3918.8 (99)	3910.1 (71)	...
C/MHz	2895.6314 (25)	2899.3606 (80)	2902.04945 (94)	2906.7259 (13)	2899.93088 (77)	2900.9983 (15)	2902.0714 (12)	...
D <sub>J</sub> /kHz	0.550 (14)	0.6319 (34)	0.6501 (96)	0.72132 (80)	0.60019 (40)	0.609971 <sup>b</sup>	0.609971 <sup>b</sup>	...
D <sub>JK</sub> /kHz	9.51 (18)	12.176382 <sup>b</sup>	12.92 (14)	12.176382 <sup>b</sup>	12.224 (25)	12.176382 <sup>b</sup>	12.176382 <sup>b</sup>	...
D <sub>K</sub> /kHz	-5.2110 <sup>b</sup>	-5.2110 <sup>b</sup>	-5.2110 <sup>b</sup>	-5.2110 <sup>b</sup>	-5.2110 <sup>b</sup>	-5.2110 <sup>b</sup>	-5.2110 <sup>b</sup>	...
d <sub>1</sub> /kHz	-0.2072 (86)	-0.244012 <sup>b</sup>	-0.2693 (45)	-0.2490 (26)	-0.244012 <sup>b</sup>	-0.244012 <sup>b</sup>	-0.244012 <sup>b</sup>	...
d <sub>2</sub> /kHz	-0.1508 (42)	-0.1893655 <sup>b</sup>	-0.1922 (22)	-0.1750 (20)	-0.1893655 <sup>b</sup>	-0.1893655 <sup>b</sup>	-0.1893655 <sup>b</sup>	...
J <sub>min</sub> J <sub>max</sub>	7/18	8/28	7/28	14/33	13/40	23/35	23/35	...
K <sub>a,min</sub> K <sub>a,max</sub>	0/5	0/1	0/5	0/3	0/3	0/2	0/2	...
N <sub>lines</sub> <sup>d</sup>	30	18	53	22	43	16	17	...
S <sub>fit</sub> <sup>e</sup> /MHz	0.055	0.089	0.046	0.048	0.042	0.121	0.082	...

<sup>a</sup> The numbers in parentheses are 1 $\sigma$  uncertainties in units of the last decimal digit.

<sup>b</sup> Fixed to the ground-state value.

<sup>c</sup> Number of distinct frequency lines in the fit.

<sup>d</sup> Root mean square deviation of the fit.

<sup>e</sup>  $\nu_a$ ,  $\nu_c$ , and  $\nu_d$  satellites could be tentatively assigned to  $\nu_{14} = 1$ , ( $\nu_{30} = 2$ ,  $\nu_{17} = 1$ ), and  $\nu_{17} = 2$  states, respectively.

## 5. REFERENCES

---

- <sup>1</sup> Solomon, P. M., Jefferts, K. B., Penzias, A. A., & Wilson, R. W. 1971, *ApJL*, 168, L107
- <sup>2</sup> Johnson, D. R., Lovas, F. J., Gottlieb, C. A., et al. 1977, *ApJ*, 218, 370
- <sup>3</sup> Belloche, A., Garrod, R. T., Müller, H. S. P., et al. 2009, *A&A*, 499, 215
- <sup>4</sup> Belloche, A., Garrod, R. T., Müller, H. S. P., & Menten, K. M. 2014, *Sci*, 345, 1584
- <sup>5</sup> Cronin, J., & Pizzarello, S. 1983, *AdSpR*, 3, 5
- <sup>6</sup> Brown, G. G., Dian, B. C., Douglass, K. O., et al. 2008, *RScI*, 79, 053103
- <sup>7</sup> Mata, S., Pena, I., Cabezas, C., López, J., & Alonso, J. 2012, *JMoSp*, 280, 91
- <sup>8</sup> Kolesníková, L., Alonso, E. R., Mata, S., & Alonso, J. L. 2017, *ApJS*, 229, 26
- <sup>9</sup> Daly, A., Kolesníková, L., Mata, S., & Alonso, J. 2014, *JMoSp*, 306, 11
- <sup>10</sup> Müller, H. S. P., Coutens, A., Walters, A., Grabow, J.-U., & Schlemmer, S. 2011, *JMoSp*, 267, 100
- <sup>11</sup> Herberich, G. 1967, *ZNatA*, 22, 543
- <sup>12</sup> Gordy, W., & Cook, R. 1984, *Microwave Molecular Spectra, Techniques of Chemistry* (New York: Wiley)
- <sup>13</sup> Kraitchman, J. 1953, *AmJPh*, 21, 17
- <sup>14</sup> Frisch, M. J., Trucks, G. W., Schlegel, H. B., et al. 2009, *Gaussian 09 Revision E.01*, Gaussian Inc. Wallingford CT 2009
- <sup>15</sup> Tatamitani, Y., Liu, B., Shimada, J., et al. 2002, *JChS*, 124, 2739
- <sup>16</sup> Blanco, S., López, J. C., Lesarri, A., Caminati, W., & Alonso, J. L. 2004, *ChemPhysChem*, 5, 1779
- <sup>17</sup> Cernicharo, J., Kisiel, Z., Tercero, B., et al. 2016, *A&A*, 587, L4
- <sup>18</sup> Daly, A. M., Bermúdez, C., Kolesníková, L., & Alonso, J. L. 2015, *ApJS*, 218, 30
- <sup>19</sup> López, A., Tercero, B., Kisiel, Z., et al. 2014, *A&A*, 572, A44
- <sup>20</sup> Daly, A. M., Bermúdez, C., López, A., et al. 2013, *ApJ*, 768, 81
- <sup>21</sup> Durig, J., & Li, Y. 1974, *JMoSt*, 21, 289
- <sup>22</sup> Kolesníková, L., Alonso, E., Cabezas, C., Mata, S., & Alonso, J. 2016, in *71st Int. Symp. on Molecular Spectroscopy* <http://hdl.handle.net/2142/91343>
- <sup>23</sup> Arenas, B. E., Gruet, S., Steber, A. L., Giuliano, B. M., & Schnell, M. 2017, *PCCP*, 19, 1751
- <sup>24</sup> Neill, J. L., Harris, B. J., Steber, A. L., et al. 2013, *OExpr*, 21, 19743
- <sup>25</sup> Loomis, F. W., & Wood, R. W. 1928, *PhRv*, 32, 223
- <sup>26</sup> Kisiel, Z., Pszczółkowski, L., Medvedev, I. R., et al. 2005, *JMoSp*, 233, 231
- <sup>27</sup> Watson, J. K. G. 1977, in *Vibrational Spectra and Structure*, Vol. 6, ed. J. R. Durig (Amsterdam: Elsevier), 1
- <sup>28</sup> Pickett, H. M. 1991, *JMoSp*, 148, 371
- <sup>29</sup> Müller, H. S. P., Walters, A., Wehres, N., et al. 2016, *A&A*, 595, A87





# CHAPTER XI.

## Rotational Spectra in 29 Vibrationally Excited States of Interstellar Aminoacetonitrile.

---

*Adapted from: Astrophysical Journal Supplement Series, 2017, 229:26 (8pp)*

*We report a detailed spectroscopic investigation of the interstellar aminoacetonitrile, a possible precursor molecule of glycine. Using a combination of Stark and frequency-modulation microwave and millimeter wave spectroscopies, we observed and analyzed the room-temperature rotational spectra of 29 excited states with energies up to  $1000\text{ cm}^{-1}$ . We also observed the  $^{13}\text{C}$  isotopologues in the ground vibrational state in natural abundance (1.1%).*



## 1. INTRODUCTION

---

The number of unidentified lines in the millimeter and submillimeter wave surveys of the interstellar medium has grown rapidly. The major contributions are due to rotational transitions in excited vibrational states of a relatively few molecules that are called the astrophysical weeds.<sup>1,2</sup> To address this problem, assignments and analyses of rotational spectra in the low-lying vibrational states of not yet identified astrophysical species are needed. The necessary data to deal with spectral lines from astrophysical weeds species can be obtained from detailed laboratory rotational measurements in the microwave and millimeter wave region.

One of the interstellar molecules to be considered is aminoacetonitrile, which has received a particular amount attention due to its implication in chemical synthesis of the smallest amino acid, glycine.<sup>3,4</sup> First detection of aminoacetonitrile was based on more than 80 ground vibrational state transitions in the line survey of the hot core of massive star-forming region Sgr B2(N),<sup>5</sup> where molecules with  $\text{-NH}_2$  and/or  $\text{-CN}$  groups are abundant. This region is well known for the elevated temperature of the gas, which suggests that a considerable part of the observed lines belong to rotational transitions in excited vibrational states. Indeed, a large amount of emission lines coming from the excited vibrational states were detected in Sgr B2.<sup>6</sup> While the ground-state rotational spectra of aminoacetonitrile and its amino deuterated isotopologues are well characterized from the microwave up to the THz frequency region,<sup>7,8,9,10,11</sup> the spectroscopic data in excited vibrational states are missing. Neither rotational spectra of  $^{13}\text{C}$  isotopic species have been reported to date. Therefore, the key to success in future astrophysical identification of more lines of aminoacetonitrile lies in new laboratory assignments and measurements for direct comparison of laboratory frequencies with those from astrophysical weeds.

In the present work, new spectroscopic measurements and analysis of aminoacetonitrile have been performed in frequency ranges 26–40 GHz, 75–115 GHz, and 170–240 GHz. Stark

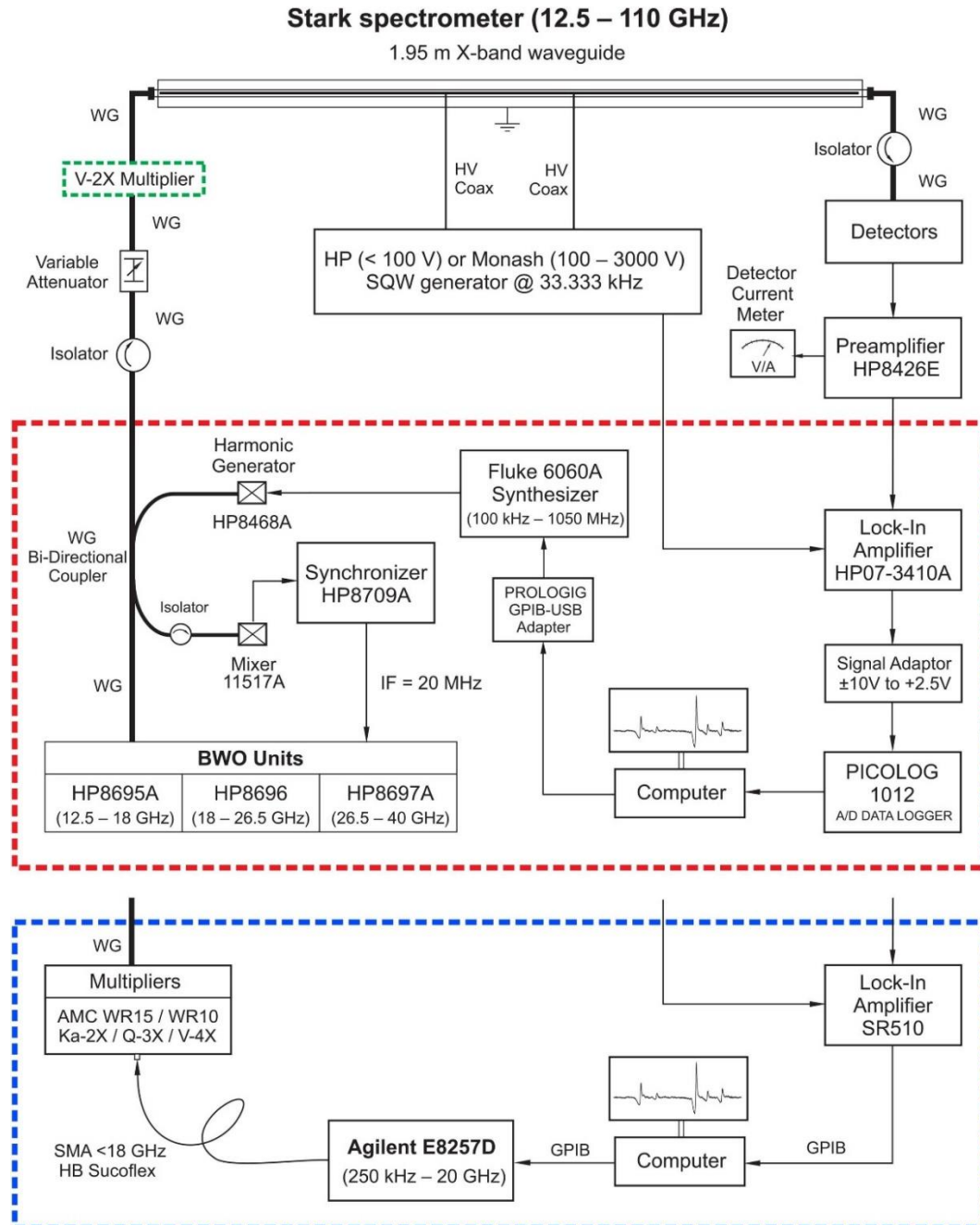
modulation microwave and frequency-modulation millimeter wave spectroscopies made it possible to identify the pure rotational transitions of 29 different excited vibrational states belonging to fundamentals, overtones, and combination states of the low-frequency torsional and bending modes. Such a large number of excited vibrational states has never been analyzed in any other observed interstellar molecule. In addition, ground state rotational transitions of two  $^{13}\text{C}$  isotopic species were measured in their natural abundances. More than 2000 new lines are reported, which should facilitate astronomers' further observations of aminoacetonitrile in the interstellar medium.

## 2. EXPERIMENTAL DETAILS

---

Stark-modulation microwave and millimeter wave spectroscopies results were fundamental in the analysis of the rotational spectra of aminoacetonitrile in excited vibrational states. A scheme of our upgraded Stark-modulation spectrometer used in the present investigation is shown in Figure 1. The spectrometer covers the frequency range from 12 to 110 GHz using either backward wave oscillators (BWOs) or an Agilent synthesizer as microwave sources. In the first case, three BWOs are available, providing the following frequency outputs: 12.5–18GHz, 18–26.5GHz, and 26.5–40 GHz (see Figure 1). The frequency stabilization of the BWOs is achieved by means of a phase-lock loop using an external frequency synthesizer, harmonic mixer, and signal synchronizer with a constant IF of 20MHz. The signal from stabilized BWOs enters directly the 1.95m long X-band waveguide or an additional passive multiplier V-2X (Spacek Labs) can be implemented to double the output of the highest-frequency BWO (see Figure 1). In the second case, an Agilent synthesizer (250 kHz–20 GHz) is used to drive the amplifier-multiplier chains WR15 and WR10 (VDI, Inc.) with multiplication factors of four and six to reach the frequency ranges of 50–75GHz and 75–110 GHz, respectively. Another option is to connect passive multipliers Ka-2X, Q-3X, and V-4X (Spacek Labs) that allow us to record the spectra in the 26–40GHz, 33–50GHz, and 50–75GHz regions, respectively. Modulation voltages up to 3000 V with a 33.3 kHz modulation frequency can be applied to the septum

of the waveguide. A Stark-modulated signal is detected by solid-state zero-bias Schottky-diode detectors (50–110 GHz) or HP crystal detectors (12.5–50GHz), pre-amplified and send to a lock-in amplifier where the phase-sensitive detection is applied.



The frequency-modulation millimeter wave spectrometer was described elsewhere<sup>12</sup> and was used to record the spectra from 75 to 115 and from 170 to 240 GHz. The spectrometer is based on the cascaded multiplication of the synthesizer frequency by a set of active and passive multipliers (VDI, Inc.) and in this case the harmonic multiplication factors of 6 and  $12 = 6 \times 2$  were applied. In the lower-frequency region, detection was made with Schottky-diode detectors (VDI, Inc.) after two passes of radiation through the cell. The rotational spectra above 170 GHz were collected using a quasioptical detector (VDI, Inc.) at a single pass configuration (see ref. 14 for details). The synthesizer output was frequency modulated at  $f = 10.2$  kHz and the modulation depth was between 20 and 40 kHz. A second derivative shape of the lines resulting from  $2f$  detection was fitted to the Gaussian profile function and the uncertainty of the line center frequency was estimated to be better than 50 kHz.

The sample of liquid aminoacetonitrile was obtained commercially and was used without any further purification. Rotational spectra were recorded at room temperature and a pressure of approximately 15  $\mu$ bar.

### 3. ROTATIONAL SPECTRA AND ANALYSIS

---

Aminoacetonitrile is a near prolate asymmetric top ( $k = -0.96$ ) with a  $C_s$  symmetry and two non-zero dipole moment components of  $|\mu_a| = 2.577(7)$  D and  $|\mu_b| = 0.5754(10)$  D<sup>8</sup>. A large  $\mu_a$  component is responsible for the intense a-type R-branch transitions that clearly dominate the room-temperature rotational spectrum. These transitions are interspersed by significantly weaker, but still observable, b-type R-branch and Q-branch transitions.

Around each ground-state line, many satellite lines attributable to pure rotational transitions in excited vibrational states were easily observed, as shown in Figure 2 for the  $4_{13} \leftarrow 3_{12}$  transition. Stark-modulation spectroscopy constitutes a definitive tool in the identification of rotational transitions in excited vibrational states.<sup>13,14,15,16,17</sup> When a molecule is exposed to both microwave radiation

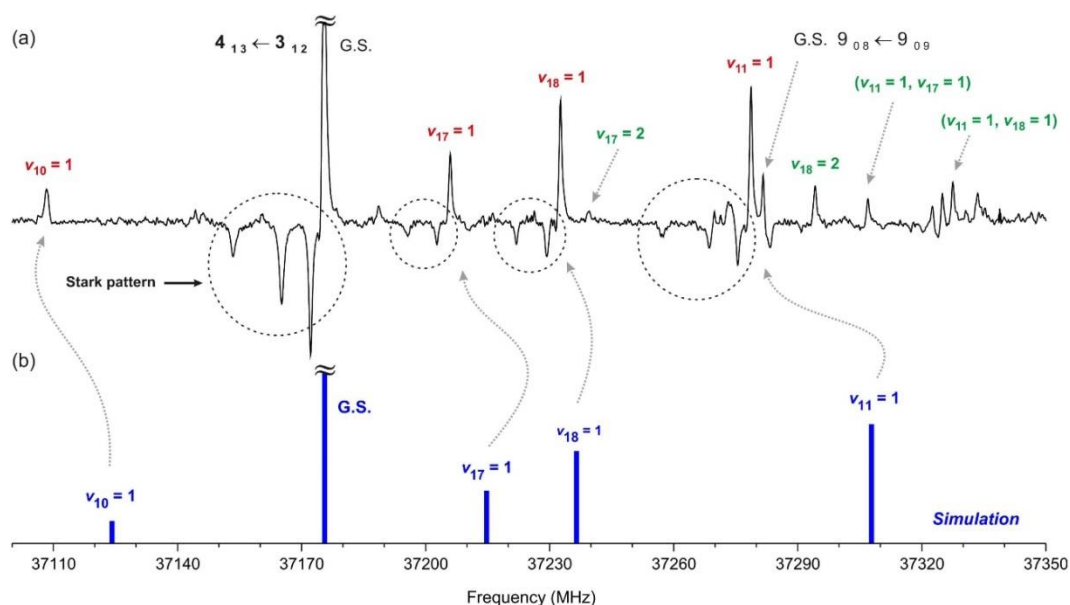


**Figure 2.** (a) Section of the Stark spectrum of aminoacetonitrile at room temperature showing the satellite pattern for the  $4_{13} \leftarrow 3_{12}$  transition. Stark components appear as narrow lobes oriented down on the left side of the unperturbed zero-field lines, which are oriented up. (b) Modeled spectrum based on the ab initio calculations. Intensities are estimated using the Boltzmann population ratio at 298.15 K.

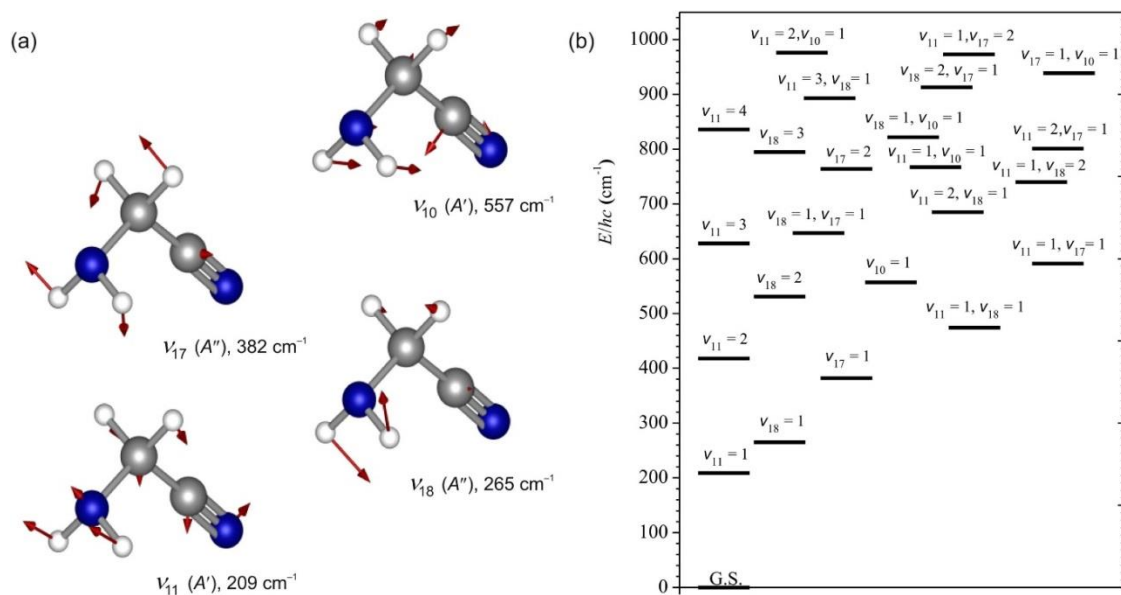


**Figure 3.** (a) Schematic visualization of four lowest frequency normal vibrational modes of aminoacetonitrile  $\nu_{11}$ ,  $\nu_{18}$ ,  $\nu_{17}$ , and  $\nu_{10}$  obtained from ab initio calculations. (b) Diagram of vibrational energy levels predicted below 1000  $\text{cm}^{-1}$  resulting from the four lowest frequency vibrational modes.

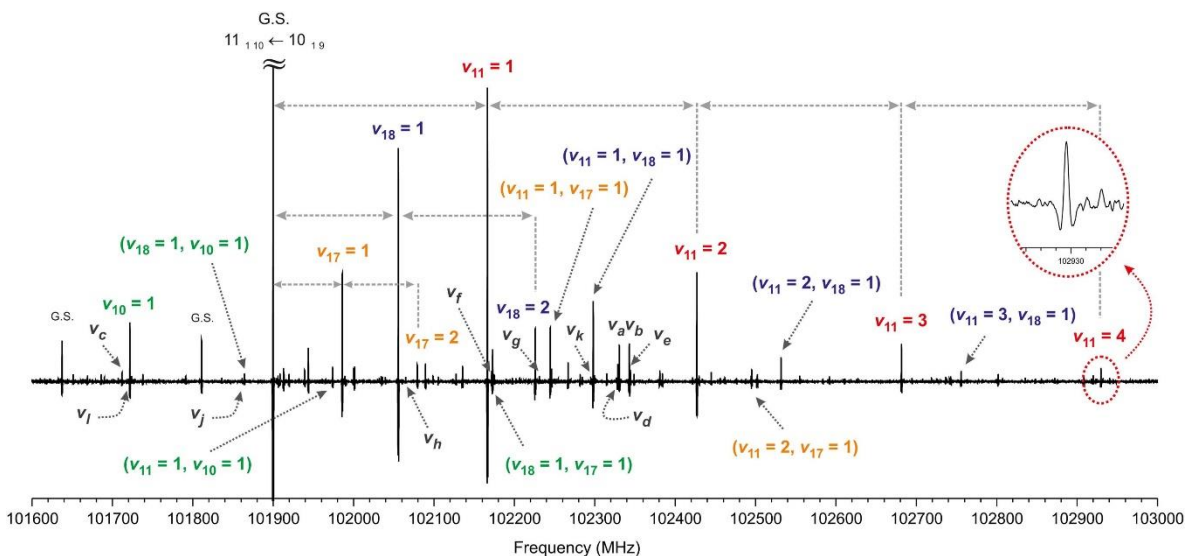


**Figure 4.** Section of 1.5 GHz of the millimeter wave spectrum of aminoacetonitrile, which illustrate assignments of many different vibrational satellites around the ground-state  $11_{1,10} \leftarrow 10_{1,9}$  transition. Almost equidistant behavior of transition frequencies in  $v_{11} = 1, 2, 3, 4$ ,  $v_{17} = 1, 2$ , and  $v_{18} = 1, 2$  sequences as well as in combination states  $(v_{11} = 1, v_{18} = 1)$ ,  $(v_{11} = 2, v_{18} = 1)$ ,  $(v_{11} = 3, v_{18} = 1)$  and  $(v_{11} = 1, v_{17} = 1)$ ,  $(v_{11} = 2, v_{17} = 1)$  is evident. Excellent signal-to-noise ratio is demonstrated on the transition in  $v_{11} = 4$ , which is expected to be located above  $800 \text{ cm}^{-1}$ .

and a square-wave modulation electric field, Stark negative lobes shifted with respect to the unperturbed line are observed in the spectrum. As shown in Figure 2(a), those satellite lines having the same pattern (circled in Figure 2(a)) as the ground-state line can be assigned to the same rotational transition in an excited vibrational state. For the vibrational assignment of these satellite lines, harmonic frequencies of the four lowest vibrational modes of aminoacetonitrile  $v_{11}$  ( $A'$ ),  $v_{18}$  ( $A''$ ),  $v_{17}$  ( $A''$ ), and  $v_{10}$  ( $A'$ ) associated with C–C≡N bending,  $\text{NH}_2$ -torsion,  $\text{NH}_2$ - $\text{CH}_2$ -torsion, and N–C–C bending motions were calculated at the MP2/6-311++G(d,p) level of the theory (Gaussian09 package)<sup>18</sup>. Harmonic frequencies together with normal coordinate displacement vectors are shown in Figure 3(a). The vibrational satellite pattern was modeled on the basis of the estimated changes of rotational constants relative to the ground-state values. This was done using the ab initio calculated first-order vibration-rotation constants  $a_i$  that define the well-known vibrational dependence of rotational constants  $B_v = B_e - \sum_i \alpha_i (v_i + 1/2)$ , where  $B_v$  and  $B_e$  substitute all three rotational constants in a given excited state and in equilibrium, respectively.  $v_i$  is the vibrational quantum number of the  $i$ th vibrational mode. The modeled pattern is shown in



Figure 2(b). The good matching in positions and intensities along with a similar Stark pattern constitute conclusive proof in the identification of rotational transitions in  $v_{11}=1$ ,  $v_{18}=1$ ,  $v_{17}=1$ , and  $v_{10}=1$  excited states. Second excited states  $v_{18}=2$  and  $v_{17}=2$  were then readily found. Finally, combination states ( $v_{11}=1$ ,  $v_{18}=1$ ) and ( $v_{11}=1$ ,  $v_{17}=1$ ) were also identified by means of linear combinations of corresponding changes in their rotational constants. A total of eight excited vibrational states were characterized in Stark spectra. These constitute only a part of the plethora of vibrational states produced by the four low-lying modes, as shown in the manifold of levels in Figure 3(b).

On this basis, in a next step of the investigation, the millimeter wave spectrum between 75 and 240 GHz was recorded. As shown in Figure 4 for the  $11_{1,10} \leftarrow 10_{1,9}$  transition, a very rich satellite pattern was also observed. After a straightforward transfer of the line assignment from the Stark spectra to this higher frequency region, additional satellite lines  $v_{11} = 2, 3, 4$  belonging to successive excitations of the lowest frequency mode  $v_{11}$  ( $A'$ ) were easily assigned. In the absence of serious perturbations, such progressions are expected to show almost equidistant behavior of transition frequencies, which is shown in Figure 4 for the  $v_{11}$  ( $A'$ ),  $v_{18}$  ( $A''$ ), and  $v_{17}$  ( $A''$ ) low-frequency modes. Similar behavior allowed the identification of the combination states progressions ( $v_{11} = 1$ ,  $v_{18} = 1$ ), ( $v_{11} = 2$ ,  $v_{18} = 1$ ), ( $v_{11} = 3$ ,  $v_{18} = 1$ ) and ( $v_{11} = 1$ ,  $v_{17} = 1$ ), ( $v_{11} = 2$ ,  $v_{17} = 1$ ). Additional ( $v_{18} = 1$ ,  $v_{17} = 1$ ), ( $v_{18} = 1$ ,  $v_{10} = 1$ ), and ( $v_{11} = 1$ ,  $v_{10} = 1$ ) combination states could be also extracted from the records leading to 17 excited states found.

Pursuing the detailed analysis, assignments of rotational transitions in another 12 excited states were achieved. These new excited states were labeled as  $v_a, v_b, \dots, v_l$ . These states might be attributable to the remaining unassigned states depicted in Figure 3(b) or even to states above  $1000 \text{ cm}^{-1}$ . Based on the predicted changes in the values of rotational constants,  $v_c$  and  $v_i$  can be tentatively assigned to first quanta of  $v_{16}$  ( $A''$ ) and  $v_9$  ( $A'$ ) calculated at  $904$  and  $855 \text{ cm}^{-1}$ , respectively. Other plausible assignments are collected in Table 3.

All of the measured rotational transitions for each of the  $v_{17} = 1$ , and  $v_{10} = 1$  excited states. Second excited states 29 excited vibrational states were analyzed using the standard Watson's S-reduced Hamiltonian<sup>19</sup> in I' representation given by

$$\begin{aligned}
 H_{ROT}^{(v)} = & A J_a^2 + B J_c^2 + C J_c^2 + D_J J^4 + D_{JK} J^2 J_a^2 - D_K J_a^4 \\
 & + d_1 J^2 (J_+^2 + J_-^2) + d_2 (J_+^4 + J_-^4) + H_J J^6 + H_{JK} J^4 J_a^2 \quad (1) \\
 & + H_{JK} J^2 J_a^4 + H_K J_a^6 + h_1 J^4 (J_+^2 + J_-^2) \\
 & + h_2 J^2 (J_+^4 + J_-^4) + h_3 (J_+^6 + J_-^6)
 \end{aligned}$$

where A, B, C are the rotational constants,  $D_{J,K}$   $d_2$  are quartic, and  $H_{J,K}$   $h_3$  are sextic centrifugal distortion constants. The need for the sixth order terms depends on the excited states data sets. Resulting spectroscopic constants for the first and higher excited states of four lowest normal vibrational modes are given in Table 1, while those for combination states and  $v_a, v_b, \dots v_l$  states are summarized in Tables 2 and 3, respectively.

Experimentally measured frequencies are collected in Table 4. It must be noted that rotational transitions with higher J and  $K_a$  than those given in Tables 1–3 were also observed, however, they could not be treated within the semi-rigid rotor model applied in this work and were not included. Figure 3(b) shows that many states may be involved in mutual interactions as a result of proximity of their vibrational energy levels. Hence, multiple perturbations in their pure rotational spectra are expected and reflected in departures of the values of their centrifugal distortion constants with respect to those for the unperturbed ground state. Despite this, in the context of future astrophysical observations, the spectroscopic data provided for the most populated excited states are of enough precision to model spectra toward interstellar sources.

**Table 1.** Spectroscopic Constants of Aminoacetonitrile in the First and Higher Successive Excitation States of Four Lowest Frequency Normal Vibrational Modes in Comparison with the Ground State (S-reduction, I<sup>r</sup>-representation)

Constant	Unit	G.S. <sup>a</sup>	$\nu_{11} = 1^b$	$\nu_{18} = 1^b$	$\nu_{17} = 1^b$	$\nu_{10} = 1$
A	MHz	30246.4887 (10) <sup>c</sup>	30018.1544 (62)	30627.7386 (71)	30143.698 (10)	30630.93 (34)
B	MHz	4761.06254 (14)	4776.36759 (43)	4769.29434 (62)	4764.23280 (41)	4752.4590 (23)
C	MHz	4310.74857 (14)	4316.76886 (41)	4314.62273 (64)	4316.43101 (36)	4302.8937 (22)
DJ	kHz	3.06687 (11)	3.06106 (33)	3.03301 (35)	3.06103 (31)	3.04255 (76)
DJK	kHz	-55.2945 (14)	-50.298 (10)	-57.563 (14)	-55.0031 (56)	-55.430 (23)
DK	kHz	714.0755 (78)	558.80 (23)	862.77 (15)	694.86 (39)	714.0755 <sup>d</sup>
d1	kHz	-0.673533 (41)	-0.67563 (27)	-0.67519 (50)	-0.67163 (14)	-0.6723 (16)
d2	kHz	-0.0299382 (96)	-0.019352 (27)	-0.039801 (99)	-0.026261 (49)	-0.0237 (10)
HJK	Hz	-0.12406 (51)	-0.2523 (82)	0.294 (13)	-0.1134 (33)	...
HKJ	Hz	-2.7126 (81)	...	...	-2.643 (12)	...
h1	Hz	0.003872 (15)	0.00434 (13)	0.00225 (27)	0.0038722 <sup>d</sup>	...
$\sigma_{fit}$ <sup>e</sup>	kHz	41	48	46	40	61
<i>N</i> lines <sup>f</sup>	...	...	215	199	226	84
<i>J</i> <sub>min</sub> / <i>J</i> <sub>max</sub>	...	1/74	6/40	8/39	8/37	8/26
<i>K</i> <sub>a,min</sub> / <i>K</i> <sub>a,max</sub>	...	0/23	0/9	0/7	0/16	0/7

Constant	Unit	$\nu_{11} = 2^b$	$\nu_{11} = 3$	$\nu_{11} = 4$	$\nu_{18} = 2$	$\nu_{17} = 2$
A	MHz	29785.189 (33)	29547.89 (18)	29303.66 (24)	31262.42 (61)	30114.89 (35)
B	MHz	4791.41661 (67)	4806.2078 (14)	4820.7240 (14)	4778.3864 (51)	4768.0546 (19)
C	MHz	4322.60427 (55)	4328.2472 (12)	4333.7020 (11)	4318.0272 (22)	4321.7582 (10)
DJ	kHz	3.06715 (46)	3.06830 (56)	3.0904 (10)	2.8141 (71)	3.1180 (19)
DJK	kHz	-45.803 (24)	-41.219 (27)	-36.621 (33)	-65.56 (11)	-40.35 (29)
DK	kHz	427.7 (25)	714.0755 <sup>d</sup>	265 (36)	714.0755 <sup>d</sup>	714.0755 <sup>d</sup>
d1	kHz	-0.67189 (25)	-0.67459 (62)	-0.67719 (55)	-0.6696 (53)	-0.7116 (18)
d2	kHz	-0.007874 (59)	-0.00364 (45)	0.01786 (50)	-0.0993 (31)	-0.0439 (13)
HJK	Hz	-0.661 (23)	-1.013 (27)	-1.150 (33)	...	...
$\sigma_{fit}$ <sup>e</sup>	kHz	44	45	40	39	24
<i>N</i> lines <sup>f</sup>	...	149	112	96	33	31
<i>J</i> <sub>min</sub> / <i>J</i> <sub>max</sub>	...	8/32	8/26	7/27	8/25	8/24
<i>K</i> <sub>a,min</sub> / <i>K</i> <sub>a,max</sub>	...	0/8	0/7	0/6	0/4	0/2

<sup>a</sup> From Motoki et al. (2013). Only those constants relevant for comparison with present results are given in this table.

<sup>b</sup> Also weaker b-type R-branch and Q-branch transitions could be observed in this state leading to assignment of *J* > 30 transitions. This explains the better statistical determination of the A rotational constant in comparison with other states.

<sup>c</sup> The numbers in parentheses are 1 $\sigma$  (67% confidence level) uncertainties in units of the last decimal digit.

<sup>d</sup> Fixed to the ground-state value.

<sup>e</sup> Root-mean-square deviation of the fit.

<sup>f</sup> Number of distinct frequency fitted lines in the specified vibrational state.

For completeness, the assignment of such a large amount of vibrational satellites and excellent signal-to-noise ratio observed in our spectra permitted also easy identification of rotational transitions of two <sup>13</sup>C isotopic species in their natural abundances (1.1%). Ground-state rotational transitions of each isotopologue were analyzed in terms of Equation (1) and the obtained spectroscopic constants can be found in Table 5.

## 4. CONCLUSIONS

The high resolution and sensitivity reached with our Stark and frequency-modulation techniques in the microwave and millimeter wave regions allowed us to analyze pure rotational spectra in 29 excited vibrational states of interstellar aminoacetonitrile molecule up to  $1000\text{ cm}^{-1}$  and record the two single substituted  $^{13}\text{C}$  isotopologues in the ground vibrational state in their natural abundance. The precise set of spectroscopic constants reported for the lowest-lying excited states will support further astrophysical identification of aminoacetonitrile in warmer regions of ISM where vibrationally excited states might be populated.

**Table 2.** Spectroscopic Constants of Aminoacetonitrile in Vibrational Combination States (S-reduction, I'-representation).

Constant	Unit	( $\nu_{11} = 1, \nu_{18} = 1$ )	( $\nu_{11} = 1, \nu_{17} = 1$ )	( $\nu_{18} = 1, \nu_{17} = 1$ )	( $\nu_{11} = 2, \nu_{18} = 1$ )	
A	MHz	30127.57 (27) <sup>a</sup>	29746.70 (40)	30716.61 (34)	29606.21 (28)	<sup>a</sup> The numbers in parentheses are 1 $\sigma$ (67% confidence level) uncertainties in units of the last decimal digit. <sup>b</sup> Fixed to the ground-state value. <sup>c</sup> Root-mean square deviation of the fit. <sup>d</sup> Number of distinct frequency fitted lines in the specified vibrational state.
B	MHz	4783.0510 (23)	4779.1113 (42)	4773.7167 (20)	4796.4049 (16)	
C	MHz	4321.1710 (14)	4322.6864 (35)	4321.6229 (16)	4327.5844 (12)	
D <sub>J</sub>	kHz	3.1536 (13)	3.1486 (51)	2.95524 (76)	3.3006 (11)	
D <sub>JK</sub>	kHz	-48.84 (11)	-48.563 (39)	-59.94 (14)	-33.321 (95)	
D <sub>K</sub>	kHz	714.0755 <sup>b</sup>	714.0755 <sup>b</sup>	714.0755 <sup>b</sup>	714.0755 <sup>b</sup>	
d <sub>1</sub>	kHz	-0.6721 (10)	-0.6785 (73)	-0.6827 (10)	-0.68108 (66)	
d <sub>2</sub>	kHz	0.06556 (48)	0.0297 (26)	-0.07166(68)	0.17549 (64)	
H <sub>JK</sub>	Hz	-3.29 (14)	...	...	-5.44 (22)	
$\sigma_{\text{fit}}^e$	kHz	55	29	59	39	
N <sub>lines</sub> <sup>f</sup>	---	77	35	49	62	
J <sub>min</sub> /J <sub>max</sub>	---	8/27	8/13	8/24	8/24	
K <sub>a,min</sub> /K <sub>a,max</sub>	---	0/4	0/5	0/3	0/4	
Constant	Unit	( $\nu_{11} = 1, \nu_{10} = 1$ )	( $\nu_{11} = 2, \nu_{17} = 1$ )	( $\nu_{18} = 1, \nu_{10} = 1$ )	( $\nu_{11} = 3, \nu_{18} = 1$ )	
A	MHz	29785.189 (33)	29547.89 (18)	29303.66 (24)	31262.42 (61)	<sup>a</sup> The numbers in parentheses are 1 $\sigma$ (67% confidence level) uncertainties in units of the last decimal digit. <sup>b</sup> Fixed to the ground-state value. <sup>c</sup> Root-mean square deviation of the fit. <sup>d</sup> Number of distinct frequency fitted lines in the specified vibrational state.
B	MHz	4791.41661 (67)	4806.2078 (14)	4820.7240 (14)	4778.3864 (51)	
C	MHz	4322.60427 (55)	4328.2472 (12)	4333.7020 (11)	4318.0272 (22)	
D <sub>J</sub>	kHz	3.06715 (46)	3.06830 (56)	3.0904 (10)	2.8141 (71)	
D <sub>JK</sub>	kHz	-45.803 (24)	-41.219 (27)	-36.621 (33)	-65.56 (11)	
D <sub>K</sub>	kHz	427.7 (25)	714.0755 <sup>d</sup>	265 (36)	714.0755 <sup>d</sup>	
d <sub>1</sub>	kHz	-0.67189 (25)	-0.67459 (62)	-0.67719 (55)	-0.6696 (53)	
d <sub>2</sub>	kHz	-0.007874 (59)	-0.00364 (45)	0.01786 (50)	-0.0993 (31)	
H <sub>JK</sub>	Hz	-0.661 (23)	-1.013 (27)	-1.150 (33)	...	
$\sigma_{\text{fit}}^e$	kHz	44	45	40	39	
N <sub>lines</sub> <sup>f</sup>	---	149	112	96	33	
J <sub>min</sub> /J <sub>max</sub>	---	8/32	8/26	7/27	8/25	
K <sub>a,min</sub> /K <sub>a,max</sub>	---	0/8	0/7	0/6	0/4	

**Table 3.** Spectroscopic Constants of Aminoacetonitrile in  $\nu_a, \nu_b, \dots, \nu_l$  States (S-reduction, I<sup>r</sup>-representation)

Constant	Unit	$\nu_a$	$\nu_b$	$\nu_c$ $\nu_{16} = 1^a$	$\nu_d$	$\nu_e$	$\nu_f$
A	MHz	31820.4 (18) <sup>b</sup>	31866.6 (10)	30048.68 (52)	31821.0 (13)	31870.3 (16)	30718.7 (11)
B	MHz	4787.1231 (78)	4787.9626 (58)	4751.4433 (19)	4787.0333 (44)	4788.0336 (49)	4773.6396 (78)
C	MHz	4313.4136 (56)	4313.3046 (39)	4305.1318 (14)	4313.3597 (40)	4313.3158 (45)	4321.602 (15)
DJ	kHz	2.929 (13)	2.9078 (79)	3.2529 (20)	2.8716 (26)	2.8841 (78)	2.9293 (41)
DJK	kHz	-65.4 (50)	-59.1 (24)	-26.96 (46)	-47.46 (51)	-52.6 (24)	-62.56 (57)
DK	kHz	714.0755 <sup>c</sup>	714.0755 <sup>c</sup>	714.0755 <sup>c</sup>	714.0755 <sup>c</sup>	714.0755 <sup>c</sup>	714.0755 <sup>c</sup>
d <sub>1</sub>	kHz	-0.6618 (39)	-0.6665 (22)	-0.7167 (11)	-0.6611 (19)	-0.6655 (21)	-0.7107 (58)
d <sub>2</sub>	kHz	-0.0282 (74)	-0.0439 (47)	0.0794 (33)	-0.0329 (42)	-0.0485 (50)	-0.02999382 <sup>c</sup>
$\sigma_{\text{fit}}^c$	kHz	117	92	34	92	75	99
$N_{\text{lines}}^d$	...	24	32	31	34	24	28
$J_{\text{min}}/J_{\text{max}}$	...	8/25	8/25	8/24	8/27	8/24	8/25
$K_{a,\text{min}}/K_{a,\text{max}}$	...	0/2	0/2	0/2	0/3	0/2	1/3

Constant	Unit	$\nu_g$ $(\nu_{11} = 2, \nu_{10} = 1)^a$	$\nu_h$	$\nu_i$ $\nu_9 = 1^a$	$\nu_j$ $(\nu_{17} = 1, \nu_{10} = 1)^a$	$\nu_k$	$\nu_l$ $(\nu_9 = 1, \nu_{11} = 1)^a$
A	MHz	30119.45 (70)	30075.33 (63)	30440.6 (37)	31011.04 (63)	29232.36 (96)	30078.0 (13)
B	MHz	4781.5021 (19)	4767.0375 (67)	4741.210 (42)	4759.7106 (35)	4780.438 (14)	4751.7783 (44)
C	MHz	4314.9693 (32)	4321.8966 (19)	4298.527 (27)	4306.5701 (36)	4328.9339 (65)	4305.0841 (52)
DJ	kHz	3.0565 (17)	3.134 (10)	2.656 (62)	3.002 (11)	3.619 (13)	3.227 (18)
DJK	kHz	-46.17 (67)	-49.57 (77)	-55.2945 <sup>c</sup>	-55.2945 <sup>c</sup>	-55.2945 <sup>c</sup>	-55.29457 <sup>c</sup>
DK	kHz	714.0755 <sup>c</sup>	714.0755 <sup>c</sup>	714.0755 <sup>c</sup>	714.0755 <sup>c</sup>	714.0755 <sup>c</sup>	714.0755 <sup>c</sup>
d <sub>1</sub>	kHz	-0.6738 (28)	-0.6921 (72)	-0.673533 <sup>c</sup>	-0.673533 <sup>c</sup>	-0.673533 <sup>c</sup>	-0.673533 <sup>c</sup>
d <sub>2</sub>	kHz	-0.0112 (40)	-0.02999382 <sup>c</sup>	-0.02999382 <sup>c</sup>	-0.02999382 <sup>c</sup>	-0.02999382 <sup>c</sup>	-0.02999382 <sup>c</sup>
$\sigma_{\text{fit}}^d$	kHz	28	40	50	40	52	56
$N_{\text{lines}}^e$	...	22	19	9	11	9	11
$J_{\text{min}}/J_{\text{max}}$	...	8/25	8/24	9/13	8/13	8/13	8/13
$K_{a,\text{min}}/K_{a,\text{max}}$	...	0/2	0/2	0/1	0/1	0/1	0/1

<sup>a</sup> Tentative assignment.  
<sup>b</sup> The numbers in parentheses are 1 $\sigma$  (67% confidence level) uncertainties in units of the last decimal digit.  
<sup>c</sup> Fixed to the ground-state value.  
<sup>d</sup> Root-mean square deviation of the fit.  
<sup>e</sup> Number of distinct frequency fitted lines in the specified vibrational state.

**Table 4.** List of the Assigned and Fitted Transitions for 29 Excited Vibrational States of the Parent Species and Ground-state Transitions of two <sup>13</sup>C Isotopologues of Aminoacetonitrile.

Specie	J'	K' <sub>a</sub>	K' <sub>c</sub>	J''	K'' <sub>a</sub>	K'' <sub>c</sub>	$\nu^a$ (MHz)	$\nu^b$ (MHz)	$\nu_{\text{obs}} - \nu_{\text{calc}}^c$ (MHz)
$\nu_{11} = 1$	11	0	11	10	0	10	98724.136	0.050	0.002
$\nu_{11} = 1$	11	1	10	10	1	9	102166.426	0.050	0.019
$\nu_{11} = 1$	10	2	8	9	2	7	91747.168	0.050	0.022
$\nu_{18} = 1$	9	0	9	8	0	8	81053.026	0.050	0.010
$\nu_{18} = 1$	9	1	9	8	1	8	79542.960	0.050	0.018
$\nu_{18} = 1$	9	2	8	8	2	7	81643.932	0.050	0.030

<sup>a</sup> Observed frequency.  
<sup>b</sup> Uncertainty of the observed frequency.  
<sup>c</sup> Observed minus calculated frequency.

**Table 5.** Ground-state Spectroscopic Constants of  $^{13}\text{C}$  Isotopic Species of Aminoacetonitrile (S-reduction, I<sup>r</sup>-representation)

Constant	Unit	$\text{NH}_2^{13}\text{CH}_2\text{CN}$	$\text{NH}_2\text{CH}_2^{13}\text{CN}$
A	MHz	29560.35 (12) <sup>a</sup>	30210.42 (13)
B	MHz	4744.2646 (10)	4735.0637 (10)
C	MHz	4282.68573 (92)	4288.7116 (10)
D <sub>J</sub>	kHz	2.98412 (33)	3.02502 (31)
D <sub>JK</sub>	kHz	-52.105 (11)	-55.5178 (65)
D <sub>K</sub>	kHz	714.0755 <sup>b</sup>	714.0755 <sup>b</sup>
d <sub>1</sub>	kHz	-0.66598 (43)	-0.65910 (45)
d <sub>2</sub>	kHz	-0.03167 (23)	-0.02915 (27)
H <sub>J</sub>	Hz	0.009535b	0.009535b
H <sub>JK</sub>	Hz	-0.1056 (79)	-0.1224 (51)
H <sub>KJ</sub>	Hz	-2.527 (36)	-2.643 (25)
$\sigma_{\text{fit}}$ <sup>e</sup>	kHz	36	31
Mlines <sup>l</sup>	...	144	129
J <sub>min</sub> /J <sub>max</sub>	...	8/27	8/27
K <sub>a,min</sub> /K <sub>a,max</sub>	...	0/14	0/14

<sup>a</sup> The numbers in parentheses are 1 $\sigma$  uncertainties in units of the last decimal digit.  
<sup>b</sup> Fixed to the ground-state value.  
<sup>c</sup> Root-mean square deviation of the fit.  
<sup>d</sup> Number of distinct frequency fitted lines.

## 5. REFERENCES

- <sup>1</sup> Goldsmith, P., Bergin, T., De Lucia, F. C., et al. 2006, Report from the Workshop on Laboratory Spectroscopy in Support of Herschel, Sofia, and Alma, Tech. Rep. (Pasadena, CA: California Institute of Technology)
- <sup>2</sup> Fortman, S. M., Medvedev, I. R., Neese, C. F., & De Lucia, F. C. 2010, ApJ, 725, 1682
- <sup>3</sup> Rimola, A., Sodupe, M., & Ugliengo, P. 2010, PCCP, 12, 5285
- <sup>4</sup> Ugliengo, P., Rimola, A., & Sodupe, M. 2011, Rendiconti Lincei, 22, 137
- <sup>5</sup> Belloche, A., Menten, K. M., Comito, C., et al. 2008, A&A, 482, 179
- <sup>6</sup> Belloche, A., Müller, H. S. P., Menten, K. M., Schilke, P., & Comito, C. 2013, A&A, 559, A47
- <sup>7</sup> MacDonald, J. N., & Tyler, J. K. 1972, J. Chem. Soc., Chem. Commun., 17, 995
- <sup>8</sup> Pickett, H. M. 1973, JMoSp, 46, 335
- <sup>9</sup> Brown, R., Godfrey, P., Ottrey, A., & Storey, J. 1977, JMoSp, 68, 359
- <sup>10</sup> Bogey, M., Dubus, H., & Guillemin, J. 1990, JMoSp, 143, 180
- <sup>11</sup> Motoki, Y., Tsunoda, Y., Ozeki, H., & Kobayashi, K. 2013, ApJS, 209, 23
- <sup>12</sup> Daly, A., Kolesníková, L., Mata, S., & Alonso, J. 2014, JMoSp, 306, 11
- <sup>13</sup> Daly, A. M., Bermúdez, C., Kolesníková, L., & Alonso, J. L. 2015, ApJS, 218, 30
- <sup>14</sup> Daly, A. M., Bermúdez, C., López, A., et al. 2013, ApJ, 768, 81
- <sup>15</sup> López, A., Tercero, B., Kisiel, Z., et al. 2014, A&A, 572, A44
- <sup>16</sup> Cernicharo, J., Kisiel, Z., Tercero, B., et al. 2016, A&A, 587, L4
- <sup>17</sup> Kolesníková, L., Alonso, E., Cabezas, C., Mata, S., & Alonso, J. 2016, in 71<sup>st</sup> Int. Symp. on Molecular Spectroscopy, TH07 <http://hdl.handle.net/2142/91343>
- <sup>18</sup> Frisch, M. J., Trucks, G. W., Schlegel, H. B., et al. 2009, Gaussian 09, Revision E.01 (Wallingford, CT: Gaussian Inc.)
- <sup>19</sup> Watson, J. K. G. 1977, in Vibrational Spectra and Structure, Vol. 6 ed. J. R. Durig (Amsterdam: Elsevier)

## CHAPTER XII.

### The glycine precursor glycinamide caught in the gas phase: A laser-ablation jet-cooled rotational study.

---

*The microwave spectrum of glycinamide, a glycine precursor, has been successfully generated in the gas phase by laser ablation of its hydrochloride salt, and is reported in the present work for the first time. The existence of one structure stabilized by a  $N_{\alpha}\text{-H}\cdots N_{\beta}\text{H}_2$  hydrogen bond has been revealed in a supersonic expansion by Fourier transform microwave spectroscopy. The complex hyperfine quadrupole coupling hyperfine structure due to the two  $^{14}\text{N}$  nuclei has been completely resolved and analyzed. The first precise data supplied about this glycine precursor could be of great importance for possible future identifications in the interstellar medium.*

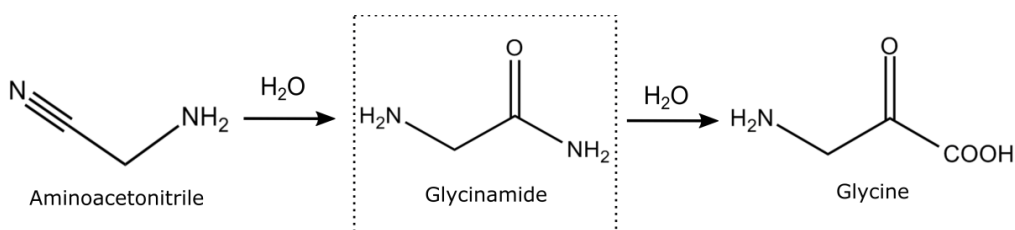




## INTRODUCTION

---

The detection of glycine in the interstellar medium (ISM) is one of the most pursued targets for the researchers in the astrochemistry and astrophysics. Its presence would confirm that complex chemical reactions in this medium can synthesize the fundamental building block of life and thus, that being in the Universe may be more widespread than accepted.<sup>1,2,3</sup> Attempts to observe glycine in the ISM have been reported<sup>4,5</sup> but its detection has never been confirmed.<sup>6</sup> Many theoretical studies have been devoted to proposing potential mechanisms of glycine formation.<sup>7,8,9,10,11,12</sup> Some of them include the participation of amino acid precursors,<sup>13</sup> and are also key candidates to be present in the ISM. The well-known famous Strecker reaction,<sup>14</sup> a mixture of ammonia, hydrogen cyanide and aldehyde in water, easily leads to the aminoacetonitrile. In laboratory or prebiotic conditions, aminoacetonitrile can be transformed in glycine by hydrolysis either basic or acidic aqueous solution.<sup>15,16</sup> This reaction is currently the most widely proposed synthesis mechanism of glycine in the ISM.<sup>17,18</sup> The hydrolysis of aminoacetonitrile occurs via the formation of the glycinamide intermediate<sup>19,20</sup> ( $\text{H}_2\text{N}-\text{CH}_2-\text{CONH}_2$ ) which is then hydrolyzed into the amino acid glycine (see Scheme 1). Therefore, the study of the precursors and their detection in the ISM is almost as important as that of the amino acid itself, to understand the chemical processes that could lead to the formation of a building block of life.



**Scheme 1.** Diagram of the Strecker reaction

Rotational spectra have been used to identify most of the compounds found in interstellar space successfully.<sup>21</sup> In 2008, aminoacetonitrile was discovered in SgrB2 by the rotational spectroscopy data.<sup>22</sup> Thus, if the hydrolysis of aminoacetonitrile occurs in the gas

phase or the grains of the ISM, glycineamide should also be present in the interstellar medium. The importance of glycineamide for prebiotic chemistry is the primary motivation to perform the present microwave investigation. The case of the glycineamide is remarkable among all the prebiotic molecules as to date no experimental investigations of this vital molecule have been reported. Its conformational landscape remains unknown.

In the pure form, the solid of glycineamide is chemically unstable, promptly reacting when exposed to the atmosphere, thus preventing easy measurement in the gas phase. It is only commercially available as a hydrochloride salt, where it appears in the protonated form. At the University of Valladolid, efficient procedures have been developed for the generation of neutral forms of proteogenic amino acids in supersonic expansion by laser ablation of their zwitterionic forms, allowing their conformational investigation using Fourier transform microwave techniques.<sup>23</sup> Very recently, a comprehensive analysis of the millimeter and submillimeter-wave spectra of aminoacetonitrile<sup>24</sup> and laser-ablated microwave spectra of hydantoin,<sup>25</sup> also a potential glycine precursor, have been reported. The microwave spectrum of glycineamide, successfully generated in the gas phase by laser ablation of its hydrochloride salt, is now first reported in the present work. In the experimental procedure, finely powdered commercial hydrochloride glycineamide sample was mixed with a small amount of a binder and pressed into cylindrical rods which were ablated using the third harmonic (355 nm) of a picosecond laser. The vaporized products were seeded in neon at backing pressures of 10-12 bar and expanded adiabatically into the vacuum chamber of the spectrometer where the glycineamide molecules liberated from the salt were probed by laser ablation broadband chirped pulse Fourier transform microwave spectroscopy (LA-CP-FTMW).<sup>26</sup> A high-power excitation pulse of 300 W was used to polarize the molecules from 6 to 11 GHz. Up to 40000 individual free induction decays at a 2 Hz repetition rate were averaged in the time domain, and Fourier transformed to obtain the broadband frequency domain spectrum shown in Fig.1.

The spectrum was inspected, and the rotational spectrum of one rotamer was quickly identified due to the very intense  $1_{01} \leftarrow 0_{00}$ ,  $2_{12} \leftarrow 1_{11}$ ,  $2_{02} \leftarrow 1_{01}$  and  $2_{11} \leftarrow 1_{10}$   $\mu_a$ -type R-branch transitions easily identified in the spectrum. Intense  $\mu_b$ -type Q-branch and weaker  $\mu_b$ -type R-branch transitions were also identified. No signals belonging to other species remained unidentified in the rotational spectra apart from known common decomposition lines (cyanoacetylene) and water complexes. All rotational transitions of glycineamide were observed split in a complicated hyperfine structure, with many components spanning several megahertz depicted in Fig. 1b for the  $1_{01} \leftarrow 0_{00}$  transition. These complex hyperfine patterns were accounted for regarding nuclear quadrupole coupling interaction effects due to the presence of two  $^{14}\text{N}$  nuclei with non-zero electric quadrupole moment ( $I=1$ ) in glycineamide, which interacts with the electric field gradient created by the rest of the molecule at the nuclei. The  $^{14}\text{N}$  nuclear quadrupole coupling splits the rotational energy levels decreasing the overall intensity of each rotational transition and giving rise to a very complex hyperfine structure.<sup>27</sup> In a first step, no attempt was made to analyze the quadrupole hyperfine structure since the hyperfine components appeared not well resolved. The rotational frequencies were measured as the intensity-weighted mean of the line clusters (see Table S1 of Supporting Information). A rigid rotor analysis generates a preliminary set of values for the rotational constants  $A=9631.61$  MHz;  $B=3986.72$  MHz;  $C=2925.51$  MHz that allows the identification of the observed rotamer of glycineamide. With this aim, a conformational search was carried out on all plausible configurations of glycineamide. Once a set of candidate structures were identified by force field and semi-empirical methods, we then employed higher-level calculations using the B3LYP density functional with the Grimme D3 dispersion interactions and Pople's 6-311++g(d,p) basis set, to optimize the four different structures below  $1000\text{ cm}^{-1}$ . The predicted spectroscopic constants are collected in Table 1. The values of the rotational constants A, B, and C, which critically depend on the mass distribution, are usually a precise tool in the identification of conformers. The values predicted for the global minimum (conformer I) in Table 1 are very close to those experimentally determined.

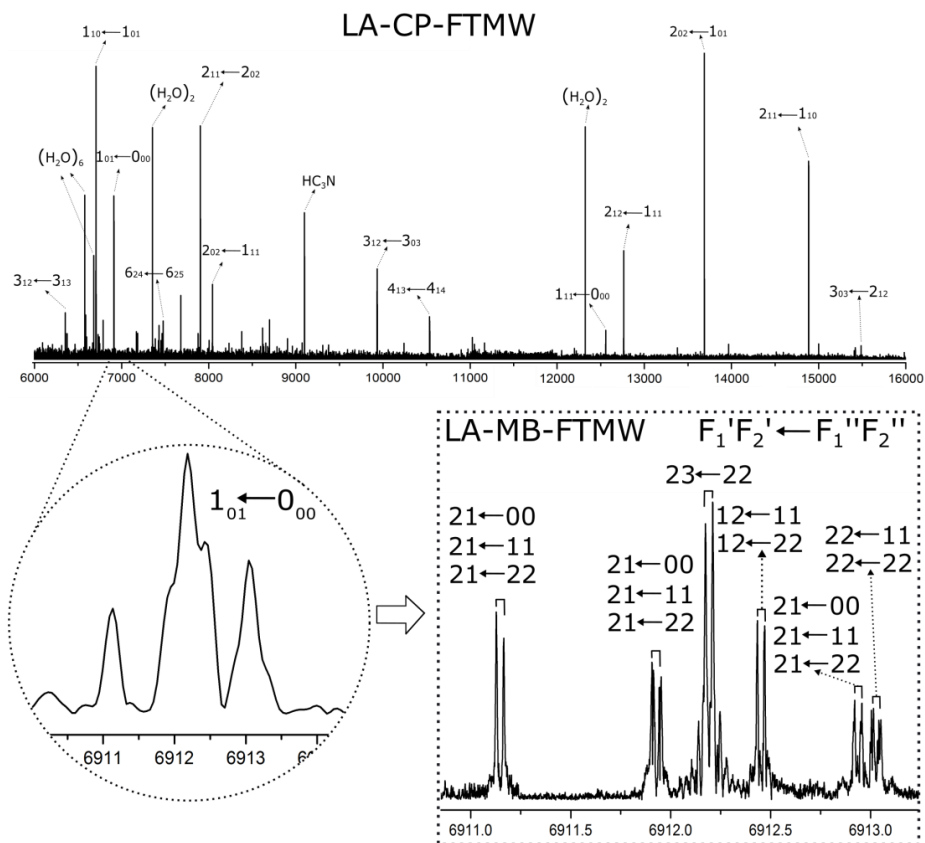
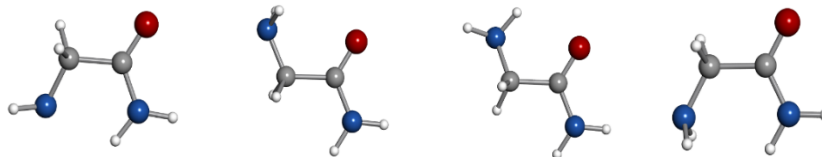


**Figure 1.** (a) Broadband LA-CP-FTMW spectrum of l-glycinamide from 6-16GHz. (b) A small section of the spectrum showing the unresolved hyperfine structure of the  $1_{01}\leftarrow 0_{00}$  transition. (c) Wholly resolved nuclear hyperfine structure of the  $1_{01}\leftarrow 0_{00}$  transition by LA-MB-FTMW. Each hyperfine component is labeled with the corresponding values of  $I'$ ,  $F'$ ,  $I''$ ,  $F''$  quantum numbers.

**Table 1.** Spectroscopic Parameters and Relative Energies Calculated at the B3LYP/6-311++G(d,p) Level of Theory for the lower energy conformers of Glycinamide.

	I	II	III	IV
$A/B/C^{[a]}$	9641/3976/2925	10066/3835/2867	9952/3939/2944	9515/3894/2855
$P_c / \text{u}\text{\AA}^2$	6.7	5.7	7.4	5.9
$ \mu_a / \mu_b / \mu_c $	3.8/1.5/0.0	1.9/2.8/0.0	1.0/3.5/1.0	2.3/3.5/0.0
$^{14}\text{N}_t \chi_{aa}/\chi_{bb}/\chi_{cc}$	2.40/-3.66/1.26	-1.48/-0.52/2.00	2.95/2.04/-5.00	-1.50/-0.91/2.41
$^{14}\text{N}_a \chi_{aa}/\chi_{bb}/\chi_{cc}$	1.79/2.19/-3.99	2.32/2.31/-4.62	2.13/2.18/-4.32	2.13/2.18/-4.32
$\Delta E/\Delta G$	0/0	745/257	1096/866	1162/934



[a] A, B, and C represent the rotational constants (in MHz);  $P_c$  is the planar inertial moment (in  $\text{u}\text{\AA}^2$ ), conversion factor:  $505379.1 \text{ MHz}\cdot\text{u}\text{\AA}^2$ ;  $\mu_a$ ,  $\mu_b$  and  $\mu_c$  are the electric dipole moment components (in D);  $\chi_{aa}$ ,  $\chi_{bb}$  and  $\chi_{cc}$  are the diagonal elements of the  $^{14}\text{N}$  nuclear quadrupole coupling tensor (in MHz),  $\text{N}_t$  and  $\text{N}_a$  correspond to the terminal and amide  $^{14}\text{N}$  nuclei, respectively;  $\Delta E$  and  $\Delta G$  are the relative and Gibbs energies (in  $\text{cm}^{-1}$ ) at 298 K with respect to the global minimum calculated at the B3LYP/6-311++G(d,p) with Grimme dispersion level of theory.

A different and independent way of identifying structures is based on the presence of  $^{14}\text{N}$  nuclei in the molecule. In our predictions, we also included the values of the quadrupole coupling constants for both  $^{14}\text{N}_t$  (amine) and  $^{14}\text{N}_a$  (amide) nuclei. While rotational constants are strongly related to mass distribution, nuclear quadrupole coupling interactions depend critically on the electronic environment, position and orientation of the  $^{14}\text{N}$  nuclei. The  $^{14}\text{N}$  nuclei introduce hyperfine rotational probes at defined sites of glycinamide and act as a reporter of the chemical environment of  $\text{N}_t$  and  $\text{N}_a$  quadrupolar nuclei. The distinct orientation of the terminal amino group in all the conformers causes a significant effect on the values of the quadrupole coupling constants for the  $^{14}\text{N}_t$  (see Table 1). To unveil, conclusively, the observed species, it becomes necessary to resolve and interpret the quadrupole hyperfine structure of glycinamide.

At this point we took advantage of the sub-Doppler resolution of our LA-MB-FTMW spectrometer<sup>28,29</sup> spectrometer to fully resolve the nuclear quadrupole hyperfine structure. Interpretation of the quadrupole coupling pattern led to the assignment of fifteen hyperfine components for the  $1_{01}-0_{00}$  rotational transition, essential as starting point of the analysis. New predictions allowed the assignment of a total of 63 hyperfine components (Table S2 of Supporting Information) belonging to four a- and two b-type transitions. They were analyzed using a Watson's A-reduced semirigid rotor Hamiltonians in the  $I'$ -representation<sup>30</sup> supplemented with a term to account for the nuclear quadrupole coupling contribution.<sup>31</sup> The quadrupole coupling Hamiltonian was set up in the coupled basis set  $(l_1 l_2 I J F)$ ,  $l_1 + l_2 = I$ ,  $I + J = F$ . The energy levels involved in each transition are thus labeled with the quantum numbers  $J, K_{-1}, K_{+1}, I, F$ . Table 2 illustrates how such analysis rendered accurate rotational and nuclear quadrupole constants. Thus, a final comparison between their experimental and theoretical values serves to the unambiguous identification of the observed rotamer as conformer I.

An unexpected fact observed in the results of Table 2 is the abnormal non-rigid behaviour reflected in the large values of the centrifugal distortion constants  $\Delta_{JK}$  and  $\Delta_K$  despite the low J values of the energy involved in the measured transitions. This fact is confirmed by the comparison of the rms deviations from the rigid and semirigid rotor analysis in Table 2. The origin of the non-rigid behavior can be attributed to the existence of a large amplitude C<sub>2</sub>-N<sub>t</sub> bond torsion controlled by a double minimum potential function with a low energy barrier to the planar configuration. For such potential functions, the vibrational energy levels occur at energy intervals with orders of magnitude like those of the rotational levels. Coriolis coupling interactions are established between the observed ground vibrational state with the first torsional excited state non-observed since it is expected to be depopulated due to vibrational cooling. When these interactions are small, they can be treated as perturbations, and their effects are reflected in abnormally high centrifugal distortion constants.

**Table 2.** Experimental rotational constants of the observed conformer I of glycineamide

	Rigid rotor analysis	Semirigid rotor analysis
<b>A<sup>a</sup></b>	9631.6462(65)	9631.998( 33)
<b>B</b>	3986.7564(34)	3986.78631(82)
<b>C</b>	2925.5858(37)	2925.58244( 58)
<b><math>\Delta_{JK}^b</math></b>	-	-0.02554( 62)
<b><math>\Delta_K</math></b>	-	-0.302( 32)
<b><math>\chi_{aa}(\text{Nterminal})^c</math></b>	2,097(23)	2,1121(57)
<b><math>\chi_{bb}(\text{Nterminal})</math></b>	-3,121(23)	-3,1135(15)
<b><math>\chi_{cc}(\text{Nterminal})</math></b>	1,024(23)	1,0014(15)
<b><math>\chi_{aa}(\text{Namide})</math></b>	1,567(26)	1,5547(32)
<b><math>\chi_{bb}(\text{Namide})</math></b>	1,968(30)	1,9597(38)
<b><math>\chi_{cc}(\text{Namide})</math></b>	-3,535(30)	-3,5145(38)
<b><math>\sigma</math> / kHz</b>	23.9	2.8

Experimental rotational parameters of glycineamide a] A, B, and C represent the rotational constants(in MHz) ;[b]  $\Delta_{JK}$ , and  $\Delta_K$  represent the centrifugal distortion constants (in MHz); [c]  $\chi_{aa}$ ,  $\chi_{bb}$ , and  $\chi_{cc}$  are the diagonal elements of the <sup>14</sup>N nuclear quadrupole coupling tensor (in MHz), N<sub>ti</sub> and N<sub>a</sub> correspond to the amino <sup>14</sup>N nuclei and amide <sup>14</sup>N nuclei, respectively.

Summarizing, the present study provides the first experimental information on the conformational properties of glycinamide. The capability of laser ablation coupled with time domain Fourier transform microwave techniques to undertake very accurate spectroscopic constants and their direct comparison with theoretical computations provides an unmatched means for the unequivocal identification of the observed species. The two  $^{14}\text{N}_t$  and  $^{14}\text{N}_a$  nuclei of glycinamide present at defined sites introduce hyperfine rotational probes that further expand the utility of this spectroscopic technique. Our results indicate that glycinamide exists in the gas phase in a single conformation, stabilized by a  $\text{N}_a\text{-H}\cdots\text{N}_t\text{H}_2$  hydrogen bond, which is the one predicted as the global minimum. The present state-of-the-art of microwave spectroscopy, as illustrated in the present study, is paving the way towards another complex, unstable systems which have been previously considered as being out of reach of high-resolution spectroscopic studies.

## REFERENCES

---

- <sup>1</sup> S. Kwok, "Organic Matter in the Universe", *Wiley-VCH 2012*
- <sup>2</sup> J.-C. Guillemin "Amino Acids in the Universe". BIO Web of Conferences, Colloquium of the CNRS Interdisciplinary Initiative "Planetary Environments and Origins of Life", 2, 2014.
- <sup>3</sup> A.M. Andrew, "Astrochemistry" John Wiley & Sons 2006.
- <sup>4</sup> R. D. Brown, P. D. Godfrey, J. W. V. Storey, M.-P. Bassez, B. J. Robinson, R. A. Batchelor, M. G. McCulloch, O. E. H. Rydbeck, A. G. Hjalmarsen, A search for interstellar Glycine, *MNRAS*, 1979, 186, 5P-8P.
- <sup>5</sup> Y.-J. Kuan, S. B. Charnley, H.-C. Huang, W.-L. Tseng, and Z. Kisiel, *ApJ*, 593, 848–867, 2003
- <sup>6</sup> L. E. Snyder, F. J. Lovas, J. M. Hollis, D. N. Friedel, P. R. Jewell, A. Remijan, V. V. Ilyushin, E. A. Alekseev, S. F. Dyubko, *ApJ*, 619, 914–9, 2005.
- <sup>7</sup> L. Largo, C. Barrientos, V. M. Rayón, A. Largo, P. Redondo, *Int. J. Mass Spectrom*, 295, 21–25, 2010.
- <sup>8</sup> P. Redondo, A. Largo, and C. Barrientos, *A&A* 579, A125, 2015.
- <sup>9</sup> A. Largo, P. Redondo, C. Barrientos, *Int. J. Quantum Chem*, 98, 355–360, 2004.
- <sup>10</sup> V. A. Basiuk, K. Kobayashi, *Viva Origino* 30, 54 – 62, 2002.
- <sup>11</sup> V. A. Basiuk *J. Phys. Chem. A*, 105, 4252-4258, 2001.
- <sup>12</sup> J.-B. Bossa, F. Duvernay, P. Theulé, F. Borget, L. d'Hendecourt, and T. Chiavassa, *A&A* 506, 601–608, 2009.
- <sup>13</sup> A. Rimola, M. Sodupe and P. Ugliengo *Phys. Chem. Chem. Phys.*, 12, 5285–5294, 2010.
- <sup>14</sup> (a)A. Strecker, *Ann.Chem.Pharm.* 75, 27-45,1850 (b)A. Strecker, *Ann.Chem.Pharm.*,91,349-351, 1854.
- <sup>15</sup> Glycine W. K. Anslow, H. King. *Org. Synth.*, 4, 31, 1925.
- <sup>16</sup> I. M. Wyzlic and A. H. Soloway *Tetrahedron Lett.* 33, 49, 7489-7490, 1992.
- <sup>17</sup> J. C. Aponte, J. E. Elsila, D. P. Glavin, S. N. Milam, S. B. Charnley, J. P. Dworkin *ACS Earth Space Chem.*, 1, 3–13, 2017.
- <sup>18</sup> S. Zhu and J.-J. Ho *J. Phys. Chem. A*, 108, 3798-3805, 2004.
- <sup>19</sup> A. Rimola, M. Sodupe, *P. Ugliengo, ApJ*, 754, 24, 2012.
- <sup>20</sup> A. Commeyras, J.Taillades, J. Brugidou, R. Sola, A. Previero, L. Mion, R. Pascal, M. Lasperas, A. Rousset, *Eur. Pat. Appl.*, EP 84470 A1 19830727, 1983.

- 
- <sup>21</sup> S.Schlemmer, H. Mutschke, T. Giesen, C. Jäger, *Laboratory Astrochemistry : From Molecules through Nanoparticles to Grains*. Ed Wiley-VCH, 2014. DOI: 10.1002/9783527653133
- <sup>22</sup> M. Bogey, H. Dubus, J.C. Guillemin, *J.Mol.Spectrosc.* 143, 180-182, 1990.
- <sup>23</sup> J. L. Alonso, J.C. López, *Topics in Current Chemistry*, Vol. 364, Springer, Heidelberg, pp. 335 –402. 2015.
- <sup>24</sup> L.Kolesnikova, E.R.Alonso, S.Mata, J.L.Alonso, *ApJ Supp. Series*,229:26(8pp), 2017
- <sup>25</sup> E. R. Alonso, L. Kolesnikova and J. L. Alonso, *J.Chem.Phys.*, 147, 124312, 2017.
- <sup>26</sup> S. Mata, I. Peña, C. Cabezas, J. C. López, J. L. Alonso, *J. Mol. Spectrosc.*, 280, 91 – 96, 2012.
- <sup>27</sup> W. Gordy, R. L. Cook, 3rd ed., Wiley, New York, 1984
- <sup>28</sup> J.L. Alonso, C. Pérez, M.E. Sanz, J.C. López, S. Blanco *Phys. Chem. Chem. Phys.*, 11, 617-627, 2009.
- <sup>29</sup> C. Bermúdez, S.Mata, C. Cabezas, and J.L. Alonso, *Angew. Chem.*, 126, 11195 –11198, 2014.
- <sup>30</sup> J.K.G. Watson, in: J.R. Durig (Ed.), *Vibrational Spectra and Structure*, vol. 6, Elsevier, Amsterdam, p. 1–89, 1977.
- <sup>31</sup> (a) H.M. Foley, *Phys. Rev.* 71, 747, 1947; (b) G.W. Robinson, C.D. Cornwell, *J. Chem. Phys.* 21, 1436, 1953.



## CHAPTER XIII.

# Laser ablated hydantoin: a high resolution rotational study

---

**Adapted from: Journal of Molecular Spectroscopy, 147, 124312 (2017)**

*Laser ablation techniques coupled with broadband and narrowband Fourier transform microwave spectroscopies has allowed the high resolution rotational study of solid hydantoin, an important target in astrochemistry as a possible precursor of glycine. The complicated hyperfine structure arising from the presence of two  $^{14}\text{N}$  nuclei in non-equivalent positions have been resolved and interpreted in terms of the nuclear quadrupole coupling interactions. The results reported in this work provide a solid base for the interstellar searches of hydantoin in the astrophysical surveys. The values of the nuclear quadrupole coupling constants have been also discussed in terms of the electronic environment around the respective nitrogen atom.*



## 1. INTRODUCTION

---

Hydantoin ( $C_3H_4O_2N_2$ ) is considered as one of the precursors of glycine in the interstellar medium<sup>1,2</sup> whose extraterrestrial evidence has been provided by analysis of carbonaceous chondrites.<sup>3</sup> As a nitrogen containing 5-membered heterocycle (see Table I), it is also assumed to participate in the primordial formation of oligopeptides and polypeptides<sup>4, 5</sup> and has been evidenced to be an intermediate in the chemistry of HCN<sup>6</sup> that is crucial to the origin of life.<sup>7</sup> Apart from the prebiotic relevance of hydantoin, it is also considered as an important molecule in medicinal chemistry due to its use as a leading compound for the synthesis of drugs with, for example, antiepileptic, antiarrhythmic, or antibacterial activities.<sup>8, 9</sup> Furthermore, substituted hydantoins act as valuable intermediates for the synthesis of enantiomerically pure amino acids<sup>10</sup> and find applications in herbicides, fungicides and insecticides.

To support the interstellar searches of hydantoin, its millimeter wave spectrum has been recently collected between 90 and 370 GHz<sup>11</sup> and rotational and centrifugal distortion constants of this prolate asymmetric rotor reported. Hydantoin bears two  $^{14}N$  nuclei with non-zero quadrupole moments ( $I_N = 1$ ) sited in non-equivalent positions ( $N_1$  and  $N_3$  in Table I) which interact with the electric field gradient created by the rest of the molecule at the nuclei. As a consequence, the nuclear spin couples to the rotational angular momentum resulting in a complicated hyperfine structure which strongly depends on the electronic environment around the nitrogen nuclei. This nuclear hyperfine structure was not observed in the reported millimeter wave rotational spectra.<sup>11</sup> It should be emphasized that at lower frequency region, those accessible for example by the Green Bank Telescope, the hyperfine pattern which can be spread over several MHz, might be of critical importance in interpreting the corresponding radioastronomical observations. Formamide<sup>12-14</sup>, ethanimine<sup>15</sup>, methylamine<sup>16</sup>, or methyl cyanide<sup>17</sup> can be mentioned as examples of neutral N-bearing molecules whose interstellar low  $J$  transitions were observed with resolved or partly resolved

nuclear quadrupole hyperfine structure. In case of cyanoallene<sup>18</sup> or methanimine<sup>19</sup>, the <sup>14</sup>N hyperfine pattern was fundamental for a conclusive detection.

Hydantoin, a solid compound with high melting point of 220 °C, is a thermally fragile molecule which cannot be easily transferred intact into the vapor phase by using conventional heating methods. Hence, heating above 150 °C was necessary to provide a sufficient number of absorbers that survive decomposition for a millimeter wave study<sup>11</sup>. Alternatively, it has been shown that laser ablation constitutes an efficient method in vaporizing solid samples of biomolecules.<sup>20</sup> In our laboratory, we have coupled a laser ablation source with high resolution Fourier transform microwave techniques.<sup>20</sup> The sub-Doppler resolution achieved with the narrowband LA-MB-FTMW technique has been crucial in the analysis of the hyperfine structure of nitrogen basis<sup>21-23</sup> amino acids<sup>24, 25</sup> nucleosides<sup>26</sup>, and dipeptides<sup>27</sup>.

In an attempt to provide a high resolution rotational signature of isolated hydantoin, we have successfully applied the above experimental approach to analyze the complex nuclear quadrupole hyperfine structure of hydantoin. The experimental values of the <sup>14</sup>N nuclear quadrupole coupling constants extracted from the analysis allow us to establish unambiguously the diketo tautomer of hydantoin. The determined spectroscopic constants provide a solid base for future searches of hydantoin in the astrophysical surveys. Details of the investigation are given in the next sections.

## 2. METHODS

---

For the experiments described here, a commercial sample of hydantoin was used without further purification. Fine powder of solid sample was mixed with a commercial binder and pressed to form a cylindrical rod that was placed into a laser ablation nozzle. The molecules of hydantoin were vaporized using the third harmonic (355 nm, 17 mJ per pulse) of a

picosecond Nd:YAG laser and were expanded into the vacuum chamber using a Ne carrier gas at a backing pressure of 8 bar. A LA-CP-FTMW spectrometer described in detail elsewhere<sup>28</sup> working in the frequency range 6 – 18 GHz was used to record the broadband rotational spectrum. Two microwave horns were used to (i) broadcast the excitation pulse created by an arbitrary waveform generator and subsequently amplified by a 300 W travelling wave tube amplifier and (ii) to receive the broadband molecular emission. At a repetition rate of 2 Hz, a total of 85000 free induction decays (4 FID emissions per gas pulse) were averaged and digitized using a digital oscilloscope. The frequency domain spectrum was obtained by taking a fast Fourier transform (FFT) after applying a Kaiser–Bessel window. The hyperfine structure due to the two  $^{14}\text{N}$  nuclei was resolved with the sub-Doppler resolution of a LA-MB-FTMW spectrometer<sup>24</sup> working from 2 to 12 GHz. A short microwave radiation pulse of 0.3  $\mu\text{s}$  duration was applied to polarize the molecules of hydantoin vaporized in the throat of the laser ablation nozzle. The registered FID was then converted to the frequency domain by Fourier transformation. All the transitions appeared as Doppler doublets due to the parallel configuration of the molecular beam and the microwave radiation. The resonance frequencies were determined as the arithmetic mean of the two Doppler components with an estimated accuracy better than 3 kHz.

In order to guide the interpretation of nuclear quadrupole hyperfine structure, geometrical optimizations and calculations of the electric field gradient tensor at the two  $^{14}\text{N}$  nuclei have been performed at the MP2/6-311++G(d,p) level of the theory (Gaussian 09 package<sup>29</sup>).

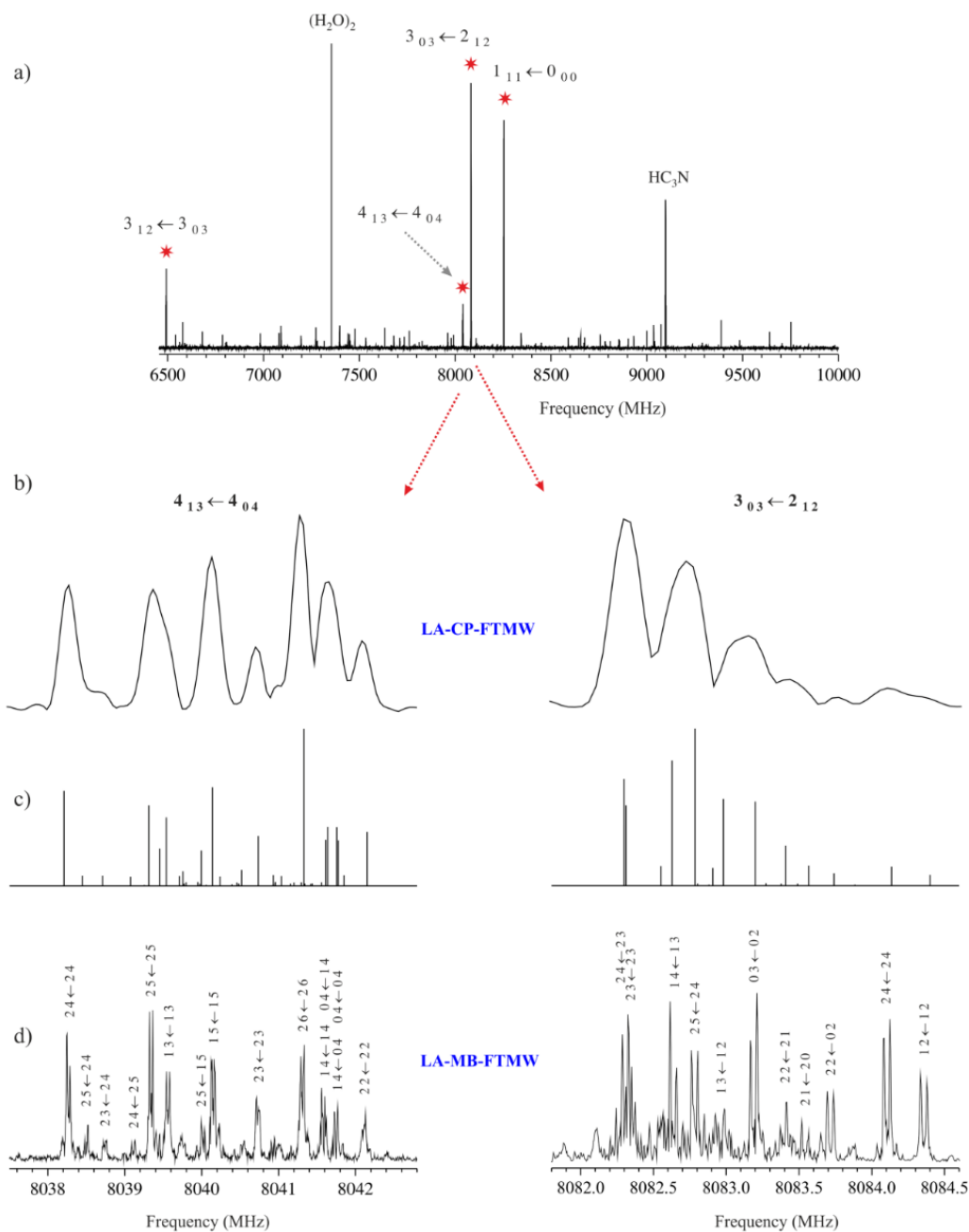


**Figure 1.** a) The broadband LA-CP-FTMW spectrum of hydantoin with assignments of its prominent spectral features. b) Hyperfine pattern of  $4_{13} \leftarrow 4_{04}$  and  $3_{03} \leftarrow 2_{12}$  rotational transitions measured by LA-CP-FTMW spectrometer. c) Modeled hyperfine pattern of the diketo form of hydantoin based on *ab initio* calculations. d) Hyperfine structure completely resolved by LA-MB-FTMW technique. Due to the coaxial configuration of the molecular beam and the microwave radiation each hyperfine component labeled as  $l' F' \leftarrow l'' F''$  appears as a doublet.

### 3. RESULTS AND DISCUSSION

---

A section of the broadband LA-CP-FTMW rotational spectrum from 6.4 to 10 GHz is shown in Fig. 1a. The spectrum is relatively sparse and the location of two intense *b*-type *R*-branch  $3_{03}\leftarrow 2_{12}$  and  $1_{11}\leftarrow 0_{00}$  transitions accompanied by weaker *b*-type *Q*-branch  $3_{12}\leftarrow 3_{03}$  and  $4_{13}\leftarrow 4_{04}$  transitions was relatively straightforward. Other strong signals corresponding to water dimer and nitrogen containing photofragmentation products<sup>26</sup> were also identified. Several *a*-type *R*-branch transitions could be also observed but due to their significant weakness, they were not further considered in the analysis. Finally, *c*-type transitions were predicted but not observed. Each rotational transition was observed splitted in many components as a consequence of nuclear quadrupole interactions of the two <sup>14</sup>N nuclei. Consequently, the overall intensity of each rotational transition is significantly decreased.<sup>30</sup> A first set of the rotational constant values  $A = 6537.7$ ,  $B = 2291.4$ , and  $C = 1716.5$  MHz was derived from a rigid rotor fit of the centre of frequency of each rotational transition.<sup>30</sup> They were in excellent agreement with those reported from the millimeter wave study.<sup>11</sup>

Hydantoin may exist in several tautomeric forms<sup>31</sup> differing from each other by the position of the hydrogens which may be bound to either nitrogen or oxygen atoms (lactam-lactim equilibrium). The rotational and nuclear quadrupole coupling constants calculated for the plausible tautomers are reported in Table S1 of the Supplementary material. In can be seen in Table S1 that the proton transfer from N–H bond to the carbonyl oxygen do not produce large changes in the rotational constants of respective tautomers. Therefore, a particular tautomer of hydantoin cannot be unambiguously identified taking into account only the above rotational constants. Although the sharp decrease in predicted relative stabilities and values of dipole moment components point to the diketo (lactam) form, a more straightforward way to conclusively identify the tautomer observed in the supersonic expansion is to take into account the nuclear quadrupole coupling constants which can be evaluated by analyzing the hyperfine structure of each rotational transition. A close look at

the predicted values of the quadrupole coupling constants ( $\chi_{aa}$ ,  $\chi_{bb}$ , and  $\chi_{cc}$ ) for  $N_1$  and  $N_3$  nuclei in Table S1 clearly indicates that they constitute a unique tool in the tautomer identification since they change dramatically from one tautomer to other as a result of different chemical environment surrounding these nuclei. Taking this into account, the predicted values of  $\chi_{aa}$ ,  $\chi_{bb}$ , and  $\chi_{cc}$  for each plausible tautomer of hydantoin were used to model the hyperfine pattern of the measured rotational transitions as shown in Fig. 1c for  $4_{13} \leftarrow 4_{04}$  and  $3_{03} \leftarrow 2_{12}$  transitions. The predicted pattern of the diketo form of hydantoin is the only one that matches with the hyperfine structure obtained from the broadband rotational spectrum as can be seen in Fig. S1 of the Supplementary material. However, the spectral resolution attainable with this LA-CP-FTMW technique is not sufficient to fully resolve the individual hyperfine components that allow a definitive analysis and identification.

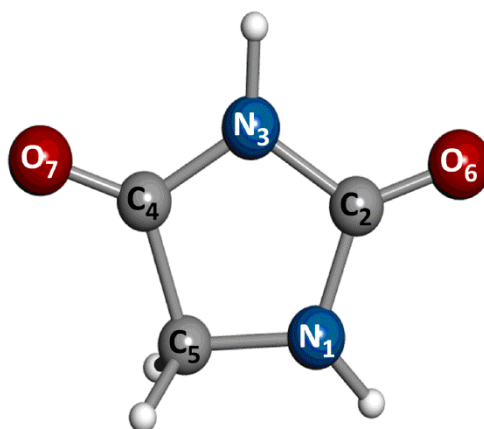
At this point we took advantage of the higher resolution of our narrowband LA-MB-FTMW spectrometer. Fig. 1d shows the above transitions under sub-Doppler resolution reached in the experiment. In this way, the nuclear quadrupole hyperfine structure could be completely resolved. 45 nuclear quadrupole hyperfine components (see Table S2 of the Supplementary material) belonging to 6 different rotational transitions ( $J$  ranging from 0 to 5) were measured and analyzed using a rigid rotor Hamiltonian in the  $I'$ -representation<sup>30</sup> supplemented with a nuclear quadrupole coupling term set up in the coupled basis set  $(I_1 I_2 I J F)$ ,  $I_1 + I_2 = I$ ,  $I + J = F$ .<sup>30</sup> The energy levels involved in each transition are thus labeled with the quantum numbers  $J$ ,  $K_a$ ,  $K_c$ ,  $I$ , and  $F$ . Only the diagonal elements of the nuclear quadrupole coupling tensors  $\chi_{aa}$ ,  $\chi_{bb}$ , and  $\chi_{cc}$  were necessary to fit the measured frequencies within the experimental uncertainty and together with the rotational constants  $A$ ,  $B$ , and  $C$  and inertial defect  $\Delta$  are collected in Table I. The inertial defect value points to the  $C_s$  effective structure of hydantoin which is consistent with the observation of  $a$ -type and  $b$ -type spectrum and the absence of the  $c$ -type one. Small deviation from  $\Delta = -3.22 \text{ u}\text{\AA}^2$ , a typical value for a rigid molecule with a plane of symmetry and one pair of out-of-plane methylene hydrogens,



reflects some additional contribution arising from atoms slightly out-of-plane or from low-frequency ring-puckering vibrations.

**Table 1.** Experimental and calculated spectroscopic parameters for the observed diketo form of hydantoin.

	Experimental	<i>Ab initio</i> diketo form <sup>a</sup>
$A$ /MHz	6537.73799 (86) <sup>b</sup>	6538
$B$ /MHz	2291.37278 (16)	2274
$C$ /MHz	1716.47204 (22)	1709
$\Delta$ / uÅ <sup>2</sup>	-3.430201 (42)	-3.82
$\chi_{aa} (^{14}\text{N}_1)$ /MHz	2.5900 (41)	2.65
$\chi_{bb} (^{14}\text{N}_1)$ /MHz	2.1438 (70)	2.18
$\chi_{cc} (^{14}\text{N}_1)$ /MHz	-4.7338 (70)	-4.83
$\chi_{aa} (^{14}\text{N}_3)$ /MHz	1.6315 (51)	1.65
$\chi_{bb} (^{14}\text{N}_3)$ /MHz	1.8321 (75)	1.92
$\chi_{cc} (^{14}\text{N}_3)$ /MHz	-3.4635 (75)	-3.57
$ \mu_a $ /D	Yes <sup>c</sup>	0.2
$ \mu_b $ /D	Yes <sup>c</sup>	2.4
$ \mu_c $ /D	No <sup>c</sup>	0.6
$\sigma_{\text{Fit}}$ / MHz <sup>d</sup>	0.003	...



<sup>a</sup> MP2/6-311++G(d,p) level of the theory ( $C_1$  symmetry).

<sup>b</sup> The numbers in parentheses are  $1\sigma$  uncertainties in units of the last decimal digit.

<sup>c</sup> Yes or No to observation of  $a$ -,  $b$ -, and  $c$ -type transitions.

<sup>d</sup> Root mean square deviation of the fit.

Under the  $C_s$  effective structure of hydantoin, the  $\chi_{cc}$  components of the nuclear quadrupole coupling tensor corresponding to  $\text{N}_1$  and  $\text{N}_3$  nuclei listed in Table I are expected to be unchanged during the transformation from the principal inertial axes to principal quadrupolar axis. These values provide information on the electric field gradient along the direction of an axis perpendicular to the heterocyclic ring. Negative value of  $\chi_{cc}$  corresponds to pyrrolic nitrogen ( $-\text{N}<$ ),<sup>32, 33</sup> while the positive value of  $\Delta_{cc}$  is typical for pyridinic nitrogen ( $-\text{N}=\text{}$ ).<sup>32-34</sup> The experimental values of  $\chi_{cc}$  of  $-4.734$  and  $-3.464$  MHz in Table I correspond to

two pyrrolic nitrogens and further confirm the identification of the diketo tautomer of hydantoin. The value  $\chi_{ccc} = -3.464$  MHz for the imide nitrogen N<sub>3</sub> is very close to those of  $-3.451$  and  $-3.420$  MHz obtained for uracil<sup>23</sup> and thymine,<sup>22</sup> respectively; the electronic environment around the N<sub>3</sub> imide nitrogen is analogous in the three systems. On the other hand, the value for the N<sub>1</sub> amide nitrogen  $\chi_{ccc} = -4.734$  MHz is significantly greater than those of  $-3.742$  MHz and  $-3.804$  MHz determined for uracil<sup>23</sup> and thymine,<sup>22</sup> respectively. The diminished coupling constants as compared with hydantoin imply a greater delocalization of  $\pi$  electrons in uracil and thymine.<sup>35</sup>

In order to derive a reliable hydantoin list of transitions for astrophysical applications (up to 110 GHz) that take the nuclear quadrupole hyperfine structure into account, we have included the quartic centrifugal distortion constants from the mm-wave study<sup>11</sup> obtained by fitting of the unsplit lines in the 90–370 GHz frequency range. The predicted list of transition frequencies is provided in Table S3 of the supplementary material.

## 5. CONCLUSION

---

The solid hydantoin has been brought into the gas phase by laser ablation and its complex nuclear quadrupole hyperfine structure due to the presence of two <sup>14</sup>N nuclei has been measured for the first time by high resolution FTMW techniques. The nuclear quadrupole coupling constants extracted from the analysis establish conclusively the diketo form for hydantoin. The spectroscopic information provided in this work could be relevant to check the existence of hydantoin in the interstellar medium.

## 6. REFERENCES

- <sup>1</sup> Y. Kebukawa, Q. H. S. Chan, S. Tachibana, K. Kobayashi and M. E. Zolensky, *Science Adv.* **3**, e1602093 (2017).
- <sup>2</sup> P. de Marcellus, M. Bertrand, M. Nuevo, F. Westall and L. Le Sergeant d'Hendecourt, *Astrobiology* **11**, 847-854 (2011).
- <sup>3</sup> A. Shimoyama and R. Ogasawara, *Orig. Life Evol. Biosph.* **32**, 165-179 (2002).
- <sup>4</sup> A. Commeyras, J. Taillades, H. Collet, L. Boiteau, O. Vandenabeele-Trambouze, R. Pascal, A. Rousset, L. Garrel, J.-C. Rossi, J.-P. Biron, O. Lagrille, R. Plasson, E. Souaid, G. Danger, F. Selsis, M. Dobrijévic and H. Martin, *Orig. Life Evol. Biosph.* **34**, 35-55 (2004).
- <sup>5</sup> C. Huber, W. Eisenreich, S. Hecht and G. Wächtershäuser, *Science* **301**, 938-940 (2003).
- <sup>6</sup> J. P. Ferris, J. D. Wos, T. J. Ryan, A. P. Lobo and D. B. Donner, *Orig. Life* **5**, 153-157 (1974).
- <sup>7</sup> J. D. Sutherland, *Angew. Chem. Int. Ed.* **55**, 104-121 (2016).
- <sup>8</sup> C. Avendaño and J. C. Menendez, in *Kirk-Othmer Encyclopedia of Chemical Technology* (John Wiley & Sons, Inc., 2000).
- <sup>9</sup> C. Sridevi and G. Velraj, *Spectrochim. Acta A* **121**, 533-543 (2014).
- <sup>10</sup> S. G. Burton and R. A. Dorrington, *Tetrahedron: Asymmetry* **15**, 2737-2741 (2004).
- <sup>11</sup> H. Ozeki, R. Miyahara, H. Ihara, S. Todaka, K. Kobayashi and M. Ohishi, *Astron. Astrophys.* **600**, A44 (2017).
- <sup>12</sup> C. A. Gottlieb, P. Palmer, L. J. Rickard and B. Zuckerman, *Astrophys. J.* **182**, 699-710 (1973).
- <sup>13</sup> J. M. Hollis, F. J. Lovas, J. R. Anthony, P. R. Jewell, V. V. Ilyushin and I. Kleiner, *Astrophys. J. Lett.* **643**, L25 (2006).
- <sup>14</sup> R. H. Rubin, G. W. Swenson, Jr., R. C. Benson, H. L. Tigelaar and W. H. Flygare, *Astrophys. J.* **169**, L39 (1971).
- <sup>15</sup> R. A. Loomis, D. P. Zaleski, A. Steber, L. J. Neill, L. T. M. Matthew, J. H. Brent, M. H. Jan, R. J. Philip, L. Valerio, J. L. Frank, Oscar Martinez, Jr., C. M. Michael, J. R. Anthony, H. P. Brooks and F. C. Joanna, *Astrophys. J. Lett* **765**, L9 (2013).
- <sup>16</sup> N. Fourikis, K. Takagi and M. Morimoto, *Astrophys. J. Lett.* **191**, L139 (1974).
- <sup>17</sup> H. E. Matthews and T. J. Sears, *Astrophys. J. Lett.* **267**, L53-L57 (1983).
- <sup>18</sup> F. J. Lovas, J. R. Anthony, J. M. Hollis, P. R. Jewell and L. E. Snyder, *Astrophys. J. Lett.* **637**(1), L37 (2006).
- <sup>19</sup> P. D. Godfrey, R. D. Brown, B. J. Robinson and M. W. Sinclair, *Astrophys. Lett.* **13**, 119-121 (1973).
- <sup>20</sup> J. L. Alonso and J. C. López, in *Gas-Phase IR Spectroscopy and Structure of Biological Molecules*, edited by A. M. Rijs and J. Oomens (Springer International Publishing, Cham, 2015), pp. 335-401.
- <sup>21</sup> J. L. Alonso, V. Vaquero, I. Peña, J. C. López, S. Mata and W. Caminati, *Angew. Chem. Int. Ed.* **52**(8), 2331 (2013).
- <sup>22</sup> J. C. López, M. Isabel Peña, M. Eugenia Sanz and J. L. Alonso, *J. Chem. Phys.* **126**(19), 191103 (2007).
- <sup>23</sup> V. Vaquero, M. E. Sanz, J. C. López and J. L. Alonso, *J. Phys. Chem. A* **111**(18), 3443-3445 (2007).
- <sup>24</sup> C. Bermúdez, S. Mata, C. Cabezas and J. L. Alonso, *Angew. Chem. Int. Ed.* **53**(41), 11015-11018 (2014).
- <sup>25</sup> C. Cabezas, M. Varela, I. Peña, S. Mata, J. C. Lopez and J. L. Alonso, *Chem. Comm.* **48**(47), 5934-5936 (2012).
- <sup>26</sup> I. Peña, C. Cabezas and J. L. Alonso, *Angew. Chem. Int. Ed.* **54**(10), 2991-2994 (2015).
- <sup>27</sup> C. Cabezas, M. Varela and J. L. Alonso, *Angew. Chem.* **129**(23), 6520-6525 (2017).
- <sup>28</sup> S. Mata, I. Peña, C. Cabezas, J. C. López and J. L. Alonso, *J. Mol. Spectrosc.* **280**(0), 91-96 (2012).
- <sup>29</sup> M. J. Frisch, G. W. Trucks, H. B. Schlegel, G. E. Scuseria, M. A. Robb, J. R. Cheeseman, G. Scalmani, V. Barone, B. Mennucci, G. A. Petersson, H. Nakatsuji, M. Caricato, X. Li, H. P. Hratchian, A. F. Izmaylov, J. Bloino, G. Zheng, J. L. Sonnenberg, M. Hada, M. Ehara, K. Toyota, R. Fukuda, J. Hasegawa, M. Ishida, T. Nakajima, Y. Honda, O. Kitao, H. Nakai, T. Vreven, J. A. Montgomery Jr., J. E. Peralta, F. Ogliaro, M. J. Bearpark, J. Heyd, E. N. Brothers, K. N. Kudin, V. N. Staroverov, R. Kobayashi, J. Normand, K. Raghavachari, A. P. Rendell, J. C. Burant, S. S. Iyengar, J. Tomasi, M. Cossi, N. Rega, N. J. Millam, M. Klene, J. E. Knox, J. B. Cross, V. Bakken, C. Adamo, J. Jaramillo, R. Gomperts, R. E. Stratmann, O. Yazyev, A. J. Austin, R. Cammi, C. Pomelli, J. W. Ochterski, R. L. Martin, K. Morokuma, V. G. Zakrzewski, G. A. Voth, P. Salvador, J. J. Dannenberg, S. Dapprich, A. D. Daniels, Ö. Farkas, J. B. Foresman, J. V. Ortiz, J. Cioslowski and D. J. Fox, (Gaussian, Inc., Wallingford, CT, USA, 2009).
- <sup>30</sup> W. Gordy and R. L. Cook, *Microwave molecular spectra.* (Wiley, New York, 1984).

<sup>31</sup> E. Kleinpeter, *Struct. Chem.* **8**(2), 161-173 (1997).

<sup>32</sup> M. Stolze and D. H. Sutter, *Z. Naturforsch. A* **42**, 49 (1987).

<sup>33</sup> C. Tanjaroon, R. Subramanian, C. Karunatilaka and S. G. Kukolich, *J. Phys. Chem. A* **108**(44), 9531-9539 (2004).

<sup>34</sup> N. Heineking, H. Dreizler and R. Schwarz, *Z. Naturforsch. A* **41**, 1210-1213 (1987).

<sup>35</sup> Y. Kawashima, R. D. Suenram and E. Hirota, *J. Mol. Spectrosc.* **219**(1), 105-118 (2003).

## **CONCLUSIONS AND FUTURE TRENDS**

---



## CONCLUSIONS

---

In this Memory is collected all the work done during the Ph.D. period. In general terms, several structural studies of different molecules have been carried out in the gas phase by rotational spectroscopy in two major subjects: the structural study of biomolecules and molecules with the aim of unveiling the relationship structure-property and the study of prebiotic molecules and amino acids precursors susceptible to be detected in the interstellar medium.

The following general conclusions can be extracted from the experimental work described in the above chapters:

- The archetypal methyl- $\beta$ -D-xyloside was the chosen molecule to experimentally prove for the first time the structural effects caused by **the *exo*-anomeric effect**. The species observed by LA-CP-FTMW microwave spectroscopy has been unequivocally attributed to conformer *cc*- $\beta$ - $^4C_1$  *g*-, where the configurational orientation adopted by the aglycon residue (-CH<sub>3</sub>) contributes towards maximization of the *exo*-anomeric effect. Furthermore, the detection of eleven isotopologues, derived from the presence of six  $^{13}\text{C}$  and five  $^{18}\text{O}$  atoms observed in their natural abundances, allowed the determination of the bond length decrease of glycosidic C<sub>1</sub>-O<sub>1</sub> (1.38 Å) bond which can only be due to the hyperconjugative interactions responsible for the *exo*-anomeric effect.
- In the gas phase isolation conditions of a supersonic expansion, three different conformers have been revealed for **the artificial sweetener D-sorbitol**, investigated for the first time using a combination of chirped pulse Fourier transform microwave spectroscopy (CP-FTMW) coupled with laser ablation (LA) source. All conformers are over-stabilized by a network of five cooperative intramolecular hydrogen bonds between vicinal hydroxyl groups in clockwise (*c*) or counterclockwise (*cc*) arrangements. They all share a characteristic structural

signature: the  $O_1H\cdots O_2$  intramolecular hydrogen bond that fulfills the requirements of the *glucophore* proposed by Shallenberger's molecular theory of sweet taste. The results provide the first linkage between sweetness and structure in sugar alcohols.

- The state of the art of our laser ablation techniques has allowed bringing the vast commonly used **artificial sweetener of saccharine** into the gas phase. The structure derived from its Fourier transform microwave spectrum indicates that in saccharine, the imine group acts as the proton donor and the oxygen of the sulfoxide group as proton acceptor according to with the Shallenberger proposal of the sweet taste.
- The benefits of vaporization by laser ablation (LA) and the high resolution and sensitivity attained by the chirped pulse Fourier transform microwave spectroscopy (CP-FTMW) have provided the first conformational map of **the phenolic acids**. The spectroscopic constants, derived from the analysis of the rotational spectra and compared with those predicted theoretically, provide an unmatched means to achieve an unambiguous identification of two conformers of trans-cinnamic acid and four conformers of trans-p-coumaric acid.
- The rotational and quadrupole coupling constants of the two  $^{14}N$  nuclei determined in the capped **dipeptide Ac-Val-NH<sub>2</sub>** using LA-MB-FTMW spectroscopy shows that non-polar side chain dipeptides exist as a mixture of two  $C_7$  and  $C_5$  conformers.  $C=O\cdots H-N$  intramolecular hydrogen bonds are closing a seven- or a five-membered ring respectively. The large isopropyl group is not able to prevent the less stable  $C_5$  conformer from forming, but it destabilizes the  $C=O\cdots H-N$  interaction.
- A general procedure has been introduced combining different time and frequency domain spectroscopic tools for providing the precise set of spectroscopic



constants for a broad characterization of the molecular emission signal of complex organic molecules of the hot cores of the interstellar medium ISM. The identification of specific species requires direct comparison of the particular frequencies observed in interstellar space with spectroscopic measurements of known species in a laboratory experiment. The millimeter and submillimeter-wave spectra of O-rich and N-rich prebiotic molecules of **acrylic acid** ( $\text{CH}_2=\text{CH}-\text{COOH}$ ), **vinyl formate** ( $\text{HCO}_2\text{CH}=\text{CH}_2$ ), **methoxyamine** ( $\text{CH}_3\text{-O-NH}_2$ ), **N-methyl hydroxylamine** ( $\text{CH}_3\text{-NHOH}$ ) and **isopropyl cyanide** ( $(\text{CH}_3)_2\text{-CN}$ ). The high resolution and sensitivity reached with our Stark, and frequency-modulation techniques in the microwave and millimeter wave regions allowed us to analyze pure rotational spectra in 29 excited vibrational states of interstellar **aminoacetonitrile** ( $\text{NH}_2\text{CH}_2\text{-CN}$ ) a possible precursor of glycine, and also observe  $^{13}\text{C}$  isotopologues in natural abundance. Present data can be confidently used in future to search for new species in the ISM as well as further astrophysical identifications in warmer regions where vibrationally excited states might be populated.

- **The glycinamide** ( $\text{H}_2\text{N-CH}_2\text{-CONH}_2$ ), a possible precursor of glycine in the interstellar space according to the Strecker reaction, has been finally caught and characterized in the gas phase by the latest developments in Fourier transform microwave techniques coupled with laser ablation vaporization methods. The glycinamide neutral form was liberated from the glycinamide hydrochloride salt using a laser ablation technique. The first precise data supplied about this glycine precursor could be of immense importance for possible future identifications in the interstellar medium.
- An essential target in astrochemistry, as a possible precursor of glycine, the solid **hydantoin** has been brought into the gas phase by laser ablation, and its complex nuclear quadrupole hyperfine structure due to the presence of two  $^{14}\text{N}$  nuclei has been measured for the first time by high-resolution FTMW techniques. The

nuclear quadrupole coupling constants extracted from the analysis establish the diketo form conclusively for hydantoin. The spectroscopic information provided in this work could be relevant to check the existence of hydantoin in the interstellar medium

## FUTURE TRENDS

---

### **Astrochemistry: Sugar in space**

Looking for biomolecules in the interstellar medium (ISM) or in laboratory simulations of this medium has known a growing attractiveness in the two last decades. The aim of these studies is to demonstrate that the synthesis of building blocks of life can be easily realized in various places of the Universe: ISM, comets, planetary atmospheres, meteorites. The hypothesis that such compounds reached the Primitive Earth and played a role in the emergency of life is still being debated.

A family of key compounds of living systems is constituted by sugars. The simplest oligomer of formaldehyde ( $(\text{CH}_2\text{O})_n$ ,  $n=2$ ), the glycolaldehyde, has been detected in the ISM by Hollis et al.<sup>1</sup> but remains, up to date, the only one hydroxylated carbonyl compound detected in the ISM. Many attempts tried to detect chiral species in the ISM, to a large extend in the aim to demonstrate a highest complexity of the chemistry of this medium than the one usually accepted, and thus the possible formation of more sophisticated molecules. In 2016, McGuire et al.<sup>2</sup> discovered the first chiral compound in the ISM, the 2-methyloxirane. The detection of a methylated derivative of a previously observed compound is quite usual since many methylated derivatives of detected compounds have been observed in the ISM. The case of lactaldehyde, the methylated derivatives of glycolaldehyde and the simplest chiral, is remarkable among all sugars as to date no microwave investigations of this relevant chiral compound have been reported to give an essential tool for its the detection in the ISM.

The microwave investigation of lactaldehyde is being undertaken in the GEM. Lactaldehyde, a solid with high melting point, is well known for its thermal instability; it rearranges in the thermodynamically more stable isomer, the hydroxyacetone. Lactaldehyde crystallizes in three different crystal forms all of them consist of hemiacetal dimers having the same 1,4-dioxane ring skeleton. We have been able to dedimerize the hemiacetal in delicate experimental conditions to record the microwave, millimetric and centimetric spectrum in the gas phase.

### **Artificial Sweeteners: Cyclamates**

Cyclamate was used commercially for many years as an artificial sweetening agent, but was banned in the US, Canada and the UK in 1970 because of suspected carcinogenic effects. Cyclamate is currently available in more than 50 countries worldwide, including several European countries, and is being used in food, drink and pharmaceuticals. In June 1994 the Sweeteners Directive of the European Union was introduced. The directive allows the use of cyclamate and saccharine how much of a sweetener may be used in each type of food or drink.

As a continuation of our study on saccharine, the solid of cyclamic acid will be study by LA-CP-FTMW. The  $\text{NH}\text{SO}_3\text{H}$  (sulfamate function) is presumed to contain the Shallenberger AH/B centres necessary for the elicitation of sweet taste of this compound. The tridimensional structure derived from the study should indicate the NH probably represents the AH entity and the B receptor centre on the sulfamate function.

### **REFERENCES**

---

<sup>1</sup> J. M. Hollis, F. J. Lovas, and P. R. Jewell, *ApJ*, 2000, 540:, L107-L110

<sup>2</sup> B. A. McGuire, P. B. Carroll, R. A. Loomis, I. A. Finneran, P. R. Jewell, A. J. Remijan, and G. A. Blake. *Science*, 2016, 352, 1449-1552



# **APPENDIX.**

## **Supplementary Information**

---



## Supplementary information for Chapter I:

**Table S1.** Observed frequencies and residuals (in MHz) for the rotational transitions of conformer cc- $\beta$ -<sup>4</sup>C<sub>1</sub> g- of methyl  $\beta$ -D-xyloside.

$J'$	$K'_{-1}$	$K'_{+1}$	$J''$	$K''_{-1}$	$K''_{+1}$	$\nu_{\text{obs}}$	$\nu_{\text{obs}} - \nu_{\text{cal}}$
3	1	2	2	0	2	6043.041	0.001
4	1	3	3	1	2	6069.136	0.010
2	2	1	1	1	1	6128.006	-0.020
5	0	5	4	1	4	6211.510	-0.004
5	1	5	4	1	4	6385.350	0.013
5	0	5	4	0	4	6525.870	0.009
5	1	5	4	0	4	6699.680	-0.004
5	2	4	4	2	3	7023.657	0.015
3	2	2	2	1	1	7077.502	-0.012
5	4	2	4	4	1	7198.054	0.008
5	4	1	4	4	0	7200.929	0.006
3	2	1	2	1	1	7267.477	0.002
5	1	4	4	1	3	7484.768	0.014
6	0	6	5	1	5	7514.553	-0.008
6	1	6	5	1	5	7603.835	0.013
5	2	3	4	2	2	7605.757	0.009
6	0	6	5	0	5	7688.394	0.011
6	1	6	5	0	5	7777.638	-0.006
3	2	2	2	1	2	7786.531	-0.003
4	1	3	3	0	3	7996.281	-0.003
4	2	3	3	1	2	8141.359	-0.004
6	2	5	5	2	4	8359.362	0.013
6	3	4	5	3	3	8653.685	-0.004
6	4	3	5	4	2	8662.870	0.007
4	2	2	3	1	2	8672.441	0.001
6	4	2	5	4	1	8675.534	0.005
7	0	7	6	1	6	8765.162	-0.011
7	1	7	6	1	6	8808.727	0.012
6	1	5	5	1	4	8818.988	0.010
7	0	7	6	0	6	8854.446	0.012
6	3	3	5	3	2	8856.284	-0.003
7	1	7	6	0	6	8897.970	-0.005
7	1	6	6	2	5	8911.639	-0.001
5	2	4	4	1	3	9095.872	-0.008
6	2	4	5	2	3	9191.319	0.008
3	3	1	2	2	0	9525.882	0.015
3	3	0	2	2	0	9530.044	0.015
4	2	3	3	1	3	9555.234	-0.008
3	3	1	2	2	1	9565.220	0.017
7	2	6	6	2	5	9662.851	0.010
6	2	5	5	1	4	9970.465	-0.009

8	0	8	7	1	7	9984.324	-0.015
8	1	8	7	1	7	10004.813	-0.007
8	0	8	7	0	7	10027.886	0.005
8	1	8	7	0	7	10048.358	-0.004
7	1	6	6	1	5	10063.143	0.008
7	5	3	6	5	2	10096.102	-0.000
7	5	2	6	5	1	10097.646	-0.001
5	1	4	4	0	4	10133.837	-0.008
5	2	3	4	1	3	10209.050	-0.013
7	3	4	6	3	3	10481.605	-0.007
7	2	5	6	2	4	10722.922	0.012
7	2	6	6	1	5	10814.326	-0.013
4	3	1	3	2	1	10893.814	0.013
8	2	7	7	2	6	10934.988	0.011
9	1	9	8	1	8	11195.798	-0.002
9	0	9	8	0	8	11206.877	-0.026
8	1	7	7	1	6	11236.668	0.010
5	2	4	4	1	4	11430.608	-0.014
8	3	6	7	3	5	11487.623	-0.001
8	5	4	7	5	3	11570.298	-0.011
8	5	3	7	5	2	11576.332	-0.011
8	2	7	7	1	6	11686.180	-0.000
6	2	4	5	1	4	11915.603	-0.016

**Table S2.** Cartesian coordinates for the  $c\text{-}\beta\text{-}^4\text{C}_1$  g- conformer. The geometries have been optimized ab initio at the MP2/6-311++G(d,p) level of theory.

Center Number	Atomic Number	Coordinates (Angstroms)		
		X	Y	Z
1	6	-0.485055	-1.767278	0.206751
2	8	0.769165	-1.361925	-0.319028
3	6	1.167421	-0.086975	0.186043
4	6	0.170860	0.983317	-0.237471
5	6	-1.229247	0.582270	0.198086
6	6	-1.575013	-0.813720	-0.274800
7	8	2.399907	0.224823	-0.345643
8	8	0.544630	2.205578	0.372347
9	8	-2.118773	1.565115	-0.316706
10	8	-2.852393	-1.121899	0.286286
11	1	-1.263157	0.586609	1.299349
12	1	-0.472843	-1.777049	1.307827
13	1	0.206632	1.056988	-1.333447
14	1	-3.226708	-1.857705	-0.207399
15	1	-0.186180	2.812940	0.206989
16	1	-0.660137	-2.785526	-0.150527
17	1	-1.617894	-0.821181	-1.371458
18	1	-3.004957	1.292092	-0.052490
19	1	1.213003	-0.141942	1.290939
20	6	3.445900	-0.580651	0.188217
21	1	4.372736	-0.205160	-0.244950
22	1	3.486938	-0.480019	1.280523
23	1	3.310316	-1.632062	-0.080230

Rotational constants (MHZ):    1774.4836143    829.1320535    595.3163125



**Table S3.** Cartesian coordinates for the  $cc\text{-}\beta\text{-}^4C_1g^+$  conformer. The geometries have been optimized ab initio at the MP2/6-311++G(d,p) level of theory.

Center Number	Atomic Number	Coordinates (Angstroms)		
		X	Y	Z
1	6	0.696995	-1.742581	-0.310050
2	8	-0.677503	-1.511035	-0.007228
3	6	-1.113457	-0.279527	-0.545334
4	6	-0.344152	0.874603	0.099077
5	6	1.135905	0.690768	-0.165897
6	6	1.577740	-0.673945	0.327180
7	8	-2.495692	-0.151814	-0.386493
8	8	-0.726832	2.120583	-0.467811
9	8	1.928558	1.665214	0.501816
10	8	2.919080	-0.949625	-0.039025
11	1	1.309179	0.744405	-1.251978
12	1	0.856831	-1.745326	-1.398218
13	1	-0.510315	0.871844	1.184507
14	1	3.432501	-0.178526	0.229322
15	1	-1.691249	2.132645	-0.488325
16	1	0.943316	-2.728550	0.086017
17	1	1.456456	-0.708872	1.419444
18	1	1.604237	2.527849	0.218231
19	1	-0.949573	-0.255622	-1.633089
20	6	-2.972615	-0.379504	0.943160
21	1	-4.055465	-0.270901	0.884604
22	1	-2.718450	-1.385713	1.281013
23	1	-2.576722	0.356791	1.651580

Rotational constants (MHZ):    1713.0814369    868.7174669    637.9641691

**Table S4.** Cartesian coordinates for the  $cc\text{-}\beta\text{-}^4C_1g^-$  conformer. The geometries have been optimized ab initio at the MP2/6-311++G(d,p) level of theory.

Center Number	Atomic Number	Coordinates (Angstroms)		
		X	Y	Z
1	6	-0.501757	-1.765569	0.165078
2	8	0.768099	-1.363015	-0.343745
3	6	1.148038	-0.108485	0.192977
4	6	0.171633	0.972445	-0.247639
5	6	-1.223613	0.605017	0.214566
6	6	-1.583903	-0.785776	-0.272908
7	8	2.398246	0.244063	-0.293799
8	8	0.485324	2.231934	0.330737
9	8	-2.206452	1.502637	-0.285792
10	8	-2.813179	-1.225859	0.280515
11	1	-1.241159	0.603474	1.315776
12	1	-0.482436	-1.820648	1.263838
13	1	0.197213	1.022815	-1.344706
14	1	-3.445400	-0.514475	0.124606
15	1	1.387724	2.438001	0.060691
16	1	-0.700632	-2.760520	-0.235327

17	1	-1.632798	-0.770807	-1.370806
18	1	-1.924261	2.388936	-0.031455
19	1	1.168026	-0.176883	1.298227
20	6	3.438425	-0.602002	0.194251
21	1	4.373317	-0.190055	-0.185043
22	1	3.451964	-0.596141	1.291513
23	1	3.308102	-1.624690	-0.167249

-----  
Rotational constants (MHz):            1771.6144990        832.9887646        595.4016216

**Table S5.** Observed frequencies and residuals (in MHz) for the rotational transitions of  $^{13}\text{C}_1$  monosubstituted isotopologue of conformer cc- $\beta$ - $^4\text{C}_1$  g- of methyl  $\beta$ -D-xyloside.

$J'$	$K'_{-1}$	$K'_{+1}$	$J''$	$K''_{-1}$	$K''_{+1}$	$\nu_{\text{obs}}$	$\nu_{\text{obs}} - \nu_{\text{cal}}$
5	1	5	4	1	4	6375.083	-0.001
5	0	5	4	0	4	6516.161	0.004
5	2	4	4	2	3	7010.851	-0.002
5	1	4	4	1	3	7471.018	0.004
5	2	3	4	2	2	7589.159	-0.015
6	1	6	5	1	5	7591.863	0.009
6	0	6	5	0	5	7677.005	0.001
6	2	5	5	2	4	8344.582	0.013
6	3	4	5	3	3	8636.767	0.008
7	1	7	6	1	6	8795.049	0.002
6	1	5	5	1	4	8804.013	0.003
6	3	3	5	3	2	8836.904	0.001
7	0	7	6	0	6	8841.214	-0.004
6	2	4	5	2	3	9171.895	0.005
7	2	6	6	2	5	9646.294	0.006
8	1	8	7	1	7	9989.434	-0.002
8	0	8	7	0	7	10012.775	-0.015
7	1	6	6	1	5	10047.434	-0.008
7	3	5	6	3	4	10063.803	-0.001
7	3	4	6	3	3	10457.906	-0.002
7	2	5	6	2	4	10701.331	-0.005
8	2	7	7	2	6	10916.822	0.009
8	1	7	7	1	6	11220.123	-0.004

**Table S6.** Observed frequencies and residuals (in MHz) for the rotational transitions of  $^{13}\text{C}_2$  monosubstituted isotopologue of conformer cc- $\beta$ - $^4\text{C}_1$  g- of methyl  $\beta$ -D-xyloside.

$J'$	$K'_{-1}$	$K'_{+1}$	$J''$	$K''_{-1}$	$K''_{+1}$	$\nu_{\text{obs}}$	$\nu_{\text{obs}} - \nu_{\text{cal}}$
4	1	3	3	1	2	6066.226	0.003
5	1	5	4	1	4	6379.105	0.008
5	0	5	4	0	4	6518.216	0.005

5	2	4	4	2	3	7019.043	0.002
5	1	4	4	1	3	7479.913	0.002
6	1	6	5	1	5	7596.018	0.000
5	2	3	4	2	2	7605.002	0.005
6	0	6	5	0	5	7679.328	0.002
6	2	5	5	2	4	8353.177	-0.001
6	3	4	5	3	3	8649.859	0.010
6	1	5	5	1	4	8811.346	0.008
7	0	7	6	0	6	8844.207	-0.002
6	2	4	5	2	3	9189.403	-0.000
7	2	6	6	2	5	9654.862	-0.012
8	1	8	7	1	7	9994.007	0.000
8	0	8	7	0	7	10016.521	-0.000
7	1	6	6	1	5	10052.248	-0.004
7	3	5	6	3	4	10078.173	-0.016

**Table S7.** Observed frequencies and residuals (in MHz) for the rotational transitions of  $^{13}\text{C}_3$  monosubstituted isotopologue of conformer cc- $\beta$ - $^4\text{C}_1$  g- of methyl  $\beta$ -D-xyloside.

$J'$	$K'_{-1}$	$K'_{+1}$	$J''$	$K''_{-1}$	$K''_{+1}$	$\nu_{\text{obs}}$	$\nu_{\text{obs}} - \nu_{\text{cal}}$
4	1	3	3	1	2	6054.732	0.007
5	1	5	4	1	4	6371.319	0.003
5	0	5	4	0	4	6511.957	0.006
5	1	4	4	1	3	7467.423	0.003
5	2	3	4	2	2	7586.733	0.001
6	1	6	5	1	5	7587.258	0.003
6	0	6	5	0	5	7672.019	-0.001
6	2	5	5	2	4	8340.276	-0.004
7	1	7	6	1	6	8789.629	0.003
7	0	7	6	0	6	8835.530	0.003
6	2	4	5	2	3	9168.656	-0.004
7	2	6	6	2	5	9641.078	-0.006
8	1	8	7	1	7	9983.208	-0.005
8	0	8	7	0	7	10006.400	-0.001
7	1	6	6	1	5	10041.312	-0.003
7	2	5	6	2	4	10697.068	0.003

**Table S8.** Observed frequencies and residuals (in MHz) for the rotational transitions of  $^{13}\text{C}_4$  monosubstituted isotopologue of conformer cc- $\beta$ - $^4\text{C}_1$  g- of methyl  $\beta$ -D-xyloside.

$J'$	$K'_{-1}$	$K'_{+1}$	$J''$	$K''_{-1}$	$K''_{+1}$	$\nu_{\text{obs}}$	$\nu_{\text{obs}} - \nu_{\text{cal}}$
4	1	3	3	1	2	6044.731	0.002
5	1	5	4	1	4	6361.598	0.004
5	0	5	4	0	4	6502.324	0.004
5	2	4	4	2	3	6996.163	-0.004
5	1	4	4	1	3	7455.400	0.002

5	2	3	4	2	2	7573.507	-0.003
6	1	6	5	1	5	7575.768	-0.001
6	0	6	5	0	5	7660.692	0.003
6	2	5	5	2	4	8327.052	-0.001
7	1	7	6	1	6	8776.395	0.001
6	1	5	5	1	4	8785.511	0.003
7	0	7	6	0	6	8822.423	-0.008
6	2	4	5	2	3	9152.915	-0.003
7	2	6	6	2	5	9626.001	0.004
8	1	8	7	1	7	9968.242	0.005
8	0	8	7	0	7	9991.514	-0.004
7	1	6	6	1	5	10026.208	-0.005
7	2	5	6	2	4	10679.122	0.003

**Table S9.** Observed frequencies and residuals (in MHz) for the rotational transitions of  $^{13}\text{C}_5$  monosubstituted isotopologue of conformer cc- $\beta$ - $^4\text{C}_1$  g- of methyl  $\beta$ -D-xyloside.

$J'$	$K'_{-1}$	$K'_{+1}$	$J''$	$K''_{-1}$	$K''_{+1}$	$\nu_{\text{obs}}$	$\nu_{\text{obs}} - \nu_{\text{cal}}$
4	1	3	3	1	2	6058.760	0.003
5	1	5	4	1	4	6363.200	0.001
5	0	5	4	0	4	6499.231	0.006
5	2	4	4	2	3	7007.191	-0.015
5	1	4	4	1	3	7467.740	0.006
6	1	6	5	1	5	7576.203	0.007
5	2	3	4	2	2	7602.195	0.005
6	0	6	5	0	5	7656.769	0.001
6	2	5	5	2	4	8337.457	0.000
6	3	4	5	3	3	8639.593	-0.000
6	1	5	5	1	4	8792.471	0.004
6	2	4	5	2	3	9183.730	-0.005
7	2	6	6	2	5	9634.735	-0.000
7	0	7	6	0	6	8818.619	0.017
8	1	8	7	1	7	9966.588	-0.008
8	0	8	7	0	7	9987.918	-0.011
7	1	6	6	1	5	10025.673	-0.008
7	3	5	6	3	4	10064.995	0.003
8	2	7	7	2	6	10900.205	0.012

**Table S10.** Observed frequencies and residuals (in MHz) for the rotational transitions of  $^{13}\text{C}_6$  monosubstituted isotopologue of conformer cc- $\beta$ - $^4\text{C}_1$  g- of methyl  $\beta$ -D-xyloside.

$J'$	$K'_{-1}$	$K'_{+1}$	$J''$	$K''_{-1}$	$K''_{+1}$	$\nu_{\text{obs}}$	$\nu_{\text{obs}} - \nu_{\text{cal}}$
5	1	5	4	1	4	6291.054	0.001
5	0	5	4	0	4	6436.200	-0.001
5	2	4	4	2	3	6908.402	0.009
5	1	4	4	1	3	7361.489	0.004
5	2	3	4	2	2	7459.199	0.006

6	1	6	5	1	5	7493.471	-0.005
6	0	6	5	0	5	7583.072	0.002
6	2	5	5	2	4	8225.702	0.002
6	3	4	5	3	3	8502.369	0.012
7	1	7	6	1	6	8682.439	0.003
6	1	5	5	1	4	8683.508	0.001
6	3	3	5	3	2	8685.050	0.007
7	0	7	6	0	6	8732.069	-0.008
6	2	4	5	2	3	9019.129	0.001
7	2	6	6	2	5	9512.597	-0.004
8	1	8	7	1	7	9862.493	0.009
8	0	8	7	0	7	9888.110	-0.003
7	3	5	6	3	4	9909.506	-0.007
7	1	6	6	1	5	9919.781	-0.003
7	3	4	6	3	3	10272.665	-0.008
7	2	5	6	2	4	10530.789	-0.009
8	2	7	7	2	6	10769.519	0.007
9	0	9	8	0	8	11049.814	-0.005
8	1	7	7	1	6	11084.802	0.002
8	3	6	7	3	5	11294.010	-0.004

**Table S11.** Observed frequencies and residuals (in MHz) for the rotational transitions of  $^{18}\text{O}_1$  monosubstituted isotopologue of conformer cc- $\beta$ - $^4\text{C}_1$  g- of methyl  $\beta$ -D-xyloside.

$J'$	$K'_{-1}$	$K'_{+1}$	$J''$	$K''_{-1}$	$K''_{+1}$	$V_{\text{obs}}$	$V_{\text{obs}} - V_{\text{cal}}$
5	0	5	4	0	4	6441.172	-0.006
5	2	4	4	2	3	6913.198	0.011
5	1	4	4	1	3	7366.256	-0.006
6	1	6	5	1	5	7499.387	-0.002
6	2	5	5	2	4	8231.492	0.003
6	3	3	5	3	2	8690.530	-0.004
7	2	6	6	2	5	9519.401	0.004
8	1	8	7	1	7	9870.397	-0.000

**Table S12.** Observed frequencies and residuals (in MHz) for the rotational transitions of  $^{18}\text{O}_2$  monosubstituted isotopologue of conformer cc- $\beta$ - $^4\text{C}_1$  g- of methyl  $\beta$ -D-xyloside.

$J'$	$K'_{-1}$	$K'_{+1}$	$J''$	$K''_{-1}$	$K''_{+1}$	$V_{\text{obs}}$	$V_{\text{obs}} - V_{\text{cal}}$
4	1	3	3	1	2	6037.757	-0.004
5	1	5	4	1	4	6317.630	0.013
5	0	5	4	0	4	6443.900	-0.010
5	2	4	4	2	3	6973.800	0.009
6	1	6	5	1	5	7519.227	0.006
6	0	6	5	0	5	7591.487	0.008
5	2	3	4	2	2	7596.672	-0.008

6	2	5	5	2	4	8292.498	0.004
6	2	4	5	2	3	9169.237	0.003
8	0	8	7	0	7	9905.722	-0.016

**Table S13.** Observed frequencies and residuals (in MHz) for the rotational transitions of  $^{18}\text{O}_3$  monosubstituted isotopologue of conformer cc- $\beta$ - $^4\text{C}_1$  g- of methyl  $\beta$ -D-xyloside.

$J'$	$K'_{-1}$	$K'_{+1}$	$J''$	$K''_{-1}$	$K''_{+1}$	$\nu_{\text{obs}}$	$\nu_{\text{obs}} - \nu_{\text{cal}}$
5	0	5	4	0	4	6420.103	0.003
5	2	4	4	2	3	6910.419	-0.010
5	1	4	4	1	3	7364.552	0.010
6	0	6	5	0	5	7563.635	-0.002
7	1	7	6	1	6	8665.660	0.003
6	1	5	5	1	4	8677.132	-0.002
7	1	6	6	1	5	9901.009	-0.003

**Table S14.** Observed frequencies and residuals (in MHz) for the rotational transitions of  $^{18}\text{O}_4$  monosubstituted isotopologue of conformer cc- $\beta$ - $^4\text{C}_1$  g- of methyl  $\beta$ -D-xyloside.

$J'$	$K'_{-1}$	$K'_{+1}$	$J''$	$K''_{-1}$	$K''_{+1}$	$\nu_{\text{obs}}$	$\nu_{\text{obs}} - \nu_{\text{cal}}$
5	0	5	4	0	4	6388.364	-0.001
5	2	4	4	2	3	6859.909	0.006
5	1	4	4	1	3	7310.097	-0.009
5	2	3	4	2	2	7410.139	0.009
6	1	6	5	1	5	7438.506	0.006
6	1	5	5	1	4	8621.494	0.005
7	0	7	6	0	6	8667.132	0.008
6	2	4	5	2	3	8959.163	-0.007
8	1	8	7	1	7	9789.646	-0.012

**Table S15.** Observed frequencies and residuals (in MHz) for the rotational transitions of  $^{18}\text{O}_5$  monosubstituted isotopologue of conformer cc- $\beta$ - $^4\text{C}_1$  g- of methyl  $\beta$ -D-xyloside.

$J'$	$K'_{-1}$	$K'_{+1}$	$J''$	$K''_{-1}$	$K''_{+1}$	$\nu_{\text{obs}}$	$\nu_{\text{obs}} - \nu_{\text{cal}}$
4	1	3	3	1	2	6047.979	0.004
5	1	5	4	1	4	6352.249	-0.002
5	0	5	4	0	4	6487.759	0.001
5	1	4	4	1	3	7454.327	-0.010
6	0	6	5	0	5	7643.379	0.011
6	2	5	5	2	4	8322.832	0.008
7	0	7	6	0	6	8803.285	-0.005
8	1	8	7	1	7	9949.474	-0.004
7	1	6	6	1	5	10007.377	-0.000

**Table S16.** Substitution coordinates for conformer cc- $\beta$ - $^4\text{C}_1$ g- of methyl  $\beta$ -D-xylopyranoside.

atom	a	b	c
C <sub>1</sub>	1.1382 (14)	0.045 (34)	0.2034 (76)
C <sub>2</sub>	0.088 (18)	0.9664 (16)	0.2479 (64)
C <sub>3</sub>	1.2172 (13)	0.5987 (27)	0.2216 (72)
C <sub>4</sub>	1.5877 (10)	0.7754 (20)	0.2747 (57)

C <sub>5</sub>	0.4925 (32)	1.77026 (90)	0.1645 (98)
C <sub>6</sub>	3.44875 (45)	0.5995 (26)	0.1930 (80)
O <sub>1</sub>	2.39812 (64)	0.2225 (70)	0.2965 (52)
O <sub>2</sub>	0.4974 (34)	2.23155 (75)	0.3137 (54)
O <sub>3</sub>	2.20226 (73)	1.5113 (11)	0.2780 (58)
O <sub>4</sub>	2.81852 (57)	1.2210 (13)	0.2730 (59)
O <sub>5</sub>	0.7529 (20)	1.3626 (11)	0.3415 (45)

<sup>a</sup>Principal inertial axis coordinates in Å; derived errors in parentheses in units of the last digit; These were calculated according to Constains formula:  $\sigma(x) = K/|x|$ ;  $\sigma(x)$  is the error in the x coordinate and  $K = 0.0012 \text{ \AA}^2$ .

**Table S17.** Experimental results of methyl  $\beta$ -D-xyloside and comparison with theoretical predictions.

	<b>Experimental</b>	MP2/B3LYP/M06HF/M05-2X /M06-2X	MP2/B3LYP/M06HF/M05-2X /M06-2X	MP2/B3LYP/M06HF/M05-2X /M06-2X
		6-311++G(d,p)	cc-pVTZ	Aug-cc-pVTZ
A <sup>a</sup> / MHz	1766.25692 (72) <sup>c</sup>	1771.6/1756.3/1779.0/1783.3/1779.3	1782.7/1765.4/1782.9/1790.2/1785.5	1777.8/1762.0/1781.9/1788.1/1783.6
B/ MHz	829.25439 (24)	833.0/ 820.0/834.9/835.6/835.2	837.4/822.7/836.1/837.8/837.2	835.4/821.2/835.2/836.7/836.2
C/ MHz	592.91443 (17)	595.4/586.9/595.8/597.1/596.2	598.6/589.2/597.0/598.9/597.8	597.2/588.1/596.4/598.1/597.0
r(C <sub>1</sub> -O <sub>1</sub> ) <sup>b</sup> /Å	1.3816 (77)	1.387/1.389/1.382/1.384/1.382	1.385/1.388/1.382/1.384/1.382	1.386/1.388/1.381/1.383/1.381

<sup>a</sup>A, B and C are the rotational constants. <sup>b</sup> C<sub>1</sub>-O<sub>1</sub> bond distance. <sup>c</sup>Standard error in parentheses in units of the last digit.

**Complete Reference 30:**

Gaussian 09 (Revision B.01), Frisch, M. J.; Trucks, G. W.; Schlegel, H. B.; Scuseria, G. E.; Robb, M. A.; Cheeseman, J. R.; Scalmani, G.; Barone, V.; Mennucci, B.; Petersson, G. A.; Nakatsuji, H.; Caricato, M.; Li, X.; Hratchian, H. P.; Izmaylov, A. F.; Bloino, J.; Zheng, G.; Sonnenberg, J. L.; Hada, M.; Ehara, M.; Toyota, K.; Fukuda, R.; Hasegawa, J.; Ishida, M.; Nakajima, T.; Honda, Y.; Kitao, O.; Nakai, H.; Vreven, T.; Montgomery, Jr., J. A.; Peralta, J. E.; Ogliaro, F.; Bearpark, M.; Heyd, J. J.; Brothers, E.; Kudin, K. N.; Staroverov, V. N.; Kobayashi, R.; Normand, J.; Raghavachari, K.; Rendell, A.; Burant, J. C.; Iyengar, S. S.; Tomasi, J.; Cossi, M.; Rega, N.; Millam, J. M.; Klene, M.; Knox, J. E.; Cross, J. B.; Bakken, V.; Adamo, C.; Jaramillo, J.; Gomperts, R.; Stratmann, R. E.; Yazyev, O.; Austin, A. J.; Cammi, R.; Pomelli, C.; Ochterski, J. W.; Martin, R. L.; Morokuma, K.; Zakrzewski, V. G.; Voith, G. A.; Salvador, P.; Dannenberg, J. J.; Dapprich, S.; Daniels, A. D.; Farkas, Ö.; Foresman, J. B.; Ortiz, J. V.; Cioslowski, J.; Fox, D. J. Gaussian, Inc., Wallingford CT, 2010.



# Supplementary information for Chapter II:

**Table S1.** Spectroscopic parameters and relative energies calculated at the MP2/6-311+ +G(d,p) level of theory for conformers with a skeletal G-TT.

Family: G-TT	G-TT/TG-/cc	G-TT/TG-/c	G-TT/G+G-/c	G-TT/G+G-/cc	G-TT/G+G-/cc'	G-TT/TT/cc	G-TT/TG-/cc	G-TT/TG+/cc	G-TT/G+G-/c'	G-TT/G+T/cc
A <sup>[a]</sup>	1686.9	1749.1	1519.1	1474.7	1509.2	1895.1	1520.4	1454.1	1557.3	1731.4
B	512.8	497.5	596.7	605.7	614.8	453.5	529.4	540.3	536.4	520.0
C	462.0	458.3	518.0	521.3	513.3	415.2	465.2	454.7	518.7	457.1
$\mu_a$	1.8	0.3	2.0	0.5	0.9	0.1	3.0	2.6	0.4	1.3
$\mu_b$	0.5	0.4	0.3	0.2	0.1	0.6	0.2	0.4	0.2	0.4
$\mu_c$	1.4	1.1	1.4	1.6	2.8	0.1	0.6	0.4	0.3	1.3
$\Delta E$	0	41	87	413.4	487.8	764.6	982.7	1015.6	1169.1	1222.1
$\Delta G$	0	-25	-29	243.0	604.4	544.3	698.4	651.4	926.6	1050.6

[a] A, B, and C represent the rotational constants (in MHz);  $\mu_a$ ,  $\mu_b$  and  $\mu_c$  are the electric dipole moment components (in D);  $\Delta E$  and  $\Delta G$  are the relative and Gibbs energies (in  $\text{cm}^{-1}$ ) at 298 K with respect to the global minimum calculated at the MP2/6-311++G (d,p) level of theory.

**Table S2.** Spectroscopic parameters and relative energies calculated at the MP2/6-311+ +G(d,p) level of theory for conformers with a skeletal G+TT.

Family: G+TT	G+TT/G+G-/cc	G+TT/G+G-/c	G+TT/G-G-/c	G+TT/TG-/c	G+TT/TG-/cc
A <sup>[a]</sup>	1745.1	1753.0	1604.4	1894.4	1853.3
B	553.5	560.5	567.9	477.1	480.3
C	503.6	499.4	475.0	428.1	427.8
$\mu_a$	2.1	0.2	1.0	2.2	2.9
$\mu_b$	0.0	0.4	1.6	1.3	1.2
$\mu_c$	2.1	2.2	2.8	0.8	0.8
$\Delta E$	396.4	417.7	503.2	831.3	1004.7
$\Delta G$	469.5	411.7	464.4	676.0	827.9

[a] A, B, and C represent the rotational constants (in MHz);  $\mu_a$ ,  $\mu_b$  and  $\mu_c$  are the electric dipole moment components (in D);  $\Delta E$  and  $\Delta G$  are the relative and Gibbs energies (in  $\text{cm}^{-1}$ ) at 298 K with respect to the global minimum calculated at the MP2/6-311++G (d,p) level of theory.

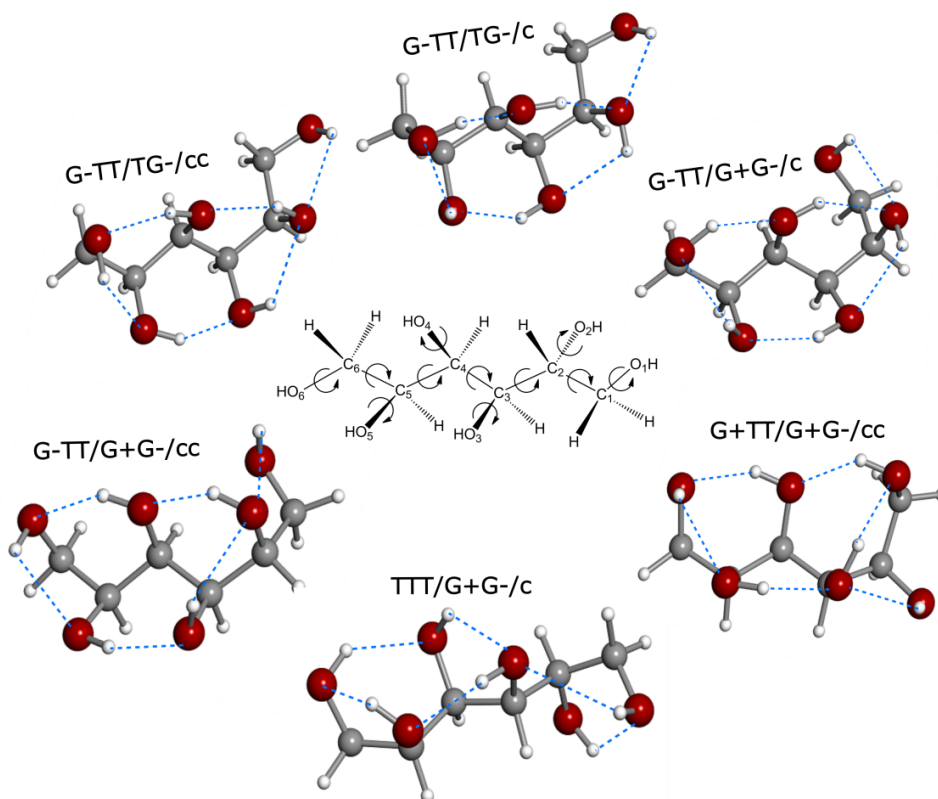
**Table S3.** Spectroscopic parameters and relative energies calculated at the MP2/6-311+ +G(d,p) level of theory for conformers with a skeletal TTT.

Family: TTT	TTT/G+G-/c	TTT/G+G-/cc	TTT/G+G-/cc'	TTT/G+G-/c'	TTT/TG-/c
A <sup>[a]</sup>	1939.6	1815.7	1915.6	1858.9	2,117.3

B	477.6	491.6	477.8	480.5	434.8
C	448.5	455.8	448.7	452.0	413.1
$ \mu_a $	0.6	1.1	0.6	1.4	1.3
$ \mu_b $	0.8	0.9	0.9	0.9	0.5
$ \mu_c $	0.5	0.4	0.4	1.1	3.0
$\Delta E$	405.4	637.2	708.4	902.7	1335.2
$\Delta G$	170.1	370.0	337.6	470.3	1008.0

**Figure S1.**  
The six more stable

[a] A, B, and C represent the rotational constants (in MHz);  $\mu_a$ ,  $\mu_b$  and  $\mu_c$  are the electric dipole moment components (in D);  $\Delta E$  and  $\Delta G$  are the relative and Gibbs energies (in  $\text{cm}^{-1}$ ) at 298 K with respect to the global minimum calculated at the MP2/6-311++G(d,p) level of theory.



conformers of sorbitol.

**Table S4.** Observed frequencies and residuals (in MHz) for conformer G-TT/TG-/ cc of D-sorbitol.

$J'$	$K'_{-1}$	$K'_{+1}$	$J''$	$K''_{-1}$	$K''_{+1}$	$\nu_{\text{obs}}$	$\nu_{\text{obs}} - \nu_{\text{calc}}$
3	2	2	2	1	2	6579.212	-0.006
3	3	0	2	2	0	8910.742	0.000
4	2	3	3	1	3	7618.178	-0.005
4	3	1	3	2	1	9873.956	-0.006
5	1	4	4	0	4	6410.009	0.010
5	2	4	4	1	4	8681.359	0.010
5	3	2	4	2	2	10831.870	0.009
6	2	5	5	1	5	9768.811	-0.016
6	1	5	5	0	5	7538.903	0.015
7	1	6	6	1	5	6911.942	0.003
7	2	6	6	2	5	6751.079	0.001
7	2	5	6	2	4	6829.844	0.001
7	3	5	6	3	4	6773.185	-0.003
7	2	6	6	1	6	10880.734	0.006

**Table S5.** Observed frequencies and residuals (in MHz) for conformer G-TT/TG-/ cc of D-sorbitol.

$J'$	$K'_{-1}$	$K'_{+1}$	$J''$	$K''_{-1}$	$K''_{+1}$	$\nu_{\text{obs}}$	$\nu_{\text{obs}} - \nu_{\text{calc}}$
3	3	0	2	2	0	9160.709	0.004
3	3	1	2	2	0	9160.709	0.018
3	3	1	2	2	1	9161.622	-0.011
3	3	0	2	2	1	9161.622	-0.025
3	2	1	2	1	1	6582.600	-0.001
3	2	2	2	1	2	6697.339	0.016
4	3	1	3	2	1	10109.674	-0.009
4	2	2	3	1	2	7482.954	0.002
4	3	2	3	2	2	10114.292	0.001
4	2	3	3	1	3	7707.714	0.013
5	2	3	4	1	3	8372.656	-0.003
5	1	4	4	0	4	6321.672	0.002
5	3	2	4	2	2	11055.223	-0.007
5	3	3	4	2	3	11068.933	0.001

7	3	4	6	3	3	6776.707	-0.001	6	1	5	5	0	5	7402.673	0.011
7	1	7	6	1	6	6574.228	-0.005	6	2	5	5	1	5	9787.965	0.001
7	0	7	6	0	6	6683.759	-0.002	6	2	4	5	1	4	9256.377	0.002
7	5	3	6	5	2	6767.854	-0.012	7	2	5	6	1	5	10139.443	-0.007
7	5	2	6	5	1	6767.854	-0.012	7	1	6	6	0	6	8511.937	-0.015
8	1	8	7	1	7	7507.416	-0.003	8	2	6	7	1	6	11027.697	0.016
8	3	5	7	3	4	7750.055	0.003	8	1	7	7	0	7	9652.473	-0.003
8	2	7	7	2	6	7710.611	0.005	8	1	8	7	1	7	7430.156	0.015
8	0	8	7	0	7	7614.257	-0.008	8	1	8	7	0	7	8225.726	-0.010
8	2	6	7	2	5	7824.854	0.006	9	1	9	8	0	8	9048.322	-0.002
8	4	4	7	4	3	7739.085	-0.005	10	1	10	9	1	9	9276.617	-0.010
8	4	5	7	4	4	7739.085	-0.005	10	1	10	9	0	9	9871.745	0.002
8	1	7	7	1	6	7890.391	-0.002								
8	3	6	7	3	5	7743.062	0.008								
8	5	4	7	5	3	7735.927	-0.004								
8	5	3	7	5	2	7735.927	-0.004								
9	2	8	8	2	7	8668.203	0.002								
9	3	7	8	3	6	8713.345	0.003								
9	1	8	8	1	7	8864.690	0.001								
9	4	5	8	4	4	8709.176	0.004								
9	4	6	8	4	5	8708.831	0.008								
9	0	9	8	0	8	8538.356	0.004								
9	3	6	8	3	5	8726.066	0.005								
9	2	7	8	2	6	8824.202	0.013								
9	1	9	8	1	8	8438.701	0.007								
9	6	4	8	6	3	8702.146	0.004								
9	6	3	8	6	2	8702.146	0.004								
10	3	7	9	3	6	9705.378	-0.007								
10	4	7	9	4	6	9679.422	-0.008								
10	1	10	9	1	9	9368.085	0.007								
10	0	10	9	0	9	9457.333	0.002								
10	3	8	9	3	7	9683.846	0.001								
10	1	9	9	1	8	9833.976	-0.016								
10	5	6	9	5	5	9673.606	0.006								
10	5	5	9	5	4	9673.606	0.006								
10	2	8	9	2	7	9826.350	-0.008								
10	2	9	9	2	8	9623.654	0.001								
10	6	5	9	6	4	9670.375	-0.001								
10	6	4	9	6	3	9670.375	-0.001								
11	2	10	10	2	9	10576.773	0.000								
11	0	11	10	0	10	10372.715	-0.002								
11	1	11	10	1	10	10295.661	0.010								
11	3	9	10	3	8	10654.311	0.014								
11	3	8	10	3	7	10688.696	-0.016								
12	2	11	11	2	10	11527.403	0.004								

**Table S7.** Cartesian coordinates of conformer G-TT/TG-/cc of D-sorbitol.

**Table S8.** Cartesian coordinates of conformer G-TT/TG-/c of D-sorbitol.

Center Number	Atomic Number	X	Y	Z
1	6	-0.574386	0.829946	-0.559942
2	1	-0.607817	1.058865	-1.637970
3	6	0.442125	-0.303222	-0.377969
4	1	0.110008	-1.137451	-1.018567
5	6	1.844057	0.070149	-0.864455
6	1	1.783604	0.254308	-1.944141
7	8	-0.260090	1.992444	0.191803
8	8	0.550807	-0.744852	0.972509
9	8	2.313707	1.275593	-0.259278
10	6	-1.986691	0.454928	-0.110414
11	1	-2.658487	1.279360	-0.381985
12	6	-2.540921	-0.828242	-0.696618
13	1	-2.489920	-0.791748	-1.788359
14	1	-1.949766	-1.684440	-0.343889
15	8	-3.908033	-0.990832	-0.356688
16	1	-3.952176	-0.902794	0.601859
17	1	0.707084	2.082758	0.156116
18	1	2.837364	0.985714	0.503723
19	1	-0.314972	-0.616831	1.391632
20	8	-2.010451	0.282710	1.317156
21	1	-1.721403	1.130831	1.681257

Center Number	Atomic Number	X	Y	Z
1	6	-0.570880	0.831844	-0.622971
2	1	-0.607544	1.049667	-1.697373
3	6	0.469307	-0.267030	-0.401273
4	1	0.210209	-1.101642	-1.074725
5	6	1.888464	0.166965	-0.794888
6	1	1.846346	0.449672	-1.860071
7	8	-0.193468	2.046536	0.031070
8	8	0.367688	-0.689630	0.956007
9	8	2.399242	1.227985	-0.006061
10	6	-1.976424	0.442592	-0.151110
11	1	-2.674525	1.212482	-0.496316
12	6	-2.466619	-0.905305	-0.656874
13	1	-2.411299	-0.944335	-1.749427
14	1	-1.842618	-1.707742	-0.240601
15	8	-3.828898	-1.096679	-0.311306
16	1	-3.889270	-0.890201	0.628634
17	1	-0.642406	2.024467	0.889521
18	1	1.655331	1.833860	0.142053
19	1	1.207017	-1.123593	1.183787
20	8	-2.051071	0.495586	1.277576
21	1	-1.349612	-0.098433	1.591370

22	6	2.857773	-1.046860	-0.597920	22	6	2.893657	-0.968516	-0.640081
23	1	3.764079	-0.861464	-1.178858	23	1	3.855216	-0.662115	-1.067092
24	1	2.435198	-2.014818	-0.895500	24	1	2.546805	-1.869277	-1.152183
25	8	3.257775	-1.043722	0.766554	25	8	3.048080	-1.312090	0.739580
26	1	2.450936	-1.221143	1.271031	26	1	3.369836	-0.505058	1.161860

**Table S9.** Cartesian coordinates of conformer G-TT/G+G-/ c of D-sorbitol.

Center Number	Atomic Number	X	Y	Z
1	6	-0.714912	0.891798	-0.573877
2	1	-0.716103	1.099729	-1.657397
3	6	0.289995	-0.242877	-0.342073
4	1	-0.058253	-1.111805	-0.918117
5	6	1.689168	0.104127	-0.851192
6	1	1.623506	0.244587	-1.936947
7	8	-0.401896	2.067068	0.161857
8	8	0.416920	-0.595207	1.034219
9	8	2.169627	1.332649	-0.298698
10	6	-2.154514	0.569973	-0.166871
11	1	-2.762281	1.435116	-0.469470
12	6	-2.763690	-0.675027	-0.795618
13	1	-3.851462	-0.638831	-0.660416
14	1	-2.553395	-0.683249	-1.869020
15	8	-2.233448	-1.881714	-0.265104
16	1	-2.513783	-1.918838	0.655194
17	1	0.566906	2.145033	0.139805
18	1	2.698002	1.069469	0.470608
19	1	-0.474986	-0.597251	1.407331
20	8	-2.237275	0.402513	1.252701
21	1	-1.838594	1.203574	1.620784
22	6	2.699806	-1.005728	-0.546791
23	1	3.603567	-0.848810	-1.140139
24	1	2.268675	-1.981715	-0.801826
25	8	3.109311	-0.950678	0.814483
26	1	2.303690	-1.103184	1.329024

## References

- [19] Gaussian 09, Revision B.01, M. J. Frisch, G. W. Trucks, H. B. Schlegel, G. E. Scuseria, M. A. Robb, J. R. Cheeseman, G. Scalmani, V. Barone, B. Mennucci, G. A. Petersson, H. Nakatsuji, M. Caricato, X. Li, H. P. Hratchian, A. F. Izmaylov, J. Bloino, G. Zheng, J. L. Sonnenberg, M. Hada, M. Ehara, K. Toyota, R. Fukuda, J. Hasegawa, M. Ishida, T. Nakajima, Y. Honda, O. Kitao, H. Nakai, T. Vreven, J. A. Montgomery, J. E. Peralta, F. Ogliaro, M. Bearpark, J. J. Heyd, E. Brothers, K. N. Kudin, V. N. Staroverov, T. Keith, R. Kobayashi, J. Normand, K. Raghavachari, A. Rendell, J. C. Burant, S. S. Iyengar, J. Tomasi, M. Cossi, N. Rega, J. M. Millam, M. Klene, J. E. Knox, J. B. Cross, V. Bakken, C. Adamo, J. Jaramillo, R. Gomperts, R. E. Stratmann, O. Yazyev, A. J. Austin, R. Cammi, C. Pomelli, J. W. Ochterski, R. L. Martin, K. Morokuma, V. G. Zakrzewski, G. A. Voth, P. Salvador, J. J. Dannenberg, S. Dapprich, A. D. Daniels, O. Farkas, J. B. Foresman, J. V. Ortiz, J. Cioslowski and D. J. Fox, Gaussian, Inc., Wallingford CT, **2010**.

## Supplementary Information for Chapter III:

**Table S1.** Observed frequencies centres and residuals (in MHz) for the rotational transitions of conformer of saccharine (LA-CP-FTMW spectrometer).

$J'$	$K'_{-1}$	$K'_{+1}$	$J''$	$K''_{-1}$	$K''_{+1}$	$\nu_{\text{obs}}$	$\nu_{\text{obs}} - \nu_{\text{cal}}$
6	0	6	5	0	5	7378.967	0.013
6	1	6	5	1	5	7370.388	-0.024
7	1	7	6	1	6	8525.713	-0.005
7	0	7	6	0	6	8528.323	0.009
8	0	8	7	0	7	9679.968	0.019
8	1	8	7	1	7	9679.201	0.001
6	1	5	5	1	4	8385.160	0.017
7	1	6	6	1	5	9489.045	-0.044
5	1	4	4	1	3	7271.341	0.030
7	1	6	6	1	5	9489.036	-0.053
6	1	5	5	1	4	8385.160	0.017
5	2	4	4	2	3	6980.104	-0.048
6	2	5	5	2	4	8219.288	-0.070
7	2	6	6	2	5	9415.578	-0.089

**Table S2.** Observed frequencies and residuals (in MHz) for the rotational transitions of conformer of saccharine (LA-MB-FTMW spectrometer).

$J'$	$K'_{-1}$	$K'_{+1}$	$F'$	$J''$	$K''_{-1}$	$K''_{+1}$	$F''$	$\nu_{\text{obs}}$	$\nu_{\text{obs}} - \nu_{\text{cal}}$
5	0	5	6	4	0	4	5	6267.335	0.002
5	0	5	4	4	0	4	3	6267.391	0.002
5	0	5	5	4	0	4	4	6267.561	0.001
5	1	5	6	4	1	4	5	6242.414	0.004
5	1	5	4	4	1	4	3	6242.477	0.000

5	1	5	5	4	1	4	4	6242.599	0.002
5	1	4	4	4	1	3	3	7306.793	0.003
5	1	4	6	4	1	3	5	7306.894	0.003
5	1	4	5	4	1	3	4	7307.375	0.003
6	0	6	7	5	0	5	6	7416.989	-0.001
6	0	6	5	5	0	5	4	7417.037	-0.001
6	0	6	6	5	0	5	5	7417.146	0.000
6	1	6	7	5	1	5	6	7408.895	-0.002
6	1	6	5	5	1	5	4	7408.948	0.000
6	1	6	6	5	1	5	5	7409.043	0.002
6	1	5	5	5	1	4	4	8424.583	0.001
6	1	5	7	5	1	4	6	8424.637	0.000
6	1	5	6	5	1	4	5	8425.048	0.000
7	1	7	8	6	1	6	7	8570.171	-0.003
7	1	7	6	6	1	6	5	8570.211	-0.004
7	1	7	6	6	1	6	5	8570.283	0.068
7	0	7	8	6	0	6	7	8572.597	-0.005
7	0	7	6	6	0	6	5	8572.638	-0.003
7	0	7	7	6	0	6	6	8572.715	-0.003
7	1	6	6	6	1	5	5	9535.095	-0.007
7	1	6	8	6	1	5	7	9535.118	-0.007
7	1	6	7	6	1	5	6	9535.422	-0.008
8	0	8	9	7	0	7	8	9730.388	-0.005
8	0	8	7	7	0	7	6	9730.417	-0.010
8	0	8	8	7	0	7	7	9730.478	-0.006
8	1	8	9	7	1	7	8	9729.695	-0.007
8	1	8	7	7	1	7	6	9729.726	-0.010
8	1	8	8	7	1	7	7	9729.784	-0.008
9	0	9	10	8	0	8	9	10888.911	0.002
9	0	9	8	8	0	8	7	10888.940	0.004

9	0	9	9	8	0	8	8	10888.980	-0.001
4	1	4	5	3	0	3	4	5166.054	0.007
4	1	4	3	3	0	3	2	5166.089	0.003
4	1	4	4	3	0	3	3	5166.464	0.008
5	1	5	6	4	0	4	5	6278.807	0.004
5	1	5	4	4	0	4	3	6278.857	0.002
5	1	5	5	4	0	4	4	6279.050	0.004
6	1	6	7	5	0	5	6	7420.368	0.001
6	1	6	5	5	0	5	4	7420.413	-0.002
6	1	6	6	5	0	5	5	7420.529	0.001
7	1	7	8	6	0	6	7	8573.551	-0.001
7	1	7	6	6	0	6	5	8573.589	-0.002
7	1	7	7	6	0	6	6	8573.667	-0.002
4	0	4	5	3	1	3	4	5026.388	0.002
4	0	4	3	3	1	3	2	5026.500	0.002
4	0	4	4	3	1	3	3	5026.571	0.000
5	0	5	6	4	1	4	5	6230.943	0.003
5	0	5	4	4	1	4	3	6231.012	0.001
5	0	5	5	4	1	4	4	6231.113	0.002
6	0	6	7	5	1	5	6	7405.519	0.000
6	0	6	5	5	1	5	4	7405.572	0.001
6	0	6	6	5	1	5	5	7405.660	0.000
7	0	7	8	6	1	6	7	8569.222	-0.002
7	0	7	6	6	1	6	5	8569.258	-0.008
7	0	7	7	6	1	6	6	8569.332	-0.004

---

**Table S3.** Theoretical calculations of the saccharine structure with different computational methods in comparison with the experimental rotational constants obtained.

	Experimental	MP2/ 6-311++(d,p)	B3LYP/ 6-311++(d,p)	M06/ 6- 311++(d,p)	M06/ cc-pTVZ	M06/ aug-cc-pTVZ	M062X/ 6-311++(d,p)	M062X/ cc-pTVZ
<b>A</b> <sup>a</sup>	1298.4982( 44)	1279.9	1279.8	1291.4	1302.1	1301.8	1293.2	1301.0
<b>B</b>	871.2573(29)	861.4	858.0	869.1	874.9	875.0	865.5	870.7
<b>C</b>	579.46230(20)	573.8	572.3	578.6	582.5	582.5	577.2	580.5
$\chi_a / \chi_b / \chi_c$	1.84(17)/ 2.502(82)/ -4.340(82)							
$\mu_a / \mu_b / \mu_c$	Obs/obs/-	4.1/1.0/0.1	4.2/1.1/0.0	4/1.1/0.0	3.7/1/0.0	3.8/1.1/0.0	4.3/1.0/0.0	4.0/0.9/0.0
<b>P<sub>cc</sub></b>	-97.1081(35)	-100.7	-100.9	-99.5	-98.2	-98.2	-99.1	-98.2

[a] A, B, and C represent the rotational constants (in MHz); P<sub>c</sub> is the planar inertial moment (in uÅ<sup>2</sup>), conversion factor: 505379.1 MHz-uÅ<sup>2</sup>;  $\mu_a$ ,  $\mu_b$  and  $\mu_c$  are the electric dipole moment components (in D);  $\chi_{aa}$ ,  $\chi_{bb}$  and  $\chi_{cc}$  are the diagonal elements of the <sup>14</sup>N nuclear quadrupole coupling tensor (in MHz).

## Supplementary Information for Chapter IV:

**Table S1.** Rotational transitions (MHz) measured of the conformer s-cis of cinnamic acid.

$J'$	$K'_{-1}$	$K'_{+1}$	$J''$	$K''_{-1}$	$K''_{+1}$	$V_{\text{obs}}$	$V_{\text{obs}} - V_{\text{cal}}$
3	0	3	2	0	2	2680.425	-0.018
4	0	4	3	0	3	3570.805	0.004
5	0	5	4	0	4	4458.496	0.000
6	0	6	5	0	5	5342.900	0.004
7	0	7	6	0	6	6223.418	0.004
3	1	2	2	1	1	2763.322	0.004
4	1	3	3	1	2	3683.635	0.005
5	1	4	4	1	3	4603.247	0.003
6	1	5	5	1	4	5521.966	-0.002
7	1	6	6	1	5	6439.593	0.000
8	1	7	7	1	6	7355.895	-0.001
3	1	3	2	1	2	2602.095	0.002
4	1	4	3	1	3	3468.688	0.001
5	1	5	4	1	4	4334.639	0.002



6	1	6	5	1	5	5199.796	-0.003
7	1	7	6	1	6	6064.048	0.002
8	1	8	7	1	7	6927.259	-0.004
3	2	2	2	2	1	2683.127	0.002
4	2	3	3	2	2	3576.983	0.005
5	2	4	4	2	3	4470.388	0.004
6	2	5	5	2	4	5363.234	0.002
7	2	6	6	2	5	6255.401	-0.009
4	3	1	3	3	0	3578.854	0.012
4	3	2	3	3	1	3578.854	0.012
5	3	2	4	3	1	4474.181	-0.001
5	3	3	4	3	2	4474.181	-0.001
7	3	4	6	3	3	6266.527	-0.004
7	3	5	6	3	4	6265.876	0.004
5	4	2	4	4	1	4473.352	-0.014
5	4	1	4	4	0	4473.352	-0.014
7	4	3	6	4	2	6263.969	0.004
7	4	4	6	4	3	6263.969	0.004
7	5	2	6	5	1	6262.995	-0.012
7	5	3	6	5	2	6262.995	-0.012
1	1	1	0	0	0	4098.111	0.001
2	1	2	1	0	1	4938.743	0.002
4	1	4	3	0	3	6541.001	0.003
5	1	5	4	0	4	7304.832	-0.002
7	0	7	6	1	6	3520.164	-0.008
8	0	8	7	1	7	4555.662	0.004
1	1	0	1	0	1	3257.478	-0.001
2	1	1	2	0	2	3311.892	0.000
3	1	2	3	0	3	3394.765	-0.002
4	1	3	4	0	4	3507.594	-0.003
5	1	4	5	0	5	3652.342	-0.003
6	1	5	6	0	6	3831.415	-0.002
7	1	6	7	0	7	4047.607	0.010
8	1	7	8	0	8	4303.956	-0.003
9	1	8	9	0	9	4603.743	-0.005
10	1	9	10	0	10	4950.208	0.002
11	1	10	11	0	11	5346.380	0.000
12	1	11	12	0	12	5794.892	0.000

**Table S2.** Rotational transitions (MHz) measured of the conformer s-trans of cinnamic acid.

$J'$	$K'_{-1}$	$K'_{+1}$	$J''$	$K''_{-1}$	$K''_{+1}$	$V_{\text{obs}}$	$V_{\text{obs}} - V_{\text{cal}}$
3	0	3	2	0	2	2701.714	0.002
4	0	4	3	0	3	3599.009	-0.009
5	0	5	4	0	4	4493.545	0.003
6	0	6	5	0	5	5384.625	-0.001
7	0	7	6	0	6	6271.663	0.003
8	0	8	7	0	7	7154.110	-0.002
3	1	3	2	1	2	2621.894	-0.003
5	1	5	4	1	4	4367.547	0.001
6	1	6	5	1	5	5239.214	0.000
7	1	7	6	1	6	6109.927	0.001
8	1	8	7	1	7	6979.558	-0.006
3	1	2	2	1	1	2786.251	-0.003
4	1	3	3	1	2	3714.180	0.005
5	1	4	4	1	3	4641.366	-0.001
7	1	6	6	1	5	6492.730	-0.004
8	1	7	7	1	6	7416.450	-0.007
3	2	2	2	2	1	2704.514	0.001
4	2	3	3	2	2	3605.477	0.004

5	2	4	4	2	3	4505.968	0.003
6	2	5	5	2	4	5405.873	-0.001
7	2	6	6	2	5	6305.086	0.003
8	2	7	7	2	6	7203.477	0.001
3	2	1	2	2	0	2707.320	0.004
4	2	2	3	2	1	3612.479	0.005
5	2	3	4	2	2	4519.951	0.005
6	2	4	5	2	3	5430.277	0.003
7	2	5	6	2	4	6343.949	-0.001
8	2	6	7	2	5	7261.383	-0.005
4	3	1	3	3	0	3607.418	-0.002
4	3	2	3	3	1	3607.418	-0.002
6	3	3	5	3	2	5413.047	0.007
6	3	4	5	3	3	5412.720	-0.006
7	3	4	6	3	3	6316.706	-0.007
7	3	5	6	3	4	6316.017	0.008
6	4	2	5	4	1	5411.411	0.001
6	4	3	5	4	2	5411.411	0.001
1	1	1	0	0	0	4086.496	-0.004
2	1	2	1	0	1	4933.220	0.003
4	1	4	3	0	3	6546.152	0.000
5	1	5	4	0	4	7314.683	0.002
6	0	6	5	1	5	2563.484	-0.005
7	0	7	6	1	6	3595.935	0.000
9	0	9	8	1	8	5692.133	0.008
10	0	10	9	1	9	6747.864	0.001
1	1	0	1	0	1	3239.786	0.004
2	1	1	2	0	2	3295.272	0.001
3	1	2	3	0	3	3379.811	-0.003
5	1	4	5	0	5	3642.798	0.002
6	1	5	6	0	6	3825.794	-0.001
7	1	6	7	0	7	4046.869	0.000
8	1	7	8	0	8	4309.214	0.001
9	1	8	9	0	9	4616.181	-0.002

**Table S3.** Rotational transitions (MHz) measured of the conformer *s-cis-a* of *p*-coumaric acid.

$J'$	$K'_{-1}$	$K'_{+1}$	$J''$	$K''_{-1}$	$K''_{+1}$	$\nu_{\text{obs}}$	$\nu_{\text{obs}} - \nu_{\text{cal}}$
4	0	4	3	0	3	2684.997	0.004
5	0	5	4	0	4	3354.585	0.002
6	0	6	5	0	5	4023.066	-0.006
7	0	7	6	0	6	4690.247	0.000
4	1	4	3	1	3	2624.685	0.010
6	1	6	5	1	5	3935.926	-0.001
7	1	7	6	1	6	4591.109	0.003
8	1	8	7	1	7	5245.923	-0.001
4	1	3	3	1	2	2748.858	0.004
6	1	5	5	1	4	4122.154	0.004
7	1	6	6	1	5	4808.308	0.003
8	1	7	7	1	6	5494.044	0.000
9	1	8	8	1	7	6179.297	-0.002

4	2	3	3	2	2	2687.038	0.003
5	2	4	4	2	3	3358.519	0.003
6	2	5	5	2	4	4029.816	0.002
7	2	6	6	2	5	4700.903	0.013
8	2	7	7	2	6	5371.703	-0.005
9	2	8	8	2	7	6042.226	-0.005
10	2	9	9	2	8	6712.411	-0.010
4	2	2	3	2	1	2689.247	-0.002
5	2	3	4	2	2	3362.944	0.002
6	2	4	5	2	3	4037.554	0.002
7	2	5	6	2	4	4713.245	-0.010
5	3	2	4	3	1	3359.774	-0.006
5	3	3	4	3	2	3359.774	0.015
7	4	3	6	4	2	4703.715	0.000
7	4	4	6	4	3	4703.715	0.001
8	4	4	7	4	3	5375.966	-0.004
8	4	5	7	4	4	5375.966	-0.003
9	4	5	8	4	4	6048.345	0.001
9	4	6	8	4	5	6048.345	0.004

**Table S4.** Rotational transitions (MHz) measured of the conformer s-cis-s of p-coumaric acid.

$J'$	$K'_{-1}$	$K'_{+1}$	$J''$	$K''_{-1}$	$K''_{+1}$	$V_{\text{obs}}$	$V_{\text{obs}} - V_{\text{cal}}$
4	0	4	3	0	3	2683.556	-0.002
5	0	5	4	0	4	3352.800	0.001
8	0	8	7	0	7	5353.106	-0.013
9	0	9	8	0	8	6016.742	-0.010
4	1	4	3	1	3	2623.378	-0.009
5	1	5	4	1	4	3278.825	-0.002
6	1	6	5	1	5	3933.997	-0.005
7	1	7	6	1	6	4588.860	-0.004
9	1	9	8	1	8	5897.484	0.013
4	1	3	3	1	2	2747.251	0.001
5	1	4	4	1	3	3433.649	0.006
6	1	5	5	1	4	4119.756	0.004
7	1	6	6	1	5	4805.503	-0.009
8	1	7	7	1	6	5490.872	0.012
4	2	3	3	2	2	2685.583	-0.004
5	2	4	4	2	3	3356.710	0.001
6	2	5	5	2	4	4027.648	0.001
7	2	6	6	2	5	4698.364	-0.002
2	1	2	1	0	1	4563.561	0.008
1	1	1	0	0	0	3923.089	0.008
4	1	4	3	0	3	5798.574	0.001
9	0	9	8	1	8	3271.319	-0.008
10	0	10	9	1	9	4052.378	0.009
11	0	11	10	1	10	4839.495	0.006
1	1	0	1	0	1	3282.607	-0.001
2	1	1	2	0	2	3313.797	0.001
4	1	3	4	0	4	3424.681	-0.001
5	1	4	5	0	5	3505.529	0.003
6	1	5	6	0	6	3604.319	-0.013
7	1	6	7	0	7	3722.055	-0.004
8	1	7	8	0	8	3859.809	0.010
10	1	9	10	0	10	4200.291	-0.006

**Table S5.** Rotational transitions (MHz) measured of the conformer s-trans-a of p-coumaric acid.

$J'$	$K'_{-1}$	$K'_{+1}$	$J''$	$K''_{-1}$	$K''_{+1}$	$V_{\text{obs}}$	$V_{\text{obs}} - V_{\text{cal}}$
4	0	4	3	0	3	2702.420	-0.008
6	0	6	5	0	5	4049.108	0.011
4	1	4	3	1	3	2641.333	0.003
5	1	5	4	1	4	3301.247	0.004
6	1	6	5	1	5	3960.887	0.007
8	1	8	7	1	7	5279.135	-0.003
11	1	11	10	1	10	7253.335	-0.001
4	1	3	3	1	2	2767.168	-0.002
5	1	4	4	1	3	3458.524	-0.004
7	1	6	6	1	5	4840.288	-0.006
9	1	8	8	1	7	6220.347	0.002
4	2	2	3	2	1	2706.817	0.010
5	2	3	4	2	2	3384.934	0.004
6	2	4	5	2	3	4063.993	-0.003
10	2	8	9	2	7	6793.122	-0.006
4	2	3	3	2	2	2704.533	0.004
6	2	5	5	2	4	4056.028	-0.005
10	2	9	9	2	8	6756.006	-0.001
10	0	10	9	1	9	4117.049	0.001
1	1	1	0	0	0	3918.176	-0.002
2	1	2	1	0	1	4562.889	-0.004
3	1	3	2	0	2	5191.971	0.008
2	1	1	2	0	2	3305.153	0.001
3	1	2	3	0	3	3353.111	-0.002
6	1	5	6	0	6	3600.552	0.002
7	1	6	7	0	7	3720.331	0.001
8	1	7	8	0	8	3860.519	-0.010
10	1	9	10	0	10	4207.323	0.013
11	1	10	11	0	11	4416.671	-0.004

**Table S6.** Rotational transitions measured of the conformer s-trans-s of p-coumaric acid.

$J'$	$K'_{-1}$	$K'_{+1}$	$J''$	$K''_{-1}$	$K''_{+1}$	$V_{\text{obs}}$	$V_{\text{obs}} - V_{\text{cal}}$
4	0	4	3	0	3	2701.187	-0.003
5	0	5	4	0	4	3374.795	0.004
6	0	6	5	0	5	4047.262	-0.004
7	0	7	6	0	6	4718.397	-0.002
9	0	9	8	0	8	6055.809	-0.004
10	0	10	9	0	9	6721.726	0.002
4	1	3	3	1	2	2765.784	0.008
5	1	4	4	1	3	3456.777	-0.012
6	1	5	5	1	4	4147.520	0.013
8	1	7	7	1	6	5527.811	0.007
9	1	8	8	1	7	6217.235	-0.007
10	1	9	9	1	8	6906.106	-0.004
4	2	2	3	2	1	2705.533	-0.010
6	2	4	5	2	3	4062.078	-0.001
7	2	6	6	2	5	4729.297	0.013
7	2	5	6	2	4	4741.919	-0.012
10	2	8	9	2	7	6789.824	0.004
11	2	10	10	2	9	7426.758	0.004

## Supplementary information for Chapter V:

**Fig. S01** The pulse sequence depicted in Fig. S01 is generated using a 32-bit counter sourced by a 20 MHz or a 100 kHz base clock, depending on the required pulse duration. The clock of the A/D conversion is phase-stabilized to a 10 MHz base clock. The signal of a 10 MHz reference standard is used to generate these base frequencies either directly or after division of the 20 MHz output signal of a frequency doubler. The trigger signal is derived from the 100 kHz basis such that all harmonics of this frequency can be used in the system. Apart from the transistor-transistor-logic (TTL) pulse sequence for the internally singly triggered jet valve (SOURCE), LASER-photolysis, LASER-ablation or flash-lamp trigger (CHARGE), DC-discharge or Q-switch trigger (DISCHARGE), the internally retriggerable MW pulse (EXCITE), DR pulse (PREPARE/MIX), MW/DR protection (PROTECT), and start trigger of the transient recorder (DETECT), additional TTL control signals (CYCLOPS I, II) are provided for the generation of an optional quadrature-phase-shift-keying (QPSK) sequence to remove possible phase and amplitude asymmetries of the input channels (I, Q) and known as the cyclically-ordered-phase-sequence (CYCLOPS). Retriggerable without trigger-delay, the segmented memory of the transient recorder captures one FID per segment. At a flight time of about 1 ms for the jet propagating along the resonator's axis, about 4 FIDs can be recorded per gas pulse without compromising the resolution while an S/N improvement of x2 is achieved. For optional double resonance (DR) experiments, the relative phase between the DR pulses can be adjusted according to the requirements of a specific DR phase sequence (PHASE I, II). All TTL status signals for phase control are only active for the duration of the corresponding radiation pulse, so that remaining coherent leakage signals during the detection period are not subjected to the phase modulation and therefore are eliminated due to the Re/Im channel rotation and +/- sign alternation in the data-acquisition cycles.

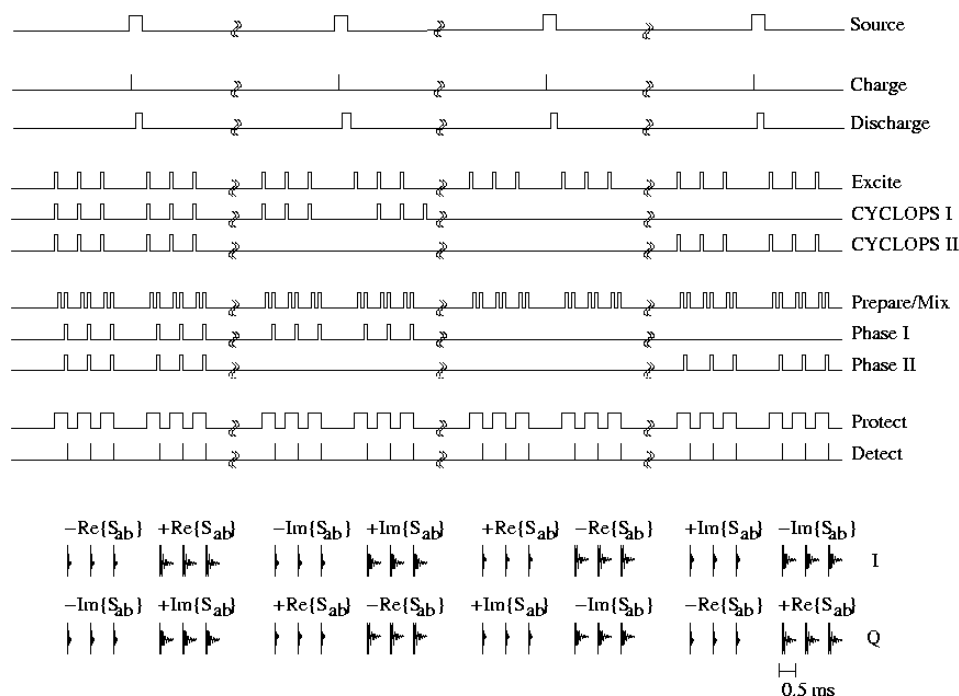


**Fig. S02** The predicted six low-energy conformers of Ac-Val-NH<sub>2</sub> in energetical order from lowest to highest. The rotational constants (in MHz) are also shown.

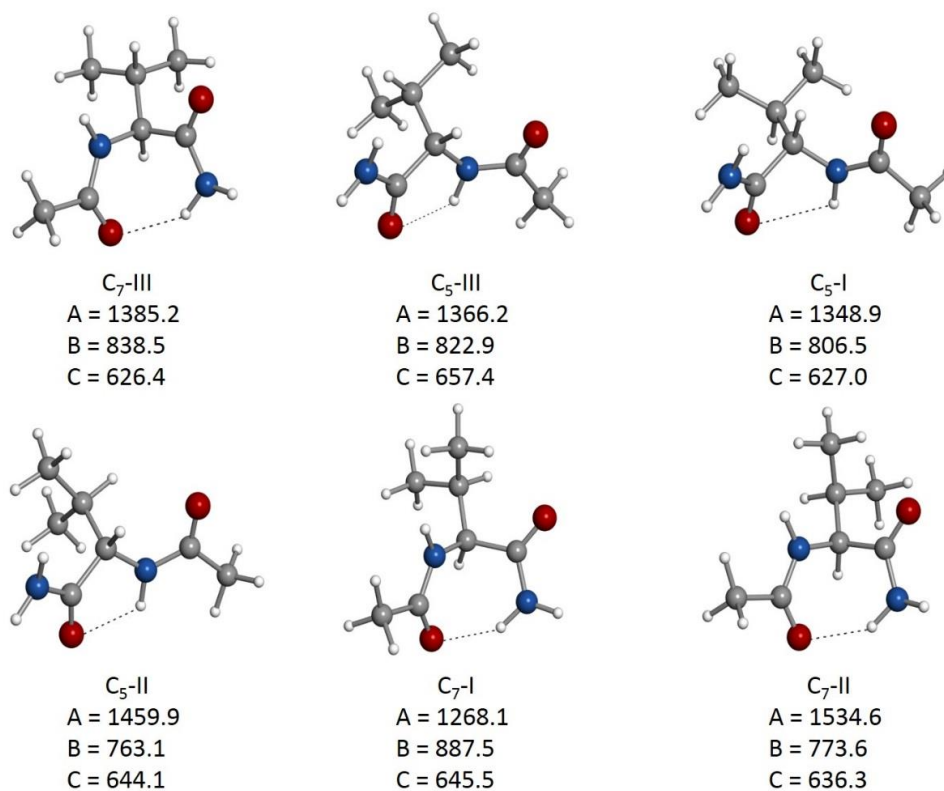


**Fig. S03** Calculated MP2/6-311++G(d,p) potential energy surface (PES) for the torsional coordinate of the isopropyl group of Ac-Val-NH<sub>2</sub>. From left to right: Conformers C<sub>5</sub>-II, C<sub>5</sub>-I and C<sub>5</sub>-III.

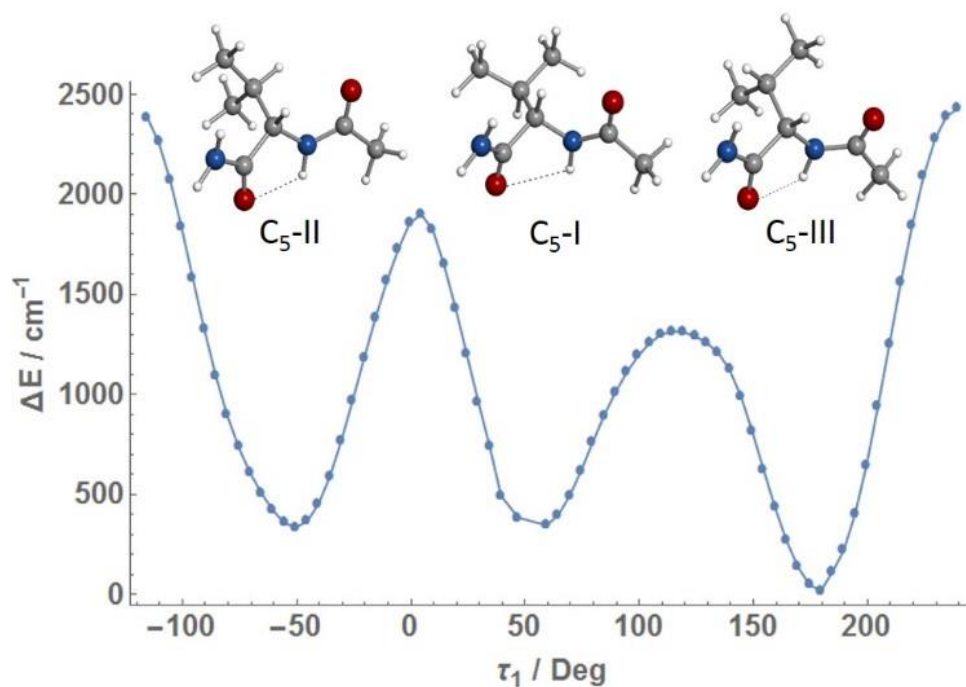


**Table S01.** Experimental and calculated spectroscopic parameters for the six lowest energy conformers of Ac-Val-NH<sub>2</sub>, including the observed rotamers (C<sub>7</sub>-III and C<sub>5</sub>-III conformers). Ab initio energies are included for the predicted species. All the calculations were done using the 6-311++G(d,p) basis set, except for B3LYP-D3BJ for which def2tzvp was used instead. A, B, and C represent the rotational constants (in MHz);  $\mu_a$ ,  $\mu_b$ , and  $\mu_c$  are the electric dipole moment components (in D);  $\chi_{aa}$ ,  $\chi_{bb}$ , and  $\chi_{cc}$  are the diagonal elements of the <sup>14</sup>N nuclear quadrupole coupling tensor (in MHz); N<sub>c</sub> and N<sub>t</sub> correspond to the central and terminal <sup>14</sup>N nuclei, respectively.  $\Delta E$  is the relative energies (in cm<sup>-1</sup>) with respect to the global minimum.  $\Delta E_{ZPE}$  is the relative energies (in cm<sup>-1</sup>) with respect to the global minimum, taking into account the zero point energy (ZPE).  $\Delta G$  is the Gibbs energies (in cm<sup>-1</sup>) calculated at 298K.

	Experimental		C <sub>7</sub> -III				C <sub>5</sub> -III				C <sub>5</sub> -I			
	Rotamer 1	Rotamer 2	MP2	M06-2X	B3LYP-D3	B3LYP-D3BJ	MP2	M06-2X	B3LYP-D3	B3LYP-D3BJ	MP2	M06-2X	B3LYP-D3	B3LYP-D3BJ
<b>A</b>	1388.6071(22)	1353.8151(58)	1385.186	1396.279	1378.672	1387.608	1366.223	1391.378	1336.571	1340.589	1348.950	1396.269	1352.620	1357.923
<b>B</b>	840.91159(42)	826.98719(28)	838.465	841.410	834.033	840.758	822.860	823.807	817.164	826.713	806.537	810.489	802.463	810.462
<b>C</b>	619.86354(17)	657.16182(21)	626.387	621.346	613.927	618.821	657.379	656.299	653.082	657.068	626.969	620.156	617.367	622.343
$ \mu_a $			1.2	1.4	1.4	1.4	2.2	2.5	2.5	2.6	0.7	1.7	1.6	1.6
$ \mu_b $			1.9	2.1	2.1	2.0	0.0	0.4	0.4	0.3	0.6	0.4	0.4	0.5
$ \mu_c $			0.8	0.8	0.8	0.8	0.3	0.2	0.2	0.2	0.1	0.3	0.3	0.3
N <sub>c</sub> / $\chi_{aa}$	2.0245(51)	2.170(11)	2.06	2.09	2.22	2.03	2.21	2.27	2.38	2.21	2.28	2.31	2.44	2.27
N <sub>c</sub> / $\chi_{bb}$	-2.987(11)	-2.286(14)	-3.22	-3.18	-3.37	-3.16	-2.29	-2.22	-2.72	-2.45	-3.46	-2.33	-3.18	-2.93
N <sub>c</sub> / $\chi_{cc}$	0.962(11)	0.116(14)	1.16	1.08	1.15	1.12	0.08	-0.05	0.34	0.24	1.18	0.01	0.74	0.65
N <sub>t</sub> / $\chi_{aa}$	-0.7689(71)	0.613(12)	-1.04	-0.80	-0.77	-0.71	0.38	0.88	0.59	0.50	-2.11	-0.76	-1.50	-1.51
N <sub>t</sub> / $\chi_{bb}$	1.902(13)	-0.925(15)	1.95	2.05	2.14	2.08	-1.23	-1.02	-1.2	-0.99	0.07	-0.76	-0.51	-0.37
N <sub>t</sub> / $\chi_{cc}$	-1.133(13)	0.312(15)	-0.91	-1.25	-1.37	-1.36	0.84	0.14	0.64	0.49	2.05	1.52	2.01	1.88
$\Delta E$			0	0	0	0	83	161	360	271	403	511	556	484
$\Delta E_{ZPE}$			0	51	0	0	45	0	187	122	267	388	372	321
$\Delta G$			113	190	115	168	154	0	0	0	0	298	122	118

**Table S01.** Cont.

	Experimental		C <sub>5</sub> -II				C <sub>7</sub> -I				C <sub>7</sub> -II			
	Rotamer 1	Rotamer 2	MP2	M06-2X	B3LYP-D3	B3LYP-D3BJ	MP2	M06-2X	B3LYP-D3	B3LYP-D3BJ	MP2	M06-2X	B3LYP-D3	B3LYP-D3BJ
<b>A</b>	1388.6071(22)	1353.8151(58)	1459.928	1478.124	1445.795	1452.532	1268.107	1296.690	1279.068	1287.992	1534.606	1555.722	1536.222	1546.055
<b>B</b>	840.91159(42)	826.98719(28)	763.069	769.803	758.491	766.400	887.512	886.970	878.761	885.804	773.625	771.279	763.985	770.868
<b>C</b>	619.86354(17)	657.16182(21)	644.125	642.501	639.507	641.934	645.512	638.250	630.885	636.035	636.289	633.483	627.149	631.908
<b> μ<sub>a</sub> </b>			2.1	2.3	2.5	2.6	1.1	1.4	1.3	-1.3	1.3	1.5	1.5	-1.51
<b> μ<sub>b</sub> </b>			0.7	0.4	0.4	-0.5	2.4	2.5	2.5	-2.5	2.4	2.4	2.4	-2.32
<b> μ<sub>c</sub> </b>			0.5	0.3	0.3	-0.3	1.3	1.4	1.3	-1.3	0.4	0.5	0.5	-0.45
<b>N<sub>c</sub>/χ<sub>aa</sub></b>	2.0245(51)	2.170(11)	2.32	2.36	2.50	2.33	2.05	2.11	2.24	2.05	2.10	2.14	2.26	2.08
<b>N<sub>c</sub>/χ<sub>bb</sub></b>	-2.987(11)	-2.286(14)	-0.58	-0.40	-0.87	-0.63	-2.40	-2.47	-2.50	-2.24	-1.27	-1.52	-1.55	-1.37
<b>N<sub>c</sub>/χ<sub>cc</sub></b>	0.962(11)	0.116(14)	-1.74	-1.96	-1.62	-1.70	0.36	0.37	0.26	0.19	-0.84	-0.62	-0.71	-0.71
<b>N<sub>t</sub>/χ<sub>aa</sub></b>	-0.7689(71)	0.613(12)	0.14	0.74	0.55	0.55	0.83	1.04	1.03	0.98	-0.05	0.10	0.12	0.14
<b>N<sub>v</sub>/χ<sub>bb</sub></b>	1.902(13)	-0.925(15)	-0.37	-0.05	-0.40	-0.12	1.83	2.03	2.11	2.03	1.58	1.70	1.78	1.70
<b>N<sub>t</sub>/χ<sub>cc</sub></b>	-1.133(13)	0.312(15)	0.23	-0.69	-0.15	-0.43	-2.67	-3.07	-3.14	-3.01	-1.52	-1.80	-1.90	-1.84
<b>ΔE</b>			342	293	417	313	440	182	193	144	588	457	406	402
<b>ΔE<sub>ZPE</sub></b>			272	241	271	179	429	176	155	134	629	497	414	416
<b>ΔG</b>			351	298	169	84	602	287	225	265	811	468	547	593



**Table S02.** Measured frequencies and residuals (in MHz) for the nuclear quadrupole coupling hyperfine components of the C<sub>7</sub>-III conformer of Ac-Val-NH<sub>2</sub>.

J'	K' <sub>-1</sub>	K' <sub>+1</sub>	J''	K'' <sub>-1</sub>	K'' <sub>+1</sub>	I'	F'	I''	F''	V <sub>obs.</sub>	V <sub>obs.</sub> - V <sub>calc.</sub>
3	0	3	2	0	2	1	2	1	1	4182.7061	0.0034
3	0	3	2	0	2	2	4	2	3	4182.7511	0.0027
3	0	3	2	0	2	2	3	2	2	4182.8731	0.0024
3	0	3	2	0	2	1	3	0	2	4182.9342	0.0043
3	0	3	2	0	2	2	5	2	4	4182.9879	0.0046
3	0	3	2	0	2	1	4	1	3	4183.1587	0.0032
3	2	2	2	2	1	2	2	2	1	4381.6986	-0.0021
3	2	2	2	2	1	1	3	1	2	4381.8243	-0.0003
3	2	2	2	2	1	1	4	1	3	4382.0074	-0.0016
3	2	2	2	2	1	2	5	2	4	4382.2344	-0.0014
3	2	2	2	2	1	0	3	0	2	4382.2853	-0.0009
3	2	2	2	2	1	2	3	2	2	4382.7738	-0.002
3	2	2	2	2	1	2	4	2	3	4382.8690	0.0028
3	2	2	2	2	1	1	2	1	1	4382.9496	-0.0008
4	0	4	3	1	3	1	3	1	2	5207.0316	0.0007
4	0	4	3	1	3	2	5	2	4	5207.0804	0.0008
4	0	4	3	1	3	0	4	0	3	5207.1285	0.0012
4	0	4	3	1	3	2	6	2	5	5207.1414	-0.0009
4	0	4	3	1	3	1	4	1	3	5207.2195	-0.0014
4	0	4	3	1	3	1	5	1	4	5207.2854	-0.0008
4	0	4	3	1	3	2	3	2	2	5207.3294	0.0021
4	0	4	3	0	3	1	5	2	4	5425.1573	-0.0007
4	0	4	3	0	3	1	5	1	4	5425.2329	-0.0030
4	0	4	3	0	3	2	3	2	2	5425.2401	0.0008
4	0	4	3	0	3	2	6	2	5	5425.3965	-0.0027
4	0	4	3	0	3	0	4	0	3	5425.4600	-0.0027
4	0	4	3	0	3	2	5	1	4	5425.5869	-0.0016
4	0	4	3	0	3	1	3	2	2	5425.6772	-0.0024

**Table S03.** Measured frequencies and residuals (in MHz) for the nuclear quadrupole coupling hyperfine components of the C<sub>5</sub>-III conformer of Ac-Val-NH<sub>2</sub>.

J'	K' <sub>-1</sub>	K' <sub>+1</sub>	J''	K'' <sub>-1</sub>	K'' <sub>+1</sub>	I'	F'	I''	F''	V <sub>obs.</sub>	V <sub>obs.</sub> - V <sub>calc.</sub>
3	1	3	2	1	2	1	4	1	3	4177.6912	-0.0001
3	1	3	2	1	2	2	5	2	4	4177.7269	-0.0001
3	1	3	2	1	2	2	3	0	2	4177.7400	-0.0001
3	0	3	2	0	2	2	3	2	2	4321.5734	-0.0028
3	0	3	2	0	2	2	4	2	3	4321.6002	0.0001
3	0	3	2	0	2	1	2	1	1	4321.6137	-0.0014
3	0	3	2	0	2	2	5	2	4	4321.7529	-0.0002
3	0	3	2	0	2	0	3	0	2	4321.9104	0.0020
3	1	2	2	1	1	2	5	2	4	4682.5783	0.0016
3	1	2	2	1	1	1	4	1	3	4682.6382	0.0045
3	1	2	2	1	1	1	2	1	1	4682.6952	-0.0045
3	1	2	2	1	1	2	4	2	3	4682.7236	0.0053
3	1	2	2	1	1	2	3	2	2	4682.8164	0.0029
4	1	4	3	1	3	2	6	2	5	5538.8507	0.0055
4	1	4	3	1	3	2	5	2	4	5538.8758	-0.0020
4	2	2	3	2	1	0	4	0	3	6193.7977	-0.0009
4	2	2	3	2	1	2	6	2	5	6193.8758	-0.0001
4	2	2	3	2	1	1	5	1	4	6194.0125	-0.0025
4	2	2	3	2	1	2	5	2	4	6194.2932	-0.0001
4	2	2	3	2	1	2	4	2	3	6194.4250	-0.0029
5	1	5	4	1	4	2	3	0	4	6883.0983	-0.0018

5	1	5	4	1	4	2	5	2	4	6883.1050	0.0034
5	1	5	4	1	4	2	6	2	5	6883.1136	-0.0013
5	1	5	4	1	4	2	7	2	6	6883.1221	0.0022
5	1	5	4	1	4	1	5	1	4	6883.1319	0.0035
5	0	5	4	0	4	1	6	1	5	6952.2332	0.0016
5	0	5	4	0	4	2	4	2	3	6952.2637	-0.0042
5	0	5	4	0	4	2	7	2	6	6952.2772	-0.0038
5	0	5	4	0	4	0	5	0	4	6952.2869	-0.0015

## Supplementary Information for Chapter IX:

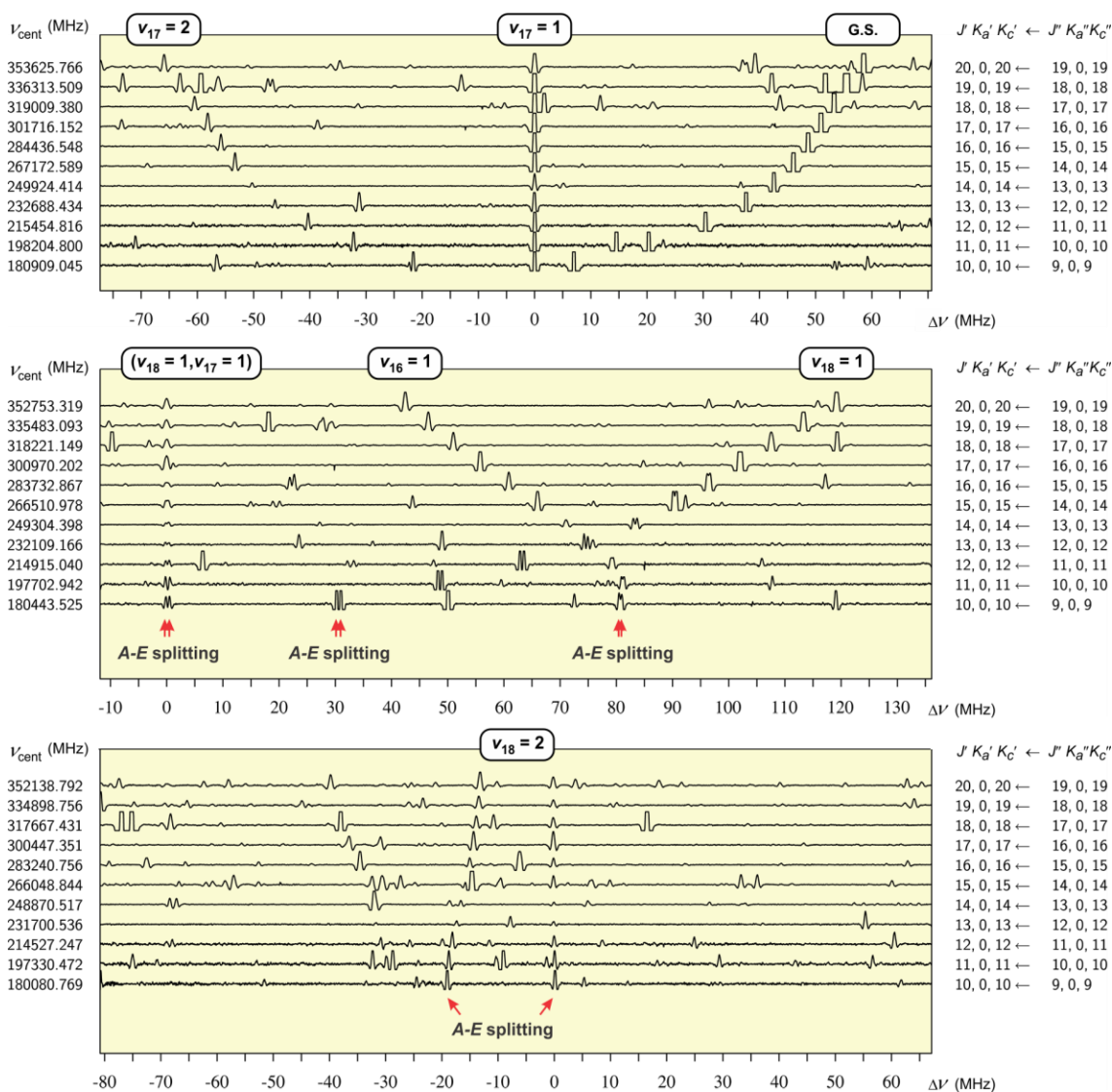


**Figure S1.** Loomis-Wood-type plots showing the identification of six different line sequences corresponding to six excited vibrational states. In each diagram, the rotational transitions are lined-up to the central frequencies  $\nu_{\text{cent}}$  of the  $K_a = 0 \leftarrow 0$  transitions of that sequence which is situated at  $\Delta\nu = 0$  where  $\Delta\nu$  is the distance from the  $\nu_{\text{cent}}$ . Rotational quantum numbers are given on the right side of each diagram.

## Supplementary information for Chapter X

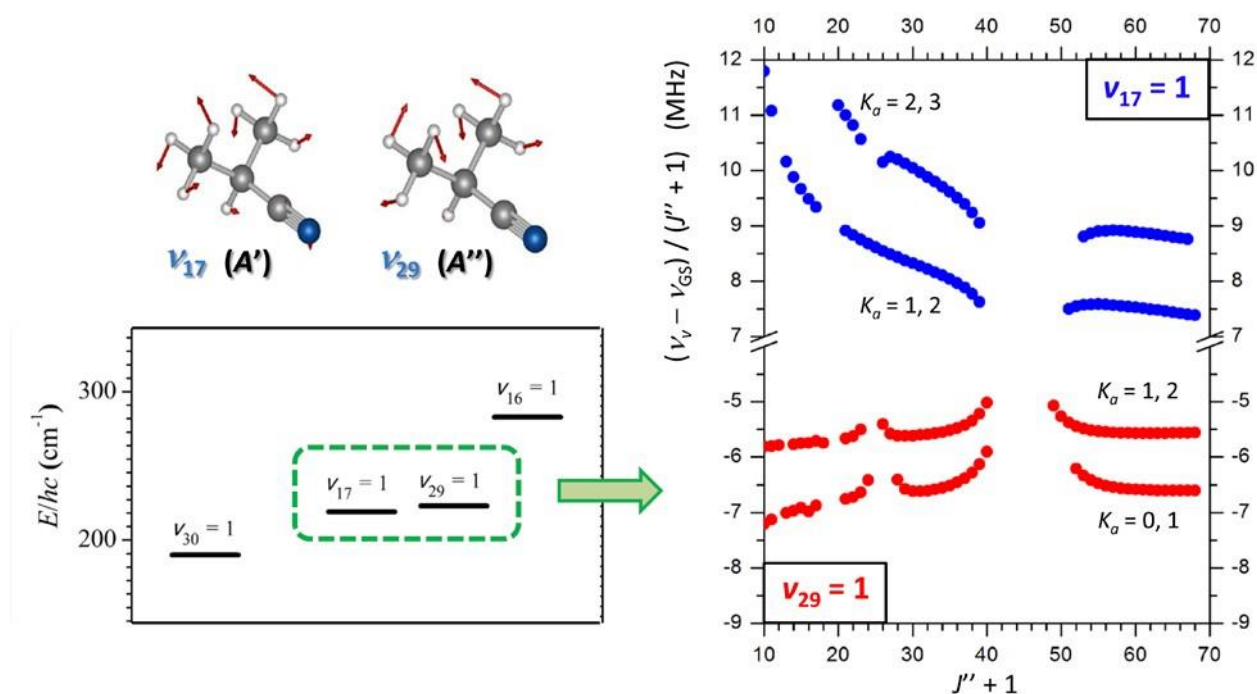


**Figure S1.** Impact of the small energy separation between  $\nu_{17} = 1$  and  $\nu_{29} = 1$  on the pure rotational transitions observed in both states. Pairwise perturbations are clearly identified by means of their characteristic mirror image in the same region of  $J$  quantum numbers. Plotted quantities are differences between the frequency  $\nu$  of a given transition in excited state and the frequency  $\nu_0$  of the same transition in the ground state, scaled by  $(J'' + 1)$  value, versus  $(J'' + 1)$ . Each dot represents an experimentally measured frequency.

## Supplementary information for Chapter XII:

**Table S1.** Observed centres of frequency and residuals (in MHz) for the rotational transitions of conformer 1 of glycynamide.

$J'$	$K'_{-1}$	$K'_{+1}$	$J''$	$K''_{-1}$	$K''_{+1}$	$V_{\text{obs}}$	$V_{\text{obs}} - V_{\text{cal}}$
1	0	1	0	0	0	6912.185	-0.042
2	0	2	1	0	1	13688.501	0.066
1	1	0	1	0	1	6706.186	0.082
2	1	1	2	0	2	7903.277	-0.051
3	1	2	3	0	3	9933.778	-0.040
2	0	2	1	1	1	8043.501	-0.034
4	1	3	4	1	4	10535.716	-0.011
3	1	2	3	1	3	6356.274	0.055
2	1	2	1	1	1	12763.220	-0.031
2	1	1	1	1	0	14885.629	-0.030
3	0	3	2	1	2	15487.127	0.034

**Table S2.** Observed frequencies and residuals with or without distortional constants (in MHz) for the rotational transitions of conformer 1 of glycynamide.

$J'$	$K'_{-1}$	$K'_{+1}$	$F'_{-1}$	$F'_{-2}$	$J''$	$K''_{-1}$	$K''_{+1}$	$F''_{-1}$	$F''_{-2}$	$V_{\text{obs}}$	$V_{\text{obs}} - V_{\text{cal}}$ with distortion	$V_{\text{obs}} - V_{\text{cal}}$ without distortion
1	1	1	1	1	0	0	0	0	0	12555.898	-0.003	-0.004
1	1	1	1	1	0	0	0	1	1	12555.898	-0.003	-0.004
1	1	1	1	1	0	0	0	2	2	12555.898	-0.003	-0.004
1	1	1	2	2	0	0	0	1	1	12556.447	-0.001	-0.004
1	1	1	2	2	0	0	0	2	2	12556.447	-0.001	-0.004
1	1	1	1	0	0	0	0	1	1	12556.938	-0.001	-0.006
1	1	1	0	1	0	0	0	0	0	12557.231	0.000	-0.005
1	1	1	0	1	0	0	0	1	1	12557.231	0.000	-0.005
1	1	1	0	1	0	0	0	2	2	12557.231	0.000	-0.005
1	1	1	2	3	0	0	0	2	2	12557.284	-0.001	-0.006
1	1	1	1	2	0	0	0	1	1	12557.774	-0.002	-0.009
1	1	1	1	2	0	0	0	2	2	12557.774	-0.002	-0.009
1	1	1	2	1	0	0	0	0	0	12558.891	-0.003	-0.012
1	1	1	2	1	0	0	0	1	1	12558.891	-0.003	-0.012
1	1	1	2	1	0	0	0	2	2	12558.891	-0.003	-0.012
1	0	1	2	1	0	0	0	0	0	6911.146	0.003	0.026
1	0	1	2	1	0	0	0	1	1	6911.146	0.003	0.026
1	0	1	2	1	0	0	0	2	2	6911.146	0.003	0.026
1	0	1	1	1	0	0	0	0	0	6911.924	-0.001	0.026
1	0	1	1	1	0	0	0	1	1	6911.924	-0.001	0.026
1	0	1	1	1	0	0	0	2	2	6911.924	-0.001	0.026

1	0	1	2	3	0	0	0	2	2	6912.191	0.006	0.032
1	0	1	1	2	0	0	0	1	1	6912.453	0.002	0.027
1	0	1	1	2	0	0	0	2	2	6912.453	0.002	0.027
1	0	1	0	1	0	0	0	0	0	6912.937	0.001	0.028
1	0	1	0	1	0	0	0	1	1	6912.937	0.001	0.028
1	0	1	0	1	0	0	0	2	2	6912.937	0.001	0.028
1	0	1	2	2	0	0	0	1	1	6913.018	-0.002	0.026
1	0	1	2	2	0	0	0	2	2	6913.018	-0.002	0.026
1	0	1	1	0	0	0	0	1	1	6913.289	0.004	0.031
1	1	0	1	2	1	0	1	0	1	6705.868	0.008	0.004
1	1	0	1	0	1	0	1	1	1	6705.879	0.002	0.002
1	1	0	2	2	1	0	1	2	3	6705.377	-0.001	0.006
1	1	0	2	3	1	0	1	2	2	6705.539	0.002	0.003
1	1	0	1	1	1	0	1	2	1	6706.205	0.001	0.018
1	1	0	1	2	1	0	1	1	2	6706.339	-0.006	0.008
1	1	0	2	3	1	0	1	2	3	6706.374	0.002	0.004
1	1	0	2	2	1	0	1	2	1	6706.421	0.002	0.012
2	0	2	0	2	1	0	1	0	1	13687.508	-0.001	0.021
2	0	2	2	1	1	0	1	2	2	13687.571	-0.002	0.020
2	0	2	2	1	1	0	1	0	1	13687.660	0.001	0.022
2	0	2	1	2	1	0	1	0	1	13687.660	0.001	0.022
2	0	2	1	2	1	0	1	1	2	13688.147	-0.001	0.021
2	0	2	1	1	1	0	1	1	0	13688.246	-0.003	0.018
2	0	2	2	4	1	0	1	2	3	13688.610	-0.001	0.021
2	0	2	1	3	1	0	1	1	2	13688.742	0.000	0.024
2	0	2	0	2	1	0	1	2	1	13689.303	0.001	0.027
2	0	2	2	3	1	0	1	2	3	13689.422	0.005	0.027
2	0	2	1	1	1	0	1	1	1	13689.609	0.000	0.020
2	1	1	2	0	1	1	0	2	1	14883.765	0.000	0.005
2	1	1	2	1	1	1	0	1	2	14884.366	-0.001	0.007
2	1	1	1	2	1	1	0	1	2	14884.681	0.001	-0.010
2	1	1	2	1	1	1	0	0	1	14884.681	0.001	-0.010
2	1	1	2	2	1	1	0	2	1	14884.777	0.000	-0.006
2	1	1	1	1	1	1	0	2	1	14885.160	-0.001	-0.009
2	1	1	2	1	1	1	0	1	0	14885.359	-0.001	-0.013
2	1	1	2	4	1	1	0	2	3	14885.634	0.002	-0.014
2	1	1	0	2	1	1	0	0	1	14885.779	0.002	-0.015
2	1	1	2	1	1	1	0	1	1	14885.810	-0.005	-0.028
2	1	1	1	3	1	1	0	2	2	14886.036	-0.002	-0.021
2	1	1	2	3	1	1	0	1	2	14886.348	-0.001	-0.014
2	1	2	2	4	1	1	1	2	3	12763.202	0.008	-0.075
2	1	2	1	3	1	1	1	2	2	12763.736	-0.002	-0.080

**Table S3.** Cartesian coordinates for the conformer I. The geometries have been optimized ab initio at the B3LYP/6-311++G(d,p) with Grimme dispersion level of theory.

Center Number	Atomic Number	Coordinates (Angstroms)		
		X	Y	Z
1	7	1.897736	-0.099394	0.081168
2	1	2.142430	-0.163903	1.063170
3	1	2.712670	0.241622	-0.413562
4	6	0.738164	0.774402	-0.125084
5	1	0.774483	1.177477	-1.140856
6	1	0.685586	1.632811	0.552982
7	6	-0.603727	0.043999	-0.011798
8	8	-1.650521	0.663051	0.079300
9	7	-0.513121	-1.308536	-0.045724
10	1	0.396146	-1.733319	-0.156283
11	1	-1.355397	-1.860062	-0.026633

Rotational constants (MHZ):  
 9640.9247968    3976.1683296    2924.8920107

**Table S2.** Cartesian coordinates for the conformer II. The geometries have been optimized ab initio at the B3LYP/6-311++G(d,p) with Grimme dispersion level of theory.

Center Number	Atomic Number	Coordinates (Angstroms)		
		X	Y	Z
1	7	1.992756	0.018030	-0.002802
2	1	2.025878	-0.586681	-0.817525
3	1	2.024957	-0.603054	0.799563
4	6	0.752468	0.766998	0.004443
5	1	0.727631	1.431641	-0.866302
6	1	0.729643	1.417635	0.885833
7	6	-0.529712	-0.083228	0.000541
8	8	-0.508114	-1.300148	0.001190
9	7	-1.692129	0.633683	-0.002476
10	1	-2.569934	0.138167	-0.003078
11	1	-1.703367	1.639925	-0.003391

Rotational constants (MHZ):  
 10065.8454778    3835.0680166    2867.3242057

**Table S4.** Cartesian coordinates for the conformer III. The geometries have been optimized ab initio at the B3LYP/6-311++G(d,p) with Grimme dispersion level of theory.

Center Number	Atomic Number	Coordinates (Angstroms)		
		X	Y	Z
1	7	-1.905384	-0.015019	0.238880
2	1	-1.737213	-1.002771	0.067659
3	1	-2.752661	0.257267	-0.243737
4	6	-0.756349	0.745651	-0.228623
5	1	-0.678602	1.692752	0.316745
6	1	-0.786089	0.995477	-1.302181
7	6	0.516166	-0.075385	-0.035331

8	8	0.505787	-1.292853	-0.069822
9	7	1.661510	0.648479	0.114210
10	1	2.529627	0.151091	0.238082
11	1	1.645999	1.642442	0.268452

-----  
Rotational constants (MHZ):

9952.0196978 3939.0588865 2943.9224471

**Table S5.** Cartesian coordinates for the conformer IV. The geometries have been optimized ab initio at the B3LYP/6-311++G(d,p) with Grimme dispersion level of theory.

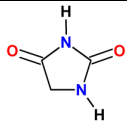
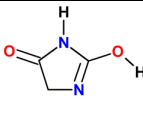
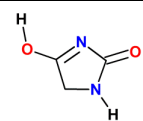
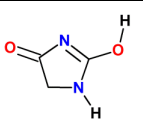
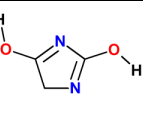
Center Number	Atomic Number	Coordinates (Angstroms)		
		X	Y	Z
1	7	-1.989402	0.030630	0.000535
2	1	-2.125548	0.591198	-0.830234
3	1	-2.126540	0.586602	0.834224
4	6	-0.763827	-0.749805	-0.000964
5	1	-0.760886	-1.408636	-0.873198
6	1	-0.760693	-1.411737	0.868866
7	6	0.603594	-0.049740	0.000105
8	8	1.632730	-0.702073	0.000605
9	7	0.590731	1.312763	-0.001107
10	1	-0.268089	1.835555	0.004928
11	1	1.470644	1.803898	0.003981

-----  
Rotational constants (MHZ):

9515.0891550 3894.2912822 2854.6530934

# Supplementary Information for Chapter XIII

**Table S1.** Experimental spectroscopic parameters of hydantoin along with those *ab initio* predicted for the plausible tautomers.

		<i>Ab initio</i> <sup>a</sup>				
		I	II	III	IV	V <sup>a</sup>
Experimental						
<i>A</i> /MHz	6537.73799 (86) <sup>b</sup>	6538	6697	6541	6524	6748
<i>B</i> /MHz	2291.37278 (16)	2274	2235	2273	2290	2230
<i>C</i> /MHz	1716.47204 (22)	1709	1694	1710	1717	1694
$\chi_{aa}$ ( <sup>14</sup> N <sub>1</sub> ) /MHz	2.5900 (41)	2.65	0.92	2.73	2.19	0.78
$\chi_{bb}$ ( <sup>14</sup> N <sub>1</sub> ) /MHz	2.1438 (70)	2.18	-0.98	2.05	2.22	-1.09
$\chi_{cc}$ ( <sup>14</sup> N <sub>1</sub> ) /MHz	-4.7338 (70)	-4.83	0.06	-4.77	-4.41	0.31
$\chi_{aa}$ ( <sup>14</sup> N <sub>3</sub> ) /MHz	1.6315 (51)	1.65	1.72	1.77	2.23	1.92
$\chi_{bb}$ ( <sup>14</sup> N <sub>3</sub> ) /MHz	1.8321 (75)	1.92	2.08	-3.36	-2.71	-3.34
$\chi_{cc}$ ( <sup>14</sup> N <sub>3</sub> ) /MHz	-3.4635 (75)	-3.57	-3.79	1.59	0.48	1.42
$ \mu_a $ /D	Yes <sup>c</sup>	0.2	2.3	3.6	3.6	1.5
$ \mu_b $ /D	Yes <sup>c</sup>	2.4	0.3	3.0	3.1	0.5
$ \mu_c $ /D	No <sup>c</sup>	0.6	0.0	0.6	0.8	0.0
$\sigma_{\text{fit}}$ / MHz <sup>d</sup>	0.003	...	...	...	...	...
$\Delta E$ / cm <sup>-1</sup> <sup>e</sup>	...	0	5501	5614	6392	9508



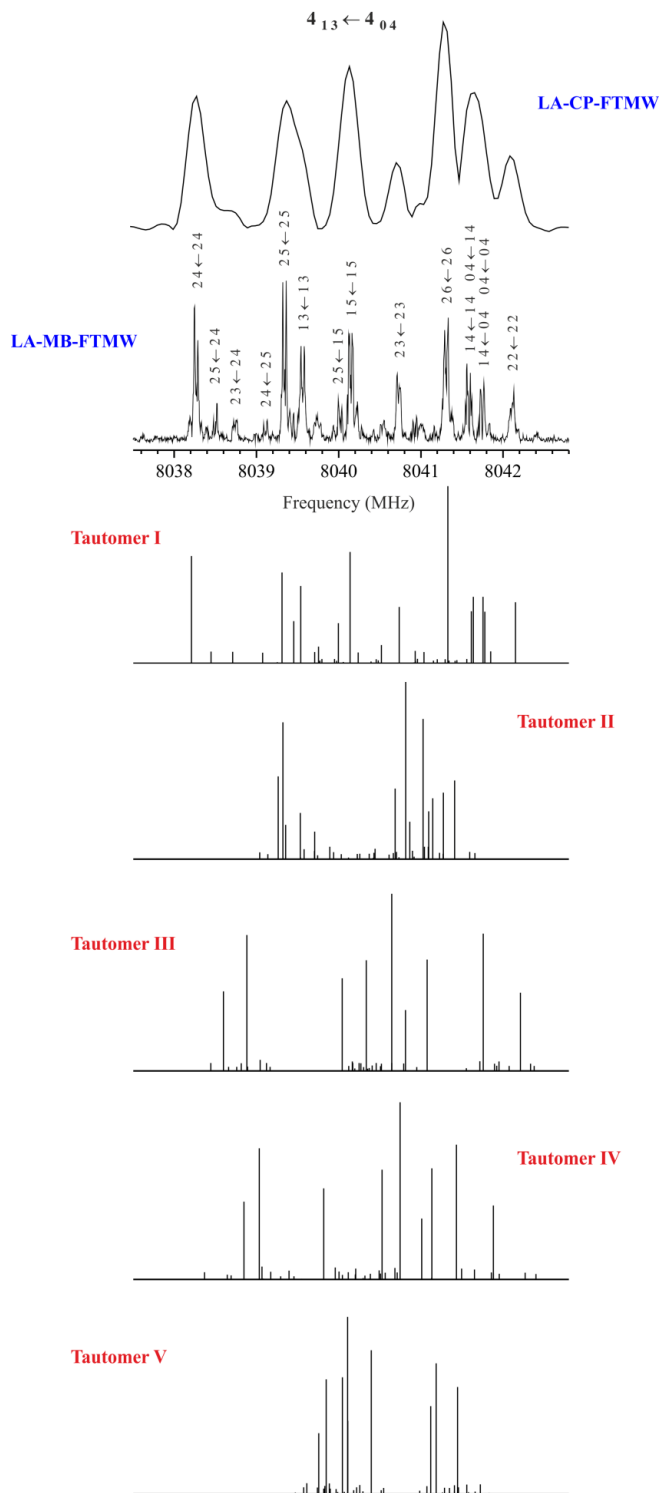


**Fig. S1.** Modeled hyperfine pattern of the plausible tautomers of hydantoin based on *ab initio* calculations in comparison with the observed spectrum.

**Table S2.** Observed frequencies and residuals (in MHz) for the rotational transitions of the conformer of hydantoin.

$J'$	$K_a'$	$K_c'$	$l'$	$F'$	$J''$	$K_a''$	$K_c''$	$l''$	$F''$	$V_{\text{obs}}$	$V_{\text{obs}} - V_{\text{calc}}$
4	1	3	2	2	4	0	4	2	2	8042.111	0.003
4	1	3	2	6	4	0	4	2	6	8041.308	0.004
4	1	3	2	3	4	0	4	2	3	8040.729	0.002
4	1	3	1	5	4	0	4	1	5	8040.146	0.003
4	1	3	2	5	4	0	4	1	5	8040.017	0.003
4	1	3	1	3	4	0	4	1	3	8039.559	-0.002
4	1	3	2	5	4	0	4	2	5	8039.343	0.002
4	1	3	2	4	4	0	4	2	4	8038.269	0.004
4	1	3	1	4	4	0	4	1	4	8041.584	-0.001
4	1	3	0	4	4	0	4	1	4	8041.601	-0.003
4	1	3	1	4	4	0	4	0	4	8041.727	0.003
4	1	3	0	4	4	0	4	0	4	8041.746	0.003
4	1	3	2	3	4	0	4	2	4	8038.741	-0.001
4	1	3	2	4	4	0	4	2	5	8039.110	0.000
4	1	3	2	5	4	0	4	2	4	8038.492	-0.004
3	1	2	1	3	3	0	3	1	3	6493.102	-0.001
3	1	2	2	1	3	0	3	2	1	6493.793	0.004
3	1	2	0	3	3	0	3	0	3	6493.326	0.002
3	1	2	1	4	3	0	3	2	4	6491.114	-0.004
3	1	2	2	4	3	0	3	2	4	6490.897	0.002
3	1	2	2	3	3	0	3	2	3	6490.011	0.005
3	1	2	2	5	3	0	3	2	5	6492.770	-0.003
3	1	2	1	4	3	0	3	1	4	6491.749	0.000
2	1	1	2	1	2	0	2	2	0	5452.424	0.004
2	1	1	2	0	2	0	2	2	1	5452.330	-0.001
2	1	1	0	2	2	0	2	0	2	5452.190	0.000
2	1	1	1	2	2	0	2	1	2	5451.754	-0.001
2	1	1	2	4	2	0	2	2	4	5451.316	0.001
2	1	1	1	3	2	0	2	1	3	5450.408	0.001
2	1	1	2	1	2	0	2	2	2	5450.094	0.003
2	1	1	1	3	2	0	2	2	3	5449.792	0.005
2	1	1	1	1	2	0	2	1	1	5449.517	0.003
2	1	1	2	3	2	0	2	2	3	5449.351	0.001
2	1	1	2	2	2	0	2	2	2	5448.725	0.002
2	1	1	2	3	2	0	2	2	2	5449.015	-0.001
2	1	1	2	2	2	0	2	2	3	5449.062	0.004
2	1	1	2	3	2	0	2	0	2	5450.957	-0.002
2	1	1	1	1	2	0	2	1	2	5450.760	-0.002
5	1	4	2	6	5	0	5	1	6	10171.387	-0.005
5	1	4	2	5	5	0	5	2	5	10169.447	-0.010
5	1	4	2	7	5	0	5	2	7	10172.758	-0.003
5	1	4	2	6	5	0	5	2	6	10170.671	0.002
1	1	1	1	0	0	0	0	1	1	8255.199	-0.004
1	1	1	2	3	0	0	0	2	2	8254.011	0.001
1	1	1	1	2	0	0	0	1	1	8254.305	-0.001
1	1	1	1	1	0	0	0	1	1	8253.712	-0.005
1	1	1	2	1	0	0	0	2	2	8252.900	0.000
1	1	1	0	1	0	0	0	1	1	8254.813	-0.004
1	1	1	2	2	0	0	0	2	2	8254.905	-0.003

3	0	3	1	2	2	1	2	1	2	8084.358	-0.002
3	0	3	2	4	2	1	2	2	4	8084.104	0.000
3	0	3	2	2	2	1	2	0	2	8083.717	0.000
3	0	3	2	2	2	1	2	2	1	8083.392	-0.002
3	0	3	0	3	2	1	2	0	2	8083.189	0.001
3	0	3	1	3	2	1	2	1	2	8082.969	0.000
3	0	3	2	5	2	1	2	2	4	8082.782	0.000
3	0	3	1	4	2	1	2	1	3	8082.637	0.003
3	0	3	2	4	2	1	2	2	3	8082.307	0.000
3	0	3	2	3	2	1	2	2	2	8082.331	0.005
3	0	3	1	3	2	1	2	1	3	8081.727	0.002
3	0	3	0	3	2	1	2	2	3	8080.593	0.000
3	0	3	2	2	2	1	2	2	2	8080.541	-0.001

---

